

230

Topics in Current Chemistry

Editorial Board:

**A. de Meijere · K.N. Houk · H. Kessler · J.-M. Lehn
S.V. Ley · S.L. Schreiber · J. Thiem · B.M. Trost
F. Vögtle · H. Yamamoto**

Springer

Berlin

Heidelberg

New York

Hong Kong

London

Milan

Paris

Tokyo

Elemental Sulfur and Sulfur-Rich Compounds I

Volume Editor: Ralf Steudel

With contributions by

B. Eckert · A.J.H. Janssen · A. de Keizer

W. E. Kleinjan · I. Krossing · R. Steudel · Y. Steudel

M. W. Wong



Springer

The series *Topics in Current Chemistry* presents critical reviews of the present and future trends in modern chemical research. The scope of coverage includes all areas of chemical science including the interfaces with related disciplines such as biology, medicine and materials science. The goal of each thematic volume is to give the nonspecialist reader, whether at the university or in industry, a comprehensive overview of an area where new insights are emerging that are of interest to a larger scientific audience.

As a rule, contributions are specially commissioned. The editors and publishers will, however, always be pleased to receive suggestions and supplementary information. Papers are accepted for *Topics in Current Chemistry* in English.

In references *Topics in Current Chemistry* is abbreviated Top Curr Chem and is cited as a journal.

Springer WWW home page: <http://www.springer.de>
Visit the TCC home page at <http://www.springerlink.com>

ISSN 0340-1022
ISBN 3-540-40191-1
DOI 10.1007/b12115
Springer-Verlag Berlin Heidelberg New York

Library of Congress Catalog Card Number 74-644622

This work is subject to copyright. All rights are reserved, whether the whole or part of the material is concerned, specifically the rights of translation, reprinting, reuse of illustrations, recitation, broadcasting, reproduction on microfilms or in any other ways, and storage in data banks. Duplication of this publication or parts thereof is only permitted under the provisions of the German Copyright Law of September 9, 1965, in its current version, and permission for use must always be obtained from Springer-Verlag. Violations are liable for prosecution under the German Copyright Law.

Springer-Verlag Berlin Heidelberg New York
a member of BertelsmannSpringer Science+Business Media GmbH

<http://www.springer.de>

© Springer-Verlag Berlin Heidelberg 2003
Printed in Germany

The use of general descriptive names, registered names, trademarks, etc. in this publication does not imply, even in the absence of a specific statement, that such names are exempt from the relevant protective laws and regulations and therefore free for general use.

Cover design: KünkelLopka, Heidelberg/design & production GmbH,
Heidelberg

Typesetting: Stürtz AG, 97080 Würzburg

02/3020 ra - 5 4 3 2 1 0 - Printed on acid-free paper

Volume Editor

Prof. Dr. Ralf Steudel

Technische Universität Berlin
Institut für Chemie / Sekr. C2
Straße des 17. Juni 135
10623 Berlin, Germany
E-mail: steudel@schwefel.chem.tu-berlin.de

Editorial Board

Prof. Dr. Armin de Meijere

Institut für Organische Chemie
der Georg-August-Universität
Tammannstraße 2
37077 Göttingen, Germany
E-mail: ameijer1@uni-goettingen.de

Prof. Dr. Horst Kessler

Institut für Organische Chemie
TU München
Lichtenbergstraße 4
85747 Garching, Germany
E-mail: kessler@ch.tum.de

Prof. Steven V. Ley

University Chemical Laboratory
Lensfield Road
Cambridge CB2 1EW, Great Britain
E-mail: svl1000@cus.cam.ac.uk

Prof. Dr. Joachim Thiem

Institut für Organische Chemie
Universität Hamburg
Martin-Luther-King-Platz 6
20146 Hamburg, Germany
E-mail: thiem@chemie.uni-hamburg.de

Prof. Dr. Fritz Vögtle

Kekulé-Institut für Organische Chemie
und Biochemie der Universität Bonn
Gerhard-Domagk-Straße 1
53121 Bonn, Germany
E-mail: voegtle@uni-bonn.de

Prof. K.N. Houk

Department of Chemistry and
Biochemistry
University of California
405 Hilgard Avenue
Los Angeles, CA 90024-1589, USA
E-mail: houk@chem.ucla.edu

Prof. Jean-Marie Lehn

Institut de Chimie
Université de Strasbourg
1 rue Blaise Pascal, B.P.Z 296/R8
67008 Strasbourg Cedex, France
E-mail: lehn@chimie.u-strasbg.fr

Prof. Stuart L. Schreiber

Chemical Laboratories
Harvard University
12 Oxford Street
Cambridge, MA 02138-2902, USA
E-mail: sls@slsiris.harvard.edu

Prof. Barry M. Trost

Department of Chemistry
Stanford University
Stanford, CA 94305-5080, USA
E-mail: bmtrost@leland.stanford.edu

Prof. Hisashi Yamamoto

School of Engineering
Nagoya University
Chikusa, Nagoya 464-01, Japan
E-mail: j45988a@nucc.cc.nagoya-u.ac.jp

Topics in Current Chemistry Also Available Electronically

For all customers with a standing order for Topics in Current Chemistry we offer the electronic form via SpringerLink free of charge. Please contact your librarian who can receive a password for free access to the full articles by registration at:

<http://www.springerlink.com>

If you do not have a standing order you can nevertheless browse through the table of contents of the volumes and the abstracts of each article by choosing *Topics in Current Chemistry* within the Chemistry Online Library.

- Editorial Board
- Aims and Scope
- Instructions for Authors

Preface

Despite more than 200 years of sulfur research the chemistry of elemental sulfur and sulfur-rich compounds is still full of “white spots” which have to be filled in with solid knowledge and reliable data. This situation is particularly regrettable since elemental sulfur is one of the most important raw materials of the chemical industry produced in record-breaking quantities of ca. 35 million tons annually worldwide and mainly used for the production of sulfuric acid.

Fortunately, enormous progress has been made during the last 30 years in the understanding of the “yellow element”. As the result of extensive international research activities sulfur has now become the element with the largest number of allotropes, the element with the largest number of binary oxides, and also the element with the largest number of binary nitrides. Sulfur, a typical non-metal, has been found to become a metal at high pressure and is even superconducting at 10 K under a pressure of 93 GPa and at 17 K at 260 GPa, respectively. This is the highest critical temperature of all chemical elements. Actually, the pressure-temperature phase diagram of sulfur is one of the most complicated of all elements and still needs further investigation.

Sulfur compounds have long been recognized as important for all life since sulfur atoms are components of many important biologically active molecules including amino acids, proteins, hormones and enzymes. All these compounds take part in the global geobiochemical cycle of sulfur and in this way influence even the earth’s climate. In interstellar space, on other planets as well as on some of their moons have elemental sulfur and/or sulfur compounds also been detected. The best known example in this context is probably Jupiter’s moon Io, first observed by Galileo Galilei in 1610, which according to modern spectroscopic observations made from the ground as well as from spacecrafts is one of the most active bodies in the solar system with quite a number of sulfur volcanoes powered by sulfur dioxide and spraying liquid sulfur onto the very cold surface of this moon.

The general importance of sulfur chemistry is reflected in the long list of monographs on special topics published continuously, as well as in the huge number of original papers on sulfur related topics which appear every year. Regularly are international conferences on organic and inorganic sulfur chemistry held, and specialized journals cover the progress in these areas.

In Volumes 230 and 231 of *Topics in Current Chemistry* eleven experts in the field report on the recent progress in the chemistry and physics of elemental

sulfur in the solid, liquid, gaseous and colloidal form, on oxidation products of elemental sulfur such as polyatomic sulfur cations and sulfur-rich oxides which both exhibit very unusual structures, on classical reduction products such as polysulfide dianions and radical anions as well as on their interesting coordination chemistry. Furthermore, the long homologous series of the polysulfanes and their industrial significance are covered, and novel methods for the removal of poisonous sulfur compounds from wastegases and wastewaters in bioreactors taking advantage of the enzymatic activities of sulfur bacteria are reviewed. In addition, the modern ideas on the bonding in compounds containing sulfur-sulfur bonds are outlined.

The literature is covered up to the beginning of the year 2003. A list of useful previous reviews and monographs related to the chemistry of sulfur-rich compounds including elemental sulfur is available on-line as supplementary material to these Volumes.

As the guest-editor of Volumes 230 and 231, I have worked for 40 years in basic research on sulfur chemistry, and I am grateful to my coworkers whose names appear in the references, for their skillful experimental and theoretical work. But my current contributions to these Volumes would not have been possible without the continuous encouragement and assistance of my wife Yana who also took care of some of the graphical work. The constructive cooperation of all the co-authors and of Springer-Verlag, Heidelberg, is gratefully acknowledged.

Berlin, April 2003

Ralf Steudel

Contents

Solid Sulfur Allotropes	
R. Steudel · B. Eckert	1
Liquid Sulfur	
R. Steudel	81
Speciation and Thermodynamics of Sulfur Vapor	
R. Steudel · Y. Steudel · M. W. Wong	117
Homoatomic Sulfur Cations	
I. Crossing	135
Aqueous Sulfur Sols	
R. Steudel	153
Biologically Produced Sulfur	
W. E. Kleinjan · A. de Keizer · A. J. H. Janssen	167
Author Index Volumes 201–230	189
Subject Index	199

Contents of Volume 231

Elemental Sulfur and Sulfur-Rich Compounds II

Volume Editor: Ralf Steudel

ISBN 3-540-40378-7

Quantum-Chemical Calculations of Sulfur-Rich Compounds

M. W. Wong

Molecular Spectra of Sulfur Molecules and Solid Sulfur Allotropes

B. Eckert · R. Steudel

Inorganic Polysulfanes H_2S_n with $n > 1$

R. Steudel

Inorganic Polysulfides S_n^{2-} and Radical Anions $S_n^{\bullet-}$

R. Steudel

Polysulfido Complexes of Main Group and Transition Metals

N. Takeda · N. Tokitoh · R. Okazaki

Sulfur-Rich Oxides S_nO and S_nO_2

R. Steudel

Solid Sulfur Allotropes

Ralf Steudel¹ · Bodo Eckert²

¹ Institut für Chemie, Sekr. C2, Technische Universität Berlin, 10623 Berlin, Germany
E-mail: steudel@schwefel.chem.tu-berlin.de

² Fachbereich Physik, Universität Kaiserslautern, 67663 Kaiserslautern, Germany
E-mail: eckert@physik.uni-kl.de

Abstract Sulfur is the element with the largest number of solid allotropes. Most of these consist of unbranched cyclic molecules with ring sizes ranging from 6 to 20. In addition, polymeric allotropes are known which are believed to consist of chains in a random coil or helical conformation. Furthermore, several high-pressure allotropes have been characterized. In this chapter the preparation, crystal structures, physical properties and analysis of these allotropes are discussed. Ab initio MO calculations revealed the existence of isomeric sulfur rings with partly rather unusual structures at high temperatures.

Keywords Sulfur homocycles · Sulfur chains · Polymerization · Physical properties · High-pressure allotropes · Crystal structures

1	Introduction	3
2	Allotropes at Ambient Pressure	4
2.1	Preparation	4
2.1.1	Allotropes Consisting of Cyclic Molecules	4
2.1.1.1	Preparation of S ₆	4
2.1.1.2	Preparation of S ₇	6
2.1.1.3	Preparation of Pure S ₈	6
2.1.1.4	Preparation of S ₉	8
2.1.1.5	Preparation of S ₁₀	8
2.1.1.6	Preparation of S ₆ ·S ₁₀	9
2.1.1.7	Preparation of S ₁₁	9
2.1.1.8	Preparation of S ₁₂	10
2.1.1.9	Preparation of S ₁₃	11
2.1.1.10	Preparation of S ₁₄	12
2.1.1.11	Preparation of S ₁₅	12
2.1.1.12	Preparation of S ₁₈	13
2.1.1.13	Preparation of S ₂₀	13
2.1.2	Allotropes Consisting of Long Sulfur Chains (Polymeric Sulfur: S _μ , S _ψ and S _ω)	14
2.2	Molecular and Crystal Structures	16
2.2.1	Allotropes Consisting of Cyclic Molecules	17
2.2.1.1	Rhombohedral S ₆	17
2.2.1.2	Allotropes of S ₇	19
2.2.1.3	Allotropes of S ₈	21
2.2.1.3.1	Orthorhombic α-S ₈	24

2.2.1.3.2	Monoclinic β -S ₈	26
2.2.1.3.3	Monoclinic γ -S ₈	27
2.2.1.4	Allotropes of S ₉	29
2.2.1.5	Monoclinic S ₁₀	29
2.2.1.6	The Compound S ₆ ·S ₁₀	30
2.2.1.7	Orthorhombic S ₁₁	32
2.2.1.8	Orthorhombic S ₁₂	33
2.2.1.9	Monoclinic S ₁₃	35
2.2.1.10	Triclinic S ₁₄	36
2.2.1.11	Solid S ₁₅	37
2.2.1.12	Allotropes of S ₁₈	37
2.2.1.13	Orthorhombic S ₂₀	38
2.2.2	Isomers of the Sulfur Homocycles	39
2.2.3	Allotropes Consisting of Long Chains	40
2.2.3.1	Fibrous Sulfur (S _{ψ})	43
2.2.3.2	2nd Fibrous and Laminar Sulfur (S _{ω1} and S _{ω2})	45
2.2.3.3	Polymeric Sulfur in Ta ₄ P ₄ S ₂₉	49
2.2.4	Concluding Remarks	50
2.3	Physical Properties	52
2.3.1	Melting Points	52
2.3.2	Thermal Behavior	53
2.3.3	Solubilities	55
2.3.4	Densities	56
2.3.5	Photochemical Behavior	57
2.4	Analysis	59
3	High-Pressure Allotropes	59
3.1	Introduction	59
3.2	Triple Points in the Vicinity of the Melting Curve	61
3.3	High-Pressure Structures	62
3.3.1	General	62
3.3.2	Photo-Induced Structural Changes ($p < 20$ GPa)	63
3.3.3	High-Pressure High-Temperature Phases ($p < 20$ GPa, $T > 300$ K)	67
3.3.4	High Pressure Phases above 20 GPa	68
3.4	Conclusion	72
	References	72

List of Abbreviations

DAC	Diamond anvil cell
DSC	Differential scanning calorimetry
MD	Molecular dynamics
S _{μ}	Polymeric sulfur usually prepared from quenched liquid sulfur
STP	Standard temperature and pressure conditions

1 Introduction

An allotrope of a chemical element is defined as a solid phase (of the *pure* element) which differs by its crystal structure and therefore by its X-ray diffraction pattern from the other allotropes of that element. This definition can be extended to microcrystalline and amorphous phases which may be characterized either by their diffraction pattern or by suitable molecular spectra.

No other element forms more solid allotropes than sulfur. At present, about 30 well characterized sulfur allotropes are known. These can be divided into ambient pressure allotropes and high-pressure allotropes depending on the conditions during preparation. While the molecular and crystal structures of the ambient pressure allotropes are known in most cases, this does not apply to all of the high-pressure forms. Therefore, in the following the two groups are described in separate sections of this chapter.

The allotropes prepared at ambient pressure can also be grouped by their molecular structures depending on whether homocyclic rings or chains of indefinite length are the constituents of the particular phase. At present, the following 20 crystalline phases consisting of rings are known:

S_6 ; $S_7(\alpha, \beta, \gamma, \delta)$; $S_8(\alpha, \beta, \gamma)$; $S_9(\alpha, \beta)$; S_{10} ; $S_6 \cdot S_{10}$; S_{11} ; S_{12} ; S_{13} ; S_{14} ; S_{15} ; *endo*- S_{18} ; *exo*- S_{18} ; S_{20}

The Greek letters given in parentheses indicate different phases of the same type of molecules. Examples are orthorhombic α - S_8 and monoclinic β - S_8 which contain molecules of the same size and the same conformation (D_{4d} symmetry) but in different packing patterns in the unit cells. However, *endo*- S_{18} (formerly α - S_{18}) and *exo*- S_{18} (formerly β - S_{18}) consist of molecules of the same size but in different conformations. The allotrope $S_6 \cdot S_{10}$ is a unique case among the many allotropes of the non-metallic elements in so far as it consists of two different molecules of the same element in a stoichiometric ratio. In addition, the solvate $S_{12} \cdot CS_2$ has been structurally characterized.

The sulfur allotropes consisting of chains are less well characterized and their nomenclature has changed in time causing some confusion in the literature. At least three ambient pressure polymeric forms are known, termed as “fibrous sulfur” or ψ -sulfur (S_ψ), “second fibrous sulfur” or $\omega 1$ -sulfur and “laminar sulfur” or $\omega 2$ -sulfur ($S_{\omega 1}$ and $S_{\omega 2}$). These allotropes are crystalline, while polymeric insoluble sulfur is usually obtained in a microcrystalline (random coil) state and is often called μ -sulfur or S_μ . These polymeric forms seem to consist, in principal, of the same type of helical molecules. In addition to long chains the polymeric allotropes are likely to contain also large sulfur rings in differing concentrations.

Another way to indicate the polymeric nature of sulfur chains is to use the symbol S_∞ ; this symbol will be reserved for the polymeric sulfur present in liquid sulfur and most probably consisting of very large rings (S_∞^R) and

diradicalic chains (S_{∞}^C) which have no end groups while the endgroups in the chain-like components of S_{μ} and S_{ω} are most probably SH or OH.

At high pressures, sulfur undergoes several phase transitions towards close-packing. In the low pressure regime (<20 GPa), the phase transitions observed by Raman and X-ray studies are complicated due to photo-induced transformations which have to be attributed to the pressure-tuned red-shift of the optical edge of sulfur. At higher pressures (around 90 GPa), metallization and superconducting states have been observed.

The chemistry of elemental sulfur has been reviewed before [1–7]. In the older literature there are many claims of doubtful sulfur allotropes which have never been characterized properly and which most probably do not consist of pure sulfur or which are identical to the well known allotropes but with a different habitus of the crystals. These materials will not be discussed here [8].

2 Allotropes at Ambient Pressure

2.1 Preparation

2.1.1 *Allotropes Consisting of Cyclic Molecules*

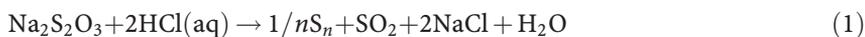
In the following, convenient methods for the preparation of the homocyclic sulfur allotropes will be described. Which method to use depends on the amount of material needed, on the skills of the experimentalist and on the chemicals and equipment available. Therefore, several alternative preparation procedures are provided.

Metastable sulfur allotropes are light-sensitive and should be protected from direct exposure to sun-light or other intense illumination. These materials are also very sensitive towards nucleophiles including alkaline glass surfaces. Therefore, pure and dry solvents should be used and the glassware should be treated with concentrated hydrochloric acid followed by rinsing with water and drying in an oven prior to use.

2.1.1.1 Preparation of S_6

cyclo-Hexasulfur S_6 forms orange-colored rhombohedral crystals which may be prepared by a variety of methods:

1. Historically, S_6 was first prepared from the two inexpensive chemicals sodium thiosulfate and hydrochloric acid [9] which, according to more recent results, yield a mixture of mainly S_6 , S_7 , and S_8 [10]:



The sulfur rings are extracted from the aqueous reaction mixture by toluene from which S_6 as the major product (69 mol%) crystallizes as orange crystals on cooling to -20°C . However, the evolution of large quantities of poisonous SO_2 gas makes this preparation somewhat unpleasant.

2. A more convenient but also slightly more expensive method to prepare S_6 uses the thermal instability of diiododisulfane which is generated in situ from simple chemicals [11]. Commercial dichlorodisulfane ("sulfur-monochloride"), dissolved in CS_2 , is stirred with aqueous potassium or sodium iodide at 20°C for 15 min whereupon iodine and elemental sulfur are formed. The latter is composed of mainly S_6 and S_8 with small concentrations of larger even-membered rings [12] of which S_{12} , S_{18} and S_{20} have been isolated from this mixture:



The iodine is reduced by reaction with stoichiometric amounts of aqueous sodium thiosulfate before the sulfur rings are separated by fractional precipitation with pentane and recrystallization from CS_2 (yield of S_6 : 36%) [11]. The formation of S_6 is likely to proceed via the intermediates S_4I_2 and S_6I_2 with subsequent ring closure by intramolecular elimination of I_2 . The larger rings probably result from the intermolecular reaction of the diiododisulfanes to give sulfur-rich homologs such as S_8I_2 and S_{12}I_2 which then undergo ring closure. The thiosulfate solution contains sodium iodide and, after all thiosulfate has been oxidized, may be used again for another reaction with S_2Cl_2 [11].

3. Titanocene pentasulfide Cp_2TiS_5 ($\text{Cp}=\eta^5\text{-C}_5\text{H}_5$) is commercially available but can easily be prepared from Cp_2TiCl_2 and aqueous sodium or ammonium polysulfide solution [13]. Using chloroform as a solvent a yield of 88% was obtained [14]. The organometallic pentasulfide forms dark-red air-stable crystals soluble in several organic solvents. The molecules contain a six-membered metallacycle in a chair conformation [15]. The pentasulfide reacts with many S-Cl compounds at $0\text{--}20^\circ\text{C}$ as a sulfur transfer reagent with formation of Cp_2TiCl_2 . For example, with SCL_2 the two rings S_6 and S_{12} are formed [16]:



Commercial "sulfurdichloride" is a mixture of SCL_2 , S_2Cl_2 , and Cl_2 which are in equilibrium with each other [17]. Therefore, this mixture needs to be distilled to obtain pure SCL_2 immediately prior to use. Due to their very differ-

ent solubilities in CS₂ (see below) [18], the reaction products Cp₂TiCl₂, S₆ and S₁₂ can easily be separated. Yields: 87% S₆, 11% S₁₂ [16].

2.1.1.2

Preparation of S₇

1. Small amounts of S₇ are best prepared from titanocene pentasulfide (see the preparation of S₆ above) by reaction with dichlorodisulfane S₂Cl₂ (“sulfur-monochloride”) in CS₂ at 0 °C [16]:



This reaction proceeds quantitatively, but the isolated yield of S₇ (23%) is lower owing to its high solubility. Since S₇ rapidly decomposes at 20 °C, it needs to be handled with cooling and should be stored at temperatures below −50 °C.

2. Liquid sulfur contains at all temperatures several percent of S₇ besides the main constituent S₈; in addition, rings of other sizes and, at higher temperatures, polymeric sulfur S_∞ are present [19]. After quenching of the melt at low temperatures it is possible to separate the main components and to isolate S₇ in 0.7% yield; see below under “Preparation of S₁₂, S₁₈, and S₂₀ from S₈”.

Depending on the crystallization conditions S₇ is obtained as either the α , β , γ , or δ allotrope [20, 21] which are all very well soluble in CS₂, CH₂Cl₂, toluene, and *cyclo*-alkanes. α -S₇ is obtained on rapid cooling of solutions in CS₂, CH₂Cl₂, or toluene and forms intense-yellow needle-shaped crystals of m.p. 38.5 °C which are disordered. β -S₇ was obtained as a powder from δ -S₇ by storage at 25 °C for 10 min. δ -S₇ crystallizes from CS₂ solutions at −78 °C and forms block-shaped, tetragonal-bipyramidal and sarcophagus-like crystals. γ -S₇ was obtained from a solution in CH₂Cl₂ containing small amounts of tetracyanoethene at −25 °C [20].

Regardless of the allotropic modification, solid S₇ decomposes at 20 °C completely within ten days but can be stored at −78 °C for longer periods of time without decomposition. The first signs of the decomposition products S₈ and S _{μ} (polymeric sulfur) can be detected already after 30 min at 20 °C [20]. In CS₂ solution S₇ is quite stable.

2.1.1.3

Preparation of Pure S₈

cyclo-Octasulfur crystallizes at ambient pressure either as orthorhombic α -S₈, monoclinic β -S₈ or monoclinic γ -S₈. Commercially available sulfur samples usually consist of mixtures of α -S₈ with some S _{μ} and traces of S₇ [22]. It is this S₇ content which causes the bright-yellow color of most commercial

sulfur samples while pure α -S₈ is greenish-yellow. Sulfur samples from volcanic areas sometimes also contain traces of S₇ but in addition minute concentrations of selenium may be present (as determined by neutron activation analysis), most probably as S₇Se heterocycles [23]. To remove these impurities the material is dissolved in toluene or CH₂Cl₂, and after filtration the solution is cooled to -50 °C. Carbon disulfide is not a good solvent for this purpose since traces of it tend to remain in the product. However, even after this treatment most sulfur samples still contain traces of carbon compounds which can best be tested for by carefully heating the sulfur in a clean test tube for 2–3 min to the boiling point (445 °C) avoiding ignition of the vapor! After cooling of the sample to room temperature black spots will be seen on the walls of the glass and the color of the sulfur itself may have changed to darker hues or even to black, caused by the formed carbon-sulfur polymer. The organic impurities can be removed by heating the sulfur for 10 h to 300 °C (with addition of 1% magnesium oxide) followed by refluxing for 1 h [24] which causes these impurities to decompose to H₂S and CS₂ which both escape; in addition, a black precipitate is formed which looks like carbon-black but is in fact a sulfur-rich polymer. After slow cooling to 125 °C and decantation from the black sludge the liquid is filtered through glass-wool. If necessary, this procedure is repeated several times. An improved method uses an immersed electrical heater to keep the sulfur boiling [25]. The purified liquid sulfur is then distilled in a vacuum resulting in a bright-yellow, odorless product. Commercial “high-purity sulfur” (99.999%) often still contains organic impurities since the purity claimed on the label applies to the metal content only. Many contradictory reports about the physical properties of elemental sulfur possibly can be explained by the differing purity of the samples investigated, especially but not exclusively in the older literature. S₈ can also be highly purified by zone melting (carbon content then $<2.4 \times 10^{-4}\%$) [26].

From most solvents S₈ crystallizes as orthorhombic α -S₈. Monoclinic β -S₈ is stable above 96 °C and is usually obtained by cooling liquid sulfur slowly below the triple-point temperature of 115 °C. At 25 °C crystals of β -S₈ convert to polycrystalline α -S₈ in less than 1 h but are stable for several weeks at temperatures below -20 °C [27]. γ -S₈ is metastable at all temperatures and occasionally crystallizes by chance, for example from ethanolic solutions of ammonium polysulfide [28], by decomposition of copper ethylxanthate [29] or in the preparation of bis(dialkylthiophosphoryl)disulfane [30]. Surprisingly, γ -S₈ occurs also naturally as the mineral rosickyite. Furthermore, γ -S₈ is a component of stretched “plastic sulfur” which is obtained by quenching liquid sulfur from 350 °C to 20 °C (in cold water) and stretching the fibers obtained in the direction of their axes. According to an X-ray diffraction study, this “fibrous” sulfur consists of helical polymeric sulfur chains (S_∞, see below) which form pockets filled with S₈ molecules as the monoclinic γ -allotrope [31].

2.1.1.4

Preparation of S₉

In principle, there is only one method to prepare S₉, and that is the reaction of titanocene pentasulfide with either S₄Cl₂ [32] or S₄(SCN)₂ [33]. The needed dichlorotetrasulfane S₄Cl₂ can be most conveniently prepared by carefully controlled chlorination of *cyclo*-S₆ in CCl₄ at 20 °C [33]:

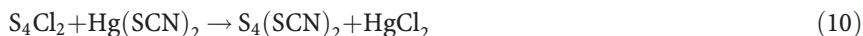


The solvent and the S₂Cl₂ are distilled off from the mixture and the residue is used for the preparation of S₉:

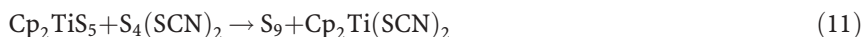


S₉ was obtained in 30% yield [32].

However, since S₄Cl₂ is an oily liquid which owing to its instability cannot be purified by distillation and consequently always contains small amounts of other dichlorosulfanes, it is recommended to convert it to S₄(SCN)₂ [identical to S₆(CN)₂]. Dicyanohexasulfane consists of chain-like molecules which form an odorless solid (m.p. 35 °C) that can be easily recrystallized for purification although it fairly rapidly polymerizes at room temperature [33]:



This reaction takes place at 0 °C in CS₂; based on the starting material S₆ the yield of S₄(SCN)₂ is 27%. This product reacts in CS₂ solution at 20 °C with titanocene pentasulfide to S₉ in 18% isolated yield:



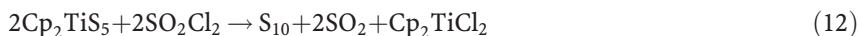
Depending on the conditions, S₉ crystallizes as either α - or β -S₉, the Raman spectra of which are very similar but not identical. α -S₉ forms intense yellow needle-shaped monoclinic crystals of melting point 63 °C [33].

2.1.1.5

Preparation of S₁₀

cyclo-Decasulfur S₁₀ can be prepared according to several different methods:

1. If several grams are needed, the sulfur transfer method is most convenient [16]:



The reagents titanocene pentasulfide and sulfurylchloride are mixed at -78 °C in CS₂ and the mixture is allowed to warm up to 0 °C with stirring. Yield of S₁₀: 35%. S₁₀ forms intense yellow crystals which slowly decompose at room temperature to S₈ with partial polymerization to S _{μ} . The reaction

mechanism for the formation of S_{10} will be explained below (see “Preparation of S_{15} ”).

2. If only small amounts of S_{10} are needed and S_6 or S_7 are available, the oxidation of either one with trifluoroperoxoacetic acid provides S_{10} in a reaction of unknown mechanism. The intermediates S_6O_2 or S_7O decompose at 5 °C in CS_2 or CH_2Cl_2 solution within several days to give S_{10} , some insoluble sulfur as well as SO_2 :



Since the homocyclic oxides do not have to be isolated, the solution of S_6 or S_7 after addition of the peroxyacid (prepared from H_2O_2 and trifluoroacetic acid anhydride in CH_2Cl_2) is simply kept in the refrigerator until S_{10} has formed which is then crystallized by cooling and purified by recrystallization [34, 35].

2.1.1.6

Preparation of $S_6 \cdot S_{10}$

When S_6 and S_{10} are dissolved together in CS_2 and the solution is cooled, then, under special concentration conditions, a stoichiometric well ordered solid solution of the two components crystallizes as orange-yellow opaque crystals of m.p. 92 °C [34]. The structure of $S_6 \cdot S_{10}$ consists of alternating layers of S_6 and S_{10} molecules in their usual conformations of D_{3d} respectively D_2 symmetry [35]. In liquid solutions the molecular mass of $S_6 \cdot S_{10}$ was determined as 258 corresponding to 8 atoms per molecule indicating complete dissociation [34]. This is the only example of an allotrope of a chemical element consisting of molecules of different sizes.

2.1.1.7

Preparation of S_{11}

The sulfur transfer reaction using titanocene pentasulfide and dichloropolysulfanes S_nCl_2 is very versatile and has made it possible to prepare S_{11} after the necessary S_6Cl_2 became accessible in sufficient purity:



The reaction is carried out in CS_2 at 0 °C and provides pure S_{11} (m.p. 74 °C) in 7% yield as yellow crystals [36]. The precursor S_6Cl_2 is best prepared by carefully controlled chlorination of *cyclo*- S_6 with elemental chlo-

rine at 0–20 °C in a CS₂/CCl₄ mixture; see Eq. (7). In the solid state the S₁₁ molecules are of approximate C₂ symmetry [37, 38].

2.1.1.8

Preparation of S₁₂

Thermodynamically, S₁₂ is the second most stable sulfur ring after S₈. Therefore, S₁₂ is formed in many chemical reactions in which elemental sulfur is a product. In addition, S₁₂ is a component of liquid sulfur at all temperatures. The same holds for S₁₈ and S₂₀ which are often formed together with S₁₂:

1. The preparation of S₁₂ from titanocene pentasulfide and SCl₂ has been described above under “Preparation of S₆”:



2. Preparation of S₁₂ from S₂Cl₂ and a polysulfane mixture H₂S_x: sulfanes H₂S_n and dichlorosulfanes S_nCl₂ react with each other with elimination of HCl forming new S-S bonds. Since pure sulfanes with more than two sulfur atoms are difficult to prepare, this synthesis uses a mixture of sulfanes, called “crude sulfane oil”, which can easily be prepared from aqueous sodium polysulfide and concentrated hydrochloric acid at 0 °C [39, 40]:



Since the aqueous sodium polysulfide contains already several polysulfide anions in equilibrium and since the acidification results in some interconversion reactions, a sulfane *mixture* H₂S_x is obtained rather than pure H₂S₄. This mixture nevertheless reacts in dry CS₂/Et₂O mixture at 20 °C with dichlorodisulfane, besides other products, to S₁₂ which has been isolated in 4% yield by extraction with CS₂ and fractional crystallization [41]:



Evidently, this reaction proceeds in several steps with H-S₆-Cl and H-S₁₂-Cl as likely intermediates.

3. Preparation of S₁₂, S₁₈ and S₂₀ from liquid sulfur: liquid sulfur after equilibration contains sulfur homocycles of all sizes [19] and some of these can be isolated by quenching, extraction, fractional precipitation and crystallization depending on their differing solubilities. Commercial elemental sulfur (several hundred gram) is heated electrically to about 200 °C for 5–10 min or longer and is then allowed to cool to 140–160 °C within ca. 15 min. As soon as the melt has become less viscous, it is poured in as thin a stream as possible into liquid nitrogen in order to quench the equilibrium. The boiling nitrogen ruptures the melt into small pieces resulting in a yellow powder. The liquid nitrogen is decanted off this powder which is then extracted with CS₂ at 20 °C (solution “A”). A small amount of polymeric sulfur remains undissolved and is filtered off. The yellow solution is

cooled to $-78\text{ }^{\circ}\text{C}$ for 20 h whereupon a mixture of much S_8 (large yellow crystals) and little $\text{S}_{12}\cdot\text{CS}_2$ (small, almost colorless crystals) crystallizes out. The latter can be separated by rapid flotation in CS_2 yielding pure $\text{S}_{12}\cdot\text{CS}_2$ in 0.2% yield based on the initial amount of elemental sulfur [42, 43]. On prolonged standing in air the crystals of $\text{S}_{12}\cdot\text{CS}_2$ lose their solvent and convert to a powder of S_{12} , single crystals of which can be obtained by recrystallization from hot benzene or toluene resulting in pale-yellow needle-like crystals of m.p. $146\text{--}148\text{ }^{\circ}\text{C}$.

The above CS_2 solution "A" from which $\text{S}_{12}\cdot\text{CS}_2$ and most of the S_8 has crystallized out is used for the preparation of S_7 , S_{18} , and S_{20} as follows. Stirring of solution "A" at $-78\text{ }^{\circ}\text{C}$ after addition of some finely ground glass powder (or S_7 seed crystals) for about 2 h results in the precipitation of finely powdered sulfur which is isolated by removing the solution by means of an immersion filter frit. The residue is extracted three times with small amounts of toluene leaving an orange residue "B". S_7 crystallizes from the toluene solution on cooling to $-78\text{ }^{\circ}\text{C}$ and may be recrystallized from CS_2 . Yield: 0.7% based on the initial amount of elemental sulfur [44].

The amorphous orange residue "B" consists of a mixture of sulfur rings S_x with x possibly ranging up to 50 or more. The mean molecular mass corresponds to an average value of $x=25$. The rings up to $x=28$ have been detected chromatographically by HPLC. S_x is stable only in CS_2 solution; on standing of a concentrated solution at $20\text{ }^{\circ}\text{C}$ for 2–3 days small crystals of *endo*- S_{18} (intense yellow orthorhombic plates) and S_{20} (pale-yellow rods) precipitate. This crystal mixture can be separated by flotation in a $\text{CHCl}_3/\text{CHBr}_3$ mixture since the density of *endo*- S_{18} is slightly higher than that of S_{20} (see below, Table 22). Yields: 0.02% *endo*- S_{18} , 0.01% S_{20} [42, 43].

4. Preparation of S_{12} , S_{18} , and S_{20} from S_2Cl_2 and potassium iodide: dichlorodisulfane, dissolved in CS_2 , reacts at $20\text{ }^{\circ}\text{C}$ with aqueous potassium iodide to a mixture of even-membered sulfur rings:



The main product is S_6 (36%; see above) but by a sequence of precipitation and extraction procedures S_{12} (1–2%), *endo*- S_{18} (0.4%) and S_{20} (0.4%) have been prepared in a pure form in the yields given in parentheses [11].

2.1.1.9

Preparation of S_{13}

To prepare S_{13} by the ligand transfer reaction requires first the synthesis of the chain-like dichlorooctasulfane which is best achieved by carefully controlled chlorination of *cyclo*- S_8 with elemental chlorine in a CS_2/CCl_4 mixture at $0\text{--}20\text{ }^{\circ}\text{C}$:



The oily product of this reaction still contains some S_8 besides S_8Cl_2 as well as other dichlorosulfanes from side-reactions. However, this product reacts with titanocene pentasulfide at 20 °C to a mixture of sulfur rings from which S_{13} was isolated as yellow crystals in 5% yield [36]:



As other sulfur homocycles, S_{13} shows a very characteristic Raman spectrum. In the solid state the molecules are of approximate C_2 symmetry [38].

2.1.1.10

Preparation of S_{14}

S_{14} was first synthesized in 1998 by a novel type of ligand transfer reaction using the zinc hexasulfido complex (TMEDA)ZnS₆ [45] with TME-DA=tetramethylethylenediamine:

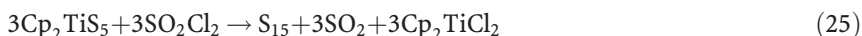


The reaction takes place in CS₂ at 0 °C and S_{14} (m.p. 117 °C) was isolated as rod-shaped intense-yellow crystals in 11% yield [46]. The S_8Cl_2 reagent is prepared by careful chlorination of S_8 ; see the "Preparation of S_{13} " above; Eq. (22).

2.1.1.11

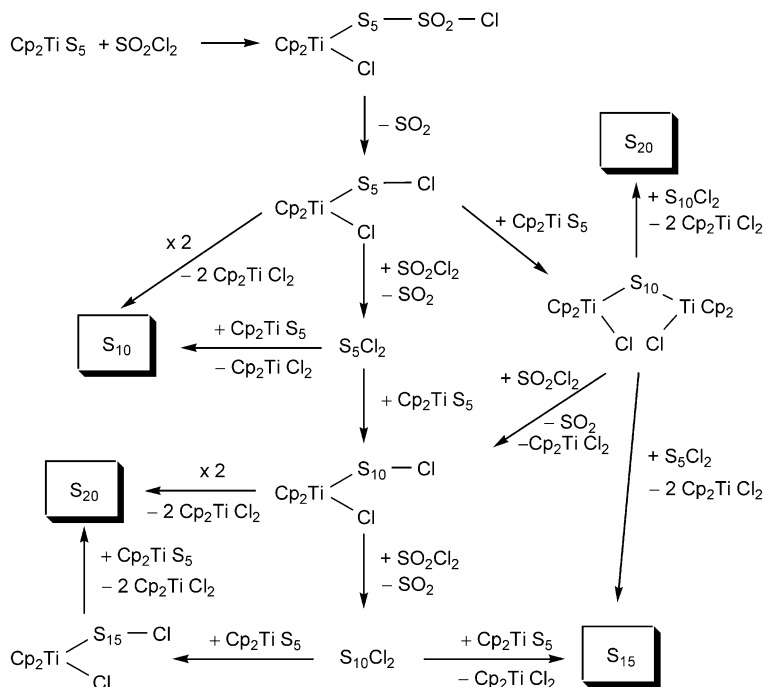
Preparation of S_{15}

cyclo-Pentadecasulfur is one of the few sulfur allotropes which have not been obtained yet as single crystals. Therefore the structure is unknown. S_{15} is formed in the reaction of titanocene pentasulfide with sulfurylchloride in CS₂ which is also used to prepare S_{10} (see above) and S_{20} (see below); the three products are separated by repeated crystallization and precipitation [47]:



S_{15} was obtained in 2% yield as a lemon-yellow powder (from toluene) which has a characteristic Raman spectrum.

The formation of S_{15} probably proceeds via several intermediates as shown in Scheme 1 [14, 47]. The first step is a ring-opening reaction of the metallacycle. The $Cp_2Ti(Cl)S_5SO_2Cl$ intermediate is likely to lose SO₂ resulting in $Cp_2Ti(Cl)S_5Cl$ which by reaction with another molecule of this type may form S_{10} or which may react with SO₂Cl₂ to S_5Cl_2 which in turn would react with Cp_2TiS_5 to S_{10} . In the latter reaction $Cp_2Ti(Cl)S_{10}Cl$ must be an intermediate which will react with another molecule of this type to S_{20} or with S_5Cl_2 to S_{15} . Several alternative pathways exist as shown in Scheme 1; *cyclo*-pentasulfur S_5 has been excluded as an intermediate [14].



Scheme 1

2.1.1.12

Preparation of S_{18}

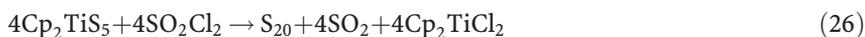
1. Preparation of S_{18} from S_2Cl_2 and potassium iodide: dichlorodisulfane, dissolved in CS_2 , reacts at 20°C with aqueous potassium iodide to a mixture of even-membered sulfur rings; see Eq. (21). The main product is S_6 (36%; see above) but by a sequence of precipitation and extraction procedures S_{12} (1–2%), *endo*- S_{18} (0.4%), and S_{20} (0.4%) have been prepared in pure form in the yields given in parentheses [11].
2. From liquid sulfur: small amounts of *endo*- S_{18} have been isolated from quenched sulfur melts by extraction and fractional crystallization; see above under “Preparation of S_{12} , S_{18} , and S_{20} from liquid sulfur”.

2.1.1.13

Preparation of S_{20}

cyclo-Eicosasulfur S_{20} has been prepared by different methods. Most convenient is the synthesis by sulfur transfer from titanocene pentasulfide which, depending on the conditions, provides either S_{10} , S_{15} or S_{20} .

1. By ligand transfer: a procedure optimized for the preparation of S_{20} uses the reaction of sulfonylchloride with titanocene pentasulfide in CS_2 at 25° :



The probable reaction mechanism of this multistep reaction is given in Scheme 1 above (see the section “Preparation of S_{15} ”). The product was obtained as pale-yellow crystals in 8% yield, sometimes still containing traces of S_{10} which can be removed by recrystallization from CS_2 . The largest sulfur ring detected by HPLC in this reaction mixture is S_{30} which has however not been isolated yet [14].

- From liquid sulfur: small amounts of S_{20} have been isolated from quenched sulfur melts by extraction and fractional crystallization; see above under “Preparation of S_{12} , S_{18} and S_{20} from liquid sulfur”.
- Preparation of S_{20} from S_2Cl_2 and potassium iodide: dichlorodisulfane, dissolved in CS_2 , reacts at 20 °C with aqueous potassium iodide to a mixture of even-membered sulfur rings; see Eq. (21). The main product is S_6 (36%; see above) but by a sequence of precipitation and extraction procedures S_{12} (1–2%), *endo*- S_{18} (0.4%), and S_{20} (0.4%) have been prepared in pure form in the yields given in parentheses [11]. Sulfur-rich diiodosulfanes S_nI_2 are probably intermediates in this reaction which eliminate I_2 intramolecularly with ring closure to S_{20} .

2.1.2

Allotropes Consisting of Long Sulfur Chains (Polymeric Sulfur: S_μ , S_ψ and S_ω)

Those forms of elemental sulfur which are insoluble even in carbon disulfide at 20 °C have been termed as polymeric sulfur. These materials consist of chain-like macromolecules but the additional presence of large rings S_n ($n > 50$) is very likely. In other words, polymeric sulfur is a mixture of chains of differing lengths and rings of differing sizes rather than a pure compound. The nature of the chain-terminating endgroups is unknown. In some cases crystalline phases have been obtained and the molecular structures were determined by X-ray crystallography. These phases are known as $\text{S}_{\omega 1}$ and $\text{S}_{\omega 2}$ and consist of helical chains (catenapolysulfur); they will be discussed later. Otherwise, polymeric sulfur is often termed as μ -sulfur or S_μ but there is no principal difference between S_μ and S_ω .

Polymeric sulfur is a component of liquid sulfur at all temperatures after the chemical equilibrium has been established which takes about 10 h at 120 °C and correspondingly less at higher temperatures [19, 43, 48]. The polymer can be isolated by quenching the melt and extracting the soluble ring molecules with CS_2 at 20 °C. The polymer content of the melt increases from 1% at 135 °C to a maximum of $45 \pm 10\%$ at 250–300 °C (different authors give differing maximum polymer concentrations) [49]. The quenching can be achieved by pouring the sulfur melt into water or, better, into liquid nitrogen [19, 43] as well as by blowing a thin stream of liquid sulfur by a jetstream of cold air against a sheet of aluminum on which the melt solidifies immediately as a thin film [50]. After quenching and extraction the polymeric sulfur is initially amorphous but tends to convert to a microcrystalline structure and, more slowly, to α - S_8 on storage at room temperature.

This conversion is accelerated by mechanical impact (e.g., grinding in a mortar), by irradiation with visible light, UV-, or X-rays, by heating, and by traces of nucleophiles like gaseous or aqueous ammonia. The spontaneous conversion is obviously a result of structural disorder of the random-coil sulfur molecules of the polymer. By heating the sample to 60 °C for 1–2 h [51] or to 80 °C for 40 h [52] the disorder can be reduced and the polymer then exhibits sharper X-ray reflections and is more stable against spontaneous conversion to S_8 than before although the heat treatment results in some loss of polymer by conversion to S_8 (see later).

To a certain degree the quenched sulfur melt can be separated into S_μ and the smallest cyclic molecules by evaporation of the latter in a high vacuum resulting in a residue of colorless, fluffy polymeric sulfur [53].

Liquid sulfur quenched in water from temperatures above 200 °C is plastic in the beginning and, if prepared in filaments, can be stretched to 3000% of its original length (fibrous sulfur, S_ψ) [54]. After some time hardening through crystallization takes place. It also should be mentioned that the quenched melt, besides S_μ and S_8 , contains other small rings like S_6 , S_7 , S_9 , S_{10} , etc. which will slowly decompose to S_μ and S_8 at room temperature [49]. Thus, the polymer content of the quenched melt first increases by a few percent before it slowly decreases due to conversion to α - S_8 on storage at room temperature [54].

Polymeric sulfur is also formed on decomposition of certain pure sulfur allotropes consisting of rings [55] (see below under “Thermal Behavior”). The temperature at which the ring-opening polymerization takes place at an observable rate depends on the ring size but is found in the region 60–140 °C, with S_7 having the lowest and S_{12} the highest polymerization temperature. Some sulfur allotropes like S_6 , S_7 , S_9 , and S_{10} decompose slowly even at room temperature with formation of S_8 and S_μ [55].

Polymeric sulfur is produced commercially as “insoluble sulfur” (IS) and is used in the rubber industry [56] for the vulcanization of natural and synthetic rubbers since it avoids the blooming out of sulfur from the rubber mixture as is observed if S_8 is used. The polymeric sulfur (trade-name Crys-tex [57]) is produced by quenching hot sulfur vapor in liquid carbon disulfide under pressure, followed by stabilization of the polymer (against spontaneous depolymerization), filtration, and drying in nitrogen gas. Common stabilizers [58] are certain olefins $R_2C=CH_2$ like α -methylstyrene which obviously react with the chain-ends (probably -SH) of the sulfur polymer and in this way hinder the formation of rings by a tail-bites-head reaction. In this industrial process the polymer forms from reactive small sulfur molecules present in sulfur vapor [59] which are unstable at ambient temperatures and react to a mixture of S_8 and S_μ on quenching.

For this reason, sulfur which has been sublimed at ambient pressure (“flowers of sulfur”) always contains some polymeric sulfur. This polymeric form of elemental sulfur is also used by wineries: Spraying of grapes with a sulfur slurry protects them from attack by certain bacteria and fungi since the sulfur is oxidized in air to SO_2 which is poisonous to many lower organisms.

Irradiation at low temperatures is another method to convert α -S₈ into polymeric sulfur [60]. Initially, the irradiation of α -S₈ with visible light ($\lambda < 420$ nm) or UV radiation at temperatures of 2–70 K produces free radicals by homolytic dissociation of S-S bonds as demonstrated by electron spin resonance (ESR) spectroscopy [61]. On warming to room temperature the ESR signals fade away since the radicals decay by recombination as well as by triggering a ring-opening polymerization resulting in the formation of polymeric sulfur [60].

2.2

Molecular and Crystal Structures

The following section provides a brief summary of the molecular and crystal structures of the solid allotropes of sulfur mentioned in the Introduction. More specific details about the structures of most of the allotropes can be found in the cited literature. A conclusion concerning the characteristics of the molecular as well as of the crystalline structures of sulfur will be drawn at the end of this section.

There are no crystalline forms known for the low atomic molecules S₂ to S₅ although these molecules are present in the gaseous and liquid phase [49, 59]. Since the cyclic molecules S₁₆, S₁₇, S₁₉, and S_{*n*} (*n* ≥ 21) have not yet been prepared, no molecular and crystal structure data are available. However, a mixture of large sulfur rings ($\langle x \rangle \approx 25$) was observed as an unstable residue during the preparation of S₁₂ (see above) [43]. The Raman spectrum of this mixture resembles that of a high pressure amorphous sulfur form as well as that of polymeric sulfur, often called S _{μ} (see the section on high-pressure forms of sulfur below).

Sulfur atoms are well known for their pronounced tendency of catenation. Since the sulfur atom has an s^2p^4 outer shell electronic configuration in the ground state the sulfur-sulfur bonds can formally be built from the two unpaired electrons in the $3p$ orbitals in which case the optimum value of the bond angle would be 90°. The observed bond angles of ca. 106° can be explained by the repulsion of the non-bonded sulfur atoms or by mixing some s -character into the covalent bonds (s - p hybridization). The two remaining electrons on the $3p$ level are non-bonding and occupy an orbital of local π -symmetry perpendicular to the neighboring S-S bonds. The repulsion of the lone-pairs of adjacent S atoms should lead to a dihedral angle of 90° at the S-S bonds in the case of a “free” chain corresponding to a minimum of configurational energy [54]. This model explains why chains of cumulated S-S bonds exhibit a three-dimensional zig-zag conformation rather than a planar configuration. In consequence, a large number of quite different cyclic and chain-like molecules is, in principal, possible. Ring closure of a sulfur chain usually causes deviations of the bond angle as well as of the dihedral angle from the ideal values due to interaction of the lone-pairs of the next-nearest S atoms. These peculiarities can be easily understood, for example, if going from simple molecules like disulfane H₂S₂ to more complex molecules with cumulated sulfur bonds, especially sulfur rings [62].

The packing of the molecules in crystalline structures has only a slight influence on the molecular geometry which is found typically in the range of a few percent variation of bond lengths and bond angles.

A characteristic parameter to describe the conformation of sulfur molecules is the sign of the dihedral angle. For a sulfur chain or ring the order of the signs of the torsion angles is the so-called "motif". Each of the molecular species shows a typical motif reflecting the molecular symmetry and shape.

2.2.1

Allotropes Consisting of Cyclic Molecules

2.2.1.1

Rhombohedral S_6

S_6 was first synthesized by Engel in 1891 [9]. Since the molecular structure was not known at that time, this sulfur allotrope was called Engel's sulfur, ρ -sulfur, as well as ε -sulfur (see [3]). Later, in 1914, Aten determined the molecular mass to S_6 molecular units [63], which has given *cyclo*-hexasulfur an additional name, Aten's sulfur. Crystals of S_6 form orange-yellow hexagonal prisms. Several attempts have been made to characterize the molecular and crystal structure by X-ray diffraction studies (see [8]). In consequence, a chair conformation for the S_6 ring molecule has been suggested; the crystal structure was attributed to a rhombohedral lattice with one molecule per primitive cell occupying a site of C_{3i} ($\equiv S_6$) symmetry.

The first complete description of crystalline S_6 was reported by Donohue et al. in 1961 on the basis of an X-ray diffraction study [64]. The rhombohedral structure was verified, and the molecular symmetry was ascertained to be D_{3d} . Since *cyclo*-hexasulfur decomposes rapidly under X-ray irradiation at standard temperature-pressure (STP) conditions Steidel et al. reinvestigated the molecular and crystal structure at 183 K giving results with a higher accuracy [65]. The molecular and crystal lattice parameters are summarized in Tables 1 and 2.

As listed in Table 2 and shown in Fig. 1, each of the S_6 molecules has 18 short intermolecular contacts in the range 350–353 pm (at ~ 300 K). This fact, in combination with the compact molecular structure, accounts for the high density of rhombohedral S_6 (for comparison see the structure data of orthorhombic sulfur, Table 6). On the other hand, the compact molecular structure is responsible for a certain strain in the bond geometry which is expressed by a relatively large deviation of the torsion angle from an unstrained value of about 90° , therefore, making the molecule unstable [66].

Since the lattice parameters depend significantly on the temperature (Table 2), it is possible to estimate the coefficient of isobaric thermal expansion roughly to about $2.8 \times 10^{-4} \text{ K}^{-1}$.

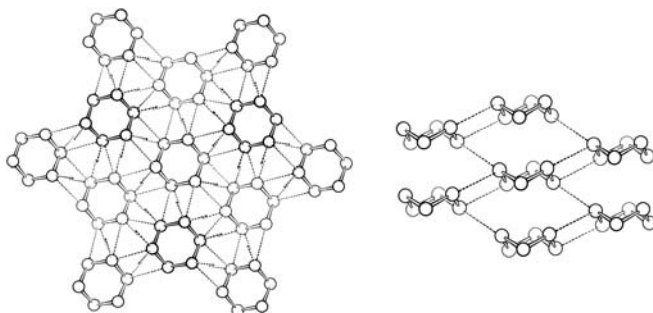
Up to now no six-membered sulfur allotrope other than rhombohedral S_6 has been found. In addition, from theoretical structure analysis it is reasonable to assume that the chair conformation is energetically more favorable than

Table 1 Molecular structure parameters of crystalline S_6 (standard deviations in parentheses). Point group of the molecule: $\bar{3}m - D_{3d}$

Temperature		
Bond length (pm)	205.7(1.8)	206.8(2)
Bond angle (°)	102.2(1.6)	102.61(6)
Torsion angle (°) ^a	74.5(2.5)	73.8(1)
Shortest intermolecular distance (pm)	320.2 pm	
Reference	[64]	[65]

^a Absolute values**Table 2** Crystal structure parameters of *cyclo*- S_6 (standard deviations in parentheses). There are three (one) molecules per unit (primitive) cell

Crystal space group	$R\bar{3} - C_{3i}^2$ (no. 148)	
Site symmetry	$\bar{3} - C_{3i}$	
Lattice constants		
$a (=b)$ (pm)	1081.8(2)	1076.6(4)
c (pm)	428.0(1)	422.5(1)
a/c	2.5275(11)	2.5482(16)
Numbers of and shortest intermolecular distances (pm)		
12	350.1	344.3(2)
6	352.6	347.1(2)
6	374.9	369.7(2)
Temperature (K)	~300	183
Reference	[64]	[65]

**Fig. 1** Structure of crystalline S_6 projected down the rhombohedral c -axis (*left*) and perpendicular to the c -axis (*right*). The direction of the crystal c -axis coincides with that of the molecular z -axis. The intermolecular distances of 350 and 353 pm are shown as *dashed lines* [8]

any other isomeric forms like boat or twisted conformations [67, 68]. The chair-boat interconversion reaction has a barrier of about 126 kJ mol^{-1} [69].

2.2.1.2

Allotropes of S_7

The first chemical preparation of *cyclo*-heptasulfur S_7 was reported by Schmidt et al. in 1968 who obtained solid S_7 as intense yellow needle-like crystals [16].

The molecular structure of homocyclic S_7 is of special interest insofar as it is not possible to construct a puckered ring in which the bond lengths, bond angles, and especially the dihedral angles typical for even membered rings such as S_6 , S_8 , and S_{12} are preserved [70]. A first X-ray structural analysis of solid S_7 was attempted by Kawada and Hellner in 1970 who only derived a two-dimensional projection of the molecule. However, it was evident that the molecule must have a chair conformation and that the various dihedral angles of the molecule must differ significantly.

Infrared and Raman spectroscopic studies have shown that S_7 crystallizes in at least four different allotropic forms (α -, β -, γ -, and δ - S_7) [21]. Most likely all of the crystalline allotropes consist of the same type of heptamer. Detailed X-ray structural studies have proved this assumption for γ - S_7 and δ - S_7 [20, 71]. In solution S_7 undergoes rapid pseudorotation, i.e., the ring atoms become equivalent on average (observed by Raman spectroscopy and by ^{77}Se NMR spectroscopy in the case of the related molecule 1,2- Se_2S_5) [72].

α - S_7 crystallizes as intense yellow needle-like, lancet shaped crystals, which are disordered [20, 21].

β - S_7 was always obtained as a powder by decomposition of δ - S_7 crystals [20, 21].

γ - S_7 crystallizes similar to α - S_7 , though under special conditions γ - S_7 can be obtained as single crystals in the monoclinic space group $P2_1/c-C_{2h}^5$ [20].

δ - S_7 forms block-shaped, tetragonal-bipyramidal and sarcophagus-like single crystals of the monoclinic space group $P2_1/n-C_{2h}^2$ [20, 21, 71].

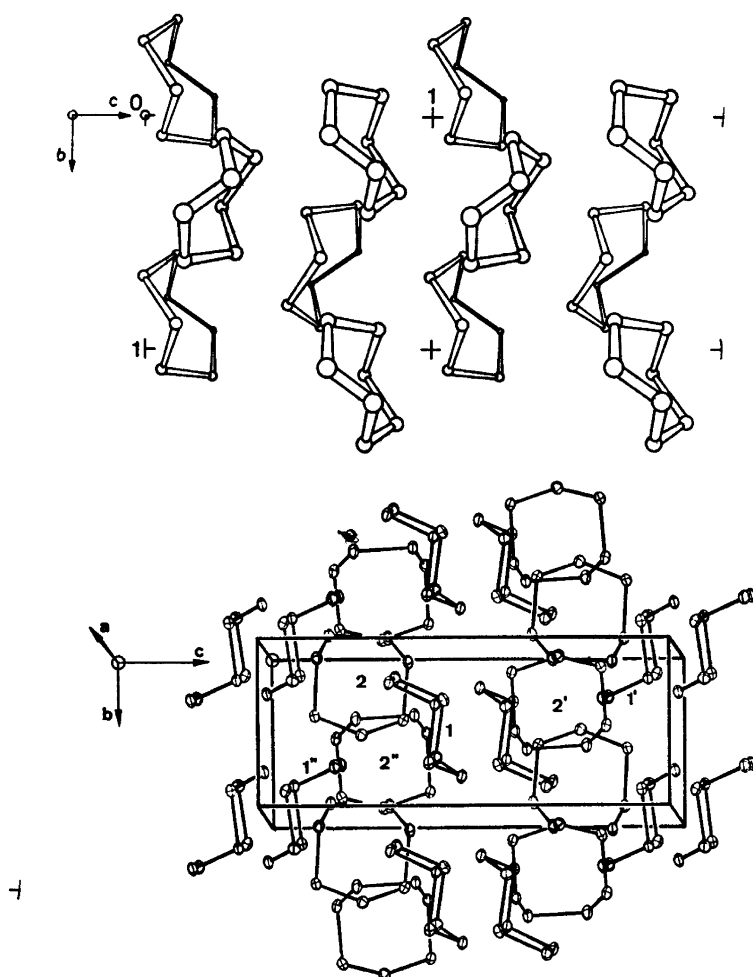
The crystalline structure parameters of γ - S_7 and δ - S_7 are summarized in Table 3. While the asymmetric unit of γ - S_7 is built by one molecule, in δ - S_7 we have to deal with two independent molecules due to intermolecular forces. Figure 2 represents a view of the unit cells of the two allotropes of S_7 which have been studied so far. A detailed analysis and modeling of the intermolecular forces in 12 sulfur allotropes using a non-spherical sulfur atom potential yielded a slightly higher lattice energy for γ - S_7 than for δ - S_7 [73].

The molecular structures of the heptamers of both allotropic forms are nearly the same. The molecules have a chair conformation and their symmetry is close to C_s , but the site symmetry is actually C_1 due to intermolecular interactions. Four neighboring atoms [S4 to S7 in Fig. 3] are located in a plane; in consequence, the torsion angle is close to the unfavorable value of 0° (motif: $+-+0-+-$). The large internuclear distance of the bond S6-S7 is the result of the repulsion of the $3p_\pi$ lone-pairs at these two atoms [21, 74].

Table 3 Crystal structure parameters of γ -S₇ and δ -S₇ at 163 K (standard deviations in brackets) [20, 71]

	γ -S ₇	δ -S ₇
Crystal space group	$P2_1/c-C_{2h}^5$	$P2_1/n-C_{2h}^2$
Site symmetry	$1-C_1$	$1-C_1$
Molecules per unit cell	4	8 ^a
Lattice constants		
<i>a</i> (pm)	968.0(3)	1510.5(5)
<i>b</i> (pm)	764.1(2)	599.8(5)
<i>c</i> (pm)	940.9(2)	1509.6(5)
β (°)	102.08	92.15(5)

^a Two molecules in the asymmetric unit

**Fig. 2** Unit cells of γ -S₇ (top) and δ -S₇ (bottom) [20]

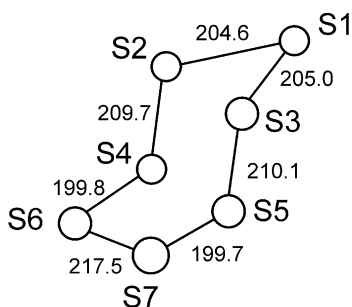


Fig. 3 Structure of the S_7 molecules in γ - S_7 and numbering of atoms; bond lengths in pm

The neighboring bonds are shortened in accordance to the common interpretation in terms of the bond-alternation concept (see [4, 75], and later). In consequence, the bond lengths of the S_7 molecules of the γ - and δ -allotropes can be divided into four sets according to the C_s mirror plane of the heptamer: 205 pm, 210 pm, 200 pm, and one very large bond length of 218 pm (see Fig. 3 and Table 4). This is in sharp contrast to the structures of homocyclic sulfur molecules of higher symmetry and regular motifs such as S_6 , S_8 , and S_{12} which contain bonds of lengths close to 205 pm as well as almost equal bond angles and torsion angles.

The mean strain energy of the S_7 molecule is approximately of the same amount as of the S_6 molecule [66]. However, the unusual bond S6-S7 is responsible for the very low stability of S_7 and, finally, for its high reactivity.

2.2.1.3

Allotropes of S_8

The only stable form of sulfur at STP conditions is the well known orthorhombic α - S_8 modification which was already known in antiquity. No wonder that this allotrope is by far the best studied. Although there is a considerable amount of knowledge on the structural and physical as well as chemical properties of α - S_8 , from the experimental and theoretical point of view there are also ambiguities. For example, the thermal volume expansion below 300 K was reported contradictorily [76, 77].

At about 369 K α - S_8 transforms to monoclinic β - S_8 which is stable up to the melting temperature of about 393 K. The transformation is reversible. One third of the molecules of β - S_8 shows a twofold orientational disorder.

Other allotropic forms of *cyclo*-octasulfur have been reported in the past. Most of these, however, are probably mixtures of well known forms or transient species (see [3, 8, 78]). Just one solid allotrope, γ - S_8 , which is quite stable, could be obtained as single crystals allowing its structure to be determined.

Table 4 Molecular structure parameters of γ -S₇ and δ -S₇ at 163 K averaged for C_s symmetry. The numbering of the atoms is shown in Fig. 3. Note that the variation of geometrical parameters of S₇ deviating from C_s symmetry—which is not reported here—is in most of the cases larger than the experimental errors. More detailed structural data are given in ref. [20]

Site symmetry of molecule	1-C ₁	
Allotrope	γ -S ₇	δ -S ₇
Bond lengths (pm) ^a		
S1-S2, S1-S3	204.8	205.0
S2-S4, S3-S5	209.9	210.2
S4-S6, S5-S7	199.8	199.6
S6-S7	217.5	218.1
Bond angles at indicated atom (°) ^b		
S1	104.97	106.10
S2, S3	102.12	102.23
S4, S5	105.34	105.28
S6, S7	107.43	107.10
Torsion angles (°) ^c		
S1-S2, S1-S3	-,+76.67	-,+5.20
S2-S4, S3-S5	+,-107.78	+,-107.45
S4-S6, S5-S7	-,+83.23	-,+84.00
S6-S7	-0.43	+1.35

^a Standard deviations of the single bond values are 0.1 pm for γ -S₇ and 0.3–0.4 pm for δ -S₇

^b Standard deviations are 0.05–0.06 ° for γ -S₇ and 0.1 ° for δ -S₇

^c Standard deviations are 0.06–0.07 ° for γ -S₇ and 0.1 ° for δ -S₇

The geometry of the molecules of the well characterized allotropes (α -, β -, and γ -S₈) is almost the same, although the bond lengths, bond angles and torsion angles are influenced by the different packing environments of the actual crystal structures. The S₈ molecule has a crown-shaped, puckered conformation; the dihedral angles alternate in sign so that a zig-zag ring with point symmetry *D*_{4d} is obtained (see Fig. 4). Ring closure causes the bond angles and the dihedral angles to deviate from the unstrained, free chain values. The variation of bond lengths in γ -S₈ is larger than in α - and β -S₈, whereas the range of valence angles is about the same. The torsion angles in γ -S₈ cover a closer range than in α - and β -S₈. The molecular structure data of the three allotropes of the sulfur octamer are compared in Table 5. The strain energy of the S₈ ring is typically within 2–3 kJ mol⁻¹ of zero which corresponds to the stability of the crown-shaped molecule [66]. In other words, the bond angles and the dihedral angles in S₈ are close to the optimum values for a sulfur ring.

Eight isomers of the crown-shaped S₈ ring below the radical formation (~150 kJ mol⁻¹) and several interconversion pathways of low energy isomers

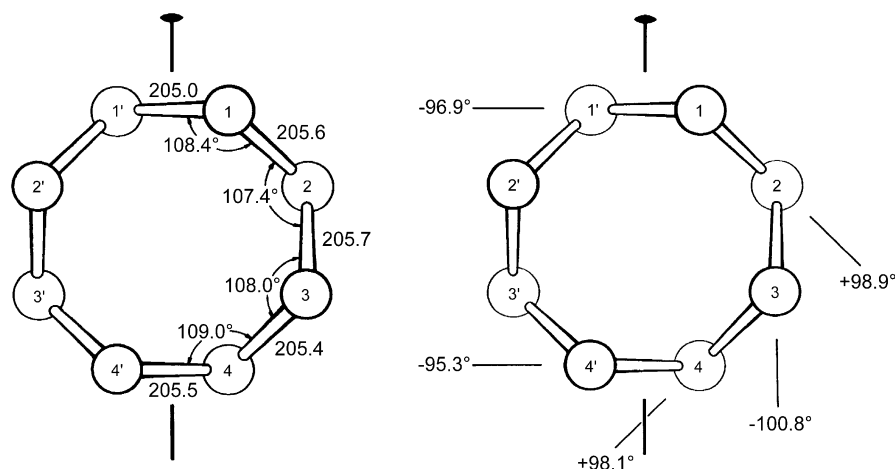


Fig. 4 Molecular structure of the S_8 molecule in orthorhombic α -sulfur with bond lengths in pm, bond angles (*left*) and torsion angles (*right*). The twofold screw axis of the molecule is indicated. Molecular parameters taken from [80]. The values of the bond lengths are those after correction for librational motion giving a mean of 205.5(2) pm in comparison with the uncorrected mean of 204.6(3) pm (Table 5)

Table 5 Molecular structure parameters of the S_8 molecule in α -, β -, and γ - S_8 . The mean values (standard deviations are in brackets) and the interval of the parameters are specified. Standard deviations have partially been calculated by the present authors

Point symmetry	$\bar{8}2m - D_{Ad}$				
Allotrope	α - S_8	β - S_8^a		γ - S_8^b	
		o	d	I	II
Bond lengths (pm)	204.6(3)	204.8(2.0)	204.2(4.4)	204.6(9)	204.5(9)
Range	203.8–204.9	200.9–207.7	194.8–213.4	203.7–206.0	203.5–205.8
Bond angles (°)	108.2(6)	107.7(7)	108.3(1.6)	108.0(4)	107.5(4)
Range	107.4–109.0	106.2–108.9	105.6–111.8	107.8–108.6	107.1–108.0
Torsion angles (°)	98.5(19)	99.1(1.7)	98.3(2.2)	98.6(5)	99.4(5)
Range	96.9–100.8	95.9–101.5	94.3–102.4	98.0–99.2	98.6–99.9
Temperature (K)	298	218 ^c		~300	
Reference	[80]	[27, 81]		[29, 30]	

^a The letters “o” and “d” refer to molecules of β - S_8 at ordered and disordered positions, respectively

^b I and II refer to the two independent molecules of γ - S_8 . Data taken from [30]

^c Data for the disordered structure above the transition temperature of $T_c \approx 198$ K taken from [27]

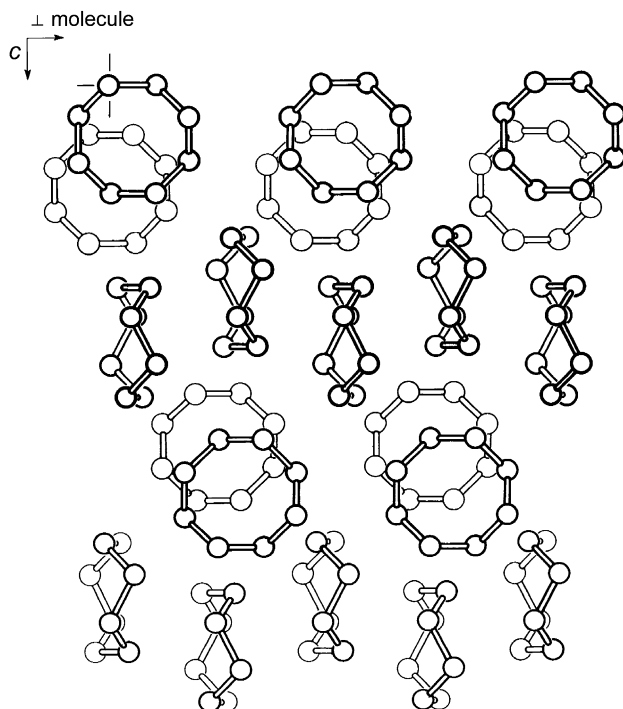


Fig. 5 The crystal structure of orthorhombic S_8 projected parallel to the c -axis showing the so-called crankshaft structure. The direction of the a - and b -axis of the crystal includes an angle of about 45° to the mean plane of the molecules in each layer [8]

of S_8 ($<55 \text{ kJ mol}^{-1}$), obtained by ab-initio quantum chemical calculations, have been reported [69, 79]. These will be discussed below.

2.2.1.3.1

Orthorhombic α - S_8

Although several early attempts had been made to analyze the structure of this allotrope, the first correct description of the crystalline as well as of the molecular structure was given by Warren and Burwell in 1935 [82], which was later improved by Abrahams in 1955 [83]. The most recent examination of the structure of α - S_8 by Rettig and Trotter in 1987 confirmed the results of the earlier studies with a somewhat higher precision [80]. The history of the attempts to characterize the structure of α - S_8 up to the 1970s has been discussed by Donohue [8].

In α - S_8 the molecules crystallize in the orthorhombic space group $Fddd-D_{2h}^{24}$. The octamers are arranged in two layers each perpendicular to the crystal c axis forming a so called “crankshaft structure” (Fig. 5). The primitive cell contains four molecules on sites of C_2 symmetry. Four non-

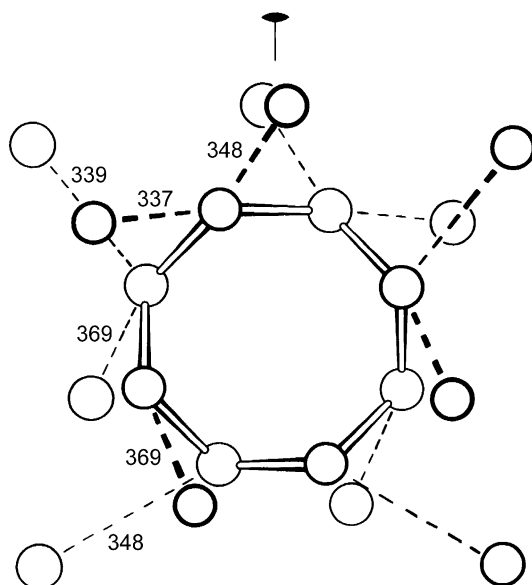


Fig. 6 Nearest intermolecular contacts in orthorhombic S_8 below 370 pm (distances in pm) [8]

Table 6 Structure parameters of α - S_8 at about 300 K (standard deviations in parentheses). There are 16(4) molecules per unit (primitive) cell [80]

Crystal space group	$Fddd-D_{2h}^{24}$ (no. 70)
Site symmetry of molecule	$2-C_2$
Lattice constants	
a (pm)	1046.46(1)
b (pm)	1286.60(1)
c (pm)	2448.60(3)
Numbers of and shortest intermolecular distances per molecule <380 pm (pm)	
2	337.4
4	350.4
4	370.4
2	377.3

equivalent atoms of the S_8 molecule have 12 intermolecular contacts shorter than 370 pm (Fig. 6). The crystal structure data are summarized in Table 6.

The molecular distortion from a perfect D_{4d} symmetry was discussed by Pawley, Rinaldi and Kurittu by means of a constrained refinement of experimental data and by theoretical calculations which made use of intermolecular and intramolecular force fields available at that time [84, 85].

Results of recently performed molecular dynamics calculations using isotropic and anisotropic S_8 model molecules for simulation of crystalline phases suggested the existence of a metastable monoclinic phase below 200 K [86]. However, no phase transition of α - S_8 in the low temperature regime was observed experimentally by several techniques [76, 87, 88].

2.2.1.3.2

Monoclinic β - S_8

This allotrope is usually obtained by heating of powdered α - S_8 to about 369 K. In single crystals of α - S_8 the transformation is kinetically hindered, for example due to the absence of impurities introduced by grain boundaries. Another way to obtain β - S_8 is by slow cooling of molten sulfur, or by crystallization from organic solvents.

The needle-like crystals of β - S_8 are of yellow color and, typically, they are twinned. Lattice parameters and space group assignment were first reported by Burwell in 1937 [89]. Atomic parameters were reported by Sands [90], and with higher accuracy by Templeton et al. [81]. The latter authors also gave a crystallographic explanation of the twinning of β - S_8 crystals.

The structure of β - S_8 (space group $P2_1/c-C_{2h}^5$, Table 7) consists of crown-shaped S_8 rings with approximate D_{4d} symmetry in two kinds of positions. Two thirds of the rings form the ordered skeleton of the crystal while the other molecules are disordered on pseudocentric sites. The disorder is twofold, a rotation of the molecules on disordered sites by 45° around the principal axis transforms the molecule in its alternate position (Fig. 7). The probability of each position is 50% well above the transition temperature of 198 K (see below).

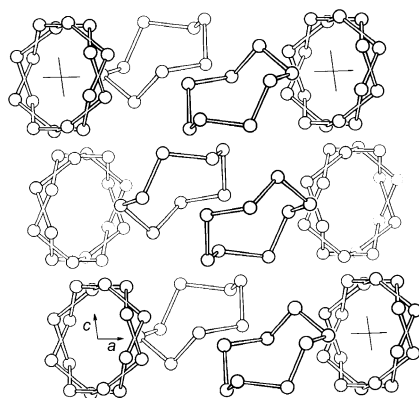
As in the case of orthorhombic sulfur, the molecules of β - S_8 are slightly distorted from a perfect D_{4d} symmetry. The effect of the intermolecular packing forces is a variation of the bond lengths and bond angles and, in general, a flattening of the crown shape. The disordered molecules thereby show a greater variation of the geometrical parameters than the molecules on ordered positions (Table 5).

The order-disorder transition is characterized by a λ -type anomaly of the heat capacity at about 198 K [91]. The temperature dependence of the transition was studied by X-ray diffraction techniques and lattice energy calculations in order to examine the mechanism of the second-order transition [27]. The authors discussed the transition in terms of the so-called Bragg-Williams model and confirmed the transition temperature of 198 K. An ordering energy of about 4.6 kJ mol^{-1} was obtained. The disorder disappears gradually at lower temperatures. The ordering of the structure is accompanied by the loss of the c glide symmetry; hence, the low temperature space group of β - S_8 is $P2_1-C_2^2$.

Table 7 Crystal structure data of β -S₈ at two temperatures^a (standard deviations are in brackets)

Space group	$P2_1/c-C_{2h}^5$ (no. 14)	$P2_1-C_2^2$ (no. 4)
Six molecules per unit cell (four in ordered general positions, two in disordered pseudocentric sites, $T > 198$ K), site symmetry: $1-C_1$		
Lattice parameters		
a (pm)	1092.6(2)	1079.9(2)
b (pm)	1085.2(2)	1068.4(2)
c (pm)	1079.0(3)	1066.3(2)
β (°)	95.92(2)	95.71(1)
Temperature (K)	297	113
Reference	[81]	[27]

^a From the temperature dependence of lattice parameters a volume expansion of about $2 \times 10^{-4} \text{ K}^{-1}$ can be estimated

**Fig. 7** Unit cell of monoclinic β -S₈ projected along the crystal b -axis. The twofold disorder of one-third of the molecules is indicated [8]

2.2.1.3.3

Monoclinic γ -S₈

This allotrope, first described by several authors in the late nineteenth century, occurs as light-yellow, nacreous-glittering, needle-like prismatic crystals (for details see [8, 78]). There was some confusion in the literature about the crystallographic structure until Watanabe in 1974 reported a complete determination of the structure of γ -S₈ [8, 29]. The most recent and accurate structure data of chemically prepared γ -S₈ are those of Gallacher and Pinkerton in 1993 [30a] and of natural γ -S₈ (rosickyite) are those of Meisser et al. [30b]. The “sheared penny roll” arrangement of the S₈ molecules in this allotrope (see Fig. 8), which has been presented earlier by De Haan [92], was

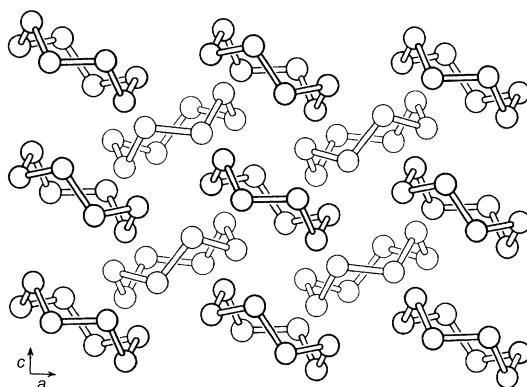


Fig. 8 The “sheared penny roll” structure of monoclinic γ -S₈ projected down to the b -axis [78]

Table 8 Crystal structure data of γ -S₈ at about 300 K (standard deviations are in brackets). There are four (two) molecules per unit (primitive) cell [30]

Space group	$P2/c-C_{2h}^4$ (no. 13)
Site symmetry	$2-C_2$
Lattice constants	
a (pm)	845.5(3)
b (pm)	1305.2(2)
c (pm)	926.7(3)
β (°)	124.89(3)

confirmed. The space group is $P2/c-C_{2h}^4$. The molecules form a pseudo-hexagonal close-packed structure. The asymmetric unit consists of two half S₈ units in which the two independent molecules have a twofold crystallographic symmetry.

The differences of the bond lengths around the S₈ ring are significant and the variation of the bond lengths is much larger than in α -S₈ and β -S₈. The shortest intermolecular distance of about 345 pm is close to the values found for the α -, and the β -modification of octasulfur. The molecular packing efficiency in γ -S₈ is comparable to that of α -S₈. The crystal structure data are given in Table 8.

2.2.1.4

Allotropes of S₉

Although crystalline S₉ was prepared in 1970 by Schmidt et al. [32], the structure was determined only in 1996 by Steudel et al. [33]. *cyclo*-Nonasulfur crystallizes as deep-yellow needles in at least in two allotropic forms (α - and β -S₉) as shown by Raman spectroscopy [33, 93]. The space group of α -S₉ is $P2_1/n(=C_{2h}^2)$ with two independent molecules in the unit cell occupying sites of C₁ symmetry. The molecular symmetry is approximately C₂. The average bond length is 205.25 pm ranging from 203.2 to 206.9 pm. One single short bond of about 203–204 pm in each of the two molecules is neighbored by two longer bonds of about 206–207 pm. The bond angles vary from 103.7° to 109.7° with an average value of 107.2° for both molecules in the cell. The torsion angles show a much wider range, the absolute values varying from 59.7° to 115.6°. The molecular structure was found to be in accordance with results of density functional and ab-initio molecular orbital calculations, especially the pattern of the torsion angles (motif) [67, 68, 94].

The lattice parameters of monoclinic α -S₉ are $a=790.2$ pm, $b=1390.8$ pm, $c=1694.8$ pm, and $\beta=103.2^\circ$ at 173 K [33]. If for each atom of the two independent molecules the shortest intermolecular distance is considered, one finds 18 of such contacts ranging from 338.9 to 364.3 pm [33].

The structure of β -S₉ has not yet been determined. However, the Raman spectrum of β -S₉ suggests that the molecules of this allotrope have the same molecular conformation as those of α -S₉ [33].

2.2.1.5

Monoclinic S₁₀

Crystalline S₁₀ was first prepared by Schmidt et al. in 1965 [16, 95]. The molecular structure of *cyclo*-decasulfur is interesting insofar as a D_{5d} symmetry was expected for this even-membered ring, in analogy to S₆ (D_{3d}) and S₈ (D_{4d}) [96]. However, X-ray studies on single crystals have shown that the S₁₀ molecule is of D_2 symmetry [35, 97]. The only symmetry elements are three orthogonal twofold axes of rotation (C₂). The conformation of the molecule is similar to the one of S₁₂ since the atoms are located in three planes (rather than two as in S₆ and S₈). In fact, S₁₀ can formally be composed of two identical S₅ units cut from the S₁₂ molecule.

The mean bond length in S₁₀ is 205.6 pm (S₁₂: 205.2 pm), but the variation of the bond lengths around the molecule shows a clear alternation (Fig. 9). Two sets of torsion angles, about -77° and $+123^\circ$, are correlated with “normal” bond distances of about 203 to 205 pm, and large distances of about 207 to 208 pm, respectively.

By ab-initio quantum chemical calculations it was found that the D_{5d} conformer is about 29 kJ mol⁻¹ less stable than the D_2 structure [68]. The lower stability of the D_{5d} structure can be explained considering the torsion angles of both structures. While the D_{5d} structure forces the torsion angles to be

Table 9 Molecular structure parameters of crystalline S_{10} (at 163 K) [35, 97]

Point symmetry	$222-D_2$
Av. bond length (pm)	205.6
Range	203.3–207.8
Av. bond angle (pm)	106.2
Range	103.4–110.2
Torsion ngle ($^\circ$) ^a	95.7
Range	75.4–123.7

^a Absolute values

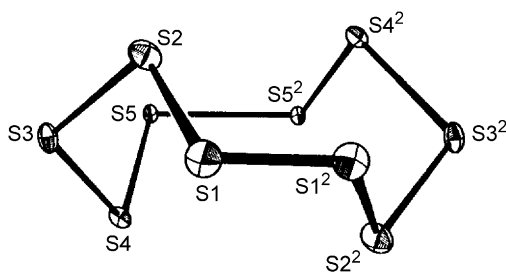


Fig. 9 Geometry of the S_{10} molecule in the crystal (the atoms S_i and S_i^2 are related by the molecular symmetry D_2) [97]

116.6° the D_2 structure has a mean absolute value of 95.7° which is much closer to the ideal value of about 90° .

The space group of crystalline S_{10} is monoclinic $C2/c-C_{2h}^6$ (no. 15) with an unusually small angle of 37° [35, 97]. Four molecules in the unit cell occupy sites of C_2 symmetry. The lattice constants are $a=1253.3(9)$ pm, $b=1027.5(9)$ pm, $c=1277.6(9)$ pm at 163 K.

The shortest intermolecular distances are 323.1, 324.0, and 329.1 pm, much less than in crystalline S_6 ; however, the S_{10} molecules are less compact. Therefore, the density of S_{10} is lower than that of S_6 (Table 22).

2.2.1.6

The Compound $S_6 \cdot S_{10}$

When S_{10} was prepared from S_6 according to several slightly different procedures (see above) the formation of a new sulfur allotrope was observed several times. This allotrope forms intense orange-yellow, opaque, hexagonal plate-like crystals [34, 35]. An X-ray study on single crystals of this allotrope proved the assumption of a molecular addition compound $S_6 \cdot S_{10}$ as had been suggested before by evaluation of the Raman spectrum [34, 35].

The space group of $S_6 \cdot S_{10}$ crystals is $I2/a$ which is an alternative setting of $C2/n(=C_{2h}^3$, no. 12) of the monoclinic crystal system. The structure consists of alternating layers of S_6 and S_{10} molecules, respectively, with four mole-

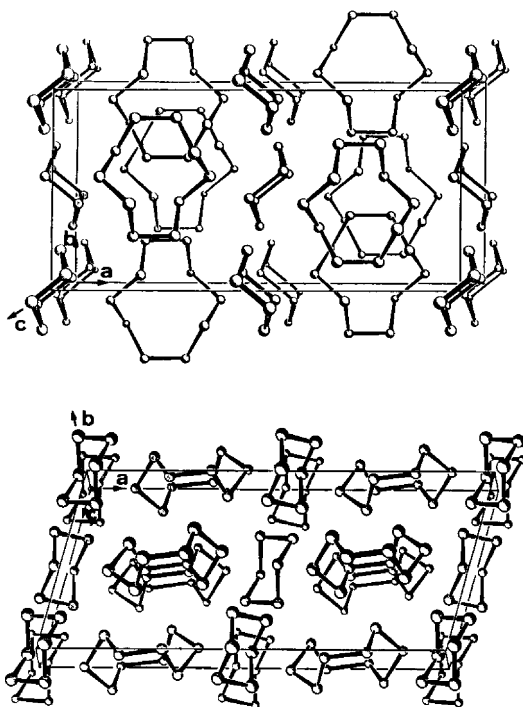


Fig. 10 Two views of the crystal structure of the sulfur allotrope $S_6 \cdot S_{10}$ [35]

cules per unit cell. The lattice parameters are $a=1954.1(8)$ pm, $b=943.1(3)$ pm, $c=883.1(3)$, and $\beta=105.11(3)^\circ$ (Fig. 10).

The molecules S_6 and S_{10} in $S_6 \cdot S_{10}$ exhibit the same molecular conformations as in the pure crystals of S_6 (D_{3d}) and of S_{10} (D_2). However, the molecular parameters of S_6 in $S_6 \cdot S_{10}$ show a slight variation of less than 1% of the mean values in the case of the bond and torsion angles and less than 0.1% in the case of the internuclear distances. As in pure S_{10} both enantiomeric molecules are present in $S_6 \cdot S_{10}$ in equal amounts. The site symmetry of S_{10} in $S_6 \cdot S_{10}$ is C_2 as in pure S_{10} . However, the site symmetry of the S_6 molecules in $S_6 \cdot S_{10}$ is reduced to C_i in comparison with C_{3i} in pure S_6 . The mean bond parameters of S_6 and S_{10} are almost identical in $S_6 \cdot S_{10}$ compared to the pure components (Table 10).

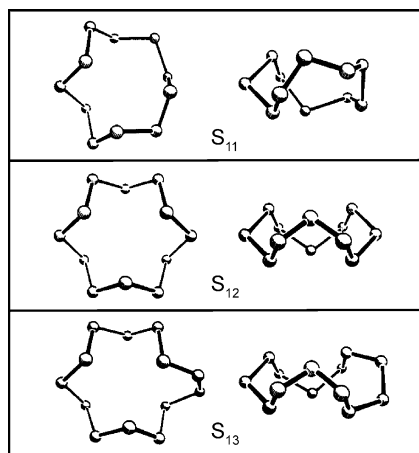
The four shortest intermolecular distances (339.9–345.2 pm) were found between S_6 and S_{10} molecules. Although these contacts are closer in comparison with other allotropes like the more dense S_6 crystal, the density of $S_6 \cdot S_{10}$ is halfway between the densities of the pure allotropes of S_6 and S_{10} , respectively (see Table 22 below).

Table 10 Mean values of molecular structure data of S_6 and S_{10} in $S_6 \cdot S_{10}$ and in the pure allotropes at 163 K [35]

Molecule	S_6		S_{10}	
Allotrope	S_6^a	$S_6 \cdot S_{10}$	S_{10}	$S_6 \cdot S_{10}$
Bond length (pm)	206.8	206.2	205.6	205.8
Bond angle ($^\circ$)	102.6	102.6	106.2	106.3
Torsion angle ($^\circ$) ^b	73.8	73.8	95.7	96.2

^a Data of crystalline S_6 at 183 K from [65]

^b Mean of absolute values of the torsion angles

**Fig. 11** Comparison of the molecular conformations of S_{11} (symmetry C_2), S_{12} (symmetry D_{3d}), and S_{13} (symmetry C_2) [38]

2.2.1.7

Orthorhombic S_{11}

The preparation of *cyclo*-undecasulfur was first reported by Sandow et al. in 1982 [36]. Results of an X-ray structural analysis of a single crystal of S_{11} were published by Steidel et al. in the same year [37] and by Steudel et al. in 1986 [38]. Crystals of S_{11} are yellow, rod-like and of rhombic-bipyramidal shape.

The unit cell contains eight molecules, although there are only two independent molecules in the asymmetric unit which occupy sites of C_1 symmetry. The crystal system is orthorhombic (space group $Pca2_1-C_{2v}^5$, no. 29) with lattice parameters $a=1493.3(10)$, $b=832.1(5)$, and $c=1808.6(12)$ pm at about 163 K. The molecular symmetry, however, is approximately C_2 with a twofold rotation axis as the only element of symmetry (see Fig. 11). As a typical odd-membered ring S_{11} shows an unusually large bond of about 211 pm

Table 11 Molecular structure data of orthorhombic S₁₁ at 163 K^a [38]

Point symmetry	2-C ₂ (approximately)	
	Molecule 1	Molecule 2
Av. bond lengths (pm)	205.7	205.5
Range	203.7–211.0	203.2–207.7
Av. bond angles (°)	106.0	106.3
Range	103.8–108.4	103.3–108.6
Av. torsion angles (°) ^b	97.1	96.9
Range	70.5–140.5	69.3–137.1

^a Errors of bond lengths 0.3–0.4 pm, of angles 0.1°

^b Absolute values

(molecule 1) and 208 pm (molecule 2) with two adjacent short bonds (203–204 pm). The related torsion angles of 141° (1) and 137° (2), respectively, are the largest ever observed in sulfur rings. However, crystalline S₁₁ is of medium stability similar to S₆, S₉, S₁₀, and S₁₃.

Both independent molecules of S₁₁ in the crystal have the same conformation, but the parameters of equivalent bonds show significant differences which are exceeded only in the case of solid S₁₃ (Table 11).

2.2.1.8

Orthorhombic S₁₂

Solid *cyclo*-dodecasulfur was first synthesized by Schmidt and Wilhelm in 1966 [98]. The authors obtained pale-yellowish, plate-like rectangular needles of solid S₁₂ (from benzene solution). In the same year an X-ray structural analysis was reported by Kutoglu and Hellner [99]. A refined analysis of crystalline S₁₂ was performed by Steidel et al. in 1981, together with an examination of the molecular addition compound CS₂·S₁₂ [100]. Accordingly, S₁₂ crystallizes in the orthorhombic space group *Pnmm*-D_{2h}¹² (no. 58) with a unit cell containing two molecules on sites of C_{2h} symmetry.

As was discussed in the case of *cyclo*-decasulfur S₁₀, for the even-membered S₁₂ ring one might have expected a highly symmetrical molecular structure of D_{6d} symmetry in analogy to S₆ (D_{3d}) and S₈ (D_{4d}). However, the X-ray single crystal analyses revealed an approximate D_{3d} conformation of S₁₂ (see Fig. 12) [99, 100]. By *ab-initio* quantum chemical calculations it has been shown that the D_{6d} structure is about 226 kJ mol⁻¹ less stable than the D_{3d} structure and, moreover, that it is not even a minimum on the potential energy surface [68].

In the S₁₂ molecule the atoms are located in three parallel planes: six atoms in the median plane and three atoms each in an upper and in a lower plane. An arrangement in which the atoms would be located in two planes (D_{6d} structure) would yield torsion angles of 129° being far from the optimum value of about 90°. As a result, the bond lengths would be larger as a consequence of bond weakening due to the large torsion angles. In the D_{3d}

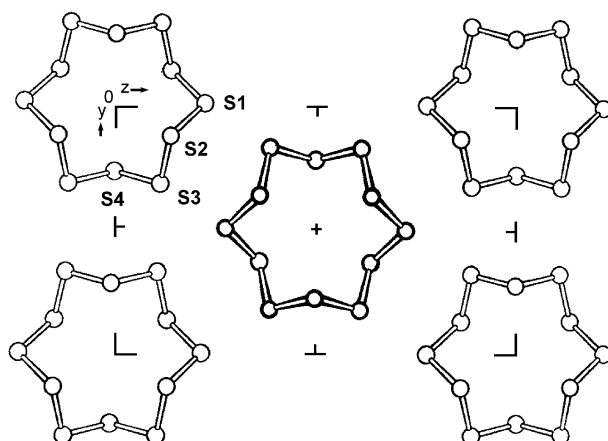


Fig. 12 Structure of the S_{12} molecule in the crystal (molecular symmetry D_{3d} , site symmetry C_{2h}). Bond lengths: S1-S2 205.7, S2-S3 204.8, S3-S4 205.2 pm; bond angles at the indicated atoms: S1 105.4°, S2 107.4°, S3 106.6°, S4 107.0° [100]

Table 12 Molecular structure parameters of orthorhombic S_{12} at about 300 K and of $CS_2 \cdot S_{12}$ at about 168 K [100]

Point group of molecule	$\bar{3}m - D_{3d}$	
Compound	S_{12}	$CS_2 \cdot S_{12}$
Av. bond lengths (pm)	205.2	205.4
Range	204.8–205.7	-
Av. bond angles (°)	106.6	106.2
Range	105.4–107.4	105.80–106.65
Av. torsion angles (°) ^a	88.0	87.2
Range	86.0–89.4	-

^aAbsolute values

structure the much more favorable value of the torsion angles of about 88° is allowed. In contrast to the structures of S_6 and S_8 in which a *cis-cis* arrangement is repeated three-times and four-times [motifs: $(+-)_3$, $(+-)_4$], respectively, the bonding in S_{12} shows a regular *cis-trans* repetition [motif: $(++--)_3$]. The average bond length is very close to values found for S_6 and S_8 , but the bond angles in S_{12} depend slightly on the planes mentioned above: The average valence angle at atoms of the median plane is 106.0° while that at the atoms of the upper and lower planes is 107.2° (Table 12).

The lattice parameters of orthorhombic S_{12} are $a=472.5(2)$ pm, $b=910.4(3)$ pm, $c=1453(3)$ pm [100]. The molecules in the crystal are arranged in layers. The molecules of adjacent layers are slightly inclined around one of the C_2 axes of molecular symmetry, and the molecular planes of the next nearest layers are parallel. While the shortest intermolecular dis-

Table 13 Molecular structure parameters of monoclinic S_{13} at 173 K^a [38]

Point group of molecule	C_2 (approximately)	
Molecule	I	II
Av. bond length (pm)	204.6	205.2
Range	197.8–207.4	199.5–211.3
Av. bond angle (°)	106.4	106.1
Range	103.3–111.1	102.8–107.8
Av. torsion angle (°) ^b	85.3	85.4
Range	30.9–116.3	29.5–114.1

^a Errors of bond lengths: 0.4–0.5 pm, of bond angles and torsion angles: 0.1–0.2°

^b Absolute values

tances in crystalline S_{12} are 335 pm (four contacts), the shortest distances in $CS_2 \cdot S_{12}$ are 372 pm (CS_2-S_{12}) and 347 pm ($S_{12}-S_{12}$), respectively. Thus, the packing effects on S_{12} due to the intermolecular forces are smaller for S_{12} in $CS_2 \cdot S_{12}$ and, therefore, the structure of the S_{12} ring is closer to a perfect D_{3d} geometry in $CS_2 \cdot S_{12}$ [100].

2.2.1.9

Monoclinic S_{13}

Crystals of S_{13} were first obtained by Sandow et al. [36] and the crystal as well as the molecular structure were studied by Steudel et al. [38] using X-ray diffraction on single crystals. S_{13} crystallizes in the monoclinic space group $P2_1/c-C_{2h}^5$ (no. 14) as hexagonal yellow plates (from CS_2 or $CHCl_3$). The unit cell is built by eight molecules on sites of C_1 symmetry. The lattice parameters are $a=1295(2)$ pm, $b=1236(1)$ pm, $c=1761(2)$ pm, $\beta=110.41(9)^\circ$ at $T=163$ K. A certain disorder of the S_{13} crystal was deduced from the crystallographic structure data and from the Raman spectrum.

The molecule *cyclo*-tridecasulfur is similar to S_{11} . The S_{13} ring can be obtained formally from S_{12} by replacing one atom by an S_2 unit. This procedure introduces a twofold rotation axis as the only symmetry element of the molecule and leaves the motif of the formerly S_{12} unit unaltered (see Fig. 11). The point group of the molecules is approximately C_2 , and the twofold axis intersects the longest bond introduced by the S_2 unit. This relatively long bond of about 209 pm is connected to a small torsion angle of about 30° and neighbored by two short bonds of about 199 pm. The two independent molecules of the asymmetric unit have different molecular parameters. As in the case of S_{11} one of them (molecule I) is closer to C_2 symmetry than the other one (see Table 13).

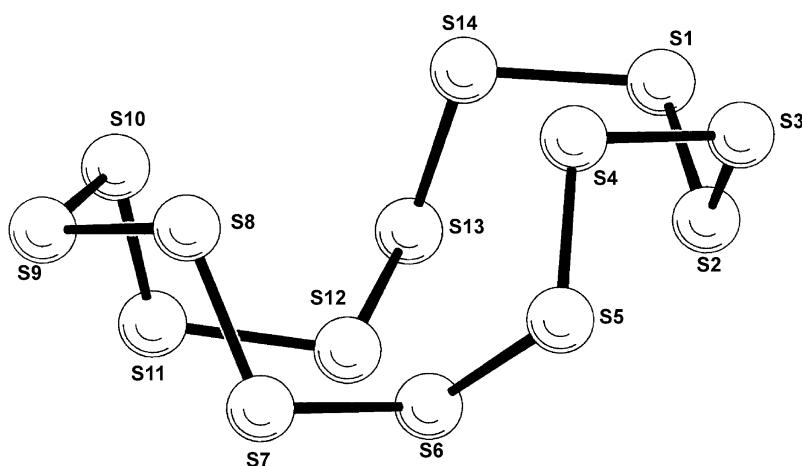


Fig. 13 Molecular conformation of the S_{14} molecule in the crystal (symmetry C_s)

Table 14 Molecular structure parameters of crystalline S_{14} at 173 K [46]

Point group of molecule	$m-C_s(\equiv C_{1h})$
Av. bond length (pm)	205.3
Range	204.7–206.1
Av. bond angle ($^\circ$)	106.3
Range	104.0–109.3
Av. torsion angle ($^\circ$) ^a	93.1
Range	72.5–101.7

^a Absolute values

2.2.1.10

Triclinic S_{14}

Although *cyclo*-tetradecasulfur has been observed in trace amounts by HPLC investigations of quenched sulfur melts and synthetic mixtures of sulfur in the 1980s, single crystals of S_{14} were obtained just a few years ago by Steudel et al. [46]. The authors reported results of X-ray structural and Raman spectroscopic studies of crystalline S_{14} which forms deep-yellow, rod-like bundles of crystallites.

The space group of crystalline S_{14} is $P\bar{1} - C_i^1$ (no. 2) of the triclinic crystal system. The lattice parameters are $a=546.9(3)$ pm, $b=966.2(5)$ pm, $c=1433.1(7)$ pm, $\alpha=95.97(4)^\circ$, $\beta=98.96(4)^\circ$, $\gamma=100.43(4)^\circ$ at 173 K [46]. The unit cell contains two molecules of approximate C_s symmetry with a mirror plane as the only symmetry element intersecting atoms S2 and S9 (Fig. 13). The molecular structure data are summarized in Table 14. The average bond length is close to those of S_8 and S_{12} . The average torsion angle of about 93° accounts for the stability of S_{14} , which is in the range of several days at room

temperature. The motif in S_{14} is similar to that of S_{12} . Therefore, the structure of S_{14} can be derived by opening the S_{12} ring and adding an S_2 fragment.

2.2.1.11

Solid S_{15}

Up to now solid forms of *cyclo*-pentadecasulfur were obtained only as a lemon-yellow powder or as light-yellow flakes, both containing traces of other sulfur rings (S_{14} , S_{16}) and slowly transforming to a sticky mass at room temperature. Attempts to grow single crystals of S_{15} were not successful [47]. However, Raman and UV spectra of S_{15} in solution have been measured which imply a ring structure [47]. The few Raman scattering lines in the stretching region ($400\text{--}480\text{ cm}^{-1}$) indicate degenerate vibrations which may exclude a very low molecular symmetry. Since in sulfur rings the wavenumber of a stretching vibration is directly correlated with the bond distance, an average value of the bond lengths of S_{15} of 207 pm (range 203–210 pm) was estimated [4, 47]. In addition, the bond length is correlated with the dihedral angle giving for the latter one a range of $30\text{--}140^\circ$ in S_{15} [47, 101].

According to a density functional calculation S_{15} molecules are of C_2 symmetry with internuclear distances ranging from 205.3 to 206.5 pm, bond angles from 104.1° to 109.4° , and absolute torsion angles from 77.1° to 112.3° [102].

2.2.1.12

Allotropes of S_{18}

cyclo-Octadecasulfur forms two crystalline allotropes each consisting of another molecular conformer usually called α - S_{18} and β - S_{18} . However, since Greek letters should generally be used to designate different crystal structures of one and the same molecule (e.g., α -, β -, and γ - S_8), we suggest here to term the allotropes with respect to the molecular conformation (see Fig. 14) in order to avoid misunderstanding. The S_{18} molecules in both allotropes are similar with the exception that four torsion angles are opposite in sign, two of them referring to the *endo*- and *exo*-conformation. In both conformers the atoms are placed in two almost parallel planes. While the *endo*-conformer is of C_{2h} symmetry (containing a twofold rotation axis and a mirror plane perpendicular to that axis) the *exo*-conformer is of the lower C_i symmetry (inversion center as the only symmetry element). The variation of bond parameters of *endo*- S_{18} is much smaller than that of *exo*- S_{18} .

Crystals of *endo*- S_{18} (α - S_{18}) are intense lemon-yellow, rhombic plates and belong to the orthorhombic crystal system. The molecules are arranged to form a pseudohexagonal close packing which accounts for the higher density of the *endo*- S_{18} crystal. Crystals of *exo*- S_{18} (β - S_{18}) are monoclinic. The crystal and molecular structure data are summarized in Table 15. A detailed analysis and modeling of the intermolecular forces in 12 sulfur allotropes

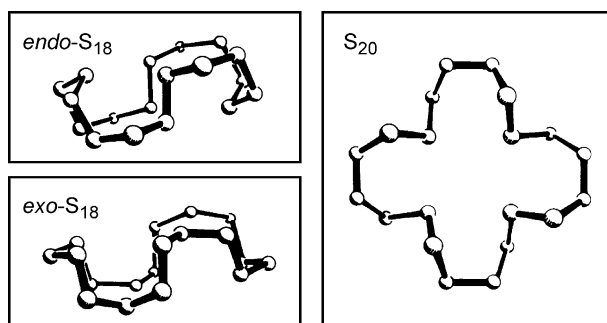


Fig. 14 Molecular conformations of the molecules in the crystals of *endo*-S₁₈, *exo*-S₁₈, and S₂₀

Table 15 Crystal and molecular structure parameters of the two allotropes of S₁₈ at room temperature [103, 104]

Allotrope	<i>endo</i> -S ₁₈ (α -S ₁₈)	<i>exo</i> -S ₁₈ (β -S ₁₈)
Space group	$P2_12_12_1-D_2^4 \equiv V^4$ (no. 19)	$P2_1/n-C_{2h}^2$ (no. 11)
Site symmetry	$1-C_1$	$\bar{1}-C_i$
Molecules per unit cell	4	2
Lattice constants		
<i>a</i> (pm)	2115.2	1075
<i>b</i> (pm)	1144.1	725
<i>c</i> (pm)	758.1	1225
β (°)	-	92.3(5)
Point group of molecule	$2/m-C_{2h}$ (approximately)	$\bar{1}-C_i (\equiv S_2)$ (averaged)
Average bond lengths (pm)	205.9(3)	207.8(5)
Range	204.4–206.7	205.3–210.3
Average bond angles (°)	106.3(1)	106.3(3)
Range	103.8–108.3	104.2–109.2
Average torsion angles (°) ^a	84.4(2)	80.0(3)
Range	79.5–89.0	66.5–87.8

^a Absolute values

using a non-spherical sulfur atom potential yielded a slightly higher lattice energy for *exo*-S₁₈ than for *endo*-S₁₈ [73].

2.2.1.13

Orthorhombic S₂₀

cyclo-Eicosasulfur crystallizes as pale-yellow needles in the orthorhombic crystal system. The unit cell contains four molecules on sites of C₂ symmetry. The space group is *Pbcn* ($D_{2h}^{14} \equiv V_h^{14}$, no. 60) with the lattice constants $a=1858.0$, $b=1318.1$, $c=860$ pm [104]. The structure of the S₂₀ ring cannot be derived from other sulfur modifications. The molecule shows approximately

Table 16 Molecular structure parameters of orthorhombic S₂₀ [104]

Point group	2-C ₂
Av. bond lengths (pm)	204.7(5)
Range	202.3–210.4
Av. bond angles (°)	106.5(2)
Range	104.6–107.7
Av. torsion angles (°) ^a	83.0(4)
Range	66.3–89.9

^a Absolute values

two twofold in-plane axes of rotation perpendicular to another C₂ axis indicating a molecular symmetry of D₂ (see Fig. 14). The atoms are arranged in five nearly parallel planes, each plane containing four atoms. The distances between the planes are small; thus, the S₂₀ molecule is a very flat ring. Surprising for an even-membered ring, there is one large bond distance (210 pm) neighbored by short bonds (202 pm) and associated with the smallest dihedral angle of the molecule (66°). Therefore, the molecular symmetry is actually C₂. This long bond may explain the low thermal stability of the molecule which decomposes in solution at room temperature (but not in the solid state). The molecular structure parameters are summarized in Table 16.

Although the S₂₀ rings are relatively flat the space required by the molecules and the unfavorable packing in the crystal result in a low density of crystalline S₂₀.

2.2.2

Isomers of the Sulfur Homocycles

Theoretical studies have demonstrated that small sulfur molecules can exist as various isomers corresponding to local minima on the potential energy hypersurface. Naturally, the S₈ molecule has been studied most extensively and at the highest level of theory, and at least nine isomers have been reported. Both ab initio MO and density functional theory (DFT) calculations have been published [69, 79, 105]. Unfortunately, the energies obtained by DFT calculations are not very reliable in the case of sulfur-rich compounds although the geometries are well reproduced at the B3LYP/6–31G(2df) level, for example. In Fig. 15 are nine isomeric forms of S₈ shown which represent local minima. Their relative energies are given in Table 17.

The reliability of the energies in Table 17 follows from the good agreement between the experimental SS bond dissociation enthalpy of 150±2 kJ mol⁻¹ and the relative enthalpy calculated for the eight-atomic S₈ chain in its triplet ground state which is 154 kJ mol⁻¹ at 298 K [79].

To a certain extent isomers of other sulfur rings have also been discovered by theoretical methods. However, as far as known the activation energies for the transformation of the ground state conformation into the next most stable structure are quite high (>25 kJ mol⁻¹) [69, 105]. An exception

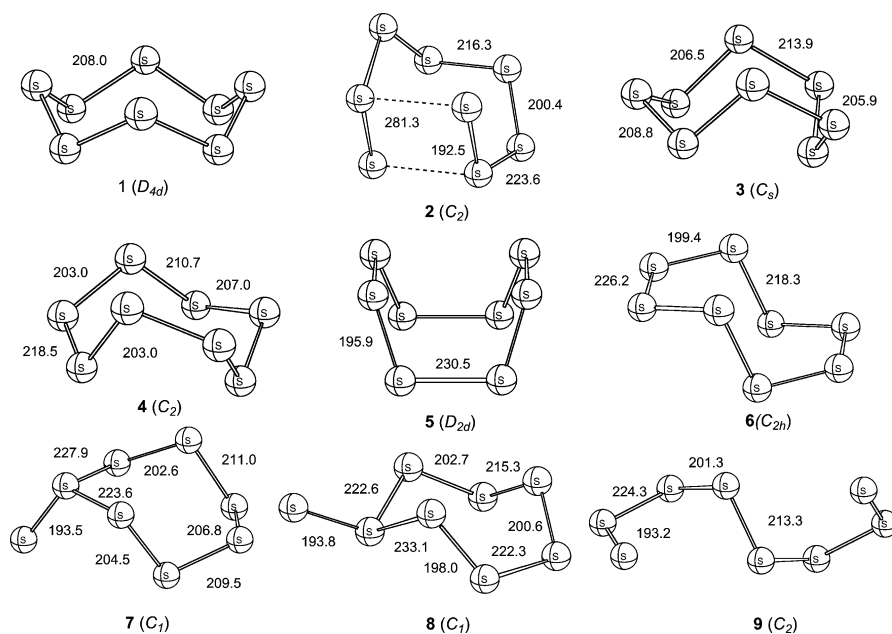


Fig. 15 Geometries of various isomers of the S_8 molecule calculated at the B3LYP/6-31G(2df) level; bond lengths in pm [79]

Table 17 Relative enthalpies of the S_8 isomers shown in Fig. 15 (in kJ mol^{-1}) calculated at the 3X(MP2) level [79]

Species	ΔH_{298}°	ΔG_{298}°
Crown- S_8 (1)	0.0	0.0
Cluster- S_8 (2)	33.3	28.3
Exo-endo- S_8 (3)	35.2	27.8
Twisted ring- S_8 (4)	37.7	30.1
Boat- S_8 (5)	44.8	41.1
Chair- S_8 (6)	57.0	48.5
$S_7=S_{ax}$ (7)	92.9	82.5
$S_7=S_{eq}$ (8)	95.8	86.6
Triplet-chain- S_8 (9)	154.4	129.1

is the S_7 ring which undergoes facile pseudorotation with an activation barrier of only 4 kJ mol^{-1} (see above, allotropes of S_7) [69].

2.2.3

Allotropes Consisting of Long Chains

One of the most interesting properties of sulfur atoms is the ability to form long polymeric chain molecules. At least three crystalline allotropes of mac-

romolecular sulfur are known at standard temperature-pressure (STP) conditions: Two slightly different fibrous forms and a laminar form. The structure of one of the fibrous allotropes (S_ψ) is well characterized. The macromolecular allotropes can be obtained only by special methods of preparation; for example, by quenching of liquid sulfur and stretching of the fibers obtained, by chemical reactions including decomposition of unstable allotropes, by UV-Vis irradiation, by drawing filaments from the melt, by sublimation of sulfur vapor, and under the action of high pressure. The materials thus obtained are in general mixtures of the polymer and of rings of different sizes. Such preparations are unstable and convert more or less slowly to the stable allotrope α - S_8 . The lifetime of the polymer content depends critically on the method of preparation and on the temperature of storage. At room temperature lifetimes of up to years have been reported. All of the polymeric forms studied up to now at ambient pressure seem to consist of the same type of helix conformation with lengths of 10^4 to 10^6 atoms. Left-handed and right-handed conformers of the helix will normally be present in one and the same allotrope.

In the past, the various techniques of preparation led to rather different results and, therefore, the elucidation of the structures of the polymeric allotropes was difficult. For example, fibrous sulfur is typically obtained by quenching a sulfur melt from above the polymerization temperature ($T_c \sim 432$ K) and subsequent extraction of the ring content as well as by stretching the fibers. Since the melt consists, besides the polymer fraction, of rings of different sizes in a temperature dependent equilibrium (see [43, 48, 49, 106]), this composition is commonly believed to be frozen by rapid quenching at temperatures well below 0 °C. However, the temperature of the melt, the temperature gradient of quenching ($-dT/dt$), and the final temperature of the quenched material have considerable impact on the resultant product. In addition, the time of the washing procedure with respect to the time of stretching induced crystallization determines the polymer content [50, 54, 107, 108]. The configuration of the polymeric molecules and their spatial arrangements in the solid state are affected by the different treatments too. It is not unusual in the history of structural determination of sulfur allotropes that the different findings reported in the literature resulted in a confusing nomenclature. In Table 18 we present a summary of the names used for polymeric sulfur. At that point, we are inclined to emphasize the necessity to label the polymeric allotropes in a consistent manner and—if delivering reports on new allotropes—to give a detailed description of the methods and conditions of preparation. For example, the polymer fraction in the liquid and in the quenched melt was often termed as S_μ regardless of the possibility that the molecular structures might be quite different. Furthermore, polymeric sulfur in the solid state comes along in different forms which may have a structural variety ranging from crystalline to amorphous (random coil) states as well as mixtures of both and mixtures of chains with very large rings. Therefore, we recommend to distinguish between the polymeric molecules in the liquid (S_∞) and the insoluble, polymeric content of a solid material (S_μ) isolated from the melt, for example. Accordingly, the term

Table 18 Nomenclature of polymeric sulfur as found in the literature. The most frequent while ambiguous terms are quoted (high-pressure allotropes are omitted; see Section 3 below)

Designation	Description, nter-relation between forms
Amorphous, vitreous, glassy or plastic sulfur	Quenched product from the melt above 160 °C; contains chains and rings of different size depending on the procedure
Polymeric or insoluble sulfur	Product after extraction of quenched liquid sulfur with CS ₂ ; synonyms are S _μ (after Smith [109]) and—sometimes—S _ω
Fibrous sulfur	Stretching the quenched product (with or without extraction of rings), drawing filaments directly from the melt; synonym for the crystallized solid was φ-sulfur, which consists of oriented helices (ψ-sulfur, S _ψ) and γ-S ₈ [31,110]; actually, ψ-S is the solid allotrope of fibrous sulfur after extraction of the rings with CS ₂
S _ω	Amorphous sulfur not stretched before extraction with CS ₂ , synonyms are "white sulfur of Das" [111, 112] and supersublimated sulfur; actually a mixture of two independent allotropes S _{ω1} (=S _ψ =2nd fibrous sulfur) and S _{ω2} (=S _χ =laminar sulfur) [54, 113–115]; sometimes also called S _μ , plastic, fibrous, or polymeric sulfur
S _μ	Synonym for polymeric or insoluble sulfur; also used for the molecule catenapolysulfur in the solid and—sometimes—in the liquid phase (S _∞) ^a
Crystex sulfur	A mixture of polymeric chains and little S ₈ rings containing organic stabilizers; also called supersublimated sulfur. Polymer fraction consists of S _{ω1} and mainly of S _{ω2} [116, 117].
S _∞	Generally used for the catenapolysulfur molecule, e.g., the biradicalic chain (·S _n ·) in sulfur melts [43, 106]; also used for the free or hypothetical helix molecule and for the polymeric chain in the solid state if the polymeric nature is to be stressed; further synonyms are polymeric sulfur, S _n chain, and S _μ ^a

^a See the recommendations in the text

S_μ ignores details in the actual molecular (and solid state) conformation, although it is clear that the molecular structure is a three-dimensional helical-like chain even if there is a certain disorder on the molecular and crystalline level. Hence, S_μ should be understood as a generic term.

The many efforts to determine the structure of polymeric sulfur allotropes have been critically reviewed by Donohue in 1974 [8]. Since that time, only a few experimental results have been reported which, however, did not introduce new structural details. Most of the more recent studies on polymeric sulfur are focused on the unique polymerization transition in the liquid. Experimental structure studies therefore often deal with quenched sulfur melts (see for example [118, 119] and literature cited therein). On the other hand, the polymerization mechanism has attracted increased interest for theoretical studies (see for example [120–123] as well as the literature cited therein).

The elastomeric properties of sulfur chains of differing lengths have been studied by means of Monte-Carlo simulations [124]. The results demonstrate a remarkable flexibility of polymeric sulfur. The configurational energy surfaces of polymeric sulfur were investigated with the use of a parameter-free density-functional method by Springborg and Jones [125]. It was found that the energy surface of the chain molecule is flat over large regions of the configurational space and contains a variety of local minima and saddle points corresponding to widely differing structures. In fact, the distinct flatness at the minimum energy is consistent with the enormous flexibility of the polymer. Finally, Ezzine et al. investigated the intermolecular interaction energies of polymeric sulfur chains by semiempirical methods. These studies were performed for several cases of chain arrangements including the S_{ω} allotropes [126].

In the following, we present a summary of the structures of the three solid allotropes of polymeric sulfur at STP conditions which have been studied so far. Doubtful forms, not verified up to now, will be omitted here. Although several authors are claiming crystalline structures in the case of certain polymeric allotropes it seems likely that in these solids regions with well defined ordered structures and regions with amorphous structures co-exist. This has clearly been shown by more or less sharp diffraction patterns in X-ray studies of different samples depending on the method of preparation.

2.2.3.1

Fibrous Sulfur (S_{ψ})

Crystalline samples of fibrous sulfur can be prepared by stretching freshly quenched liquid sulfur or by drawing filaments directly from a hot sulfur melt. The quenched melt (plastic sulfur) is viscoelastic and transparent yellow but slowly transforms into an opaque crystalline material at room temperature. After several days the material contains besides the polymer a fraction of S_8 rings and traces of S_7 while all other rings have converted to either polymer or S_8 [22]. The ring fraction can be extracted by washing the material with CS_2 . The insoluble fraction of polymeric sulfur is then allowed to crystallize (termed S_{μ} after Smith [109] or sometimes S_{ω} after Das [112]).

If plastic sulfur is stretched (by a factor of thousand of its original length!) crystallization will be induced [127]. The resulting filaments are mixtures of S_8 rings and polymeric sulfur. After extraction of the soluble ring fraction a fibrous crystalline allotrope is obtained (called S_{ψ} after Prins et al. [31, 110]).

Because of the complications introduced by the special treatments and the interconversion of the ring and polymer fractions during the preparation the elucidation of the structure was a long-standing puzzle. An important contribution to the determination of the molecular structure came from Prins et al. in the late 1950s [31, 110]. The authors showed that the diffraction patterns of filaments of sulfur can be understood assuming a superposition of the patterns of two constituents, namely *catena*-polysulfur and monoclinic γ - S_8 . From then on the true fibrous sulfur was termed S_{ψ} . Prins

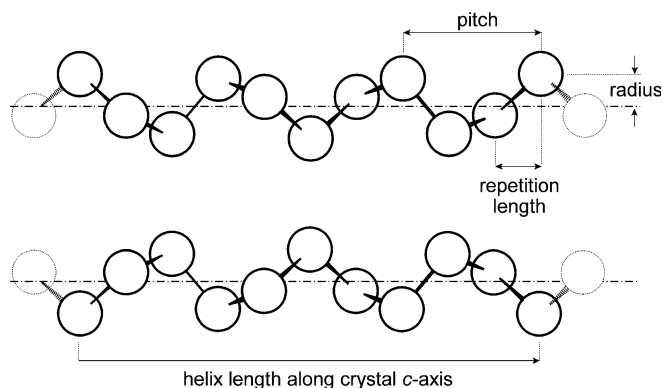


Fig. 16 View of the sulfur helix present in the fibrous allotrope. Left-handed helix (*top*) and right-handed helix (*bottom*) together with characteristic parameters are shown (cf. Fig. 17 and Table 19)

et al. also showed that crystalline polymeric sulfur can be obtained by washing the material with CS_2 which removes the monoclinic ring fraction. In addition, Prins et al. proposed a helical chain molecule with a period of ten atoms in three turns with a length of 1370 pm of the repeating unit. In the following years several structures have been discussed. With the work of Tuninstra [54, 128] and Lind and Geller [129, 130] the molecular and crystalline structure of fibrous sulfur seems to be well characterized.

The chain molecules of fibrous sulfur have a helical conformation (Fig. 16). The bond parameters are similar to those of the most stable ring molecules (S_8 , S_{12}). The bond length of 206.6 pm is slightly larger than in S_8 while the torsion angle of 85.3° is practically identical to the unstrained value [62] of sulfur chains. Crystalline S_ψ consists of parallel helices, which are regularly left-handed and right-handed. The unit cell contains eight ten-atom segments of the helices on a monoclinic indexing [129]. Efficient packing of the helices is attained by relative shifts and rotations of the individual helices such that the interlocking is maximal (Fig. 17). The molecular and crystal structure parameters are summarized in Table 19. The thermal expansion of solid S_ψ has been measured and found to be different from other known helical structures of the chalcogen family (trigonal Se and Te) [131].

It is interesting to note that fibrous sulfur (S_ψ) is identical to an allotrope obtained from high-temperature and high-pressure conditions ($T \sim 470\text{--}670$ K, $p \sim 2\text{--}6$ GPa, at conditions above the melting curve) [129, 130, 132–134]. However, results of a more recently performed in-situ structural analysis at 670 K and 3 GPa suggest that the previously obtained high-pressure fibrous forms result from the back-transformation of another high-pressure polymorph at pressures below 0.5 GPa (see the section High Pressure Allotropes below) [135].

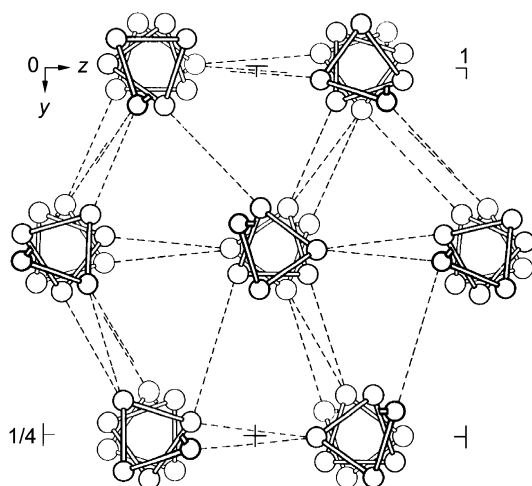


Fig. 17 Structure of fibrous sulfur projected along the fiber axis showing the arrangement of left- and right-handed helices in a pseudo-orthorhombic setting ($x=1380$ pm, $y=3240$ pm, $z=925$ pm); the orthorhombic x -axis corresponds to the monoclinic c -axis (cf. Fig. 16 and Table 19). The shortest intermolecular distances (333–348 pm) are indicated by *dashed lines* [8]

2.2.3.2

2nd Fibrous and Laminar Sulfur ($S_{\omega 1}$ and $S_{\omega 2}$)

Polymeric sulfur or, generally speaking, insoluble sulfur can be obtained by various methods apart from quenching sulfur melts from temperatures above 160 °C. The methods which have been reported are:

- “Chilling” liquid sulfur [112] (a somewhat slower process than quenching) or quenching without stretching the product
- Sublimation of sulfur vapor onto a (relatively) cold substrate [112]
- Quenching of sulfur vapor in a cold solvent like carbon disulfide (“super-sublimation”; product commercially available under the trade-name Crystex)
- Irradiation of solutions of sulfur rings at room temperature [113, 114, 136] or of solid S_8 at low temperatures [137]
- Thermal decomposition of metastable allotropes like S_6 , S_7 , etc. (see 2.3.2 below)
- Application of high pressure in combination with high temperature or intense light (see below)

Older reports that certain chemical reactions (hydrolysis of S_2Cl_2 [111], reaction of SO_2 with H_2S [138]) would produce polymeric sulfur are in error since the yellow product also contains long-chain polythionates which make it hydrophilic [139].

Table 19 Crystal and molecular structure parameters of fibrous sulfur, S_ψ [8, 54, 128–130]. The pseudo-orthorhombic unit cell proposed by Tuinstra has been overcome in favor of a monoclinic structure. The unit cell contains eight segments of ten atoms of the helices

Crystal system	Monoclinic
Space group	$P2=C_2^1$ (no. 3)
Lattice constants	
a	1760 pm
b	925 pm
c	1380 pm (=three times the pitch) ^b
β	113°
Helix parameters	
Screw order, k^a	$\sim 10/3$ (=ten atoms in three turns)
Radius	95.0(3) pm
Pitch, P^b	460 pm
Atomic repetition length, p^c	137 pm
Rotation, γ^d	108°
Bond parameters	
Bond length	206.6 pm
Bond angle	106.0°
Torsion angle	85.3°

^a The screw order, k , is defined as the number of atoms per turn. Here, the repetition of the helix is ten atoms in three turns ($^{10}S_3$) giving $k \sim 3.33$. The screw order is connected with the pitch, P , and the atomic repetition length, p , through the relation $k = P/p$

^b The pitch, P , is the distance along the axis of the helix after one turn

^c The atomic repetition length, p , is defined as the distance of successive atoms in the helix projected to the helical axis

^d The rotation of successive atoms is given by $\gamma = 360^\circ/k$

The diffraction patterns of crystalline samples of insoluble sulfur prepared by chilling and by sublimation have been found to be identical, but different from fibrous sulfur, S_ψ . These crystalline forms have been termed S_ω by Das [111, 112]. Later, it was shown by Erämetsä and Suonuuti [113, 114] that S_ω consists of two independent allotropes which they have called S_μ and S_ν , respectively. If insoluble sulfur was prepared under the influence of bright sunlight S_ω was the predominant form. During investigations of the insoluble residues of Crystex and of “home-made” specimens of polymeric sulfur obtained by quenching Tuinstra [54, 115] confirmed the statement of Erämetsä. Tuinstra called the two different allotropes $S_{\omega 1}$ (= S_ω) and $S_{\omega 2}$ (= S_μ), respectively. The ordinary quenched insoluble sulfur S_ω of Das (= $S_{\omega 1} + S_{\omega 2}$) gave best oriented diffraction patterns if the specimens were stretched to about 1000% of their original length. Additional stretching caused a transformation to the well-known fibrous sulfur, S_ψ . It has been reported that $S_{\omega 1}$ can be obtained by carefully heating of Crystex and followed by extraction of the soluble ring fraction [54, 115, 140]. However, the temperature of 110 °C reported by Tuinstra is in conflict with the thermal depolymerization of insoluble sulfur observed by Hendra et al. in Raman spectra

Table 20 Crystal structure parameters of “2nd fibrous sulfur” ($S_{\psi}=S_{\omega_1}$) and of “laminar sulfur” ($S_{\chi}=S_{\omega_2}$) [54, 115]. The molecular parameters were claimed to be very similar to those of fibrous sulfur, S_{ψ}

Allotrope	2nd fibrous ^a	Laminar
Crystal system	Orthorhombic	Tetragonal (body-centered)
Space group	$Pccn-D_{2h}^{10}$ (no. 56)	$I\bar{4}-S_4^2$ (no. 82)
Lattice onstants		
a (pm)	902	458 ($\sim 1380/3$) ^b ($a=b$)
b (pm)	833	
c (pm)	458 ($\sim 1380/3$) ^b	1632

^a Data have been derived from partly stretched samples. Strong extended fibers gave diffraction pattern of fibrous sulfur, S_{ψ}

^b Coincides with one third of the $^{10}S_3$ helix axis of repetition length 1380 pm

at sample temperatures of 80–110 °C [116] and by Steudel et al. by DSC and other experiments [55].

On the other hand, S_{ω_2} is obtained by heating samples, “home-made” by quenching, cautiously to 80 °C [54, 115], or by quenching sulfur vapor followed by extraction, or by extraction of commercially available polymeric sulfur with CS_2 at low temperatures (~ 195 K) [140]. In addition, Tuinstra reported the diffraction pattern of both forms, S_{ω_1} and S_{ω_2} , to be complementary and to coincide with that of the untreated Crystex.

X-ray studies of Crystex demonstrated that this form is at least partially crystalline [116]. The diffraction lines are broadened in comparison with recrystallized material (α - S_8). The diffraction pattern of commercial Crystex is identical to that of a mixture of S_{ω_1} and S_{ω_2} with the latter being the predominant component [116, 117, 140]. These results are in accordance with Raman and infrared spectra of Crystex and sublimed sulfur [116, 117, 141, 142] which are identical to those of quenched melts with the exception of the lines of α - S_8 [106, 143]. Michaud et al. reported the decomposition of polymeric sulfur to α - S_8 by recording the time-dependent evolution of the Raman spectrum [140].

From the coincidence of the X-ray layer lines of S_{ω_1} and S_{ω_2} with those of S_{ψ} Tuinstra concluded that these polymers have the same molecular conformation. Since the diffraction patterns of S_{ω_1} and S_{ω_2} were much poorer than that of S_{ψ} the exact positions of the atoms of the helices remained uncertain [54, 115]. However, the gross arrangement of the helices in the units of S_{ω_1} and S_{ω_2} could be determined. Accordingly, the structure of S_{ω_1} is an orthorhombic lattice which has nearly the same size as the unit cell of S_{ψ} on a pseudo-orthorhombic setting (Table 20). In these structures the helices are arranged parallel to each other. Since the densities of both were found to be the same the unit cell was expected to be built by four helices as in the case of S_{ψ} . A maximum of interlocking of the helices was estimated for the direction of the b -axis which consists of alternating helices with opposite turns (see Fig. 18). Because of the similarity with the fibrous sulfur allotrope S_{ψ} ,

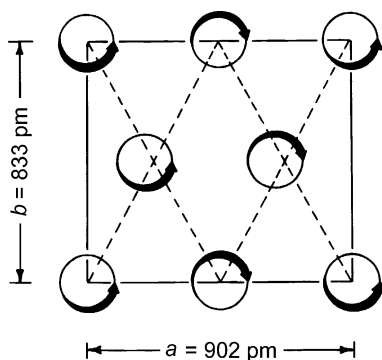


Fig. 18 Schematic view of the crystal structure of $S_{\omega 2}$ (=2nd fibrous sulfur or S_{ψ}) along the c -axis showing the handedness of the helices [8]

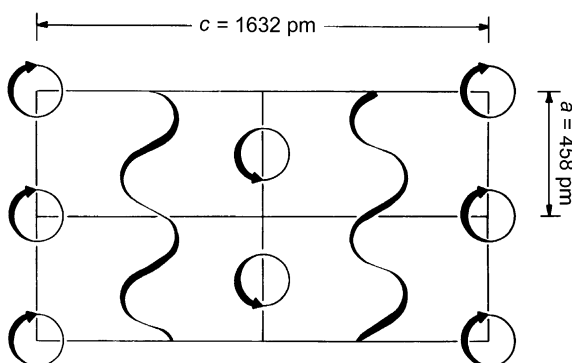


Fig. 19 Schematic view of the crystal structure of $S_{\omega 2}$ (=laminar sulfur or S_{χ}) along the b -axis showing the “cross-grained plywood” arrangement of the helices (after [8, 54])

Tuinstra proposed the name “2nd fibrous sulfur” or S_{ψ} for the $S_{\omega 1}$ modification [115].

On the other hand, the structure of $S_{\omega 2}$ was reported as tetragonal with the helices perpendicular to the c -axis of the unit cell (Table 20). The only reasonable possibility in structure determination was the one in which adjacent layers of helices are oriented perpendicular to each other. The helices of the layers have the same molecular structure and all the helices in one layer have the same handedness. The closest packing of the helices is achieved if the molecules of parallel layers have opposite turns (see Fig. 19). This structure is unusual but not unlikely since the pitch of the sulfur helix is the same as the intermolecular distance of neighboring helical axes, about 460 pm (see Table 20). The structure of $S_{\omega 2}$ is a “cross-grained plywood structure”. This peculiarity has caused Tuinstra to label this modification “laminar sulfur” (S_{χ}).

Furthermore, polymeric sulfur ($S_{\omega 1}+S_{\omega 2}$) also seems to be obtainable at high pressures and high temperatures (1.7–2.8 GPa, 460–600 K), e.g., the so-called Geller's phase I [144]. However, this phase was later indexed by Roof as a monoclinic structure similar to Geller's high pressure phase III (~ 3 GPa, ~ 540 K) [145].

From measurements of the molar heat capacity of $S_{\omega 2}(=S_{\gamma})$ in the temperature range 5–370 K this allotrope was suspected to undergo a transition to a more stable phase above 310 K, the structure of the new phase being unknown [146].

Based on the structures of $S_{\omega 1}$ and $S_{\omega 2}$ as proposed by Tuinstra [54, 115], Ezzine et al. studied theoretically the repulsive and attractive interaction energies of both crystalline allotropes in order to determine the relative atomic positions of the interdepending chains in these solids [126]. It was found that the $S_{\omega 2}$ allotrope is more stable than $S_{\omega 1}$ (at 0 K). From the energy calculations it turned out that the (idealized) structures of $S_{\omega 1}$ and $S_{\omega 2}$ are sufficiently represented by three helix atoms per elementary cell rather than ten. The parity of the helices claimed by Tuinstra was confirmed. Moreover, the authors stated the most stable structure to be the one in which neighboring helices are shifted relative to each other by one half of the atomic repetition length, that is about 70 pm. The mutual arrangements of the helices resulting from minimal total energies correspond to a maximum of interlocking of the polymers.

Up to now, the various solid allotropes of polymeric sulfur can only be identified by X-ray structural analysis since the molecular vibrations and therefore the Raman spectra are very similar [151]. A chance to distinguish between the different allotropes by vibrational spectroscopy may only exist if the lattice vibrations are recorded which are expected to be different enough, especially for the fibrous and the laminar structures. However, this experiment requires samples of a high degree of crystallinity; such measurements have to be performed at low temperatures to avoid broadening of the Raman lines.

2.2.3.3

Polymeric Sulfur in $Ta_4P_4S_{29}$

Polymeric sulfur was found as a constituent in the three-dimensional tunnel structure of the tantalum thiophosphate $Ta_4P_4S_{29}$ [147]. The basic framework consists of TaS_6 groups linked by PS_4 units sharing the sulfur atoms. This structure leaves two parallel channels in the unit cell along the c -axis which both are occupied by sulfur helices of the type $(S_{10})_{\infty}$. Only right-handed helices were found in the crystal investigated. The molecular structure parameters are close to the polymeric forms mentioned above: The average bond length and bond angles are 205.2 pm and 105.75° , respectively. The S_{10} unit has a length of 1365 pm projected down to the helical axis coinciding with the lattice parameter c of the network crystal. The polymeric chains are weakly bound to the network structure by van der Waals forces. The next,

non-bonded atoms of the tunnel structure are sulfur atoms of the TaPS₆ units of the framework with distances not shorter than about 330 pm.

2.2.4

Concluding Remarks

The flexibility of the sulfur-sulfur bond with its relatively low torsional barrier of 27 kJ mol⁻¹ [148] allows the formation of many more or less stable molecular conformations of rings S_n ($n \geq 5$) and chains [4]. The conformation of the various molecular species can be described in terms of the sign (+ or -) of the dihedral angles around the ring or along the chain. This motif was extensively discussed by Tuinstra for hypothetical sulfur molecules and by Schmidt for several ring molecules known at that time [54, 96, 149].

Considering the symmetry of the cyclic sulfur molecules the rings can be divided into two groups [35]:

- Highly symmetrical species with almost equal bond parameters (bond lengths, bond angles and torsional angles) and with regular motifs, e.g., S₆:(+-)₃, S₈ (+-)₄, and S₁₂ (++--)₃.
- Less symmetrical species with unequal bond parameters and usually alternating long and short bonds around the ring (S₇, S₉, S₁₁, S₁₃, etc.). The conformation of these molecules is characterized by a less regular motif (e.g., S₇: +-+0-+-, see Table 4) due to their low symmetry (S₇: C_s).

From this point of view one may expect a higher degree of stability for the high symmetrical rings. However, this is not always the case: S₆ is quite unstable. In fact, the molecules S₆ and S₇ have comparable mean bond energies [19] and strain energies [66]. Since the torsion angles in S₆ (*D*_{3d} symmetry) are all equal and ca. 74° which is an unfavorable value, the strain is “stored” in the whole ring. On the other hand, in S₇ there is one very long bond as the result of a torsional angle of about 0° which accounts for the strain in the ring. Not only S₇, which is the most prominent example, but also all other rings show that a longer bond is always neighbored by shorter ones (Fig. 21).

This general peculiarity of cumulated sulfur-sulfur bonds can be interpreted in terms of a simple lone-pair electron repulsion model [150] and furthermore indicates a strong bond-bond interaction [21]. In other words, shorter bonds are stronger (bond order higher than one) and vice versa. The longest bonds in sulfur rings are those of which the torsion angles show the largest deviation from the optimum value of 90±10°. There exists a certain correlation between a given torsion angle and the corresponding bond distance [148]. From Fig. 20 it can be seen that the most favorable values of the dihedral angle are those near 90° while those which deviate from this value result in longer and therefore weaker bonds. These experimental findings are very well reproduced by ab-initio molecular dynamics calculations on sulfur clusters [67].

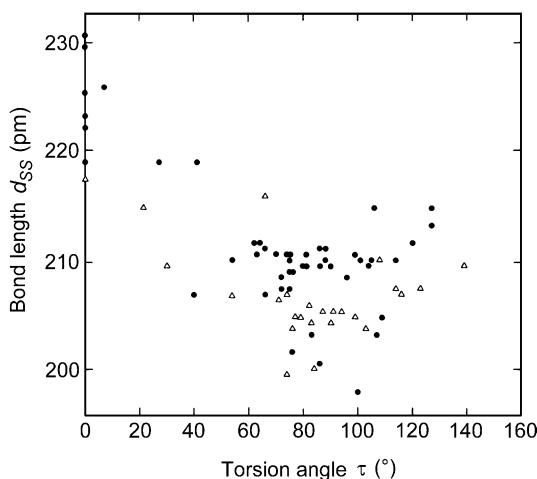


Fig. 20 Dependence of the S-S bond distance in sulfur homocycles on the torsion angle τ_{SS} . Experimental values are shown by *open triangles*, values obtained by MD calculations are shown by *full circles* [67]

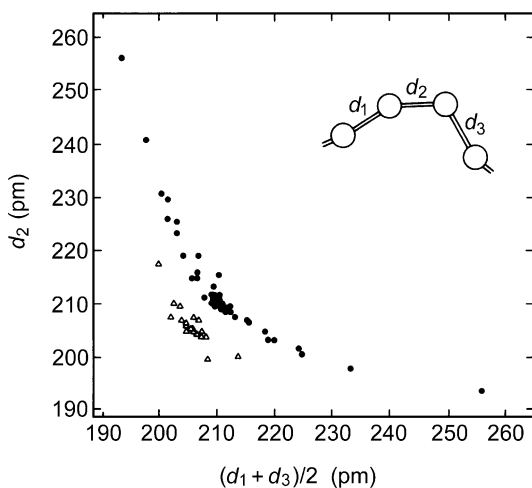


Fig. 21 Relationship between the bond lengths in sulfur rings S_5 to S_{13} indicating strong bond-bond interactions. The bond length d_2 is plotted as a function of the two neighboring bonds, $1/2(d_1 + d_3)$, see the inset. Experimental values are shown by *open triangles*, MD calculated values by *full circles* [67]

In the crystalline state, the site symmetry is in general lower than the symmetry of the free molecule. The preferred lattice structures of sulfur homocycles are of the orthorhombic and monoclinic crystal systems. The molecular packing arrangements of the solid allotropes are quite different. In orthorhombic S_{12} , for example, the asymmetric unit is given by one quarter

of the molecule while, on the other hand, in monoclinic δ -S₇, orthorhombic S₁₁, monoclinic S₁₃ and monoclinic *exo*-S₁₈ (β -S₁₈) the asymmetric unit is much larger containing two molecules [73]. With the exception of S₁₈ all rings S_{*n*} which form different solid allotropes (S₇, S₈, S₉, S₆, S₁₀, S₆·S₁₀, S₁₂, S₁₂·CS₂) show up with the same molecular conformation. The same is true for the polymeric modifications at STP conditions although one has to consider that the polymeric solids may, at least partly, consist of a random coil network.

The variety of structures and symmetries both of the molecular and crystalline forms of sulfur gives rise to significantly different vibrational spectra which, therefore, can serve as a fingerprint for an actual allotropic form [151].

2.3

Physical Properties

2.3.1

Melting Points

None of the sulfur allotropes melts without (some) decomposition [55]. Therefore, the melting points measured depend on the heating rate. As lower the heating rate as lower the melting point observed since the decomposition products lower the melting temperature. Only in the case of S₈ a constant triple point temperature (115 °C) can be measured since the composition of the melt reaches an equilibrium after some time (usually 10 h). In the case of the other cyclic allotropes the melting process yields S₈ and S_∞ as the primary decomposition products from which other ring molecules are then formed. Nevertheless, S₇ and S₈ show reversible melting temperatures if the heating is done quickly enough and if the melt is cooled down immediately before the last crystal has disappeared. With the exception of S₈ all sulfur allotropes decompose already at temperatures slightly below the melting temperature if kept at such a temperature for some time. Therefore, the following “melting points” should be taken with caution (for more details see under “Thermal Behavior”):

S ₆	88 °C [55]
S ₇	39 °C [16, 55]
α -S ₈	115 °C [152] (112 °C [153], 116 °C [55])
β -S ₈	120 °C [152] (119 °C [153, 154], 120 °C [155], 121 °C [55]; triple point: 115 °C [48])
γ -S ₈	109 °C [152]
S ₉	63 °C [33]
S ₁₀	92 °C [55]
S ₆ ·S ₁₀	92 °C [35]
S ₁₁	74 °C [36]

S_{12}	148 °C at heating rate 10 K min ⁻¹ , 141 °C at 5 K min ⁻¹ , 135 °C at 2.5 K min ⁻¹ [55]
S_{13}	Polymerizes at ca. 90 °C prior to melting at 114 °C [55]
S_{14} :	117 °C [46]
S_{15}	No melting point has been reported for this allotrope
<i>endo</i> - S_{18} (α - S_{18})	126–128 °C [104]
S_{20}	121 °C [55] (124–125 °C [104], 120–130 °C [43])
S_{μ}	ca. 110 °C [55]

In this context it should be mentioned that the heat conductivity of elemental sulfur is extremely low. Therefore, heating rates should not be chosen too high.

Obviously, melting temperatures also depend on the external pressure, a phenomenon which has been most extensively studied in the case of S_8 [156]; see below.

2.3.2

Thermal Behavior

The thermal decomposition of the sulfur allotropes has been studied extensively by Steudel et al. [55].

S_6 : pure solid *cyclo*-hexasulfur decomposes only slowly at 20 °C [157] and even at 50 °C the reaction is still slow. Storage at 20 °C in diffuse daylight for 10 days resulted in a decomposition of only 3% of the original S_6 and the only decomposition product was S_{μ} . Storage at 50 °C (in an oven) for 5 days gave 8% S_{μ} and 2% S_8 [106]. At 120 °C, in the liquid state, the decomposition is complete within 1 min yielding S_7 , S_8 and S_{μ} . DSC diagrams show the melting of pure S_6 to begin at 88 °C (endothermic melting peak centered at 100 °C) followed by the exothermic polymerization to S_{∞} (peak centered at 110 °C) and its exothermic depolymerization to mainly S_8 and some S_7 [55].

S_7 : *cyclo*-heptasulfur is the least stable of all sulfur allotropes. After 2 h at 20 °C a sample of γ - S_7 had decomposed to a mixture of S_8 and S_{μ} containing only trace amounts of S_7 . After 4 days at 20 °C (in the dark) the decomposition was complete and yielded 81% S_{μ} and 19% S_8 [106]. The melting of γ - S_7 at 39 °C is reversible, but on further heating the melt polymerizes exothermically at 70–110 °C followed by the exothermic depolymerization of S_{∞} to the equilibrium melt in the region above 115 °C [55].

S_8 : below 96 °C, *cyclo*-octasulfur is stable as orthorhombic α - S_8 . However, the conversion to monoclinic β - S_8 at temperatures just above the triple point of 96 °C is kinetically hindered and requires lattice defects or imperfections as present in a powder but usually not in a single-crystal [158]. Therefore, single-crystals of α - S_8 usually melt at 115 °C without prior conversion to the β -form. For the same reason the temperature at which the transition $\alpha \rightarrow \beta$ is observed by DSC measurements depends on the heating rate and is often found well above 100 °C, even if a powder-like sample is used. The activation energy for the $\alpha \rightarrow \beta$ transition is approximately identical to the enthalpy of sublimation of α - S_8 (100 kJ mol⁻¹) [158]. Heating of S_8 to 90–110 °C, just be-

low the melting point of the α -phase at 115 °C, does not result in any decomposition of the eight-membered rings, but as soon as a melt has formed equilibration with other ring sizes takes place [49]. High purity liquid sulfur shows a strong tendency for supercooling: it can be kept liquid in bulk at about 50 °C for 20 min or so. At temperatures closer to the melting point this period of supercooling is even extended [24]. γ -S₈ is metastable at all temperatures but in a clean environment it survives at 20 °C for longer periods of time. However, in the laboratory atmosphere it was reported to convert fairly rapidly to α -S₈ even at 20 °C [31]; the rate of transformation into α -S₈ reaches a maximum at 80 °C. These phase transitions are catalyzed by traces of carbon disulfide but hindered by the presence of polymeric sulfur [158].

S₉: if solid α -S₉ is heated with a rate of 2–20 K min⁻¹ to the melting point of 63 °C and the melt is rapidly cooled to room temperature, it consists mainly of S₉ with traces of S₇ and S₈. At 25 °C S₉ is about as stable as S₆ [33].

S₁₀: if S₁₀ is heated at a rate of 5 K min⁻¹ in a DSC apparatus one observes the melting at 92 °C and an exothermic polymerization reaction in the temperature range 95–119 °C followed by depolymerization to mainly S₈ and some S₇ together with traces of other sulfur rings. If rapidly heated to 120 °C, S₁₀ decomposes within 1 min [55].

S₆·S₁₀: This allotrope can be stored at 20 °C for several days, at -30 °C for several months without decomposition [35].

S₁₁: at 20 °C S₁₁ can be handled for several days without decomposition. On heating it polymerizes to S_∞ [38].

S₁₂: on heating at a rate of 5 K min⁻¹ S₁₂ decomposes within the temperature range of 140–155 °C with simultaneous formation of S_∞, S₈, and some S₇. At room temperature S₁₂ can be stored for indefinite periods of time without decomposition [55].

S₁₃: as in the case of other sulfur allotropes S₁₃ polymerizes on heating and a well separated melting process cannot be observed. Instead, the two processes take place more or less simultaneously. At 20 °C crystalline S₁₃ does not decompose for several days [38, 55].

S₁₄: at 25 °C crystalline S₁₄ is stable for several days. On heating to the melting point of 117 °C it decomposes to S₇ and S₈ while S₆ is not formed. Probably the dissociation into two molecules of S₇ is the first step followed by the interconversion of S₇ to S₈ [46].

S₁₅: at 23 °C solid S₁₅ can be kept for several hours without decomposition. The thermal behavior at higher temperatures has not been reported [47].

endo-S₁₈ (α -S₁₈): this allotrope can be kept at room temperature for extended periods of time without decomposition but no DSC measurements have so far been reported, and no information is available about the thermal behavior of *exo*-S₁₈ (β -S₁₈).

S₂₀: like crystalline S₁₂ and S₁₈ this allotrope can be kept at 25 °C for indefinite periods of time without decomposition. On heating S₂₀ melts near 121 °C and simultaneously polymerizes followed by depolymerization of the

S_{∞} with formation of S_8 and S_7 . In fact, the observed melting may apply already to a mixture of S_{20} and S_{∞} [55].

S_{μ} : the thermal behavior of S_{μ} depends on its preparation since S_{μ} is a mixture of long chains and large rings and not a well defined chemical substance. This mixture is thermodynamically unstable with respect to α - S_8 at 20 °C and in fact depolymerizes slowly at moderate temperatures already. DSC measurements of polymeric sulfur prepared from quenched melts as well as from sublimed sulfur show the polymer to melt at 100 °C followed immediately by the exothermic depolymerization. Stabilized commercial polymeric sulfur (Crystex) starts to melt only at 110 °C but otherwise behaves similarly (heating rate 10 K min⁻¹) [55].

2.3.3

Solubilities

As a general rule, the solubility of the sulfur allotropes in organic solvents decreases with increasing molecular size. Carbon disulfide is by far the best solvent, followed by toluene and dichloromethane while *cyclo*-alkanes are suitable for the smaller ring molecules only as far as ambient temperatures are concerned. For example, at higher temperatures S_{12} is fairly well soluble in benzene and toluene; on cooling S_{12} crystallizes as monoclinic needles. This molecule is the only sulfur allotrope which forms a stoichiometric solvate with a solvent molecule: From carbon disulfide it crystallizes as orthorhombic plates of composition $S_{12}\cdot CS_2$ the structure of which has been elucidated by X-ray crystallography [100]. The CS_2 molecules occupy empty spaces in the special layer structure of S_{12} with no other than van der Waals interactions of the two molecules.

Quantitative solubility data at various temperatures are available only for S_6 [159], S_7 [106], S_8 [1, 159, 160], and S_{12} [159]. The following data [159] may serve as examples:

- In 100 g CS_2 at 17 °C are soluble: 9.11 g S_6 , 37.4 g α - S_8 , or 0.21 g S_{12}
- In 100 g benzene at 17 °C dissolve: 1.5 g S_6 , 1.6 g α - S_8 , or 0.02 g S_{12}

The highest solubility of any sulfur allotrope in CS_2 is observed for S_7 . At 20 °C the two compounds can be mixed in practically any ratio since even small concentrations of CS_2 lower the melting point of γ - S_7 to room temperature. The solubilities (g/100 g CS_2) listed in Table 21 were measured at low temperatures [159].

It is evident from the data in Table 21 that the solubility of S_7 increases with increasing temperature much more so than that of S_8 .

During studies on the composition of quenched liquid sulfur it was observed that the solubilities of S_7 and S_8 in CS_2 are considerably enhanced by the presence of larger sulfur rings (S_x , mean value of $x \approx 25$ [106]). For example, 7.7 g S_8 dissolve in 100 g CS_2 at -78 °C in the presence of 2.3 g S_x [106]. For more information on S_x see above under "Preparation of S_{12} , S_{18} ,

Table 21 Solubilities of γ -S₇ [106] and α -S₈ in carbon disulfide at various temperatures

T (°C)	γ -S ₇	T(°C)	α -S ₈
		-80	2.40
-77	1.7	-70	3.09
-53	5.5	-51	5.76
-40	9.1	-41	7.40
-26	17.2	-25	11.5

and S₂₀ from liquid sulfur". The solubility of S₁₈ is 240 mg in 100 g CS₂ at 20 °C [104].

At higher temperatures (65–120 °C) elemental sulfur is also soluble in compressed gases like nitrogen, methane, carbon dioxide, and hydrogen sulfide, a fact which is of tremendous technical importance for the gas industry since many natural gas reservoirs also contain H₂S and elemental sulfur. During production of the gas the sulfur is partly transported to the surface and precipitates on decompression and/or cooling of the gas mixture at the well-head [160–165]. Clogging of pipelines may then result [166].

Polymeric sulfur S _{μ} is usually considered to be insoluble in all common solvents, even in CS₂. However, polymeric sulfur is unstable with respect to small sulfur rings like S₈, and in the presence of solvents it slowly depolymerizes at 20 °C, faster at higher temperatures, even with exclusion of light. If S _{μ} is shaken with either CS₂ or *cyclo*-hexane at room temperature the concentrations of S₆, S₇, and S₈ in the solution increases from day to day. From 500 mg S _{μ} and 50 ml CS₂ a solution containing 12 mg soluble sulfur rings was obtained after 14 days at 20 °C in the dark (ratio S₈:S₇=2:1). After several weeks a yellow solution was obtained which also contained traces of S₉, S₁₀, and S₁₂. Complete dissolution can be achieved by heating the mixture to 100 °C for 1–2 days (in an ampoule). The solution obtained in this way contains all the sulfur rings observed in liquid sulfur but in differing concentration ratios [55].

Sulfur is normally considered to be insoluble in water and, in fact, the solubility of α -S₈ at 20 °C is only 5 $\mu\text{g l}^{-1}$ [167]. However, if neutral surfactants are added to the aqueous phase the solubility of α -S₈ (and other sulfur allotropes) increases dramatically, provided the critical micelle concentration of the surfactant is reached [168]. These surfactants do not alter the S₈ molecule chemically. For example, a concentration of 50 g l⁻¹ of sodium dodecyl-sulfate C₁₂H₂₅SO₄Na increases the solubility of α -S₈ at 22 °C by a factor of 4000. Even higher factors were observed with hexadecyl(trimethyl)ammonium bromide, especially at higher temperatures [168].

2.3.4

Densities

The densities of 16 solid sulfur allotropes consisting of rings are given in Table 22. These data have been calculated from the most recent crystallograph-

Table 22 Densities of solid sulfur allotropes

Allotrope	Density (g cm ⁻³)	Temperature (K)	Reference
S ₆	2.260	183	[65]
γ-S ₇	2.190	163	[20]
δ-S ₇	2.182	163	[20]
α-S ₈	2.108/2.066	173/298	[76]
β-S ₈	2.088/2.008	113/298	[27, 81]
γ-S ₈	2.08	298	[29]
α-S ₉	2.114	173	[33]
S ₁₀	2.103	163	[35]
S ₆ S ₁₀	2.17	163	[35]
S ₁₁	2.08	163	[38]
S ₁₂	2.045	298	[100]
S ₁₃	2.09	173	[38]
S ₁₄	2.045	173	[46]
α-S ₁₈	2.090	298	[104]
β-S ₁₈	2.009	298	[103]
S ₂₀	2.023	298	[104]

ic results. The comparison shows that S₆ has the highest density and therefore should be thermodynamically favored at high pressures. This is in fact the case; see later.

The density of Crystex, the commercial polymeric sulfur, is 1.95 g cm⁻³ [169].

2.3.5

Photochemical Behavior

All sulfur allotropes are light sensitive both in the solid state and in solution. If the energy of the absorbed photons is sufficiently high homolytic cleavage of the sulfur-sulfur bonds will occur and free radicals are formed. The thermal bond dissociation energy in liquid sulfur [170] is 150±2 kJ mol⁻¹ corresponding to a wavelength of 800 nm. However, the extinction coefficient of most sulfur molecules (rings and long chains) is very low at wavelengths >430 nm [171]. Therefore, in most photochemical experiments radiation of shorter wavelengths has been used. The following discussion will be restricted to solid phases.

The irradiation of solid sulfur allotropes or of solid solutions of sulfur rings produces not only free radicals but also new absorbing and unstable species the identity of which is however not always certain (for a discussion, see [61]). The properties of the radicals as well as their mode of generation are summarized in Table 23 [172, 173]. In addition to the formation of radicals and colored species the irradiation of sulfur induces also luminescence and enhanced electrical conductivity [174].

The three types of radicals observed in irradiated sulfur samples have been interpreted as follows: Radical β is a sulfur chain-end with the terminal

Table 23 Sulfur radicals generated by irradiation of solid sulfur with neutrons or photons

Sample	Radical generation	Sample temperature	<i>g</i> tensor values	Radical type	Reference
α -S ₈	Neutrons	77 K	2.025	α	[172]
α -S ₈	Neutrons	77–195 K	2.040/2.022/2.002	β	[172]
α -S ₈	Neutrons	77–273 K	2.051/[2.024] ^a /[2.002] ^a	β'	[172]
α -S ₈ ^b	$\lambda < 420$ nm	2–180 K	2.0254	α	[61]
α -S ₈ ^b	$\lambda < 420$ nm		2.041/2.025/2.0027	β	[61]
α -S ₈ ^b	$\lambda < 420$ nm	2–298 K	2.052/[2.025] ^a /[2.003] ^a	β'	[61]
Quenched liquid sulfur	$\lambda = 380$ – 450 nm	77 K	2.041/2.026/2.003	β	[173]

^a Signals not directly observed due to superimposition, therefore taken from [170d]

^b Signals also observed with quenched liquid sulfur irradiated under the same conditions

torsion angle positive, while this angle is negative for radical β' . Radical α is the same as β or β' but neighboring to another radical resulting in a broad absorption line lacking any fine structure or anisotropy due to spin-spin interaction. Radical α is therefore the least stable thermally since recombination of the two chain ends can easily occur. This species is obviously the primary product of the homolytic dissociation if the two chain ends are trapped by the cage effect of the surrounding molecules [61]. On warming the concentration of radical α steadily decreases and practically disappears at 210 K. The signals due to radicals β and β' could be observed up to much higher temperatures and even in irradiated samples stored for some days at 298 K [61]. Radicals β and β' have also been observed in quenched liquid sulfur (without irradiation) [170d].

Bombardment of thin sulfur films, cooled to low temperatures, by He^+ ions of MeV energy (sputtering) results in erosion and loss of material by sublimation [175]. These results are of relevance to the surface properties of Jupiter's moon Io large parts of which are covered by elemental sulfur [176] which is constantly bombarded by fast particles from the magnetosphere of nearby Jupiter.

2.4

Analysis

Qualitatively, solid sulfur allotropes can best be characterized by Raman spectroscopy which is an extremely sensitive method. Depending on the number of atoms in the molecule and of the molecular symmetry quite different spectra are obtained [151]. A quantitative analysis of even complex mixtures of sulfur rings can be achieved by reversed-phase HPLC analysis after dissolution in carbon disulfide and using a UV absorbance detector [49]. This method is also extremely sensitive and only minute amounts of sample are needed [49]. The polymer content is simply determined by weighing of the extraction residue after the solvent has been removed in a vacuum.

3

High-Pressure Allotropes

3.1

Introduction

Application of high pressure in the megabar range (up to a few hundred GPa) has become a valuable tool in solid state physics as well as in solid state chemistry. Molecular systems under high pressure are experiencing extreme forces which cause the intermolecular distances to approach values of the intramolecular bond distances. As a result, there is an increased overlap between adjacent molecular orbitals which gives rise to a number of consequences such as structural changes (towards close packing), electronic tran-

sitions (e.g., alteration of coordination number and metallization) and pressure induced chemical reactions (e.g., polymerization).

The most striking observation in the case of sulfur is the formation of a superconducting phase at about 93 GPa with the highest critical temperature T_c , about 10 K, amongst the non-metallic elements [177–179]. The transition temperature reaches a maximum value of about 17 K at pressures of around 160 GPa. Both peculiarities are correlated with structural transitions and changes in the coordination number under high pressure (see below).

The various techniques to generate high pressures up to a few hundred GPa are beyond the scope of this review. The diamond anvil cell (DAC) technique has gained high popularity during the last decades thanks to its feasibility and wide range of experimental techniques which can be applied [180]. High-pressure techniques and experimental applications have been reviewed by Eremets [181] and by Hemley et al. [182]. X-ray diffraction and absorption studies utilizing the DAC technique were discussed by Briester [183].

Sulfur has been studied over a wide range of temperatures (a few ten mK to 1500 K) and static pressures (up to about 230 GPa). The pressure-temperature (p - T) phase diagram has already been reviewed during the last three decades by several authors (by Donohue, Meyer, Cannon, and Pistorius in the 1970s [3, 8, 184, 185], by Liu and Bassett in 1986 [186], by Young [187] and by Tonkov in the 1990s [188]). Therefore, we focus here only on the results of the last 15 years with the emphasis on high-pressure structures of solid sulfur. Unfortunately, numerous results on the p - T diagram of elemental sulfur reported in the literature are contradictory and often irreproducible from one laboratory to another. The most frequent experimental methods applied in high-pressure studies on sulfur during the last decade are X-ray diffraction techniques, vibrational spectroscopy (mainly Raman spectroscopy), optical absorption spectroscopy, measurements of the electrical resistivity, and, more recently, measurements of the magnetic susceptibility. While the DAC technique allows samples to be subjected to very high pressures, theoretical calculations of the electronic band structure of sulfur under ultrahigh pressure conditions have been developed simultaneously [189–192].

The p - T phase diagram of sulfur is about the most complicated amongst the chemical elements, and many open questions still exist with respect to phase boundaries, structures in detail, and kinetics of phase transitions in the solid as well as in the liquid state. Not only the molecular and crystalline variety of sulfur contributes to this complexity but also the metastability of high-pressure phases which is related to the application of different experimental procedures. For example, early structural studies on the p - T phase diagram of sulfur could not be performed in-situ. Therefore, in these experiments the sulfur samples were quenched from a selected temperature-pressure point to STP conditions. The results obtained by such a procedure depend strongly on the variables ΔT and Δp as well as on their time derivatives (gradients), dT/dt and dp/dt , respectively. Especially, dynamic compression (shock wave) methods may introduce further complications since melting of

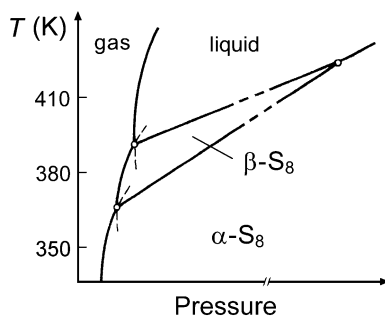


Fig. 22 Schematic phase diagram of sulfur around the α - β -liquid-gas states at low pressures (cf. Table 24). Pressure scale is in arbitrary units

the sample combined with large gradients of the thermodynamic parameters of state along the shock front have to be taken into account [193].

When the high intensity synchrotron X-ray sources became available a major problem of the former structural investigations was overcome. However, the low X-ray scattering intensity of sulfur makes detailed structural analyses still difficult, particularly in high-pressure apparatuses dealing with extremely small sample volumes of the order of 10^{-4} mm³.

3.2

Triple Points in the Vicinity of the Melting Curve

The melting curve of sulfur with respect to metastability and experimental procedures has been critically analyzed by Vezzoli and Walsh [194]. The authors also discussed the previously reported phase boundaries of the solid high-pressure allotropes in the range up to 4 GPa and from room temperature up to about 670 K [132]. However, the structures of these high-pressure polymorphs are unknown and their probability to exist under equilibrium conditions is still awaiting confirmation.

The p - T phase diagram near the α - β transition of crystalline S₈ has been studied and the triple-points of the solids in equilibrium with the vapor and the liquid were determined; see Fig. 22.

Under higher pressures, liquid sulfur shows several additional transitions [195]. Near the melting point at 12 GPa and 1100 K, the melt transforms to a metallic liquid state the pressure of metallization being much lower than in the solid state (\sim 80–90 GPa at room temperature) [196]. The most reliable critical points in the vicinity of the melting curve of sulfur are listed in Table 24.

Table 24 Critical points in the high-pressure high-temperature phase diagram of sulfur

Phase boundary	Pressure (Pa)	Temperature (K)	Reference
α - β -gas ^a	0.50	368.7	[74]
β -liquid-gas	2.4	393	
α - β -liquid	$0.131 \cdot 10^9$	424	
IV-VI-liquid ^b	$0.85(1) \cdot 10^9$	508(5)	[197]
	$0.9(1) \cdot 10^9$	528(2)	[132, 194]
VI-VIII-liquid ^b	$1.2(5) \cdot 10^9$	563(5)	[197]
	$1.8(2) \cdot 10^9$	617(2)	[132, 194]
VIII-XII-liquid ^c	$2.06 \cdot 10^9$	648	[132, 194]
VIII-XI-XII ^c	$2.6 \cdot 10^9$	508	[132, 194]
γ -L-L' ^d	$7.8(4) \cdot 10^9$	960(30)	[196]
δ -L'-L''	$12(5) \cdot 10^9$	1100(30)	

^a The α -phase and the β -phase are often called SI and SII, respectively, which should be avoided since the use of Roman numbers is not consistent in the literature

^b Data derived from in-situ visual inspection

^c Phase XII can be assigned to (solid) polymeric sulfur on the basis of X-ray diffraction and Raman spectroscopic results. The critical points are results of temperature-pressure quenching experiments. Therefore, the data may only reflect the range of p - T conditions from which S XII has been obtained. The nature of the other forms (IV, VI, VIII, XI) is unknown

^d L and L' denote non-metallic liquid phases. The phase L'' is believed to be a metallic phase of the melt. The symbols γ and δ denote solid phases; however, neither the structures of these solids nor their relationships to known phases have been mentioned by the authors

3.3

High-Pressure Structures

3.3.1

General

Generally, the group 16 elements of the periodic table show a tendency towards close-packing and increasing coordination number (CN) with increasing atomic number. The progression is: diatomic molecule (O_2 , CN=1)→insulating molecular solid (S_8 , CN=2)→semiconductor (Se and Te chain, CN=2+2)→metal (Po, CN=6). Under increasing high pressure these elements exhibit the same tendency [198]. From similarities of the melting curves of S, Se, and Te and from an analysis of the high-pressure structures of Se and Te it was to be expected that sulfur would undergo analogous phase transitions including metallization [195, 199–201]. A transition of sulfur to conducting and superconducting states has been reported several times. The transition pressures were found in the range 17.5 to 50 GPa (by measurements of electrical resistivity and extrapolation from optical absorption data), but at last it was stated that sulfur is “not very metallic” or “still a semiconductor” up to 50 GPa [202, 203]. More recent high-pressure X-ray

structural and optical studies revealed a transition to a metallic state in the range 80–100 GPa [200, 201, 204] besides several structural transitions up to ~200 GPa which will be summarized below.

3.3.2

Photo-Induced Structural Changes ($p < 20$ GPa)

In the pressure range up to about 20 GPa at least five phase transitions have been observed by Raman and X-ray investigations, in which however transition pressures and pressure ranges of phase stabilities were reported with significant discrepancies. These confusing results can partially be understood by taking into account the pressure dependence of the indirect optical absorption edge of sulfur as well as the different experimental conditions, mainly the energy and the power density of the laser light used to excite the Raman spectra and/or the ruby fluorescence for pressure determination [205].

In detail, Wang et al. observed by X-ray diffraction a structural transition of orthorhombic α -S₈ to a triclinic structure at 5.3 GPa. Raman spectra at high pressures, using the 515 nm line of an Ar ion laser, showed the lines of α -S₈ up to 5.13 GPa; at about 6 GPa, the spectra were reported as featureless [206]. Later, Nagata et al. on the basis of own X-ray diffraction studies claimed that the triclinic lattice parameters reported by Wang et al. can be transformed into the orthorhombic parameters of α -S₈ at that pressure [207]. In addition, these authors reported X-ray diffraction patterns of α -S₈ up to the maximum pressure of 8.3 GPa which did not reveal any indication of a phase transition. On the other hand, Nagata et al. have observed changes in the Raman spectrum of α -S₈ at 5.2 GPa indicating a transformation to a phase which had previously been reported by other investigators [208, 209]. It was concluded that the sample transformed only at the spot illuminated by the laser (wavelength of the laser line: 515 nm). Wolf et al. studied this phase transition by Raman spectroscopy using different laser energies [208]. The authors found that near 6 GPa radiation of 515 nm wavelength could initiate the phase transformation, but light of 488 and 530 nm was less efficient, and light of 600 nm was not effective at all. These findings are in accordance with results of previous Raman studies up to 9 GPa and 12 GPa, respectively, employing red laser light [210, 211]. Furthermore, by infrared spectroscopy it was shown that α -S₈ is observable up to about 10 GPa, although the ruby fluorescence method was used for pressure determination [212]. In the studies by Wolf et al., 600 nm light was effective to induce the transition at 12 GPa, but not 515 nm light. Therefore, the authors concluded that the transformation was due to a photo-reaction of sulfur [208]. In contrast to the results of Nagata et al., Wolf et al. observed a hysteresis upon decompression according to Raman studies of Eckert et al. [209] in which the transition to the photo-induced sulfur, p-S, could be initiated under nearly the same conditions as those reported by Nagata et al. [207].

Prior to these studies, the Raman spectrum of the photo-induced sulfur, p-S, has never been reported. Based on the discrete features of the Raman spectrum shown in Fig. 23 a certain molecular and crystalline structure for

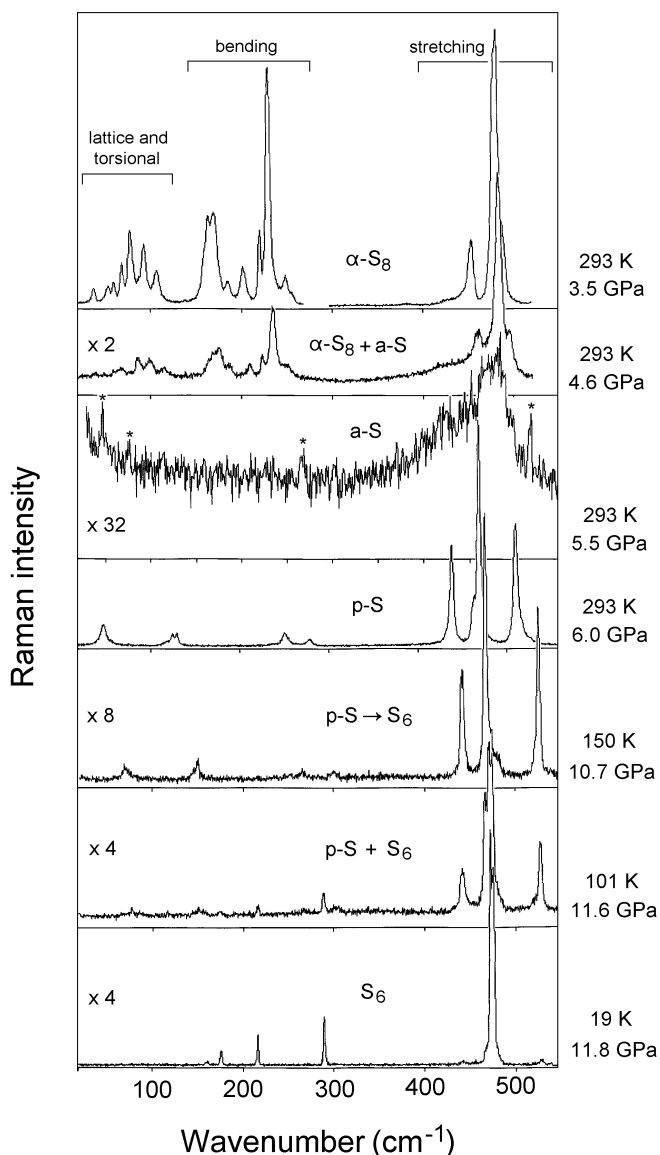


Fig. 23 Evolution of the Raman spectra during a high-pressure low-temperature experiment on elemental sulfur (from *top to bottom*, factor of magnification of the intensity scale is indicated). The wavenumber range of characteristic vibrations in sulfur is shown in the case of α -S₈ (wavelength of the laser: 515 nm; power density at the sample: ca. 150 μ W μ m⁻²). Starting with α -S₈ the onset of amorphization is seen at about 5 GPa, the transformation to p-S occurred at about 6 GPa, upon further increasing the pressure and cooling down the sample a transformation to S₆ took place. At low temperatures, the transition p-S \rightarrow S₆ is thermally hindered resulting in a larger background scattering due to structural reorientation. Plasma lines of the Ar ion laser are marked by *asterisks*

p-S was suggested. Considering the negative slope of the frequency of one of the S-S stretching vibrations under pressure, the low number of Raman lines and their intensity ratios (stretching vs bending) as well as the kinetics of the transition a chain structure was proposed [205, 207, 213].

The investigation of the high-pressure behavior of sulfur was additionally complicated by the observation of an amorphous phase in the Raman spectra around 5 GPa when a laser line of wavelength 515 nm was applied [209]. Later, it was proved that amorphous sulfur (a-S) appears as an intermediate state between two crystalline phases, the orthorhombic α -S₈ and the photo-induced structure, p-S [205, 213–215]. Moreover, the amorphous phase was found to be photo-induced, too. Systematic Raman studies on the disappearance of the α -S₈ lines and on the amorphization transition, which made use of different excitation laser energies, provided strong evidence for a correlation of the pressure-tuned red shift of the (indirect) optical absorption edge and the photo-induced ring-opening due to the laser illumination [205, 213, 216].

The controversies in the Raman studies were also reflected by the results of X-ray structural studies. Krüger et al. [217] and Akahama et al. [201] did not observe any transition of α -S₈ up to about 35 GPa and 25 GPa, respectively. However, Luo and Ruoff [218] could follow the diffraction pattern of α -S₈ up to 4.9 GPa, but at 5.3 GPa the diffraction lines indicated a transition to a monoclinic lattice which then was observed up to about 24 GPa. It should be noted that the authors used the 488 nm line of an Ar ion laser for ruby pressure determination. Shortly after, Yoshioka and Nagata [219] reported X-ray diffraction patterns of α -S₈ up to 7.6 GPa proving that the pattern at 5.3 GPa obtained by Luo and Ruoff agrees with that of orthorhombic sulfur at 6 GPa according to their previous results [207].

Furthermore, by application of a higher laser power a transformation of p-S to S₆ at a pressure of around 11 GPa could be induced [205, 208, 211, 215, 219, 220]. With increasing pressure, the Raman lines of S₆ could be observed up to about 45 GPa. However, at about 30–35 GPa new lines appeared in the spectra indicating the formation of a novel high-pressure species [211, 221]. Apart from pressure induced frequency shifts and intensity changes, the Raman spectrum of high-pressure S₆ is identical with that of rhombohedral S₆ chemically prepared at ambient conditions [34, 211, 222–224]. Although S₆ was considered to be a high-pressure high-temperature phase of sulfur [211], a more recently performed Raman investigation of the high-pressure low-temperature phase diagram has found S₆ as the dominant allotrope below 100 K at about 11 GPa (see Fig. 23) [205]. On the other hand, results of in-situ X-ray diffraction studies of sulfur at temperatures much higher than room temperature and at pressures of about 10–13 GPa were interpreted controversially with respect to the presence of S₆ [225, 226].

In summary, upon compression of orthorhombic sulfur a sequence α -S₈→a-S→p-S→S₆ with transition pressures of about 5 GPa, 6 GPa, and 11±2 GPa, respectively, were found in Raman studies if laser light with a wavelength of 515 nm was applied and if a certain threshold of the power density of the laser at the sample was exceeded. Since the Raman spectra

show a coexistence of the phases within a pressure range of 1–2 GPa it is likely that the transitions are of second order. In addition, a reverse sequence was found upon decompression accompanied by pressure hysteresis effects of the order of a few GPa. The full reversible back-transformation to α -S₈ occurs below about 0.5 GPa. However, the lattice needs ca. one day for structural healing at room temperature and 0.25 GPa as was deduced from the time evolution of the Raman spectra [213]. It is interesting to note, that upon increasing the pressure on the sample the time constants of the transitions were found significantly smaller than upon decreasing (seconds to minutes *vs.* hours to days) according to the persistence of metastable states.

If the (averaged) power density of the laser was below about $30 \mu\text{W} \mu\text{m}^{-2}$ no transition of a-S to p-S could be induced. Then, a-S was observable up to 15 GPa, the maximum pressure in the experiments, even if the laser light was of relatively high energy (488 nm) [205].

The transformation of α -S₈ to a-S is correlated to the pressure-tuned red-shift of the optical absorption of sulfur. The amorphization mechanism was interpreted in terms of ring-opening by photo-excitation in accordance with molecular dynamics simulations on bond scission in liquid sulfur [123, 227] and observations of biradicals after irradiation (see the section “Photochemical Behavior” above and [61]). After photo-induced bond breaking the chain-ends of the molecular fragments are allowed to recombine randomly leading to a disordered molecular structure. In the Raman spectra this transition is observable by the simultaneous disappearance of discrete features of the bending, torsional and lattice modes as well as by broadening and frequency shifts of the stretching vibrations [228]. The onset of amorphization has been reported at pressures where the laser energy was about 0.22 ± 0.04 eV above the absorption edge which agrees reasonably well with the torsional *trans*-barrier of about 0.28 eV ($\sim 27 \text{ kJ mol}^{-1}$) in S_n chains [148]. Therefore, the laser light also provides the activation energy for torsional isomerizations. The role of pressure is to act as a tool in tuning the equilibrium between the recombination into rings or chains (Table 25).

The pressure at which p-S can be obtained is about 1 GPa higher than the pressure of amorphization. While a-S was found at low temperatures too, the generation of p-S is favored at higher temperatures (about >200 K). Upon decompression (<1.5 GPa) Raman spectra of a solid identical to those as reported for S_μ appeared. Upon further unloading a reversible back-transformation to α -S₈ took place. However, the Raman spectra of S_μ retained, and at STP conditions the spectra could be observed for months while the sample showed slow recrystallization to α -S₈. Raman spectra of S_μ were obtained only if the sample had previously been transformed to p-S. Upon unloading of pure a-S only α -S₈ was observed as the result of decompression.

Once a formation of p-S was induced a relatively high power density of about $0.1\text{--}3 \text{ mW} \mu\text{m}^{-2}$ is required to initiate the formation of S₆ [205, 232]. It appears that if there is a dependence on the laser energy to induce S₆ it must be small. In contrast, amorphization and formation of p-S depend strongly on the laser energy (Table 25).

Table 25 Correlation of the photo-induced amorphization of α -S₈ with the laser energy and the pressure tuned absorption edge [205, 216]

Laser		Transition pressure (GPa) ^a		Absorption edge (eV) ^b
Wavelength (nm)	Energy (eV)	Loading	Unloading	
488.0	2.541	3.5 (2.6–4.3) 4.0 ^c	1.9 (2.7–1.0)	2.37
514.5	2.410	4.7 (3.8–5.5) 5.7 ^c	2.8 (4.1–1.5)	2.14
600.0	2.067	10.1 (8.8–11.4)	9.3 (10.2–8.3)	1.86 -
632.8	1.960	12.0 ^c	-	1.70

^a Mean values of the transition (pressure range in brackets) obtained from single crystal samples. Error $< \pm 0.1$ GPa

^b Absorption edge energy at the onset pressure of amorphization based on the optical absorption data given by Peanasky et al. [229], by Lorenz and Orgzall [214], and by Syassen [230]. Data have partly been adjusted to the indirect absorption edge of α -S₈ at STP conditions reported by Abass et al. [231]

^c Pressure values at which the lines of α -S₈ disappeared in the Raman spectra [216]. These values correspond to those reported [205] at which the amorphization transition was completed

3.3.3

High-Pressure High-Temperature Phases ($p < 20$ GPa, $T > 300$ K)

Only a few in-situ X-ray structural studies have been performed at high-pressure and high-temperature conditions [135, 225, 226]. By laser-heating of sulfur at 11 GPa a mixture of two phases was observed which consisted of room-temperature sulfur (α -S₈) and a phase which was not indexed by the authors [225]. However, by evaluation of the diffraction lines it was concluded that this phase cannot be interpreted as S₆ as had previously been suggested on the basis of Raman studies [211].

In the pressure-temperature range up to 16 GPa and 1170 K three phases of sulfur were found as “stable”, namely in the pressure ranges of 3–8 GPa, 8–15 GPa, and above 15 GPa, respectively [226]. All phase transitions were reported to occur only at temperatures above 570 K. In addition, the phases were found to be unquenchable to STP conditions. The structure of the lower pressure phase was automatically indexed as a hexagonal unit cell with the parameters $a=697.6(1)$ and $c=429.1(2)$ pm at 4.2 GPa and 300 K, containing nine atoms. The crystal structure was compared with those of hexagonal selenium and tellurium, and therefore a helical structure of sulfur was assumed. The phase at 8–15 GPa was interpreted as S₆ with a hexagonal unit cell containing 18 atoms. The phase above 15 GPa remained unsolved in these studies. All three phases showed a large hysteresis.

Independently, a two-chain helical structure was found at 3 GPa and 673 K by Chrichton et al. [135]. A hexagonal unit cell with $a=709.08(5)$ and $c=430.28(6)$ pm has been obtained which was refined to a trigonal lattice

($P3_221=D_3^6$, no. 154). The unit cell contains nine atoms on two unique sites. The two helices are reported as non-chiral having repetitions along the c -axis with one turn including three atoms (3S_1 helix). The bond lengths and the bond angles of the two helices are similar in deviating from those of the sulfur helix in the fibrous allotrope S_{ψ} [helix 1: 207.0(4) pm, 102.7(2)°; helix 2: 209.6(7) pm, 101.7(3)°; S_{ψ} : 206.6 pm, 106.0°]. A calculation of the torsion angles (applying Tuinstra's formula [54]) gives 100.4° and 99.7° for helix 1 and helix 2, respectively, in comparison with 85.3° in the S_{ψ} chain. Although temperature-quenchable, this two-chain phase was observed to transform below 0.5 GPa to a phase which has been reported earlier by other authors as high-pressure fibrous sulfur or S-XII (see the above section "Allotropes Consisting of Long Sulfur Chains").

3.3.4

High Pressure Phases above 20 GPa

In the pressure range (20–80 GPa) there are also contradictions between the reported phase transitions. While Krüger et al. [217] detected only one phase transition up to 40 GPa, Luo et al. [200, 218] and Akahama et al. [201] reported two phase transitions. In fact, the phase transition observed by Krüger et al. was interpreted as a first order transition from orthorhombic α - S_8 to a trigonal modification at about 33 GPa. A similar transition pressure was mentioned by Häfner et al. based on X-ray studies but without providing further details [233]. Raman spectroscopic studies demonstrated that S_6 may have partly been transformed to another allotrope above 35 GPa [211]. By means of impedance spectroscopy, a change in the behavior of the sulfur sample around 37 GPa was reported [234]. Luo and Ruoff [200] could follow the monoclinic phase (which possibly has been a result of a photo-induced reaction at about 5 GPa due to the laser irradiation) up to about 24 GPa while above 18 GPa a significant decrease in intensity and broadening of the diffraction lines took place. At about ≥ 25 GPa, the diffraction pattern was reported as characteristic of an amorphous structure making a quantitative analysis impossible. The pressure-induced amorphization was found to start at about 18 GPa and to be completed at 25 GPa.

Optical absorption studies by Luo et al. revealed a discontinuity of the energy gap, E_{gap} , between 23 and 30 GPa (of about +0.2 eV) accompanied by a change of the slope dE_{gap}/dp above 30 GPa down to 20% [204, 235]. In reflectivity spectra, an increase of the signal intensity of about 3% (at 0.5 eV) and 9% (at 3.0 eV) was observed upon rising the pressure to 23 GPa which on further compression to 88 GPa increased by only a few additional percent.

On the other hand, Akahama et al. [201] could observe a diffraction pattern up to 17.5 GPa which they assigned to α - S_8 . Similar to the X-ray studies of Luo et al., the intensity of the diffraction lines decreased with increasing pressure, and at about 26.5 GPa no lines could be recognized any longer.

Although the transition pressures and the starting phases were reported differently, it is plausible that there is a (second order) phase transition with an onset pressure of about 18 GPa and completion at about 25–26 GPa. This

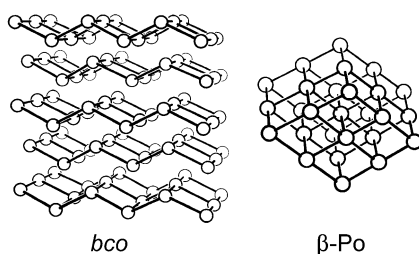


Fig. 24 Proposed structures for the observed high-pressure phases of sulfur above ca. 80 GPa [8]. For the more simple *sc*, *bcc*, and *fcc* structures, see textbooks on solid state physics/chemistry

phase is amorphous; however, nothing is known about its structure. It is not clear yet if this pressure-induced amorphous sulfur has any relation to the photo-induced amorphous sulfur observed in high-pressure Raman studies. Indeed, as in the case of the photo-induced transformations ($\alpha\text{-S}_8 \rightarrow \text{a-S} \rightarrow \text{p-S}$) the pressure-induced amorphization is an intermediate state between two crystalline forms towards close-packing upon further compression [236].

At 34 GPa, Akahama et al. [201b] recorded diffraction patterns indicating the presence of a single crystal since the Bragg reflections were observed as “spotty”. The transition was interpreted as a process of recrystallization and reorientation. Luo et al. [200] reported a transition from the amorphous phase at 37 GPa at which a single intense peak appeared in the diffraction spectra. A second intense peak was observed at 42 GPa and the transition was found to be accomplished at 75 GPa. In both investigations the structures were not analyzed. However, there might be some relation to the trigonal phase observed by Krüger et al. above 32 GPa [217]. The diffraction lines of this unknown phase, termed S-II by Akahama et al., became weaker with increasing pressure, and at 89 ± 2 GPa, the lines had completely vanished [201].

Amaya et al. reported a stepwise change of the electrical resistivity of sulfur at room temperature and pressures of about 40 and 90 GPa, respectively [178b]. The changes in electrical resistivity can be reasonably interpreted as insulator-to-semiconductor and semiconductor-to-metal transitions.

At 82–84 GPa, in the studies of Akahama et al. [201] and Luo et al. [200], respectively, new diffraction lines appeared which were indexed as a base-centered orthorhombic (*bco*) lattice (Fig. 24). On theoretical grounds, such a structure should be metallic [190, 237]. Luo et al. stated that the transformation from the unknown phase to the *bco* phase was not completed until about 100 GPa because of the persistence of a diffraction peak from the previous phase. On the other hand, Akahama et al. reported a transition pressure of about 89 GPa. The *bco* phase showed a hysteresis of about 6 GPa upon lowering the pressure [201]. Further evidence for the transition to a metallic phase comes from the optical reflectivity measurements of Luo et al. [204]. Below 88 GPa, the reflectivity was reported to be low (typically

1–7% in the spectral range from the infrared to the ultraviolet). Under increasing compression from 88 GPa to 95 GPa an abrupt and large increase of the reflectivity (up to about 30%) was found which on further compression reached a value of about 62% reflectivity below about 2 eV incident photon energy. From visual observation both groups reported that “the appearance of the sample has become even shinier than the metallic gasket” surrounding the sulfur sample. Thus, it was suspected that sulfur has been transformed to a metallic phase at around 93 GPa [201, 204].

By comparison of the lattice constants of the *bco* phase of sulfur (termed S-III by Akahama et al.) with those of *bco* selenium (termed Se-IV) Akahama et al. obtained a unique value of about 1.16 for the ratios as compared to the ratio of 1.15 for the bond lengths of selenium and sulfur at STP conditions. In addition, the intensity ratios of the diffraction peaks of S-III resemble those of Se-IV. Therefore, the authors concluded that the crystal structure of S-III should be isomorphous to *bco* selenium (Se-IV) [201].

The structural model of metallic *bco* sulfur is proposed as puckered layers in which the sulfur atoms have a coordination number of 4 within the layer (see Fig. 24). The unit cell contains segments of three layers. The layers are stacked in the *b*-axis direction whereas adjacent layers are shifted alternately by one-half of the cell parameter *c*. The *b*-*c* plane provides the base-center of the *bco* structure. The primitive cell then contains four atoms [201].

The optimized lattice constants of a slightly simplified model structure for the *bco* phase of sulfur have been calculated by pseudo-potential ab-initio and energy minimization methods [190]. The results obtained agree with the experimental results within a few percent. The experimental lattice parameters of *bco* sulfur are summarized in Table 26.

The transition to the metallic *bco* phase at room temperature has found its counterpart at low temperatures in the formation of a superconducting state. At a pressure of about 93 GPa the critical temperature T_c of the superconducting transition was found at about 10 K [179]. With increasing pressure T_c increases to about 17 K near pressures of about 160 GPa at which an additional room-temperature phase transition, from the *bco* phase to the β -Po structure, was reported. The increase in T_c was attributed to a stiffening of the lattice or, in other words, due to the contribution of higher energy phonons rather than changes of the electron-phonon coupling [192].

The transition from the *bco* structure to the β -Po structure was observed at 162 ± 5 GPa and characterized as “very gradually and subtly” [200]. In the β -Po structure the S atoms are sixfold coordinated with nearest neighbors at a distance of 258.4 pm (Fig. 24). The rhombohedral unit cell, which can be derived from a body-centered cubic structure by a rhombohedral distortion, contains one atom. The transition from the *bco* to the β -Po structure was interpreted as of second order due to the absence of any volume change at the transition (both structures have the same atomic volume of $8.5 \text{ \AA}^3 = 8.5 \times 10^6 \text{ pm}^3$) [200]. On the other hand, the transition is expected to be of first order due to symmetry considerations [191]. In fact, the *bco* structure is of $Cmcm$ (D_{2h}^{17}) symmetry while β -Po belongs to $R\bar{3}m$ (D_{3d}^5). To solve this discrepancy a model for the lower pressure β -Po structure was

Table 26 Lattice parameters of sulfur at room temperature and pressures above 20 GPa obtained by X-ray diffraction studies [200, 201, 217, 218]

Structure	Pressure (GPa)	Lattice parameters (pm)	Z^a	
CN ^b				
Monoclinic ^c	5.3	$a=983$ $b=1033$ $c=2065$ $\beta=79.34^\circ$?	?
Trigonal	38–40	$a=b\sim 724$ $c\sim 385$?	?
Base-centered orthorhombic (bco)	89.4	$a=346.96(36)$ $b=524.22(68)$ $c=222.02(34)$	4	4
^d $Cmcm$ (D_{2h}^{17})	145	$a=330.93$ $b=496.98$ $c=214.46$		
β -Po (rhombohedral) ^e	207	Trigonal setting $a=207.9$ $\alpha=104.03^\circ$	1	6
$R\bar{3}m(D_{3d}^5)$		Hexagonal setting $a=327.7$ $c=258.4$ $c/a=0.789$	3	6

^a Z =Atoms per unit cell

^b CN=Coordination number

^c The monoclinic form at above 5.3 GPa reported by Luo et al. might be assessed as an incorrect assignment [219]

^d Metallic phase with superconducting temperatures of about 10 K (at ~ 90 GPa) raising to 17 K (at ~ 160 GPa, where the transition to the β -Po structure occurs)

^e Metallic phase with decreasing superconducting temperature upon increasing pressure (~ 15 K at 231 K) [179]

proposed based on a monoclinic distortion of the rhombohedral unit. In this model, the rhombohedral structure was considered as a base-centered monoclinic structure of $B2/m$ (C_{2h}^3) symmetry with $Z=6$ atoms per unit cell [191].

In the X-ray studies of Luo et al. the β -Po phase could be observed up to at least 212 GPa, the highest pressure achieved in the experiments [200]. From an analogy of the ratio of the lattice constants c/a in Se and Te (~ 0.72), at pressures where the body-centered cubic (bcc) structure is reached, a similar transition for sulfur was estimated to take place around 700 GPa [200].

Zakharov and Cohen predicted a pressure of about 550 GPa for the β -Po to bcc transition on the basis of pseudopotential ab-initio calculations [190]. In addition, a critical temperature of 15 K for the superconducting transition in the vicinity of the β -Po to bcc transition was estimated. This relatively high value was attributed to an enhancement of the electron-phonon coupling near the structural transition. Although the lattice parameters of bco and β -Po sulfur have fairly been reproduced by the calculations, the model failed in reproducing the experimentally observed bco to β -Po transition. At 145 GPa, the calculated total energy of the bco structure was found higher than that of the β -Po structure.

On the other hand, Rudin et al. [192] found theoretically a progression β -Po \rightarrow simple cubic (sc) \rightarrow bcc instead of the previously expected β -Po \rightarrow bcc transition for sulfur by analogy with selenium and tellurium. In addition, the face-centered cubic (fcc) structure of Se (and Te) stable at pressures

above the *bcc* structure was found to be energetically unfavorable in the case of sulfur. Accordingly, the differences between the structural sequences of sulfur and selenium were interpreted in terms of differences in the electronic core states, especially arising from the presence of a strongly attractive *d*-pseudopotential in sulfur due to the lack of *d*-states. On the other hand, the *d*-pseudopotential in selenium, which has *d*-states in the core region, is relatively weak. Therefore, in the energy calculations the electron-ion contribution was found to stabilize the *sc* structure for sulfur in comparison with the *bcc* structure.

A drop of the temperature of the superconducting transition in *sc* sulfur down to 7 K (at 280 GPa) and 1 K (at 550 GPa) was predicted on the basis of changes in the phonon density of states, that is a distinct stiffening of the *sc* lattice in comparison with the β -Po and the *bcc* structures [192].

3.4

Conclusion

In conclusion, orthorhombic sulfur α -S₈ seems to be stable up to at least 20–30 GPa. However, in this pressure range several additional phases (*a*-S, *p*-S, S₆) were observed which are generated by photo-induced ring-opening and re-crystallization processes due to the application of laser radiation. At high-pressure high-temperature conditions (3–8 GPa, >600 K) a two-chain structure with a trigonal unit cell was found. In the pressure range of about 20–35 GPa sulfur exists in an amorphous state and, upon increasing pressure, transforms to an unknown (trigonal?) phase existing up to about 80–90 GPa. Around 90 GPa, sulfur undergoes a transition to a *bco* phase and at about 160 GPa to the β -Po phase both structures being metallic with superconducting properties below 20 K.

A transition to the more close-packed *bcc* structure was estimated to occur at pressures ranging from 500 to 700 GPa. However, theoretical calculations suggest the existence of a *sc* phase stable between 280 and 500 GPa prior to the *bcc* structure. Accordingly, the structural phase sequence of sulfur is different from those of selenium and tellurium in following the order *bco*→ β -Po→*sc*→*bcc* at pressures above ~80 GPa.

Acknowledgements One of the authors (B.E.) appreciates the support of parts of the work (Photo-induced Amorphization of Sulfur at High Pressures and High-Pressure Low-Temperature Phase Diagram of Sulfur) by NATO research grants and by the European Community (LENS facility). This work has also been supported by the Deutsche Forschungsgemeinschaft and the Verband der Chemischen Industrie.

References

1. Gmelin *Handbuch der Anorganischen Chemie*, 8. Aufl., Schwefel, Teil A, Lieferung 2, Springer, Berlin, 1974, and Lieferung 3, VCH, Weinheim, 1953.
2. M. Schmidt, *Angew. Chem.* **1973**, *85*, 474; *Angew. Chem. Int. Ed. Engl.* **1973**, *12*, 445.
3. B. Meyer, *Chem. Rev.* **1976**, *76*, 367.
4. R. Steudel, *Top. Curr. Chem.* **1982**, *102*, 149.

5. R. Steudel, in: *Sulfur—Its Significance for Chemistry, for the Geo-, Bio- and Cosmo-sphere and Technology* (A. Müller, B. Krebs, eds.), Elsevier, Amsterdam, 1984, p. 3.
6. R. Steudel, in: *The Chemistry of Inorganic Homo- and Heterocycles*, Vol. 2. (I. Haiduc, D. B. Sowerby, eds.), Academic Press, London, 1987, p. 737.
7. R. Laitinen, P. Pekkonen, R.J. Suantamo, *Coord. Chem. Rev.* 1994, 130, 1.
8. For a critical review see: J. Donohue, *The Structures of the Elements*, Wiley, New York, 1974, p. 324.
9. M. Engel, *Compt. Rend. Hebd. Scean. Acad. Sci.* 1891, 112, 866.
10. R. Steudel, H.-J. Mäusle, *Z. Anorg. Allg. Chem.* 1979, 457, 165.
11. H.-J. Mäusle, R. Steudel, *Z. Anorg. Allg. Chem.* 1980, 463, 27.
12. R. Steudel, H.-J. Mäusle, D. Rosenbauer, H. Möckel, T. Freyholdt, *Angew. Chem.* 1981, 93, 402; *Angew. Chem. Int. Ed. Engl.* 1981, 20, 394.
13. (a) H. Köpf, B. Block, M. Schmidt, *Chem. Ber.* 1968, 101, 272; (b) H. Köpf, B. Block, *Chem. Ber.* 1969, 102, 504.
14. R. Steudel, R. Strauss, *J. Chem. Soc. Dalton Trans.* 1984, 1775.
15. E. F. Epstein, I. Bernal, *J. Organomet. Chem.* 1971, 26, 229.
16. M. Schmidt, B. Block, H.D. Block, H. Köpf, E. Wilhelm, *Angew. Chem.* 1968, 80, 660.
17. R. Steudel, D. Jensen, B. Plinke, *Z. Naturforsch. Part B* 1987, 42, 163.
18. M. Schmidt, H.-D. Block, *Z. Anorg. Allg. Chem.* 1971, 385, 119.
19. R. Steudel, R. Strauss, L. Koch, *Angew. Chem.* 1985, 97, 58; *Angew. Chem. Int. Ed. Engl.* 1985, 24, 59.
20. R. Steudel, J. Steidel, J. Pickardt, F. Schuster, R. Reinhardt, *Z. Naturforsch., Part B* 1980, 35, 1378.
21. R. Steudel, F. Schuster, *J. Mol. Struct.* 1978, 44, 143.
22. R. Steudel, B. Holz, *Z. Naturforsch. Part B* 1988, 43, 581.
23. R. Steudel, E.-M. Strauss, M. Papavassiliou, P. Brätter, W. Gatschke, *Phosphorus Sulfur* 1986, 29, 17.
24. R. F. Bacon, R. Fanelli, *Ind. Eng. Chem.* 1942, 34, 1043.
25. H. v. Wartenberg, *Z. Anorg. Allg. Chem.* 1956, 286, 243; O. Skjerven, *Z. Anorg. Allg. Chem.* 1957, 291, 325 and 1962, 314, 206.
26. F. Fehér, H. D. Lutz, K. Obst, *Z. Anal. Chem.* 1967, 224, 407.
27. L. M. Goldsmith, C. E. Strouse, *J. Am. Chem. Soc.* 1977, 99, 7580.
28. W. Muthmann, *Z. Krist.* 1890, 17, 336.
29. Y. Watanabe, *Acta. Cryst.* 1974, B30, 1396.
30. a: A. C. Gallacher, A. A. Pinkerton, *Acta. Cryst.* 1993, C49, 125. b: N. Meisser, K. J. Schenk, E. Spangenberg, *Schweiz. Mineral. Petrogr. Mitt.* 2000, 80, 299.
31. J. A. Prins, J. Schenk, L. H. J. Wachters, *Physica* 1957, 23, 746.
32. M. Schmidt, E. Wilhelm, *J. Chem. Soc. Chem. Commun.* 1970, 1111.
33. R. Steudel, K. Bergemann, J. Buschmann, P. Luger, *Inorg. Chem.* 1996, 35, 2184.
34. R. Steudel, J. Steidel, T. Sandow, F. Schuster, *Z. Naturforsch. Part B* 1978, 33, 1198.
35. R. Steudel, J. Steidel, R. Reinhardt, *Z. Naturforsch. Part B* 1983, 38, 1548.
36. T. Sandow, J. Steidel, R. Steudel, *Angew. Chem.* 1982, 94, 782; *Angew. Chem. Int. Ed. Engl.* 1982, 21, 794.
37. J. Steidel, R. Steudel, *J. Chem. Soc. Chem. Commun.* 1982, 1312.
38. R. Steudel, J. Steidel, T. Sandow, *Z. Naturforsch. Part B* 1986, 41, 958.
39. F. Fehér, W. Laue, G. Winkaus, *Z. Anorg. Allg. Chem.* 1956, 288, 113.
40. See the Chapter on "Inorganic Polysulfanes" by R. Steudel, *Top. Curr. Chem.* 2003, in print.
41. M. Schmidt, G. Knippschild, E. Wilhelm, *Chem. Ber.* 1968, 101, 381.
42. R. Steudel, H.-J. Mäusle, *Angew. Chem.* 1979, 91, 165; *Angew. Chem. Int. Ed. Engl.* 1979, 18, 152.
43. R. Steudel, H.-J. Mäusle, *Z. Anorg. Allg. Chem.* 1981, 478, 156.
44. R. Steudel, H.-J. Mäusle, *Angew. Chem.* 1978, 90, 54; *Angew. Chem. Int. Ed. Engl.* 1978, 17, 56.
45. A. K. Verma, T. B. Rauchfuss, S. R. Wilson, *Inorg. Chem.* 1995, 34, 3072.

46. R. Steudel, O. Schumann, J. Buschmann, P. Luger, *Angew. Chem.* **1998**, *110*, 2502; *Angew. Chem. Int. Ed.* **1998**, *37*, 2377.
47. R. Strauss, R. Steudel, *Z. Naturforsch. Part B* **1988**, *43*, 1151.
48. For a review of the literature up to 1980, see: R. Steudel, *Z. Anorg. Allg. Chem.* **1981**, *478*, 139.
49. See the review on liquid sulfur by R Steudel, *Top. Curr. Chem.* **2003**, in this Volume.
50. J. C. Koh, W. Klement, *J. Phys. Chem.* **1970**, *74*, 4280.
51. E. C. Missbach, Stauffer Chem. Co., U.S. Patent Nr. 2419324 (1947).
52. F. Tuinstra, *Acta Cryst.* **1966**, *20*, 341.
53. D. B. Nash, *Icarus* **1987**, *72*, 1.
54. F. Tuinstra, *Structural Aspects of the Allotropy of Sulfur and the Other Divalent Elements*, Waltman, Delft, **1967**.
55. R. Steudel, S. Passlack-Stephan, G. Holdt, *Z. Anorg. Allg. Chem.* **1984**, *517*, 7.
56. H. Bartsch, *Kautschuk Gummi Kunststoffe* **1988**, *41*, 455 and **1974**, *27*, 72.
57. Crystex HS OT 10 is insoluble sulfur of high stability treated with 10% oil; Crystex HS OT 33 AS is a mixture of insoluble high stability sulfur with silica and 25% oil. The oil content suppresses dust formation.
58. J. N. Haimsohn, Stauffer Chem. Co., *US Patent Nr. 2757075* (1956).
59. See the review on sulfur vapor by R. Steudel, Y. Steudel, M. W. Wong, *Top. Curr. Chem.* **2003**, in this Volume.
60. R. Steudel, G. Holdt, A. T. Young, *J. Geophys. Res.* **1986**, *91*, 4971.
61. R. Steudel, J. Albertsen, K. Zink, *Ber. Bunsenges. Phys. Chem.* **1989**, *93*, 502 and references cited therein.
62. R. Steudel, *Angew. Chem.* **1975**, *87*, 683; *Angew. Chem. Int. Ed. Engl.* **1975**, *14*, 655.
63. A. W. H. Aten, *Z. Phys. Chem.* **1914**, *88*, 321.
64. J. Donohue, A. Caron, E. Goldish, *J. Am. Chem. Soc.* **1961**, *83*, 3748.
65. J. Steidel, J. Pickardt, R. Steudel, *Z. Naturforsch. Part B* **1978**, *33*, 1554.
66. D. S. Warren, B. M. Gimarc, *J. Phys. Chem.* **1993**, *97*, 4031; and literature cited therein.
67. D. Hohl, R. O. Jones, R. Carr, M. Parrinello, *J. Chem. Phys.* **1988**, *89*, 6823.
68. K. Raghavachari, C. M. Rohlfing, J. S. Binkley, *J. Chem. Phys.* **1990**, *93*, 5862.
69. J. Cioslowski, A. Szarecka, D. Moncrieff, *J. Phys. Chem. A* **2001**, *105*, 501.
70. The same argument holds for other odd-membered sulfur homocycles like S₉ or S₁₁, but the effect in these molecules is less dramatic.
71. R. Steudel, R. Reinhardt, F. Schuster, *Angew. Chem.* **1977**, *89*, 756; *Angew. Chem. Int. Ed. Engl.* **1977**, *16*, 715.
72. R. Steudel, M. Papavassiliou, K. Seppelt, *Z. Naturforsch. Part B* **1988**, *43*, 245.
73. A. Abraha, D. E. Williams, *Inorg. Chem.* **1999**, *38*, 4224.
74. R. Steudel, *Chemie der Nichtmetalle*, W. de Gruyter, Berlin, **1998**, p. 274.
75. R. Steudel, *Spectrochim. Acta Part A* **1975**, *31*, 1065.
76. P. Coppens, Y. W. Yang, R. H. Blessing, W. F. Cooper, F. K. Larsen, *J. Am. Chem. Soc.* **1977**, *99*, 760.
77. J. Wallis, I. Sigalas, S. Hart, *J. Appl. Cryst.* **1986**, *19*, 273.
78. B. Meyer, in *Elemental sulfur* (B. Meyer, ed.), Interscience, New York, **1965**, p. 71.
79. M. W. Wong, Y. Steudel, R. Steudel, *Chem. Phys. Lett.* **2002**, *364*, 387.
80. S. J. Rettig, J. Trotter, *Acta Cryst.* **1987**, *C43*, 2260.
81. L. K. Templeton, D. H. Templeton, A. Zalkin, *Inorg. Chem.* **1976**, *15*, 1999.
82. B. E. Warren, J. T. Burwell, *J. Chem. Phys.* **1935**, *3*, 6.
83. S. C. Abrahams, *Acta Cryst.* **1955**, *8*, 661.
84. G. S. Pawley, R. P. Rinaldi, *Acta Cryst.* **1972**, *B28*, 3605.
85. J. Kurittu, G. S. Pawley, *Acta Cryst.* **1973**, *A29*, 615.
86. C. Pastorino, Z. Gamba, *J. Chem. Phys.* **2001**, *115*, 9421. C. Pastorino, Z. Gamba, *Chem. Phys.* **2000**, *261*, 317.
87. B. Eckert, H. O. Albert, H. J. Jodl, P. Foggi, *J. Phys. Chem.* **1996**, *100*, 8212.
88. M. Becucci, R. Bini, E. Castellucci, B. Eckert, H. J. Jodl, *J. Phys. Chem.* **1997**, *101*, 2132.
89. J. T. Burwell, *Z. Krist.* **1937**, *97*, 123.

90. D. E. Sands, *J. Am. Chem. Soc.* **1965**, *87*, 1395.
91. R. L. Montgomery, *Science* **1974**, *184*, 562.
92. Y. M. De Haan, *Physica* **1958**, *24*, 855.
93. R. Steudel, T. Sandow, J. Steidel, *Z. Naturforsch. Part B* **1985**, *40*, 594.
94. S. Millefiori, A. Alparone, *J. Phys. Chem. A* **2001**, *105*, 9489.
95. M. Schmidt, E. Wilhelm, *Inorg. Nucl. Chem. Lett.* **1965**, *1*, 39.
96. F. Tuinstra, *J. Chem. Phys.* **1967**, *46*, 2741.
97. R. Reinhardt, R. Steudel, F. Schuster, *Angew. Chem.* **1978**, *90*, 55; *Angew. Chem. Int. Ed. Engl.* **1978**, *17*, 57.
98. M. Schmidt, E. Wilhelm, *Angew. Chem.* **1966**, *78*, 1020; *Angew. Chem. Int. Ed. Engl.* **1966**, *5*, 964.
99. A. Kutoglu, E. Hellner, *Angew. Chem.* **1966**, *78*, 1021; *Angew. Chem. Int. Ed. Engl.* **1966**, *5*, 965.
100. J. Steidel, R. Steudel, A. Kutoglu, *Z. Anorg. Allg. Chem.* **1981**, *476*, 171.
101. R. Steudel, *Z. Naturforsch. Part B* **1983**, *38*, 543.
102. L. Peter, *Phosphorus Sulfur Silicon* **2001**, *168*, 287.
103. T. Debaerdemaeker, A. Kutoglu, *Cryst. Struct. Commun.* **1974**, *3*, 611.
104. M. Schmidt, E. Wilhelm, T. Debaerdemaeker, E. Hellner, A. Kutoglu, *Z. Anorg. Allg. Chem.* **1974**, *405*, 153.
105. R. O. Jones, P. Ballone, *J. Chem. Phys.* **2003**, *118*, 9257.
106. H.-J. Mäusle, R. Steudel, *Z. Anorg. Allg. Chem.* **1981**, *478*, 177.
107. J. Schenk, *Physica* **1957**, *23*, 546.
108. J. Schenk, *Physica* **1957**, *23*, 325.
109. A. Smith, *Z. physik. Chem.* **1906**, *54*, 257.
110. J. A. Prins, J. Schenk, P. A. M. Hospel, *Physica* **1956**, *22*, 770.
111. S. R. Das, *Ind. J. Phys.* **1938**, *12*, 163.
112. S. R. Das, K. Ghosh, *Ind. J. Phys.* **1939**, *13*, 91.
113. O. Erämetsä, H. Suonuuti, *Suom. Kemi. Part B* **1959**, *32*, 47.
114. (a) O. Erämetsä, *Suom. Kemi. Part B* **1963**, *36*, 6. (b) O. Erämetsä, *Suom. Kemi. Part B* **1963**, *36*, 213.
115. F. Tuinstra, *Physica* **1967**, *34*, 113.
116. P. Hendra, P. Wallen, A. Chapman, K. Jackson, J. Loadman, M. van Duin, B. Kip, *Kautschuk Gummi Kunststoffe* **1993**, *46*, 694.
117. F. Cataldo, *Angew. Makromol. Chem.* **1997**, *249*, 137.
118. R. Bellisent, L. Descôtes, P. Pfeuty, *J. Phys. Condens. Matter* **1994**, *6*, A211.
119. M. Stolz, R. Winter, W. S. Howells, R. L. McGreevy, P. A. Egelstaff, *J. Phys.: Condens. Matter* **1994**, *6*, 3619.
120. F. H. Stillinger, T. A. Weber, R. A. LaViolette, *J. Chem. Phys.* **1986**, *85*, 6460. (b) F. H. Stillinger, T. A. Weber, *J. Chem. Phys.* **1987**, *91*, 4899.
121. J. S. Tsu, D. D. Klug, *Phys. Rev. B* **1999**, *59*, 34.
122. L. Descôtes, C. Bichara, *J. Non-Cryst. Solids* **1995**, *192 & 193*, 627.
123. (a) F. Shimojo, K. Hoshino, Y. Zempo, *J. Phys. Condens. Matter* **1998**, *10*, L177. (b) S. Munejiri, F. Shimojo, K. Hoshino, *J. Phys. Condens. Matter* **2000**, *12*, 7999. (c) S. Munejiri, F. Shimojo, K. Hoshino, *Comp. Phys. Comm.* **2001**, *142*, 131.
124. J. E. Mark, J. G. Curro, *J. Chem. Phys.* **1984**, *80*, 5262.
125. (a) M. Springborg, R. O. Jones, *Phys. Rev. Lett.* **1986**, *57*, 1145. (b) *J. Chem. Phys.* **1988**, *88*, 2652.
126. (a) M. Ezzine, A. Pellegatti, C. Minot, R. J.-M. Pellenq, *J. Phys. Chem. A* **1998**, *102*, 452. (b) M. Ezzine, A. Pellegatti, C. Minot, R. J.-M. Pellenq, J. Olivier-Fourcade, A. Boutilab, *New J. Chem.* **1998**, 1505.
127. J.-J. Trillat, J. Forestier, *Bull. Soc. Chim. France* **1932**, *51*, 248.
128. F. Tuinstra, *Acta Cryst.* **1966**, *20*, 341.
129. M. D. Lind, S. Geller, *J. Chem. Phys.* **1969**, *51*, 348.
130. S. Geller, M. D. Lind, *Acta Cryst. Part B* **1969**, *25*, 2166.
131. C. M. Looman, F. Tuinstra, *Physica* **1969**, *42*, 291.

132. G. C. Vezzoli, F. Dachille, R. Roy, *Science* **1969**, *116*, 218.
133. G. C. Vezzoli, R. J. Zeto, *Inorg. Chem.* **1970**, *9*, 2478.
134. C. B. Sclar, L. C. Carrison, W. B. Gager, O. M. Stewart, *J. Phys. Chem. Solids* **1966**, *27*, 1339.
135. W. A. Chrichton, G. B. M. Vaughan, M. Mezouar, *Z. Kristallogr.* **2001**, *216*, 417.
136. E.-M. Strauss, R. Steudel, *Z. Naturforsch. Part B* **1987**, *42*, 682.
137. R. Steudel, G. Holdt, A. Young, *J. Geophys. Res.* **1986**, *91*, 4971.
138. S. R. Das, *Silicon-Sulfur-Phosphates*, Colloq. Sec. Inorg. Chem. (IUPAC), Verlag Chemie, Weinheim, **1955**, p. 103.
139. See the review on aqueous sulfur sols by R. Steudel, *Top. Curr. Chem.* **2003**, in print.
140. (a) F. Michaud, J. Fourcade, E. Philippot, M. Maurin, M. Discours, in: *Proc. Int. Symp. Elemental Sulfur in Agriculture*, Vol. 2. Syndicat Française du Soufre, Marseille, **1987**, p. 789. (b) F. Michaud, *Thesis*, Université de Montpellier II, **1989**.
141. A. T. Ward, *J. Phys. Chem.* **1968**, *72*, 4133.
142. R. E. Barletta, W. Brown, *J. Phys. Chem.* **1971**, *75*, 4059.
143. W. Dultz, H. D. Hochheimer, W. Müller-Lierheim, in: *Proc. 5th Int. Conf. Amorphous and Liquid Semicond.* (J. Stuke, W. Brenig, eds.) Taylor and Francis, London, **1974**, p. 1281.
144. S. Geller, *Science* **1966**, *152*, 644.
145. R. B. Roof, *Aust. J. Phys.* **1972**, *25*, 335.
146. J. C. van Miltenburg, J. Fourcade, M. Ezzine, C. Bergmann, *J. Chem. Thermodyn.* **1993**, *25*, 1119.
147. M. Evain, M. Queignec, R. Brec, J. Rouxel, *J. Solid State Chem.* **1985**, *56*, 148.
148. Y. Drozdova, K. Miaskiewicz, R. Steudel, *Z. Naturforsch. Part B* **1995**, *50*, 889.
149. M. Schmidt, in: *New Uses of Sulfur, Part II* (D. J. Bourne, ed.), American Chemical Society, Washington, **1978**, p. 1.
150. L. Pauling, *Proc. Natl. Acad. Sci.* **1949**, *35*, 495.
151. See the review on molecular spectra of sulfur molecules and solid sulfur allotropes by B. Eckert, R. Steudel, *Top. Curr. Chem.* **2003**, in print.
152. M. Thackray, *J. Chem. Eng. Data* **1970**, *15*, 495.
153. B. R. Currel, A. J. Williams, *Thermochim. Acta* **1974**, *9*, 255.
154. J. Chiu, *Anal. Chem.* **1963**, *35*, 933.
155. F. Fehér, G. P. Görler, H. D. Lutz, *Z. Anorg. Allg. Chem.* **1971**, *382*, 135.
156. G. C. Vezzoli, P. J. Walsh, *High Temp. High Pressures* **1977**, *9*, 345.
157. P. D. Bartlett, G. Lohaus, C. D. Weis, *J. Am. Chem. Soc.* **1958**, *80*, 5064.
158. M. Thackray in: *Elemental Sulfur* (B. Meyer, ed.), Interscience, New York, **1965**, p. 45.
159. M. Schmidt, H. D. Block, *Z. Anorg. Allg. Chem.* **1971**, *385*, 119.
160. J. M. Austin, D. Jensen, B. Meyer, *J. Chem. Eng. Data* **1971**, *16*, 364.
161. H. T. Kennedy, D. R. Wieland, *Petrol. Trans. AIME* **1960**, *219*, 166.
162. J. G. Roof, *Soc. Petrol. Engrs. J.*, Sept **1971**, 272.
163. S. C. Swift, *Soc. Petrol. Engrs. J.* **1976**, *16*, 57.
164. E. Brunner, W. Woll, *Soc. Petrol. Engrs. J.*, Oct **1980**, 377; *Erdoel-Erdgas* **1979**, *95*, 314.
165. W. Woll, *Erdoel-Erdgas* **1983**, *99*, 297.
166. J. B. Hyne, G. D. Derdall, *World Oil*, Oct **1980**, 111.
167. J. Boulegue, *Phosphorus Sulfur* **1978**, *5*, 127.
168. R. Steudel, G. Holdt, *Angew. Chem.* **1988**, *100*, 1409; *Angew. Chem. Int. Ed. Engl.* **1988**, *27*, 1358.
169. Prospectus by Kali-Chemie, Hannover, Germany.
170. (a) D. M. Gardner, G. K. Fraenkel, *J. Am. Chem. Soc.* **1956**, *78*, 3279. (b) J. A. Poullis, C. H. Massen, P. v. d. Leeden, *Trans Faraday Soc.* **1962**, *58*, 474. (c) D. C. Koningsberger, T. De Neef, *Chem. Phys. Lett.* **1970**, *4*, 615. (d) D. C. Koningsberger, Dissertation, Techn. Hochschule Eindhoven, **1971**.
171. R. Steudel, D. Jensen, P. Göbel, P. Hugo, *Ber. Bunsenges. Phys. Chem.* **1988**, *92*, 118.

172. (a) J. Buttet, *Helv. Phys. Acta* **1969**, *42*, 63. (b) A. Chatelain, *Helv. Phys. Acta* **1969**, *42*, 117. (c) A. Chatelain, J. Buttet, in: *Elemental Sulfur* (B. Meyer, ed.), Interscience, New York, **1965**, p. 209. (d) A. Chatelain, J. Buttet, *Helv. Phys. Acta* **1964**, *37*, 77.
173. S. R. Elliott, *J. Phys. (Paris)* **1981**, *42*, C4–387.
174. (a) W. E. Spear, A. R. Adams, *J. Phys. Chem. Solids* **1966**, *27*, 281. (b) B. E. Cook, W. E. Spear, *J. Phys. Chem. Solids* **1969**, *30*, 1125. (c) S. Oda, M. A. Kastner, E. Wasserman, *Phil. Mag. B* **1984**, *50*, 373.
175. (a) L. Torrisi, S. Coffa, G. Foti, G. Strazzula, D. Fink, *Radiation Effects* **1986**, *99*, 293. (b) G. Strazzula, L. Torrisi, S. Coffa, G. Foti, *Icarus* **1987**, *70*, 379.
176. J. S. Kargel, P. Delmelle, D. B. Nash, *Icarus* **1999**, *142*, 249.
177. (a) V. V. Struzhkin, R. J. Hemley, H.-K. Mao, Y. A. Timofeev, *Nature* **1997**, *390*, 382; (b) R. J. Hemley, H.-K. Mao, *J. Phys.: Condens. Matter* **1998**, *10*, 11157.
178. (a) S. Kometani, M. I. Eremets, K. Shimizu, M. Kobayashi, K. Amaya, *J. Phys. Soc. Jpn.* **1997**, *66*, 2564. (b) K. Amaya, K. Shimizu, M. I. Eremets, T. C. Kobayashi, S. Endo, *J. Phys. Condens. Matter* **1998**, *10*, 11179.
179. E. Gregoryanz, V. V. Struzhkin, R. J. Hemley, M. I. Eremets, H.-K. Mao, Y. A. Timofeev, *Phys. Rev. B* **2002**, *65*, 064504.
180. In a DAC, high pressure is achieved by two opposed diamonds which transform the acting force of the device onto a relatively small volume. In general, the sample volume is enclosed by a thin metal plate (~100 μm thickness, ~200 μm central hole) serving as a gasket. In the case of sulfur, an additional pressure transmitting medium (e.g., a noble gas) provides for hydrostatic conditions. Very often, the sulfur sample itself is used as a pressure transmitting medium, too, because of its softness. However, this preparation technique may give rise to considerable pressure gradients through the sample volume. The determination of pressure makes use of well calibrated pressure standards such as the pressure dependence of the ruby fluorescence (optical studies) or the equation of states of metals or salts like Au or NaCl (X-ray diffraction studies). The role of the diamonds is not only to serve as an anvil (due to its hardness) but also to serve as an optical window with a wide range of spectral transparency and, in combination with the gasket material, as a sealing of the sample volume against leakage.
181. M. I. Eremets, *High pressure experimental methods*, Oxford University Press, Oxford **1996**, and literature cited in the preface.
182. R. J. Hemley, H.-K. Mao, R. E. Cohen, in: *Ultrahigh Pressure Mineralogy Physics and Chemistry of the Earth's Deep Interior* R. J. Hemley (ed.), Reviews in Mineralogy, Vol. 37. Mineralogical Society of America, Washington, **1998**.
183. K. Briester, *Rev. Sci. Instrum.* **1997**, *68*, 1629.
184. J. F. Cannon, *J. Phys. Chem. Ref. Data* **1974**, *3*, 781.
185. C. W. F. T. Pistorius, in: *Progress in Solid State Chemistry*, Vol. 11, (O. McCaldin, G. Somorjai eds.), Pergamon, London, **1976**.
186. L.-G. Liu, W. A. Bassett, *Elements, Oxides and Silicates—High Pressure Phases with Implications to the Earth's interior*, Oxford University Press, New York, **1986**.
187. D. A. Young, *Phase diagrams of the elements*, University of California Press, Berkeley, **1991**.
188. (a) E. Y. Tonkov, *High pressure phase transformations. A handbook*, Vol. 2, Gordon and Breach, Philadelphia, **1992**; (b) E. Y. Tonkov, *High pressure transformations. A handbook*, Vol. 3, Gordon and Breach, Philadelphia, **1996**.
189. D. A. Boness, J. M. Brown, *J. Geophys. Res.* **1990**, *95*, 21721.
190. O. Zakharov, M. L. Cohen, *Phys. Rev. B* **1995**, *52*, 12572.
191. (a) A. Nishikawa, K. Niizeki, K. Shindo, K. Ohno, *J. Phys. Chem. Solids* **1995**, *56*, 551; (b) A. Nishikawa, K. Niizeki, K. Shindo, *Phys. Stat. Sol. (b)* **1999**, *211*, 373.
192. (a) S. P. Rudin, A. Y. Liu, *Phys. Rev. Lett.* **1999**, *83*, 3049. (b) J. K. Freericks, S. P. Rudin, A. Y. Liu, *Physica B* **2000**, *284*. (c) S. P. Rudin, A. Y. Liu, K. Freericks, A. Quandt, *Phys. Rev. B* **2001**, *63*, 224107.
193. T. Yamada, K. Kani, K. Mori, in: *Proceedings of the 22nd Japan Congress of Materials Research*, Kyoto, **1978**, p. 331.

194. G. C. Vezzoli, P. J. Walsh, *High Temp.-High Press.* **1977**, 9, 345.
195. G. C. Vezzoli, R. J. Zeto, in: *Sulfur Research Trends. Adv. Chem. Series* **1972**, 110, 103.
196. (a) V. V. Brazhkin, R. N. Voloshin, S. V. Popova, A. G. Umnov, *Phys Lett A* **1991**, 154, 413; (b) V. V. Brazhkin, R. N. Voloshin, S. V. Popova, A. G. Umnov, *High Press. Res.* **1992**, 10, 454; (c) V. V. Brazhkin, S. V. Popova, R. N. Voloshin, *Physica B* **1999**, 265, 64.
197. S. Block, G. J. Piermarini, *High Temp. High Press.* **1973**, 5, 567.
198. In accordance with this order, Te is more semiconducting than Se. Further, Te shows metallic behavior at a lower pressure than Se. The transition pressures for Se and Te are 28 and 6 GPa, respectively. Moreover, high-pressure oxygen transforms to a metallic state too (~90 GPa).
199. G. C. Vezzoli, L. W. Doremus, P. J. Walsh, *Phys. Stat. Sol. (a)* **1975**, 32, 683.
200. (a) H. Luo, R. G. Greene, A. L. Ruoff, *Phys. Rev. Lett.* **1993**, 71, 2943. (b) H. Luo, A. L. Ruoff, in: *High Pressure Science and Technology* (S. C. Schmidt, J. W. Shaner, G. A. Samara, M. Ross, eds.), American Institute of Physics, New York, **1994**, p. 1527.
201. (a) Y. Akahama, M. Kobayashi, H. Kawamura, *Phys. Rev. B* **1993**, 48, 6862; (b) Y. Akahama, M. Kobayashi, H. Kawamura, in: *High Pressure Science and Technology* (S. C. Schmidt, J. W. Shaner, G. A. Samara, M. Ross; eds.), American Institute of Physics, New York, **1994**, p. 425.
202. F. P. Bundy, K. J. Dunn, *Phys. Rev. B* **1980**, 22, 3157.
203. D. A. Golopentiana, A. L. Ruoff, *J. Appl. Physics* **1981**, 52, 1328.
204. H. Luo, S. Desgreniers, Y. K. Vohra, A. L. Ruoff, *Phys. Rev. Lett.* **1991**, 67, 2998.
205. B. Eckert, R. Schumacher, H. J. Jodl, P. Foggi, *High Press. Res.* **2000**, 17, 113.
206. L. Wang, Y. Zhao, R. Lu, Y. Meng, Y. Fan, H. Luo, Q. Cui, G. Zou, in: *High Pressure Research in Mineral Physics* (M. H. Manghnani, Y. Syono, eds.), Terra Scientific Publ., Tokyo, **1987**, p. 299.
207. K. Nagata, T. Nishio, H. Taguchi, Y. Miyamoto, *Jpn. J. Appl. Phys.* **1992**, 31, 1078.
208. P. Wolf, B. Baer, M. Nicol, H. Cynn, in: *Molecular Systems under High Pressure* (R. Pucci, G. Piccitto, eds.), Elsevier, Amsterdam, **1991**, p. 263.
209. B. Eckert, H. J. Jodl, H. O. Albert, P. Foggi, in: *Frontiers of High Pressure Research* (H. D. Hochheimer, R. D. Etters, eds.), Plenum Press, New York, **1991**, p. 143.
210. M. L. Slade, R. Zallen, B. Weinstein, *Bull. Am. Chem. Soc.* **1982**, 27, 163; R. Zallen, *Phys. Rev. B* **1974**, 9, 4485.
211. W. Häfner, J. Kritzenberger, H. Olijnyk, A. Wokaun, *High Press. Res.* **1990**, 6, 57.
212. A. Anderson, W. Smith, J. F. Wheeldon, *Chem. Phys. Lett.* **1996**, 263, 133.
213. B. Eckert, *Doctoral Thesis*, University of Kaiserslautern, **2001**.
214. (a) B. Lorenz, I. Orgzall, in: *High Pressure Science and Technology* (S. C. Schmidt, J. W. Shaner, G. A. Samara, M. Ross; eds.), American Institute of Physics, New York, **1994**, p. 259; (b) B. Lorenz, private communication of unpublished results.
215. I. Orgzall, B. Lorenz, *High Press. Res.* **1995**, 13, 215.
216. H. Luo, A. L. Ruoff, in: *High Pressure Science and Technology* (S. C. Schmidt, J. W. Shaner, G. A. Samara, M. Ross; eds.), American Institute of Physics, New York, **1994**, p. 43.
217. T. Krüger, G. Parthasarathy, O. Schulte, W. B. Holzapfel, in: *Jahresbericht 1988 - HASYLAB* (G. Materlik, ed.), Hamburg, **1989**, p. 313.
218. H. Luo, A. L. Ruoff, *Phys. Rev. B* **1993**, 48, 569.
219. A. Yoshioka, K. Nagata, *J. Phys. Chem. Solids* **1995**, 56, 581.
220. P. Rossmanith, W. Häfner, A. Wokaun, H. Olijnyk, *High Press. Res.* **1993**, 11, 183.
221. This phase has been termed "high-pressure low-temperature" (hplt) sulfur, although low temperature means room temperature. Later, this phase was tentatively assigned by the authors to S_{II} or S_{XII} , respectively [220].
222. R. Schumacher, B. Eckert, H. J. Jodl, *High Press. Res.* **1996**, 15, 105.
223. J. Berkowitz, W. Chupka, E. Bromels R. L. Belford, *J. Chem. Phys.* **1967**, 47, 4320.
224. L. A. Nimon, V. D. Neff, R. E. Cantley, R. O. Buttlar, *J. Mol. Spectrosc.* **1967**, 22, 105.
225. N. Sakurai, H. Hirano, A. Onodera, Y. Akahama, H. Kawamura, in: *SPring-8 User Experiment Report (1997B)*, Japan Synchrotron Radiation Research Institute, **1998**, p. 55.

226. (a) K. Kusaba, T. Kikegawa, in: *Photon Factory Activity Report*, High Energy Accelerator Research Organization (KEK), Japan, 2000, 18B, p. 200. (b) K. Kusaba, T. Kikegawa, in: *Photon Factory Activity Report*, High Energy Accelerator Research Organization (KEK), Japan, 2000, 17B, p. 228.
227. J. S. Tse, D. D. Klug, *Phys. Rev. B* 1999, 59, 34.
228. The spectral peculiarities of a-S resemble those of the more or less disordered chains in S_{μ} as well as those of large rings S_x ($x \sim 20-50$) [43, 151, 205]. Therefore, it is likely that there is no principal difference between large disordered rings (S_x) and disordered chains (present in S_{μ} , for example).
229. M. J. Peanasky, C. W. Jurgensen, H. G. Drickamer, *J. Chem. Phys.* 1984, 81, 6407.
230. K. Syassen private communication of unpublished results.
231. (a) A. K. Abass, A. K. Hasen, R. Misho, *J. Appl. Phys.* 1985, 58, 1640. (b) A. K. Abass, N. H. Ahmad, *J. Phys. Chem. Solids* 1986, 47, 143.
232. W. Häfner, J. Kritzenberger, H. Olijnyk, A. Wokaun, in: *Twelfth International Conference on Raman Spectroscopy* (J. R. Durig, J. F. Sullivan, eds.), Wiley, Chichester, 1991, p. 448.
233. W. Häfner, H. Olijnyk, A. Wokaun, *High Press. Res.* 1990, 3, 248.
234. Y. A. Kandrina, A. N. Babushkin, S. N. Shkerin, Y. Y. Volkova, *Defect Diffusion Forum* 2002, 208-209, 295.
235. In these studies the optical absorption edge was defined as the energy of light at a transmission of 1%, that is an optical density of 2 ($OD=2$). Although common, this definition does not reflect the true absorption edge, which has to be evaluated more strictly, for example, using the so-called Urbach equation.
236. S. K. Sikka, *Metals Materials and Processes* 1992, 3, 303; S. M. Sharma, S. K. Sikka, *Progress in Material Science* 1996, 40, 1.
237. G. Doerre, J. D. Joannopoulos, *Phys. Rev. Lett.* 1979, 43, 1040.

Liquid Sulfur

Ralf Steudel

Institut für Chemie, Sekr. C2, Technische Universität Berlin, 10623 Berlin, Germany
E-mail: steudel@schwefel.chem.tu-berlin.de

Abstract The molecular composition as well as the physical properties (including spectra) of liquid sulfur are reviewed starting with a historic Introduction to explain the terms π -sulfur and μ -sulfur. At all temperatures the melt contains homocyclic rings of between 6 and at least 35 atoms with S_8 as the majority species as well as polymeric sulfur (S_∞) which becomes a major component only above 170 °C. The polymer probably consists of very large rings at temperatures below 157 °C but above this temperature very long diradicalic chains occur in addition. At temperatures above 300 °C highly colored small molecules like S_3 and, at even higher temperatures, S_4 can be detected spectroscopically. According to quantum-chemical calculations branched rings (clusters) will be minor components at temperatures near the boiling point only. The temperature dependence of the composition is explained and the various polymerization theories for the transformation of S_8 into S_∞ as well as the molecular nature of the polymer are discussed. In addition, the various analytical techniques applied to solve the composition problem of liquid sulfur are described.

Keywords Sulfur rings · Sulfur chains · Branched rings · Thermodynamics · Polymerization · Photochemistry

1	Introduction	82
2	Historical Review [18].	84
2.1	π -Sulfur	84
2.1.1	Preparation and Properties of π -Sulfur	84
2.1.2	Molecular Mass of π -Sulfur.	85
2.1.3	Concentration of π -Sulfur in Sulfur Melts	85
2.1.4	Rates of Formation and Decay of π -Sulfur	86
2.1.5	Enthalpy of Formation of π -Sulfur	86
2.1.6	Molecular Nature of π -Sulfur	87
2.2	Polymeric Sulfur (μ -Sulfur and S_∞)	87
2.2.1	Preparation of Polymeric Sulfur and its Concentration in Sulfur Melts 87	
2.2.2	Properties of μ -Sulfur	89
2.2.3	Rate of Formation of Polymeric Sulfur	90
2.2.4	Molecular Nature of Polymeric Sulfur.	90
2.3	Doping of Sulfur Melts.	92
3	Recent Results	94
3.1	Analysis of Liquid Sulfur by Vibrational Spectroscopy	94
3.1.1	Raman Spectra of Liquid Sulfur.	95
3.1.2	Raman Spectra of Quenched Sulfur Melts	96

3.1.3	Infrared and Raman Spectra of π -Sulfur	96
3.2	Analysis of Quenched Sulfur Melts by HPLC	97
3.3	UV-Vis Spectroscopy of Liquid Sulfur.	102
3.4	Photochemistry of Liquid Sulfur	105
3.5	Electrical Conductivity of Liquid Sulfur	106
3.6	Polymerization Theories for Liquid Sulfur.	108
	References	113

List of Abbreviations

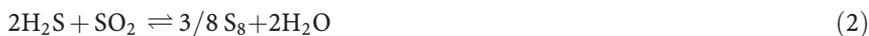
DSC	Differential scanning calorimetry
ESR	Electron spin resonance
HPLC	High performance liquid chromatography
HOMO	Highest occupied molecular orbital
LUMO	Lowest unoccupied molecular orbital
MD	Molecular dynamics
S_π	Mixture of soluble sulfur rings excepting S_8
S_x	Mixture of soluble sulfur rings with $x > 8$
S_∞	Polymeric sulfur present in liquid sulfur
S_μ	Polymeric sulfur prepared from liquid sulfur

1

Introduction

Liquid sulfur is produced industrially on a huge scale: Worldwide ca. 35 million tonnes are produced annually with an increasing trend. There are only two major processes which yield elemental sulfur: The Claus process involves oxidation of hydrogen sulfide to sulfur and water while the Frasch process is based on underground sulfur deposits and the application of a sophisticated mining procedure invented by Hermann Frasch [1]. The latter process is mainly used in the Southern part of the United States of America including off-shore mines. A modified version is applied in Poland. Basically, in the Frasch process the elemental sulfur in underground deposits is melted by pressurized hot water continuously pumped into the well and the generated liquid sulfur is mixed with compressed air and pumped simultaneously to the surface [2]. The Claus process is applied worldwide since hydrogen sulfide is a product of the desulfurization of crude oil by catalytic hydrogenation (hydrodesulfurization [HDS] process) which is performed in all oil refineries. Furthermore, H_2S is a component of so-called sour gas which is a natural gas containing up to 50% of H_2S (sometimes even more). Sour gas is produced in Northern Germany and Western Canada (Alberta), for example. The Claus process consists of two steps: The partial combus-

tion of H_2S to SO_2 in the Claus oven (or furnace) followed by the catalytic comproportionation of H_2S and SO_2 to sulfur and water in a second reactor:



Both the Frasch and the Claus process produce sulfur as a liquid, and in this form, at ca. 140 °C, sulfur is usually transported to the customers using either steam-heated pipelines, railroad cars, or ships, the latter with a sulfur capacity of up to 25,000 tonnes. Sometimes, the sulfur is first solidified before shipping.

The main users of elemental sulfur are the chemical industry for the production of chemicals such as sulfuric acid, phosphorus sulfides, etc., as well as the rubber industry for the vulcanization of natural or synthetic rubber.

Liquid sulfur has unique physical properties which have puzzled scientists and engineers for more than 100 years and which have no parallel in any other substance. For example, the color of the liquid changes reversibly from honey-yellow near the melting point (120 °C) to dark red-brown at the boiling point (445 °C) [3]. The dynamic viscosity η of the melt exhibits a minimum of 0.007 Pa s (0.07 Poise) at 157 °C but increases by more than four orders of magnitude in the small temperature range of 155–190 °C; the maximum viscosity of 93.2 Pa s (932 Poise) is reached at 187 °C [4, 5]. Other measurements using commercial and not purified sulfur resulted in a minimum viscosity of 0.009 Pa s at 154 °C [6]. On heating to temperatures above 190 °C the viscosity decreases again to 0.1 Pa s at the boiling point. Obviously, a substantial concentration of polymeric sulfur molecules (S_∞) is building up at temperatures above 159 °C. This so-called “polymerization temperature” (or “transition temperature”) depends on the external pressure: As higher the pressure as lower the polymerization temperature [7, 8]. At 840 bar (84 MPa) the polymerization takes place at 145.5 °C which is identical to the melting temperature of monoclinic β - S_8 at this pressure. In other words, under these conditions β - S_8 melts directly to a liquid containing a high concentration of S_∞ [9]. According to DTA measurements by Kuballa and Schneider the curve for the experimental pressure dependence of the polymerization temperature intercepts the melting curve of β - S_8 at 155.5 °C and 1300 bar (130 MPa) [10].

The density of liquid sulfur (at ambient pressure) decreases with increasing temperature from 1.802 g cm⁻³ at 120 °C to 1.573 g cm⁻³ at 440 °C but the temperature coefficient of the specific volume shows a unique discontinuity at 159 °C when the density change has a minimal value (density at this temperature: 1.770 g cm⁻³) [11–13]. Similarly, the heat capacity C_p of the melt exhibits a discontinuity at 161 °C [14]. The dielectric constant shows a distinct minimum at 159 °C [15, 16]. The temperature of 159 °C (sometimes given as 159.5 or 160 °C) has therefore also been called a transition temperature (“first order λ -transition” at “ T_λ ”).

All these temperature-related changes of the physical properties are completely reversible if the melt is cooled down slowly. It must be pointed out, however, that only measurements made with highly purified sulfur using the method by Bacon and Fanelli [4] produce reliable results.

The melting point of β -S₈ (120 °C) is reversible only if the freshly produced melt is cooled down immediately before the last crystal has disappeared. If the melt is kept for some hours at temperatures above 120 °C the freezing point is observed at a constant temperature of 115 °C (triple point). This phenomenon is explained by the formation of novel low molecular weight molecules S_n with $n \neq 8$. In the older literature these molecules have been termed collectively as π -sulfur or S _{π} (in contrast to S₈ which was termed λ -sulfur [17]). In addition, polymeric sulfur S _{∞} is a component of liquid sulfur at all temperatures. After isolation from the melt the polymer is usually called μ -sulfur [17] or S _{μ} . In the following sections we will show how the molecular nature of π -sulfur has been found out and how the physical properties of liquid sulfur can be understood on the basis of the rather complex but very interesting molecular composition.

2 Historical Review [18]

2.1 π -Sulfur

2.1.1 *Preparation and Properties of π -Sulfur*

If liquid sulfur, after the chemical equilibrium has been established (12 h at 120 °C or 1 h at 250 °C), is rapidly quenched to low temperatures and immediately extracted with carbon disulfide the polymeric S _{μ} will remain undissolved while S₈ and S _{π} will dissolve. After filtration, most of the S₈ will crystallize out on cooling of the solution to -78 °C while S _{π} together with some S₈ remains in solution. It is not possible to isolate S _{π} completely free of S₈. Therefore, in the literature the mixture S₈+S _{π} has often been simply termed “S _{π} ” but in this chapter we will differentiate between S _{π} on the one hand and mixtures of S _{π} with S₈ on the other hand (“S₈+S _{π} ”). If a solution of S₈+S _{π} is evaporated in a vacuum a yellow resin-like mass is obtained which solidifies at low temperatures as a glass but decomposes at room temperature within a few days to a crystalline mixture of S₈ and S _{μ} [19].

Because of the instability of S _{π} at room temperature the quenching of the sulfur melt has to be very rapid and efficient. Different authors have used ice water [20–22], liquid air [23], or sheets of glass [19] or metal [19, 24] onto which the melt was blown by a strong jet of cold gas to produce either a thin film or small particles. Because of the low heat conductivity of elemental sulfur the quenching in water is insufficient and water is not even inert chemically towards hot sulfur. The quenched melt has to be extracted by CS₂ at

20 °C immediately after quenching (and not after storage). In CS₂ solution S_π is stable for weeks at 20 °C provided that light and nucleophiles are strictly excluded. Such solutions may be prepared with a rather high concentration of S₈+S_π. If the quenched sulfur melt is extracted by a solution of S₈+S_π from a former extraction or if the sulfur melt is poured directly into a solution of S₈+S_π it is possible to obtain mixtures with 140 g S_n/100 g CS₂ at 20 °C which is four times the solubility of S₈ in CS₂! At -78 °C, after the precipitated S₈ has been removed, such solutions may contain 26.8 g S_n/100 g CS₂ corresponding to ten times the solubility of S₈ at this temperature [25, 26].

2.1.2

Molecular Mass of π-Sulfur

Carefully performed cryoscopic measurements of solutions of S₈+S_π in CS₂ yielded a relative molecular mass of 260 corresponding to 8.1 atoms per molecule. This value did not depend significantly on the concentration of the solution nor on the temperature of the sulfur melt (130–350 °C) from which the S₈+S_π solution was prepared [26].

2.1.3

Concentration of π-Sulfur in Sulfur Melts

Using Raoult's Law several authors have tried to calculate the concentration of S_π in sulfur melts of different temperatures from the melting point depression assuming that the polymeric sulfur does not contribute to this depression owing to its high molecular mass. Schenk and Thümmeler used the melting point of β-S₈ (119.3 °C) and the triple point of the melt (114.5 °C) and obtained the S_π content of the equilibrium melt at the triple point as 5.5% by mass corresponding to 5.5 mol% since the molecular masses of S₈ and S_π are seemingly identical (see above) [26]. However, these authors used the cryoscopic constant of equilibrium sulfur melts as determined by Beckmann and Platzmann [27] which most probably is not identical to that of pure liquid S₈. Similarly, Wiewiorowski et al. equilibrated sulfur melts at 130, 140, and 150 °C followed by rapid cooling to the freezing point and measurement of the freezing temperature. These authors observed melting point depressions of 5.0, 6.0, and 7.7 K, respectively, indicating an increasing S_π content with increasing temperature [28]. For the calculation of the S_π content, however, they used a much too small value for the melting enthalpy of β-S₈ (9.81 kJ mol⁻¹). If the currently accepted value of this enthalpy (12.98 kJ mol⁻¹) [29] is applied instead the S_π concentrations are obtained as 5.0, 6.0, and 7.6%, numerically almost identical to the corresponding freezing point depressions. These concentrations must be considered as lower limits since some S_π will decompose during the cooling from the equilibration temperature to the freezing point.

If more recent data for the melting temperature of β-S₈ (120.1 °C) [30] and the triple point of liquid sulfur (115.2 °C) [31] are used the freezing point depression of 4.9 K yields an S_π content of 4.8% at the triple point.

2.1.4

Rates of Formation and Decay of π -Sulfur

Several authors have reported that the formation of S_π from S_8 in liquid sulfur is a slow reaction which takes at least 8 h at 120 °C and at least 3 h at 150 °C [28, 32]. The back reaction $S_\pi \rightarrow S_8$ is much faster requiring ca. 30 min at 120 °C and ca. 2 h at 97–112 °C (in the solid state) [32]. However, the back reaction is not complete: Even after 15 days at 100 °C there are still traces of S_π present in the (solid) sample [21]. At 20 °C S_π decomposes within two days to a mixture of S_8 and S_μ in an approximate 1:1 ratio [33]. In solution S_π is much more stable: On heating of $S_8 + S_\pi$ in toluene to 100 °C no conversion was observed within 20 h [20] while heating of such a sample in CS_2 to 100 °C resulted in a slow decrease of the S_π concentration within several days [21].

In the presence of traces of ammonia the reactions $S_\pi \rightarrow S_8$ and S_∞ (or S_μ) $\rightarrow S_8$ are fast and ammonia accelerates also the formation of S_π and S_∞ in sulfur melts [21, 34–36]. Therefore, investigations on these systems should be carried out in laboratories in which no ammonia (aqueous or gaseous) is stored. Illumination with visible light also accelerates the interconversion reactions [36].

Assuming a first order reaction, Wiewiorowski et al. [28] calculated the Arrhenius activation energy for the formation of S_π in the temperature range of 130–150 °C using the concentrations derived from the freezing point depression. An activation energy of 134 kJ mol⁻¹ was obtained. However, since these authors—as outlined above—used an outdated value for the enthalpy of melting of β - S_8 their cryoscopically determined S_π concentrations are too low. If the concentrations corrected by the present author (see above) are used [18] the activation energy is obtained as 144 kJ mol⁻¹ which agrees fairly well with the activation energy of 150 kJ mol⁻¹ for the formation of free radicals by homolytic S-S bond dissociation in sulfur melts as determined by ESR spectroscopy [37, 38] and magnetic measurements [39]. It should be pointed out however that in the above calculations the back reaction has been neglected despite the fact that it is much faster than the forward reaction (S_π formation).

2.1.5

Enthalpy of Formation of π -Sulfur

From the corrected concentrations of S_π at various temperatures (see above) and taking the concentration of polymeric sulfur into account the equilibrium constants $K_c = c(S_\pi)/c(S_8)$ can be calculated for the temperature range 115–150 °C. The linear regression $-\log K_c$ vs $1/T$ then yields the enthalpy of formation of S_π as +22 kJ mol⁻¹ [18].

2.1.6

Molecular Nature of π -Sulfur

The molecular mass of 260 determined for S_π (see above) has puzzled some authors who tried to identify meaningful molecular species in liquid sulfur. Schenk and Thümmeler [26] who had first determined reliable data for the (average) molecular mass proposed a chain of eight sulfur atoms which was assumed to be a singlet molecule with a delocalized π -bond rather than a di-radical. Wiewiorowski and Touro [40] proposed that these eight-membered chains function as Lewis bases and the S_8 rings as Lewis acids forming "adducts" of the type *catena-S₈-n cyclo-S₈*. Several authors [15, 32, 41, 42] suspected that S_π is simply a cyclic S_8 molecule in a conformation different from the well-known crown-shaped D_{4d} molecule. All these hypotheses proved to be wrong.

Krebs and Beine [43] were the first who succeeded to separate S_π into fractions using counter-current distribution between the two solvents methanol and carbon disulfide. They obtained fractions containing S_n molecules with average molecular masses corresponding to between 6.5 and 33 atoms per molecule but were unable to isolate pure components. These very interesting results indicated that S_6 might be a component of S_π as had first been suspected by Aten in 1914 [36].

Harris [44] finally reviewed all the data available in 1970 and concluded that S_π must be a mixture of both S_6 and S_7 as well as of rings larger than S_8 . At that time Schmidt and Block [45] had already isolated traces of S_{12} from sulfur melts quenched from temperatures of between 120 and 370 °C. The hypothesis by Harris turned out to be correct as will be shown below where reliable qualitative and quantitative data obtained by modern analytical methods will be presented.

2.2

Polymeric Sulfur (μ -Sulfur and S_∞)

2.2.1

Preparation of Polymeric Sulfur and its Concentration in Sulfur Melts

After equilibration liquid sulfur contains a certain concentration of polymeric molecules (S_∞) at all temperatures. This polymer can be isolated and determined by quenching the melt at very low temperatures, extracting the smaller molecules immediately by pure carbon disulfide at 20 °C, and drying the residue of S_μ in a vacuum. Extraction and drying should be done with exclusion of light and nucleophiles and avoiding higher temperatures which would initiate the conversion of the polymer to *cyclo-S₈*. The content of μ -sulfur thus obtained depends on the purity of the melt. In addition, it has to be obeyed that the π -sulfur present in the quenched melt is unstable at 20 °C and partly polymerizes to S_μ for which reason the extraction has to be done without any delay if the true polymer content of the melt is to be determined. If, on the other hand, simply S_μ is to be prepared it is possible to in-

crease its yield by extraction of the quenched melt *after* the π -sulfur has decomposed which takes ca. two days at 20 °C or one day at 40–60 °C (see above). Since the quenching and extraction procedures may alter the molecular identity of the polymer it is convenient to use two different symbols for the polymer dissolved in the melt (S_∞) and for the isolated product (S_μ). Below it will be shown that S_∞ is most probably a mixture of large rings and long chains at temperatures above 159 °C.

The most reliable determinations of S_μ in the older literature are those by P.W. Schenk [19] and by J. Schenk [23] while the data reported by Koh and Klement [24] are probably too high, at least in the high temperature region. P.W. Schenk equilibrated liquid sulfur in an aluminum oven and allowed the melt to flow in a thin stream from the oven through a valve in the bottom. Using a jet of cold gas to blow the melt against a sheet of glass (P.W. Schenk) or copper or aluminum metal (Koh and Klement) the authors tried to rapidly quench the melt as a thin layer. In some experiments J. Schenk used liquid air to quench the melt, a coolant which is to be preferred over water since it yields very small particles of sulfur which are efficiently quenched. After extraction with CS_2 at 20 °C the S_μ content was determined as insoluble residue.

In general, the polymer content of liquid sulfur increases first slowly from the melting point to 155 °C, but more steeply above 158 °C although there is no indication for a *sudden* increase as dramatically as the viscosity increases in the region 159–190 °C (see above). While the viscosity decreases above 190 °C the polymer content increases further to a maximum of 40% [19]. Therefore, the claim [26, 34, 46, 47] that the sudden viscosity increase is caused by a precipitation of polymer from the melt and a sudden shift of the equilibrium from the monomer S_8 to the polymer above 159 °C is not justified. For systems like liquid sulfur with highly entangled but not crosslinked chains the viscosity is proportional to the product $N^3 \cdot \rho^3$ where N is the chain-length and ρ is the concentration of chain-atoms [48].

The following polymer contents are representative examples for high-purity sulfur melts quenched from the temperatures indicated:

- 120 °C: 0.5% [23]; 130 °C: 1.0% [23]; 160 °C: 4.5% [23]; 350 °C: 37% [19]

More recent data indicate that these concentrations are all slightly too high (see later). According to Koh and Klement who quenched the sulfur melts at room temperature the polymer content rises from ca. 1% at 135 °C melt temperature, to 10% at 162 °C, 36% at 200 °C, and 56% at 250 °C at which temperature a plateau is reached which extends to at least 300 °C [24]. Since these authors did not purify the sulfur by the method recommended by Bacon and Fanelli [4] and since a quenching temperature of 20 °C is probably too high the reliability of these data may be disputed. Sulfur melts containing various types of impurities show higher polymer contents after extraction (max. 65%), but this polymer is less stable at 20 °C with regard to conversion to α - S_8 [19].

Previous authors [19, 21–23, 34] also reported that the polymer concentration is nearly constant in the region 250–420 °C although their absolute values in some cases differ from more recent results because of deficiencies in the quenching procedure or the impact of impurities including the water used for chilling the melt. Generally, it is assumed that the polymer is present as an ideal solution in a melt of small ring molecules.

Ward and Myers [49] tried to determine the S_{∞} content of the sulfur melt *directly* using Raman spectroscopy. The Raman spectra of hot sulfur melts are characterized by very broad and overlapping signals. The authors assumed identical Raman scattering intensities for the stretching vibrations of S_8 and S_{∞} and an identical temperature dependence of these intensities. In addition, they neglected the S_{π} content of the melt. The obtained concentrations scatter considerably but indicate that the S_{∞} content increases from practically zero at 150 °C to ca. 70% by mass at 260 °C. From the temperature dependence of the S_{∞} content the enthalpy of formation of was estimated as 19 kJ mol⁻¹ (for more recent data, see later).

The occurrence of higher concentrations of S_{∞} above 160 °C results in a birefringence of sulfur melts [50] with a maximum between 175 and 185 °C at which temperature the viscosity also attains its maximum value.

If sulfur melts are quenched at temperatures below -30 °C a material is obtained which initially is elastic and amorphous at room temperature but rapidly crystallizes to become a mixture of microcrystalline sulfur rings and polymeric molecules. The glass-transition temperature of the elastic material is ca. -30 °C. Below this temperature the conversion to a microcrystalline mixture is very slow [51, 52].

For reasons of completeness it should be pointed out that polymeric sulfur is also obtained if sulfur vapor is quenched from very high temperatures (e.g., 600 °C) to very low temperatures (liquid nitrogen) followed by warming the condensate to +20 °C and extraction with carbon disulfide. Up to 60% S_{μ} have been obtained in this way [53]. Commercially polymeric sulfur (trade name Crystex) is produced by a similar process (see the chapter on “Solid Sulfur Allotropes” in this volume). The glass transition temperature of Crystex is +75 °C [51].

2.2.2

Properties of μ -Sulfur

Polymeric or insoluble sulfur prepared from quenched sulfur melts by extraction is a yellow powder which slowly converts to S_8 at 20 °C. This reaction takes months to years but is accelerated by irradiation, by grinding, by heating as well as by catalysts like aqueous or gaseous ammonia. Heating to 100 °C for 10 h destroyed all S_{μ} in a quenched and aged melt which originally contained 2.8% of S_{μ} [54, 55]. If S_{μ} is treated with liquid carbon disulfide at 100 °C (in a sealed thick-walled glass ampoule) it partly dissolves as a mixture of S_8 and S_{π} , in other words by depolymerization [21]. The melting (depolymerization) temperature of solid S_{μ} has been reported as 105–115 °C [56, 57]. The molecules in the melt thus obtained rapidly equilibrate with

Table 1 Polymerization temperature of liquid sulfur as a function of the heating rate starting with pure S_8 samples [58]

Rate ($K \text{ min}^{-1}$)	1.25	2.5	5	10	20	40
$T_{\text{polym.}}$ ($^{\circ}\text{C}$)	161	167	172	183	191	203

each other and the composition of the melt after equilibration is identical to that of a melt obtained from S_8 [34, 57]. In liquid sulfur S_{μ} dissolves with depolymerization to S_8 and S_{π} [57].

2.2.3

Rate of Formation of Polymeric Sulfur

The formation of S_{∞} in sulfur melts is a slow reaction, and it takes about 1 h at 160 $^{\circ}\text{C}$ to establish the equilibrium concentration [24, 58]. From the temperature dependence of the polymer content, from the heat capacity C_p of the melt [29] as well as from calorimetric measurements [56, 58] it was concluded that the reaction $S_8 \rightarrow S_{\infty}$ is endothermic with an estimated activation energy of ca. 120 $\text{kJ mol}^{-1}(S_8)$ [58]. The same value was derived from DSC measurements of liquid sulfur [58]. In this context it was observed that the sudden viscosity increase of liquid sulfur takes place at exactly 159 $^{\circ}\text{C}$ only if the heating rate approaches zero. If the heating rate is varied between 1.25 and 40 K min^{-1} higher “transition temperatures” are observed as the data in Table 1 show [58].

Furthermore it was observed that the polymerization temperature at finite heating rates depends on the thermal history of the sulfur! The data in Table 1 apply to pure S_8 and fresh samples in each experiment. If sulfur is used which had been melted (and then solidified) before or had been kept liquid for some time at a temperature below $T_{\text{polym.}}$ the polymerization takes place at lower temperatures but never below 159 $^{\circ}\text{C}$ [58]. This indicates that the polymerization is triggered by molecules which form from S_8 after melting, most probably by some component of π -sulfur. This has been convincingly demonstrated by the following experiment. Addition of 2% of crystalline S_6 to an equilibrium sulfur melt at 150 $^{\circ}\text{C}$ resulted in immediate polymerization of the entire melt [59]. Therefore, it was concluded that the polymerization of sulfur melts is triggered by free radicals originating from the thermal ring opening of S_6 and S_7 molecules the dissociation energy of which is smaller than that of S_8 [60, 61].

2.2.4

Molecular Nature of Polymeric Sulfur

The molecular nature of S_{∞} and S_{μ} has been disputed many times. While some of the earlier authors believed that polymeric sulfur is a mixture of large rings (S_{∞}^{R}) [46, 47, 62, 63], others preferred chain-like macromolecules (S_{∞}^{C}) [39, 64–68]. These macromolecules should have “dangling

bonds” at the chain-ends (i.e., free radicals). In fact, Gardner and Fraenkel [37] obtained ESR spectra of very pure sulfur melts in the temperature range of 189–414 °C and observed an increasing spin concentration with increasing temperature. These spectra consist of a single broad line at $g=2.024$. The radicals are formed by homolytic cleavage of sulfur-sulfur bonds:



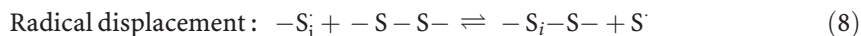
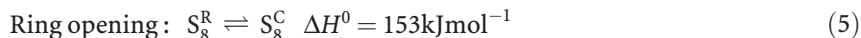
From the temperature dependence of the signal intensity (amplitude) the activation energy for this reaction was derived as $140 \pm 20 \text{ kJ mol}^{-1}$ (SS bonds) or 70 kJ mol^{-1} (spins). From the line-width and its temperature dependence the lifetime of the free radicals was estimated which is obviously determined by the following rapid radical displacement reaction:



The activation energy for reaction (4) was derived as 12 kJ mol^{-1} and the lifetime was estimated from the line-width as $1.6 \times 10^{-9} \text{ s}$ at 216 °C and $6.5 \times 10^{-10} \text{ s}$ at 414 °C. Evidently, the radicals move rapidly around in the melt and novel chain-like and cyclic molecules are constantly formed and destroyed. If the melt is cooled to temperatures below 150 °C irreversible radical recombination will occur.

Koningsberger and DeNeef used a spectrometer of high sensitivity and applied time-averaging techniques to improve the signal-to-noise ratio. They observed isotropic ESR signals of Lorentzian line-shape ($g=2.017 \pm 0.005$) already at 153 °C (but not at lower temperatures) and up to 800 °C [38]. The spin concentration was estimated as two electrons per 5×10^7 atoms at 172 °C and per 5×10^3 atoms at 445 °C (boiling point) [69]. These numbers would represent the average chain-lengths of the diradicals at the given temperatures if only chains and no rings were present which is of course not the case. Therefore, these numbers are upper limits for the average chain-lengths of the diradicals in liquid sulfur.

The chemistry in liquid sulfur was modeled by the following four reactions (C=diradical chain, R=ring) and the enthalpy values given were derived using a theoretical analysis presented in [69] for the temperature region of 250–550 °C:



The enthalpy of the last reaction is of course zero.

Poullis et al. [39] measured the magnetic susceptibility of liquid sulfur in the temperature range of 120–580 °C. The susceptibility is strongly influ-

enced by the paramagnetic contribution of the diradicals. These authors derived the enthalpy of the bond dissociation reaction of sulfur chains as 148 kJ mol^{-1} at $578 \text{ }^\circ\text{C}$. The mean chain-length of the polymer in liquid sulfur was estimated as 10^4 atoms near $400 \text{ }^\circ\text{C}$ and 10^3 atoms near $550 \text{ }^\circ\text{C}$. These data were confirmed by Radscheit and Gardner who obtained 152 kJ mol^{-1} for the dissociation enthalpy above $550 \text{ }^\circ\text{C}$ [70].

2.3

Doping of Sulfur Melts

Many authors have shown that the physical properties of liquid sulfur as reported in the Introduction change dramatically with even small concentrations of “impurities” or “dopants”. These dopants react chemically with the elemental sulfur at the temperatures of the liquid and therefore change the composition and in particular the chain-length of the polymeric sulfur. This is one of the reasons that studies on the properties of sulfur should be performed only with samples of extremely high purity as obtained by the method of Bacon and Fanelli [4, 71]. The latter authors investigated the impact of impurities such as organic matter, SO_2 , H_2SO_4 , H_2S , H_2S_x , amines and halogens. *Organic substances* of unknown nature are present as impurities in all commercial sulfur samples including the so-called 99.999+% sulfur! On heating to $200 \text{ }^\circ\text{C}$ a sulfur sample containing 0.038% oil and 0.05% H_2SO_4 produced, inter alia, hydrogen sulfide which has a pronounced impact on the chemical equilibria in liquid sulfur lowering the viscosity in the range $160\text{--}230 \text{ }^\circ\text{C}$ to less than 4 Pa s (40 Poise). On repeated heating and cooling these samples more and more behaved like pure sulfur with its pronounced viscosity maximum at $187 \text{ }^\circ\text{C}$ since the hydrogen sulfide either evaporated or was oxidized to elemental sulfur and water which escapes [4]. Sulfur dioxide and sulfuric acid have no effect on the viscosity of liquid sulfur.

If gaseous *hydrogen sulfide* is passed through pure liquid sulfur while rising its temperature from 125 to $190 \text{ }^\circ\text{C}$ within 90 min the sample does not attain the viscous state. Its viscosity at the end of this period is only 0.09 Pa s as compared to about 93 Pa s for untreated sulfur [4]. The dependence of the viscosity on the H_2S content of the melt at temperatures of between 170 and $300 \text{ }^\circ\text{C}$ has been determined [72]. The H_2S reacts with sulfur in a reversible reaction to polysulfanes H_2S_n which have been detected by infrared [73] and $^1\text{H NMR}$ [74] spectroscopy in such melts. For this reason the solubility of H_2S in liquid sulfur *increases* with temperature up to $385 \text{ }^\circ\text{C}$ [72, 73, 75] while usually gases are less soluble if the temperature is increased. Polysulfanes therefore lower the viscosity of liquid sulfur as efficiently as hydrogen sulfide does [4]. The freezing point of sulfur is also lowered by H_2S [76]. Many commercial samples of elemental sulfur contain traces of hydrogen sulfide or polysulfanes which are not easy to remove.

The viscosity maximum of sulfur treated for several days with *ammonia* is only slightly lower (ca. 78 Pa s) than that of untreated samples which has been explained by the formation of minute amounts of H_2S and H_2S_x . For

the same reason, some amines lower the viscosity because of reactions of the organic groups with sulfur producing some hydrogen sulfide [4].

The impact of the *halogens* chlorine, bromine and iodine on the viscosity of liquid sulfur has been studied most extensively. They all lower the viscosity dramatically, even in low concentrations, and the effectiveness in this respect decreases from chlorine to iodine. At the same time the maximum of the viscosity curve is shifted to higher temperatures. For example, the addition of 0.02% of I₂ gives a viscosity maximum of 5.7 Pa s at 225 °C while 0.75% chlorine, added as sulfur chloride, give maximum viscosity values below 0.2 Pa s in the entire temperature region of 150–320 °C [4]. It is generally assumed that the halogens as well as the sulfur chlorides react with liquid sulfur to chain-like dihalopolysulfanes S_nX₂. In this way the chain-length of the polymeric sulfur molecules is reduced and the viscosity thus lowered:



Since these reactions are reversible and since the elemental halogens as well as the low molecular mass sulfur chlorides are volatile they slowly escape from the hot melt if the sample is kept open to the atmosphere. In this case, the viscosity rises again with the heating time [4].

If *selenium* is added to liquid sulfur the transition temperature is somewhat lowered since mixed selenium-sulfide chains and rings are formed [77] the dissociation energy of which is lower than for sulfur-sulfur bonds. The maximum viscosity is also lower compared to pure sulfur. Above a concentration of 70% Se the melt is highly viscous and obviously consists mainly of polymeric molecules at all temperatures as is the case with pure selenium [23].

The effects of *phosphorus* and *arsenic* are more complicated. These elements are added as such or as P₄S₃ or As₂S₃, respectively, followed by heating to 400 °C for homogenization and cooling to the melting point. The maximum viscosity of these melts is lowered by approximately one order of magnitude if between 0.25% and 1.5% of arsenic are added but the increase in viscosity begins at much lower temperatures compared to pure sulfur [23, 78]. The polymer obtained from such melts is more stable thermally since the three-valent phosphorus or arsenic atoms obviously knit the sulfur chains together in a process similar to the vulcanization of organic polymers by elemental sulfur resulting in oligosulfane bridges of the type R-S_x-R with x=1, 2,...[79].

Dilution of liquid sulfur with an inert organic solvent shifts the polymerization temperature to higher values.

3 Recent Results

Since about 1970 it has been shown that almost all metastable sulfur homocycles between S_6 and S_{20} can be prepared as pure solids by kinetically controlled syntheses at moderate temperatures [71]. The investigation of their physical properties and in particular of their spectra allowed the molecular composition of liquid sulfur to be determined using modern spectroscopic and chromatographic techniques. As a result of these investigations the pure sulfur rings S_7 , S_{12} , S_{18} , and S_{20} can now be prepared from quenched sulfur melts by fractional crystallization [71]. The analytical work will be described below while the preparation of solid sulfur allotropes is reported elsewhere [71].

3.1 Analysis of Liquid Sulfur by Vibrational Spectroscopy

The interpretation and assignment of the vibrational spectra of liquid sulfur and of quenched sulfur melts requires the knowledge of the spectra of the likely components of these mixtures. Therefore, the infrared and Raman spectra of all sulfur allotropes existing at ambient pressure had to be recorded to collect the data needed to assign the spectra of the melt. It turned out that the vibrational spectra of the various sulfur rings and of polymeric chains are different enough to identify each species by this method in mixtures, provided the particular concentration is not too low and the composition of the mixture is not too complex. The differences in the spectra result from the increase in the vibrational degrees of freedom with increasing number of atoms in the molecule. But in addition, the molecular symmetry plays a major role since high-symmetry molecules like S_6 (D_{3d}), S_8 (D_{4d}), and S_{12} (D_{3d}) give simpler spectra than molecules of similar size such as S_7 (C_s) due to degeneracies of some of their vibrational modes.

Most of the sulfur rings have either no or only small dipole moments owing to the low or lacking polarity of the sulfur-sulfur bonds. Therefore, infrared spectra of these species are of low intensity as a result of the selection rule for infrared absorption. In contrast, the Raman scattering intensity of S-S bonds is very strong and Raman spectra are therefore the best technique to study sulfur melts and samples prepared from the melt like π -sulfur and μ -sulfur. In Fig. 1 a schematic comparison is made to demonstrate the differences in the Raman spectra of the homocycles with between 6 and 12 atoms.

Compounds containing S-S bonds are light sensitive and this holds particularly true for solid sulfur allotropes. Since Raman spectroscopy involves the irradiation with a high-intensity laser beam one has to take care that the sample composition is not affected by the irradiation. Therefore, red (krypton ion) or infrared (Nd:YAG) laser lines are recommended and the solid samples should be cooled to at least -100 °C whenever possible. The low sample temperature at the same time improves the spectral resolution since

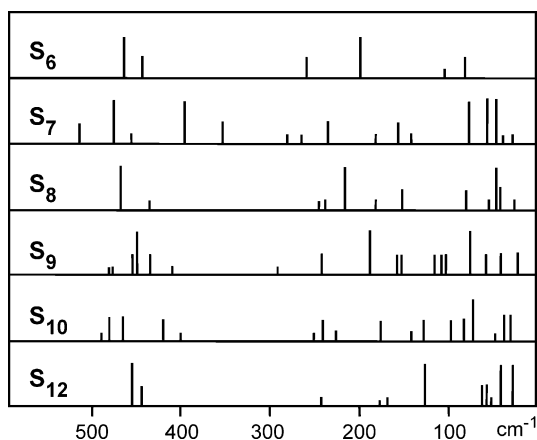


Fig. 1 Schematic representation of the Raman spectra of some sulfur allotropes consisting of homocycles (fundamental modes given only; after [80])

narrower Raman lines are obtained. Green and blue laser lines usually initiate photoreactions even at low temperatures.

3.1.1

Raman Spectra of Liquid Sulfur

Several authors have reported Raman spectra of sulfur melts without obtaining any novel information besides the fact that *cyclo-S*₈ is the main constituent and that the polymer content increases with temperature, in particular above 159 °C [49, 81–85]. These spectra show the strong lines of S₈ at 151, 218 and 474 cm⁻¹ and—at higher temperatures—the broad line of S_∞ at ca. 460 cm⁻¹ which prevents the detection of any weaker lines of the other components of the melt. With rising temperature the S₈ lines also get broader and broader [83]. Only the use of modern spectrometers revealed the weak lines of additional components [80]: High-purity sulfur sealed in a glass ampoule was measured in the range 110–300 °C using a krypton ion laser (647.1 nm) after the thermal and chemical equilibria had been established. In addition to the lines of S₈ two weak lines at 264 and 235 cm⁻¹ (± 1 cm⁻¹) were observed at temperatures above 130 °C. These lines can definitely be assigned to the symmetrical ring bending vibrations of S₆ and S₇, respectively [86]. The additional Raman signals of these two molecules are obscured by the dominating and very broad S₈ lines. Compared to the solid allotropes α - and β -S₈ the lines of liquid S₈ of a₁ and e₂ symmetry are shifted to lower wavenumbers as higher the temperature of the melt [80]. At temperatures where the melt contains a substantial concentration of polymeric sulfur a broad Raman “band” in the region 350–460 cm⁻¹ was observed which partly must be caused by the polymer [80].

3.1.2

Raman Spectra of Quenched Sulfur Melts

To avoid the problems with the rather broad Raman signals of S_8 and S_∞ in the spectra of hot sulfur melts it seemed helpful to record spectra of liquid sulfur rapidly quenched in liquid nitrogen [80]. To prepare such samples the equilibrated melt of high-purity sulfur was allowed to flow into stirred liquid nitrogen in as thin a string as possible resulting in a fine yellow powder of solid sulfur provided the melt temperature was below 160 °C. At higher melt temperatures thin wires of solidified sulfur were obtained. All samples were handled and measured at temperatures below -78 °C. The spectra now showed clearly the presence of S_6 (268 cm^{-1}) and S_7 (175, 288, 360, 402, 518 cm^{-1}) by the lines given in parentheses. In addition, β - S_8 was detected [80].

The time-dependent formation of S_7 from S_8 in liquid sulfur at 120 °C was monitored using the two neighboring Raman lines of S_7 (360 cm^{-1}) and S_8 (196 cm^{-1}) in the spectra of the melt quenched at certain time intervals after the start of the melting procedure of pure S_8 in the aluminum oven. The intensity ratio $I(360)/I(196)$ continuously increased from zero to 0.28, the final value being reached after ca. 10 h. By independent experiments it had been shown before that this intensity ratio is proportional to the S_7 concentration in liquid S_8 . The temperature dependence of $I(360)/I(196)$ was used to demonstrate that the S_7 concentration in liquid sulfur increases from 115 to 159 °C approximately by a factor of 2 but absolute concentrations could not be determined in this way [80].

3.1.3

Infrared and Raman Spectra of π -Sulfur

Above it has been shown that the Raman spectra of liquid sulfur and of quenched sulfur melts are obscured to a large extent by the strong lines of the main component S_8 . Therefore, to obtain spectral information on the minority species one has to reduce the S_8 concentration in the quenched samples by extraction with carbon disulfide at 25 °C followed by cooling of the filtered extract to -78 °C whereupon most of the S_8 together with some $S_{12}\cdot\text{CS}_2$ crystallizes out (see above). The α - S_8 is obtained as large yellow crystals while $S_{12}\cdot\text{CS}_2$ forms almost colorless small plates which can easily be separated from the S_8 by flotation. These plate-like crystals have been characterized by X-ray structure analysis as well as by vibrational spectra [87]. Infrared and Raman spectra of the filtered solution of S_8+S_π as well as of its evaporation residue showed once more the presence of S_8 , S_7 , and S_6 but in addition a Raman line at 460 cm^{-1} was observed which was assigned to the S-S stretching vibrations of soluble rings larger than S_8 (in the following termed as S_x). All these components were observed in sulfur melts quenched from temperatures of 120, 140, 250, 350, and 445 °C [80].

To obtain quantitative data on the composition of the S_8+S_π solution calibration curves were recorded using solutions of pure S_6 , S_7 , and S_8 in CS_2 .

Table 2 Molecular composition of liquid sulfur determined by vibrational spectroscopy of quenched melts (T: equilibration temperature; concentrations in mass %; S_x are soluble rings larger than S_8 ; the homocycles S_6 , S_7 , and S_x are the constituents of S_π) [88]

T (°C)	S_8 (%)	S_μ (%)	S_π (%)	S_6 (%)	S_7 (%)	S_x (%)
115	95	0.05	4.9	0.6	2.8	1.5
130	94	0.2	5.9	0.9	3.6	1.4
145	93.4	0.4	6.2	0.9	4.0	1.3
159	90.4	2.4	7.2	1.4	4.7	1.1
250	43.8	51.3	4.9	0.9	3.3	0.7
350	42.8	52.0	5.2	1.0	3.5	0.7

The concentration of S_x was obtained as the difference between the total sulfur concentration and the sum of the concentrations of S_6 , S_7 , and S_8 . To double-check the results the molecular mass of the S_8+S_π solution was determined osmometrically and the result compared with the molecular mass calculated from the analytical composition data assuming an average value of $x=25$; excellent agreement was obtained [88]. The final results were then used to calculate the composition of the melt with the assumption that the quenching procedure does not change the composition. These analytical results are given in Table 2.

The data in Table 2 demonstrate that the concentration ratio $c(S_i)/c(S_8)$ increases with increasing temperature for rings with $i<8$ but decreases for rings with $i>8$ as is to be expected from the impact of the entropy. The data obtained for the S_π content are in agreement with earlier values derived from the depression of the melting temperature of liquid sulfur (see above).

The maximum amounts of pure sulfur allotropes [71] isolated from 400 g liquid sulfur quenched from 160 °C, extracted at 20 °C by CS_2 followed by fractional crystallization are as given below [88]:

– S_7 : 0.8 g S_{12} : 0.25 g S_{18} : 80 mg S_{20} : 40 mg

The maximum amount of S_x isolated from 400 g melt was 1.2 g.

By chromatography on silica gel 60 at a column temperature of -40 °C the S_x mixture has been separated into six fractions; the mean molecular mass of the sulfur rings dissolved in these fractions ranged from 1100 (first fraction) to 733 (last fraction). In other words, S_x must contain rings with up to 35 atoms at least [88]. A more sophisticated chromatographic separation will be described in the following section.

3.2

Analysis of Quenched Sulfur Melts by HPLC

High-performance liquid chromatography (HPLC) using the reversed phase technique is used to separate the most complex mixtures of organic and inorganic molecules with base-line separation quality. In the case of sulfur ho-

mocycles so-called C18 stationary phases have turned out to be the best, e.g., silica gel the surface OH groups of which have been modified by substitution of the hydrogen atoms by dimethyloctadecylsilyl groups ($\text{Me}_2\text{C}_{18}\text{H}_{37}\text{-Si-}$). While untreated silica gel decomposes metastable sulfur rings such as S_7 to S_8 , the C18 phases are inert provided the surface OH groups have been substituted quantitatively. High-purity methanol is used as a mobile phase. Addition of *cyclo*-hexane to the methanolic eluent (up to 30 vol.%) reduces the retention time and at the same time enhances the solubility of the larger sulfur rings, while addition of water (up to 5%) increases the retention time [89, 90]. In some cases ethanol has been added as a third component, and gradient techniques helped to reduce the retention time of the larger rings [91]. All homocycles S_n with $n=6-28$ have been separated and can be determined in this way alongside one another. The rings larger than S_{28} which are definitely present in π -sulfur (see above) cannot be separated by this technique owing to their low solubility in the polar mobile phase, owing to their low concentration in the quenched sulfur melt and owing to their large retention times which result in broad and therefore small peaks due to diffusion broadening.

The retention times t_R of sulfur homocycles systematically increase at identical conditions with the ring size allowing the estimation of t_R for new S_n species by inter- or extrapolation. The capacity factors

$$k' = (t_R - t_0)/t_0 \quad (11)$$

are linearly dependent on the number n of the sulfur atoms in a semilogarithmic plot (t_0 : dead time of the chromatographic system) [89, 91]. The most sensitive detection technique for the separated components is the measurement of the UV absorption at or near 254 nm since all compounds containing S-S bonds show a very strong absorbance in this wavelength region [92]. The samples are injected into the flowing mobile phase as very dilute CS_2 solutions (1 mg $\text{S}_n/100$ ml CS_2).

Chromatograms of quenched sulfur melts, of π -sulfur and of S_x demonstrate that sulfur melts contain all homocycles from S_6 to at least S_{28} [91]. There is no reason to assume that larger rings are absent; it is just not possible to detect them by the presently available techniques. If these rings are too large they will be insoluble and in this way become components of the polymeric sulfur S_{∞} .

To analyze sulfur ring mixtures quantitatively by HPLC requires the determination of the calibration functions $A=f(c)$ by analysis of solutions of differing concentrations c for all the allotropes available as pure materials (A : peak area). In most cases this function has the form $A=a \cdot c$ with the slope depending systematically on the ring size or the number of sulfur atoms, respectively [89].

The quantitative composition of liquid sulfur as determined by HPLC analysis after quenching in liquid nitrogen, extraction with CS_2 and separation from the insoluble S_μ is shown in Table 3 [93]. These data are the most reliable information about the composition of liquid sulfur in the tempera-

Table 3 Molecular composition of equilibrated liquid sulfur (mass %) after quenching the melt from temperatures of between 116 and 387 °C to -196 °C. S_μ is the fraction insoluble in carbon disulfide (polymeric sulfur)

T [°C]	S ₈	S _{μ}	S ₆	S ₇	S ₉	S ₁₀	S ₁₁	S ₁₂	S ₁₃	S ₁₄	S ₁₅	S ₁₆	S ₁₇	S ₁₈	S ₁₉	S ₂₀	S ₂₁	S ₂₂	S ₂₃	ΣS
116	93.63	0.17	0.51	3.05	0.30	0.10	0.03	0.39	0.02	0.03	0.06	0.03	0.03	0.06	0.08	0.07	0.05	0.04	0.02	98.67
122	93.08	0.24	0.56	3.29	0.35	0.10	0.04	0.42	0.03	0.04	0.07	0.03	0.03	0.07	0.08	0.07	0.06	0.04	0.02	98.62
141	92.69	0.31	0.75	4.51	0.54	0.17	0.06	0.48	0.05	0.06	0.09	0.05	0.05	0.09	0.12	0.10	0.07	0.05	0.03	100.27
159	83.43	3.01	0.93	5.20	0.62	0.21	0.07	0.49	0.06	0.07	0.11	0.06	0.06	0.09	0.13	0.12	0.08	0.05	0.03	94.82
178	68.82	19.91	0.89	4.87	0.57	0.14	0.07	0.45	0.05	0.07	0.10	0.06	0.06	0.07	0.12	0.10	0.08	0.06	0.04	96.53
197	60.64	28.42	0.91	4.86	0.51	0.12	0.07	0.42	0.04	0.06	0.10	0.06	0.06	0.11	0.12	0.11	0.09	0.06	0.04	96.80
220	54.33	34.21	0.89	4.55	0.58	0.19	0.07	0.40	0.05	0.07	0.10	0.06	0.06	0.09	0.11	0.08	0.06	0.04	0.03	95.97
243	51.48	39.85	0.91	4.73	0.61	0.20	0.07	0.40	0.05	0.07	0.10	0.07	0.06	0.10	0.12	0.11	0.08	0.06	0.03	99.10
269	50.70	38.96	0.89	4.44	0.58	0.20	0.07	0.39	0.05	0.07	0.10	0.06	0.06	0.06	0.11	0.08	0.06	0.04	0.02	96.94
293	54.02	37.80	0.90	4.61	0.61	0.20	0.08	0.40	0.05	0.07	0.10	0.06	0.06	0.08	0.11	0.08	0.06	0.04	0.03	99.36
316	54.89	35.22	0.81	3.87	0.51	0.18	0.07	0.41	0.04	0.06	0.10	0.05	0.05	0.06	0.11	0.08	0.06	0.03	0.02	96.62
339	56.40	34.47	0.83	4.18	0.56	0.19	0.07	0.39	0.04	-	0.10	0.05	0.06	0.08	0.10	0.08	0.06	0.04	0.02	97.72
387	56.28	33.91	0.86	4.13	0.50	0.18	0.06	0.40	0.04	0.06	0.09	0.05	0.05	0.09	0.10	0.09	0.07	0.05	0.03	97.04

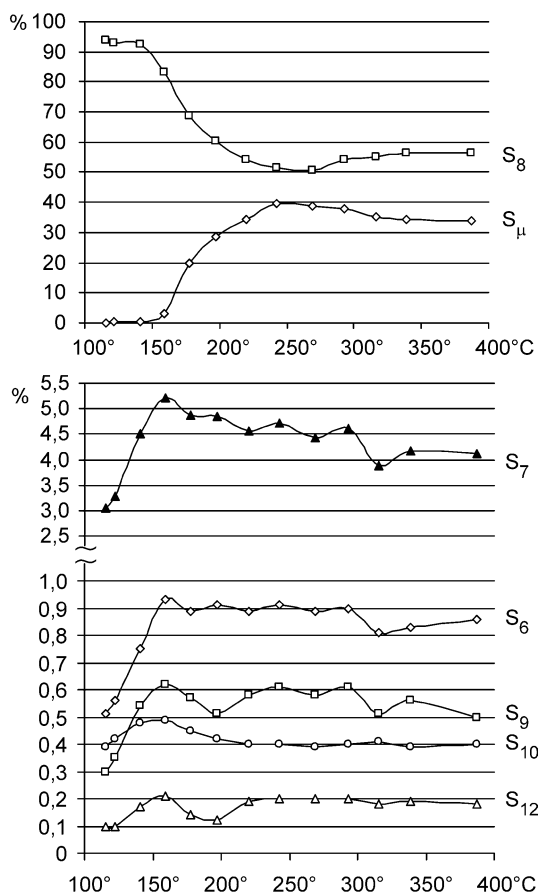


Fig. 2 Temperature dependence of the concentrations of S₈ and of the polymer S_μ (top), of S₇ (center), and of S₆, S₉, S₁₀, and S₁₂ (bottom) in liquid sulfur according to the data in Table 3. Note the two different ordinate scales

ture region 116–387 °C available at present. The temperature dependence of the concentrations of the major components of liquid sulfur is shown in Fig. 2.

According to the data in Table 3 the S₈ content decreases from 93.6 mass % at 116 °C via 83.4% at 159 °C to 50.7% at 269 °C at which temperature it reaches a minimum followed by a slight increase to 56.3% at 387 °C. Simultaneously, the polymer content increases from 0.2% at 116 °C via 3.0% at 159 °C to a maximum of 39.9% at 243 °C followed by a slight decrease to 33.9% at 287 °C. Of all the rings soluble in CS₂ the concentration of S₈ is highest, of course; second comes S₇ the concentration of which first increases from 3.1% at 116 °C to 5.2% at 159 °C followed by a decrease at higher temperatures as a consequence of the decreasing S₈ concentration. At 159 °C the order of decreasing ring concentration is S₈ >> S₇ >> S₆ > S₉ > S₁₂ > S₁₀ > S₁₉,

$S_{20}, S_{15} > S_{18} > S_{11}, S_{13}, S_{14}, S_{16}, S_{17}, S_{21}, S_{22} > S_{23}$. Larger rings, though present, could not be determined quantitatively [93].

The chemical equilibria



are governed by the Gibbs energy $\Delta G^\circ = \Delta H^\circ - T \cdot \Delta S^\circ$. At higher temperatures the entropy term favors the rings smaller than S_8 since ΔS° will be positive in these cases and $-T \cdot \Delta S^\circ$ overcompensates the always positive term ΔH° resulting in a negative value of ΔG° . The rings larger than S_8 are thermodynamically unfavorable and their concentrations remain small at all temperatures; only the entropy of mixing may work in favor of them. However, since a large number of different ring sizes is possible including an increasing number of different conformations of the same ring size they cumulatively contribute substantially to the concentration of π -sulfur. The missing “rest” of the 100% assay in the last column of Table 3 is attributed to the soluble rings with more than 23 atoms as well as to analytical errors [93].

In principle, one would also expect the homocyclic S_5 to be present in hot sulfur melts but this species may be too unstable to survive the quenching and extraction procedure since never has ever a peak at the expected retention time been observed. However, according to Rau et al. [94] saturated sulfur vapor contains only 0.7 mol% S_5 but 20% S_6 and 12% S_7 at 200 °C. At higher temperatures the melt will also contain traces of S_4 , S_3 and S_2 [61]; see also the next section. The sum of the concentrations of the non- S_8 rings at 116 °C is 4.87%, practically identical to the concentration of π -sulfur as derived from the freezing point depression (see above), thus confirming the reliability of the HPLC analysis.

The data in Table 3 have been used to calculate the enthalpies of formation of the various rings in liquid sulfur from S_8 using Eq. (12). From these enthalpies the mean bond energies of the sulfur homocycles were derived. The differences of these mean bond energies to the value of S_8 (266.6 kJ mol⁻¹ [95]) are shown in Fig. 3 [93]. As can be seen, S_{12} and the rings larger than S_{17} are most stable (besides S_8) with mean bond energies of just 1 kJ mol⁻¹ below that of S_8 . Of the smaller rings S_6 seems to be most strained but even in this case the difference in bond energies of ca. 4 kJ mol⁻¹ is only 1.5% of the total bond energy. Density functional calculations confirmed that the mean bond energies of sulfur rings larger than S_{12} are practically identical [96].

Ludwig et al. have tried to model the composition of liquid sulfur by quantum-chemical calculations [97] which is not accurately possible since the polymeric molecules—a major component above 159 °C—cannot be calculated. Therefore, the results are of little use and no novel insights were achieved.

The critical parameters of sulfur have been determined as follows: $T_c=1313$ K, $p_c=179.7$ atm (18.2 MPa), $\rho_c=0.563$ g cm⁻³ [98]; $T_c=1313$ K, $p_c=20.3$ MPa, $\rho_c=0.58$ g cm⁻³ [99].

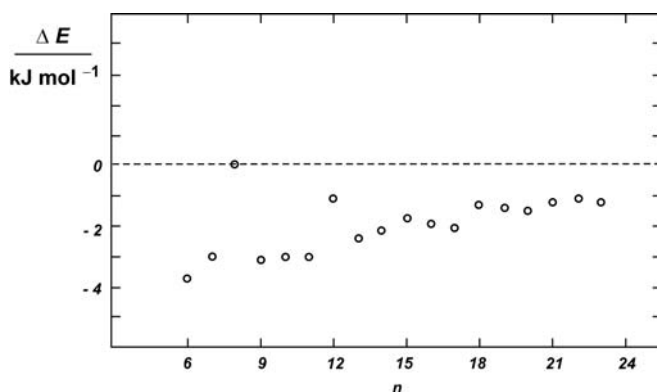


Fig. 3 Mean bond energies of the sulfur homocycles $S_6 \dots S_{23}$ in liquid sulfur relative to S_8 . ΔE is the difference in mean bond energies between S_8 and the particular ring (in kJ mol^{-1}) [93]

If equilibrated liquid sulfur was allowed to cool down from 122 to 35 °C at a controlled rate of between 2.4 and 0.01 K min^{-1} (cooling time between 0.6 and 145 h) all the metastable rings S_n ($n \neq 8$) partly or completely decomposed to a mixture of S_8 and polymeric sulfur [100]. The slower the cooling the more S_8 was formed in this way while the concentration of the polymer was maximum at a cooling time of 2–15 h, depending on the purity of the sample. However, even if the cooling rate was very low and the solidified product was stored for several months at 20 °C it still contained traces of S_7 (0.1–0.2%) as some kind of memory to its former liquid state. Since commercial sulfur samples are prepared from liquid sulfur it is not surprising that they always contain between 0.10 and 0.56% S_7 which, by the way, is responsible for the bright-yellow color of these samples while pure α - S_8 , obtained by recrystallization of the commercial samples from organic solvents, is greenish-yellow [100]. The traces of S_7 in solid S_8 may be considered as “matrix-isolated molecules” or as stable solid state “defects” or simply as a solid solution of little S_7 in S_8 .

3.3

UV-Vis Spectroscopy of Liquid Sulfur

At 200 °C liquid sulfur is as deep-yellow as a synthetic mixture of its components S_8 , S_n and S_μ would be. With increasing temperature the color changes via orange and dark-red to dark red-brown [3]. The saturated sulfur vapor shows the same colors. Several research groups have tried to use absorption spectroscopy in the UV-Vis region to detect and identify the molecular species responsible for the color changes [101–105]. Because of the extremely high absorbance of sulfur one usually obtains spectra characterized by a steep absorption edge. At 120 °C melt temperature this edge begins to rise at 480 nm (2.6 eV) and is very steep near 450 nm (path length 0.1 mm). With

increasing temperature the edge shifts to larger wavelengths. This red-shift is explained by the increasing excitation of molecular vibrations resulting in a broadening of the absorption bands of S_8 . This view is in agreement with the measured activation energy for the red-shift of $10 \pm 1 \text{ kJ mol}^{-1}$ [106]. From about $400 \text{ }^\circ\text{C}$ a strong increase of the absorption in the region of $950 \pm 100 \text{ nm}$ (ca. 1.3 eV) is observed resulting in shoulders at the absorption edge. This new absorption has been assigned to the chain-end atoms of the free radicals since the temperature dependence of this additional absorption has been shown to be about the same as that of the ESR signal intensity (while in fact it is slightly smaller) [103, 105]. The band gap between the valence and conduction bands of liquid sulfur is 3.65 eV at $150 \text{ }^\circ\text{C}$; it slightly decreases with increasing temperature [105].

The spectra of very thin films of liquid sulfur exhibit absorptions which are not present in the spectra of pure S_8 . Even at as low a temperature as $145 \text{ }^\circ\text{C}$ a shoulder at 360 nm is observed which has been assigned to S_6 [103]. This absorption band can also be seen in the spectra of liquid sulfur at $250 \text{ }^\circ\text{C}$ [102, 103] and in the spectrum of the melt quenched from $250 \text{ }^\circ\text{C}$ [102]. The assignment to S_6 is rather unlikely since this molecule has practically no absorption in this region [92]. Furthermore, the S_6 concentration at $145 \text{ }^\circ\text{C}$ is only 0.8% [93]. Most probably the 360 nm band is caused by the collective absorption of the components of π -sulfur and in particular by the S_x content of the melt, i.e., the rings larger than S_8 which have higher extinction coefficients at 360 nm than the smaller rings [92].

However, Tamura et al. [105] found a linear correlation between the absorbance at 380 nm and the polymer content of the melt quenched from temperatures in the region $160\text{--}300 \text{ }^\circ\text{C}$ as determined by Koh and Klement [24]; they consequently assigned this band to the central atoms in the polymeric chains of S_∞ .

At temperatures of $300\text{--}700 \text{ }^\circ\text{C}$ another additional absorption is observed at 400 nm , and in the region of $500\text{--}900 \text{ }^\circ\text{C}$ another one at 520 nm [102, 103]. By comparison with the spectra of sulfur vapor [61] as well as with the spectra of photolytic dissociation products of S_3Cl_2 and S_4Cl_2 [102] the absorption at $520\text{--}530 \text{ nm}$ was assigned to the *cis*-planar isomer of the S_4 molecule and the $400\text{--}410 \text{ nm}$ band to the cherry-red S_3 molecule [102]. The saturated sulfur vapor contains about $1 \text{ mol}\%$ each of S_3 and S_4 at $500 \text{ }^\circ\text{C}$ but about $10 \text{ mol}\%$ each at $1000 \text{ }^\circ\text{C}$ [61, 94]. At temperatures below $300 \text{ }^\circ\text{C}$ these species are practically absent and therefore can hardly play any significant role in liquid sulfur. The deep red-brown color of sulfur melts at temperatures above $400 \text{ }^\circ\text{C}$ has also been assigned to the red S_3 molecule [102] but in addition S_4 and the diradicals S_x^C will contribute. The extinction coefficient of S_3 is one order of magnitude larger than that of S_4 [107]. The diradicals probably absorb at practically any wavelength owing to their widely differing chain-lengths x [102].

However, in addition to the chain-like and cyclic species discussed so far the presence of branched rings and chains in sulfur vapor and in liquid sulfur has also been discussed [108] but no conclusive *experimental* evidence for such isomers is presently available. For example, an isomer of *cyclo*- S_8

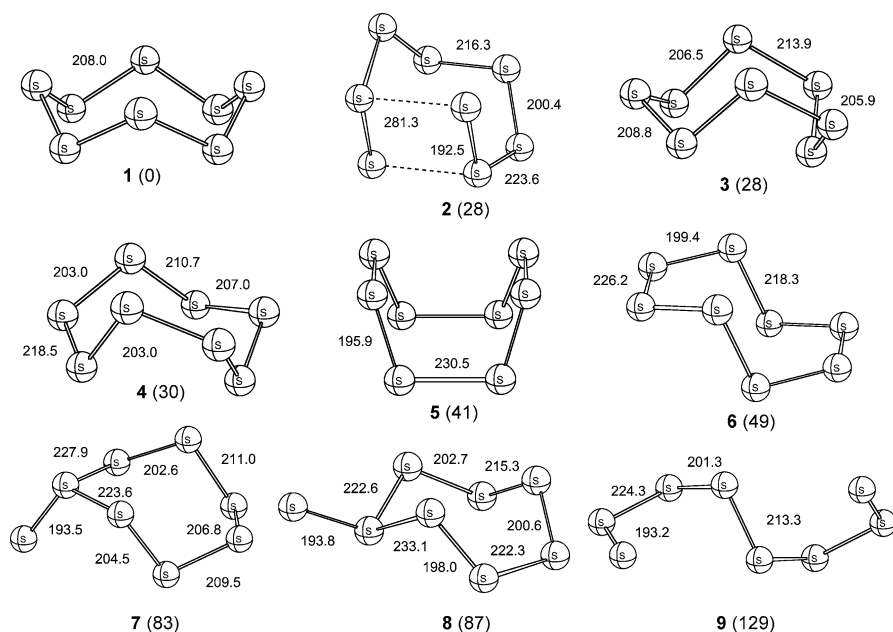


Fig. 4 Structures of nine isomeric molecules of composition S₈ with internuclear distances (in pm) as optimized at the B3LYP/6-31G(2df) level of theory. The relative Gibbs energies ΔG°₂₉₈ are given in parentheses [109]

could be a candidate since *ab initio* MO calculations at the very high G3X(MP2) level of theory place the lowest energy isomer of S₈ at only ΔG°₂₉₈=28.3 kJ mol⁻¹ above the eight-membered ring [109]. This isomer is of C₂ symmetry [110] and has the structure of a partly opened ring or a cluster-like spiral (species 2 in Fig. 4); its concentration in liquid sulfur was estimated from the calculated Gibbs energy of formation as ca. 1% of all S₈ species at the boiling point. The structurally related homocyclic sulfur oxide S₇=O is known as a pure compound and has been well characterized by X-ray crystallography and vibrational spectroscopy [111].

In addition, S₈ ring conformations of lower symmetry than D_{4d} are likely candidates in liquid sulfur. For example, the *exo-endo* isomer 3 (Fig. 4) is by only ΔG°₂₉₈=27.8 kJ mol⁻¹ less stable than the ground state conformation and therefore its relative concentration in liquid sulfur at the boiling point will be also ca. 1% of all S₈ species [109].

The HOMO/LUMO gaps of the isomeric sulfur molecules shown in Fig. 4 (generally of branched rings and chains) are considerably smaller than for the crown-shaped S₈ ring [109]. Therefore, the UV-Vis spectra of these species will exhibit absorption bands at longer wavelengths than the ground state species S₈. In addition, these species possess a dipole moment in contrast to the S₈ ring of D_{4d} symmetry. All of these species can be expected to be present in liquid sulfur at high temperatures, and from the Gibbs energies

of formation their relative concentrations at the melting point and the boiling point of sulfur have been calculated as follows (related to the concentration of species 1) [109]:

- At 393 K (melting point):
- 1 : 2 : 3 : 4 : 5 : 6 : 7 : 8 : 9 =
 $1 : 2 \times 10^{-4} : 2 \times 10^{-4} : 1 \times 10^{-4} : 3 \times 10^{-6} : 4 \times 10^{-7} : 1 \times 10^{-11} : 3 \times 10^{-12} : 7 \times 10^{-18}$
- At 718 K (boiling point):
- 1 : 2 : 3 : 4 : 5 : 6 : 7 : 8 : 9 =
 $1 : 9 \times 10^{-3} : 9 \times 10^{-3} : 6 \times 10^{-3} : 1 \times 10^{-3} : 3 \times 10^{-4} : 1 \times 10^{-6} : 5 \times 10^{-7} : 4 \times 10^{-10}$

Branched long *chains* of the type -S-S-S(=S)-S-S- must also be components of the polymeric S_{∞} present in liquid sulfur at higher temperatures since the model compound H-S-S-S(=S)-S-S-H was calculated to be by only $\Delta G^{\circ}_{298} = 51 \text{ kJ mol}^{-1}$ less stable at the G3X(MP2) level than the helical isomer of hexasulfane, H_2S_6 [109].

Isomeric forms of *cyclo-S₆* and *cyclo-S₇* can also be suspected as components of liquid sulfur at high temperatures. However, their relative energies have not been calculated yet on a high enough level of theory to obtain realistic concentrations.

The reflectance spectra of solidified liquid sulfur previously equilibrated at temperatures of between 120 and 440 °C have been measured at 25 °C and color pictures of these solidified melts were published [112]. These data are used to explain the yellow, orange and red colors of the sulfur flows on Jupiter's moon Io on which a number of very active sulfur volcanoes have been discovered [113]. These volcanoes are powered by SO_2 gas which forces the liquid sulfur from its underground deposits to the surface.

If hot sulfur melts or hot vapors at low pressure are condensed at low temperatures highly colored samples are obtained which may be black, green or red depending on the temperature and pressure conditions and the rate of quenching. These colors originate from the small molecules and radicals present at high temperatures and which are trapped in the solid sample. At room temperature these samples turn yellow, or—if not—the sulfur has not been pure.

3.4

Photochemistry of Liquid Sulfur

The photochemistry of elemental sulfur has been studied using solid, liquid and dissolved sulfur rings as well as solid polymeric sulfur. The general outcome is that the absorption of photons of sufficient energy triggers a homolytic bond dissociation with formation of free radicals as well as a breakdown of S_8 rings into smaller singlet molecules like $S_3 + S_5$ or two S_4 . In liquid solutions photochemical interconversion as well as polymerization reactions of sulfur homocycles are observed [114]. In the case of liquid sulfur only very few investigations are available. Sakaguchi and Tamura [115] illuminat-

ed very thin samples of liquid sulfur with a pulsed laser (355 nm) and observed the time dependence of the transient absorption spectra of the photo-generated species. Irradiation at sulfur temperatures of between 130 and 150 °C produced two types of species with relaxation times of 60 s and 40 min at 130 °C, respectively. Both species showed absorption maxima near 3.5 eV (354 nm). The short-lived product was formed by repeated illumination with 1.0 mJ pulses and was interpreted as polymeric chains of sulfur atoms. The long lived product was originally assigned to the short chains which were assumed to bind to S₈ rings as charge-transfer complexes [115]. As a seemingly more convincing species the branched S₇=S structure was later proposed as the long-lived product which had been found by molecular dynamics simulations of the photochemistry in liquid sulfur [116] (see below). However, as has been demonstrated in the previous section, the most likely candidate(s) for the long lived product absorbing near 360 nm is the π -sulfur in the sulfur melt, especially the medium-sized rings S_x(x>8) which form from polymeric sulfur by depolymerization. This follows from the rates of formation and decay of the long-lived product when it was generated thermally [115]; these rates agree very well with the rates of formation and decay of π -sulfur of which the Japanese authors were however not aware.

3.5

Electrical Conductivity of Liquid Sulfur

Under ambient conditions elemental sulfur is one of the best electrical insulators known. In fact, sulfur is the prototype of a non-metal defined as a material of zero electrical conductivity at 0 K. However, this statement applies to ambient pressures only. At very high pressures sulfur—like other typical non-metals—becomes an electrical conductor and, at very low temperatures, even a superconductor [117]. Because of the very low conductivity at standard conditions (e.g., 10⁻⁷ Ω⁻¹ cm⁻¹ at 550 °C) impurities play a major role and those studies which reported the lowest conductivity must be considered the most trustworthy.

The electrical conductivity σ of liquid sulfur increases with temperature except near the viscosity maximum of ca. 170 °C where a minimum of the conductivity is observed. Above 200 °C the plot of log σ vs 1/*T* was found by several authors to be linear but the slopes of these linear relationships as well as the absolute conductivities vary considerably [118–122]. On the assumption that the conductivity at these temperatures is intrinsic, values of about 1.6 eV were derived for the activation energy at high temperatures (up to 900 °C) [121, 122], an energy which is much higher than the activation energy for the formation of free spins by homolytic bond dissociation (see above).

In a more recent investigation the conductivity of highly purified sulfur was measured in the range of 300–900 °C using gold electrodes and a quartz cell. It was found that the slope of the linear function log σ vs 1/*T* changes relatively sharply near 550 °C (see Fig. 5). Activation energies of 1.9 eV below this temperature and of 1.05 eV above 550 °C were obtained for the gen-

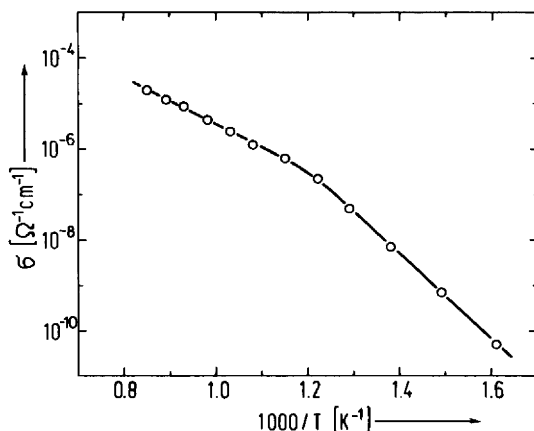


Fig. 5 Temperature dependence of the electrical conductivity of very pure liquid sulfur [123]

eration of the charge carriers [123]. In other words, liquid sulfur at high temperatures is a semiconductor. It was assumed that the conductivity is caused by the unpaired electrons at the chain-end atoms (“dangling bonds”) of polymeric sulfur which are assumed to form acceptor states within the bandgap. Using an activation energy of 0.8 eV for the formation of a “dangling bond” (free spin) from the ESR measurements of Koningsberger et al. (see above) the activation energy above 550 °C was calculated as 1.3 eV in agreement with the position of the optical absorption band of 1.25 eV associated with the sulfur atoms at the chain-ends [123] (see above). The higher value observed at lower temperatures was explained by the influence of impurities at the ppm level; the deviating results of the earlier authors were explained similarly [123].

From measurements of the dielectric constant of liquid sulfur in the temperature range 134–206 °C [15] it was concluded that the molar polarization increases from 134–159 °C which was explained by the assumption of a temperature dependent equilibrium between S_8 (crown) and S_8 (chair) molecules, the latter possessing a permanent dipole moment owing to their low symmetry (C_s). However, the most natural rationalization of the findings is that certain components of π -sulfur like S_7 and S_9 —molecules of low symmetry possessing a dipole moment—contribute to the molar polarization. Since their concentration increases with temperature up to the polymerization transition it is to be expected that the molar polarization changes accordingly. Above 159 °C the molar polarization is proportional to the polymer content of the melt.

3.6

Polymerization Theories for Liquid Sulfur

The polymerization reaction of liquid sulfur above 157 °C, often termed as “ S_λ - S_μ transition” or simply “ λ -transition”, cannot be considered as a phase transformation in the normal sense but is a kinetically controlled equilibrium reaction. In fact, over the whole temperature range there is an equilibrium between small cyclic monomer molecules and polymeric sulfur molecules of differing molecular sizes and types (rings and chains). Thus, there is no spontaneous and complete polymerization reaction at a defined temperature but only an *additional polymer formation* on rising the temperature above 157 °C! This temperature follows from the temperature dependence of the heat capacity [14] and of the polymer concentration [124]. Neutron diffraction measurements on liquid sulfur support this view [125]. Since the equilibrium is established only slowly owing to the high activation energy the polymerization reaction is considerably heating-rate dependent.

Several authors have tried to simulate the *mechanism of the reactions* in liquid sulfur by molecular dynamics (MD) calculations. The starting reaction, that is the opening of the S_8 ring by homolytic bond dissociation, was achieved either thermally [126] or photochemically [116, 127]. The thermal treatment of a theoretical system initially consisting of 125 S_8 rings resulted in mixtures of diradical-chains of various sizes together with some medium sized rings like S_{12} besides S_8 . However, the rather simple potential function used and the restriction of the density to a fixed value are probably responsible for the fact that the molecular composition of this system shows hardly any similarity to the real sulfur melt [126].

The same kind of criticism has to be applied to a MD calculation based on density functional theory in which only nine S_8 molecules placed in a cubic box were heated or photoexcited followed by quenching [128]. As expected the rings turned into chains of different lengths but no rings other than S_8 were produced.

A more realistic treatment is the simulation of a ring opening polymerization by Ballone and Jones [129]. These authors investigated the behavior of 10,000 cyclic particles in a periodically squared (cubic) simulation box. To start the reaction one molecule of an initiator was added, and the development of the system as a function of temperature, density and “reaction time” was studied. At low densities the initially present cyclic tetramers turned into a mixture of smaller and larger rings while at higher densities one huge chain-like polymer molecule resulted together with a “background” of medium sized rings consisting of up to several thousand monomers (since the initiator molecule is incorporated into the polymer only one such molecule can form in such a simulation). The formation of these species is entropy-driven since the reaction enthalpy was assumed to be zero. The larger number of possible configurations in the polymer as well as in the medium sized rings results in a positive reaction entropy. In addition, the fact that a “living polymer” is formed which is able to undergo bond interchange reactions also adds to the entropy gain. Although sulfur was not considered specifical-

ly in this work the results show many similarities to the experimental findings regarding the composition and thermal behavior of sulfur as described in the previous sections.

To simulate the first step in the *photochemical polymerization* of liquid sulfur by ab initio molecular dynamics calculations one electron of an S_8 ring was promoted from the HOMO to the antibonding σ^* orbital (LUMO) which resulted in immediate ring opening [127]. This electron configuration was then relaxed. The following adjustment in a system of ten S_8 rings at 400 K revealed interesting reactions [116]. The eight-atomic diradical-chain, now in the ground state, did not recombine back to the original S_8 ring nor did it react with another S_8 molecule to form an S_{16} chain but instead it isomerized to a novel type of structure which is best described as $S_7=S$:



One atom of this structure is exocyclic while the others form an asymmetrical seven-membered ring. Even if another S_8 chain was generated by electron excitation in the same system of ten S_8 rings it also relaxed to $S_7=S$ rather than recombining to *cyclo*- S_8 or reacting with a neighboring S_8 ring. This $S_7=S$ structure survived for a long time in the MD simulation [116]. However, if the concentration of S_8 diradical-chains was increased (by exciting four electrons in the system of ten S_8 rings) it was found that, after the excitation was terminated, the four S_8 chains recombined pairwise forming two S_{16} chains. The reaction of an S_8 chain with the $S_7=S$ species also resulted in an S_{16} chain [116]. These results indicate that diradical-chains as well as the branched rings or the other isomers of S_8 shown in Fig. 4 may be important intermediates in the polymerization of liquid sulfur.

Numerous authors have tried to model the *equilibrium composition and the related physical properties* of liquid sulfur theoretically assuming certain reversible reactions and adjusting the thermodynamic functions ΔH° and ΔS° in such a way that the polymerization behavior, that is the polymer content of the melt at various temperatures as known at the particular time, could be simulated or “explained”. In almost all cases, however, the melt was considered to consist entirely of S_8 rings (S_8^R) and polymeric chain-like diradicals (S_x^C). The other small and/or medium sized rings were neglected despite the fact that at the time there was already experimental evidence available for the presence of such species in liquid sulfur. Nevertheless, we will discuss some of these theories or models here to illustrate the complexity of the problem.

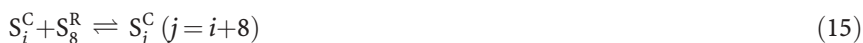
Powell and Eyring [65] in 1943 proposed the equilibrium



and used a reaction enthalpy of $\Delta H^\circ=115 \text{ kJ mol}^{-1}(S_x^C)$ which was assumed to be independent of the chain-length x and of the temperature T . The reaction entropy was assumed to depend on x as follows: $\Delta S^\circ=99.8-0.0031 \cdot x$ ($\text{J mol}^{-1} \text{K}^{-1}$). With these assumptions the temperature dependence of the polymer concentration could be reproduced very nicely including the pla-

teau of ca. 50% S_∞ reached at temperatures above 250 °C as was later observed by many authors including Koh and Klement [24]. Also, the polymer content started to increase right from the melting point of β - S_8 in agreement with the experimental observations and not only above 157 °C. However, this model is nevertheless unsatisfactory since it predicts a diradical concentration of 7% at 150 °C in contradiction to the ESR spectroscopic results which show first *traces* of free spins at 153 °C only [69] (see above). If these radicals are assumed to be extremely long chains (resulting in a low spin concentration) one would expect an increase in viscosity from 120 to 150 °C in contrast to the observed decrease. Furthermore, the existence of rings other than S_8 in liquid sulfur is ignored in this model.

In 1952, Gee [64] analyzed the thermal behavior of liquid sulfur. He was aware of the fact that the melt contains traces of *cyclo*- S_6 (since he noticed that S_6 is present in sulfur vapor) besides S_8 rings as well as diradical chains but initially he based his model solely on the following ring addition reaction:



Assuming $\Delta H^0 > 0$ and $\Delta S^0 > 0$, Gee derived the equation

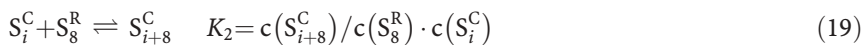
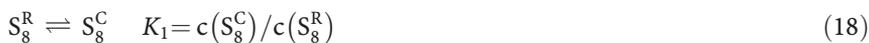
$$-\ln(1 - \Phi) = \Delta H^0 (1/T_\Phi - 1/T)/R \quad (16)$$

using Flory's polymerization theory. The polymer concentration Φ is then predicted as zero below a certain "critical transition temperature" T_Φ at which Φ suddenly increases. Using older literature data for the temperature dependence of the polymer content of the sulfur melt Gee derived $\Delta H^0 = 17 \text{ kJ mol}^{-1}$ for the ring addition reaction at Eq. (15). Equation (16) predicts a continuous increase of the polymer content Φ with increasing temperature resulting in a value of ca. 80% at 400 °C while for temperatures below T_Φ the equation is invalid. This behavior is in sharp contrast to many experimental observations. Therefore, the author proposed a second equilibrium reaction:



With a number of assumptions regarding the enthalpy of this reaction and the maximum chain-length of the polymer another mathematical equation was derived which is applicable at all temperatures but yields a polymer concentration of only $10^{-12}\%$ at 120 °C in contradiction to all analytical data available at the time. In a supplementary publication by Gee et al. [66] the enthalpy of the ring addition reaction was reduced to 13.3 kJ mol^{-1} and the reaction entropy assumed as $31 \text{ J mol}^{-1} \text{ K}^{-1}$ but novel results were not obtained. The authors discussed however the possibility that the sulfur melt may contain rings larger than S_8 and that the polymer S_∞ present at temperatures below 159 °C may consist of very large rings rather than chains.

Tobolsky and Eisenberg [67, 68] presented another general analysis of equilibrium polymerization systems and based their model for liquid sulfur on the following reversible reactions:



The diradical chain S_8^C obtained by ring opening of a cyclic S_8 molecule is assumed to act as an initiator in the following stepwise ring addition polymerization shown in Eq. (19). It was assumed that the equilibrium constant $K_2 = c(S_{i+8}^C)/c(S_8^R) \cdot c(S_i^C)$ is independent of the chain-length i . The number average chain length P is then given by Eq. (20):

$$M_0 = (P - 1)/P \cdot K_2 + K_1 \cdot P(P - 1)/K_2 \quad (20)$$

$M_0 = 3.90 \text{ mol kg}^{-1}$ is the total concentration of pure sulfur. Using crude literature data for the polymer content and for P at various temperatures (as estimated before by Gee), the following thermodynamic data were derived from plots of $\log K$ vs $1/T$:

- $\Delta H^0(18) = 137 \text{ kJ mol}^{-1}$, $\Delta S^0(18) = 96 \text{ J mol}^{-1} \text{ K}^{-1}$
- $\Delta H^0(19) = 13.3 \text{ kJ mol}^{-1}$, $\Delta S^0(19) = 19.4 \text{ J mol}^{-1} \text{ K}^{-1}$

However, this model also predicts a continuous increase in the polymer content with temperature resulting in 48% at 250 °C and 68% at 350 °C while the best analytical data show that the maximum value for S_∞ in high-purity sulfur melts is 40% [93]. In addition, the equilibrium reactions between rings other than S_8 and the polymer as well as the substantial polymer content at temperatures below 157 °C are neglected in this model. Therefore, the polymerization theory by Tobolsky and Eisenberg as well as its slightly modified versions [42, 69, 130–132] are also unsatisfactory.

In 1963 Gee [133] published a modified version of his polymerization theory which in principle allows for the incorporation of small rings other than S_8 . The general description of a ring addition reaction (Eq. 21) is given by Eq. (22) if no solvent is present:



$$-R \ln(1 - \Phi) = \Delta S^0 - \Delta H^0/T \quad (22)$$

This assumption is approximately valid in the case of liquid S_8 which is always the majority ring species in sulfur melts below 170 °C. For S_7 , the second most abundant ring in liquid sulfur, the term $R \cdot \ln c$ must be added to Eq. (22) (c is the fraction of that ring in the mixture of S_8 and dissolved polymer):

$$-R \cdot \ln(1 - \Phi) = \Delta S - \Delta H/T + R \cdot \ln c \quad (23)$$

In the case of S_8 the ring addition reaction is endothermic and endentropic ($\Delta S > 0$). This results in a “floor temperature” for the polymerization and Eq. (23) can be simplified to the form Eq. (16) given above [133]. No poly-

mer can exist below the floor temperature, and above the floor temperature the polymer concentration rises steeply.

The polymer dissolved in liquid S_8 must be in equilibrium with all dissolved species. Steudel et al. have shown in 1984 that the addition of an S_7 ring to a polymeric diradical-chain is exothermic and endentropic if pure liquid S_7 is considered [124]. Therefore, pure *cyclo-S₇* is thermodynamically unstable with respect to polymeric chains at all temperatures while in the case of pure *cyclo-S₆* the ring addition is exothermic and exentropic resulting in a (very high) “ceiling temperature” for the polymerization above which no polymer can exist [124]. Since the enthalpy and entropy data for the ring addition reactions of S_6 and S_7 are not accurately known the consequences for liquid sulfur can be discussed only qualitatively. At the so-called onset of the polymerization at 157 °C liquid sulfur contains about 1% S_6 and 5% S_7 [93]. The term $R \cdot \ln c$ in Eq. (23) has then values of $-38 \text{ J mol}^{-1} \text{ K}^{-1}$ for S_6 and $-25 \text{ J mol}^{-1} \text{ K}^{-1}$ for S_7 . Under these circumstances the addition of both rings *in liquid sulfur* to the polymer is exentropic. However, the ceiling temperatures cannot be calculated as long as the necessary polymerization enthalpies and entropies are not known accurately.

Whether the polymer in liquid sulfur actually consists of long chains or very large rings does not make any difference since the thermodynamic properties of the ring addition reactions (Eq. 21) are independent of the structure of the polymer as long as it is macromolecular. In fact, it is highly unlikely that the polymer present in liquid sulfur at temperatures below 157 °C is exclusively chain-like. This follows not only from the high dissociation enthalpy of S-S bonds of 150 kJ mol^{-1} which is not available at moderate temperatures. More convincing is the following argument: the viscosity *minimum* of liquid sulfur is observed at 157 °C at which temperature the melt contains already ca. 3% of polymeric sulfur! At 157 °C the viscosity suddenly rises sharply while the polymer content rises only gradually. Obviously, a *new type of polymer* is formed at this temperature which must be responsible for the dramatic increase in viscosity. This polymer is evidently chain-like and a diradical in agreement with the first observation of free radicals near 153 °C by ESR spectroscopy [38]. Only chain-like macromolecules can form catenane-like molecules and entangled chains which cannot longer flow and slip easily without breaking covalent bonds and which therefore give rise to the observed viscosity increase. This view is supported by the analytical data of quenched melts which showed the presence of relatively large rings up to at least S_{35} (see above). There is no reason to exclude even larger rings which, above a certain molecular mass, will be insoluble in carbon disulfide and therefore qualify as “polymeric sulfur”.

On quenching and extraction the long diradical-chains of polymeric sulfur will pick up some impurity atoms from the solvent or from the air to chemically satisfy the chain ends with, for example, H or OH groups. Therefore, polymeric sulfur prepared in this way is diamagnetic (S_μ). If this view is correct the polymer generated at temperatures below 157 °C is mainly composed of very large rings, formed by some kind of ring-fusion reaction with no or little involvement of radicals, while the polymer formed at tem-

peratures higher than 157 °C mainly consists of long chains together with a certain percentage of very large rings. However, never has any author reported a qualitative difference in the properties of polymeric sulfur isolated from below or above the “polymerization temperature” of ca. 157 °C, respectively.

Finally, it should be mentioned that several times species with four-coordinate sulfur atoms (tetrathiasulfuranes) have been claimed to be present in polymeric sulfur [134] or to be intermediates in the interconversion of sulfur rings and chains [135, 136]. However, recent high-level ab initio MO calculations [137] demonstrated that tetrathiasulfuranes like $S(SH)_4$ are much too unstable (endothermic) to play any role in liquid sulfur.

Acknowledgement I am grateful to Dr. Yana Steudel for assistance with the figures. This work has been supported by the Deutsche Forschungsgemeinschaft and the Verband der Chemischen Industrie.

References

1. W. Botsch, *Chemie unserer Zeit* **2001**, 35, 324.
2. R. Steudel, *Chemie unserer Zeit* **1996**, 30, 226 and *Chemie unserer Zeit* **1980**, 14, 73.
3. For color pictures of the melt at different temperatures, see ref [2].
4. F. Bacon, R. Fanelli, *J. Am. Chem. Soc.* **1943**, 65, 639.
5. T. Doi, *Rev. Phys. Chem. Japan* **1963**, 33, 41.
6. J. Ruiz-Garcia, E. M. Anderson, S. C. Greer, *J. Phys. Chem.* **1989**, 93, 6980.
7. A. Eisenberg, *J. Chem. Phys.* **1963**, 39, 1852.
8. G. C. Vezzoli, P. J. Walsh, *High Temp. High Pressure* **1977**, 9, 345.
9. K. Bröllos, G. M. Schneider, *Ber. Bunsenges. Phys. Chem.* **1974**, 78, 296.
10. M. Kuballa, G. M. Schneider, *Ber. Bunsenges.* **1971**, 75, 513.
11. F. Fehér, E. Hellwig, *Z. Anorg. Allg. Chem.* **1958**, 294, 63.
12. H. Patel, L. B. Borst, *J. Chem. Phys.* **1971**, 54, 822.
13. K. M. Zheng, S. C. Greer, *J. Chem. Phys.* **1992**, 96, 2175.
14. F. Fehér, E. Hellwig, *Z. Anorg. Allg. Chem.* **1958**, 294, 71.
15. M. E. Baur, D. A. Horsma, *J. Phys. Chem.* **1974**, 78, 1670.
16. S. C. Greer, *J. Chem. Phys.* **1986**, 84, 6984.
17. A. Smith, *Z. Physik. Chem.* **1906**, 54, 257.
18. For an extensive review, see R. Steudel, *Z. Anorg. Allg. Chem.* **1981**, 478, 139.
19. P. W. Schenk, *Z. Anorg. Allg. Chem.* **1955**, 280, 1.
20. A. H. W. Aten, *Z. Phys. Chem.* **1913**, 83, 442.
21. A. H. W. Aten, *Z. Phys. Chem.* **1914**, 86, 1.
22. D. L. Hammick, W. R. Cousins, E. L. Langford, *J. Chem. Soc.* **1928**, 797.
23. J. Schenk, *Physica* **1957**, 23, 325, 546.
24. J. C. Koh, W. Klement, *J. Phys. Chem.* **1970**, 74, 4280.
25. U. Thümmler, Doctoral Dissertation. Freie Universität Berlin **1959**.
26. P. W. Schenk, U. Thümmler, *Z. Elektrochem. Ber. Bunsenges. Phys. Chem.* **1959**, 63, 1002.
27. E. Beckmann, C. Platzmann, *Z. Anorg. Allg. Chem.* **1918**, 102, 201.
28. T. K. Wiewiorowski, A. Parthasarathy, B. L. Slaten, *J. Phys. Chem.* **1968**, 72, 1890.
29. F. Fehér, G. P. Görler, H. D. Lutz, *Z. Anorg. Allg. Chem.* **1971**, 382, 135.
30. M. Thackray, *J. Chem. Eng. Data* **1970**, 15, 495.
31. E. D. West, *J. Am. Chem. Soc.* **1959**, 81, 29.
32. M. F. Churbanov, I. V. Skripachev, G. G. Devyatikh, *Russ. J. Inorg. Chem.* **1976**, 21, 1272.
33. P. W. Schenk, U. Thümmler, *Z. Anorg. Allg. Chem.* **1962**, 315, 271.

34. A. Smith, B. Holmes, *Z. Phys. Chem.* **1906**, *54*, 257.
35. A. Smith, C. M. Carson, *Z. Phys. Chem.* **1907**, *57*, 685.
36. A. H. W. Aten, *Z. Phys. Chem.* **1914**, *88*, 321.
37. D. M. Gardner, G. F. Fraenkel, *J. Am. Chem. Soc.* **1956**, *78*, 3279; J. E. Van Aken, *Physica* **1968**, *39*, 107.
38. D. C. Koningsberger, T. DeNeef, *Chem. Phys. Lett.* **1970**, *4*, 615.
39. J. A. Poulis, C. H. Massen, P. v. d. Leiden, *Trans. Faraday Soc.* **1962**, *58*, 474; J. A. Poulis, W. Derbyshire, *Trans. Faraday Soc.* **1963**, *59*, 559.
40. T. K. Wiewiorowski, F. J. Touro, *J. Phys. Chem.* **1966**, *70*, 3528.
41. M. F. Churbanov, I. V. Skripachev, G. G. Devyatykh, *Russ. J. Inorg. Chem.* **1976**, *21*, 439.
42. W. J. MacKnight, J. A. Poulis, C. H. Massen, *J. Macromol. Sci. Chem. A.* **1967**, *1*, 699.
43. H. Krebs, H. Beine, *Z. Anorg. Allg. Chem.* **1967**, *355*, 113.
44. R. E. Harris, *J. Phys. Chem.* **1970**, *74*, 3102.
45. M. Schmidt, H.-D. Block, *Angew. Chem.* **1967**, *79*, 944.
46. H. Krebs, E. F. Weber, *Z. Anorg. Allg. Chem.* **1953**, *272*, 288.
47. H. Krebs, *Z. Naturforsch. B* **1957**, *12*, 795.
48. K. E. Evans, S. F. Edwards, *J. Chem. Soc. Faraday Trans. II.* **1981**, *77*, 1929.
49. A. T. Ward, M. B. Myers, *J. Phys. Chem.* **1969**, *73*, 1374.
50. K.-D. Pohl, R. Brückner, *Phys. Chem. Glasses* **1982**, *23*, 23.
51. A. V. Tobolsky, W. MacKnight, R. B. Beevers, V. D. Gupta, *Polymer.* **1963**, *4*, 423.
52. A. Eisenberg, L. A. Teter, *J. Phys. Chem.* **1967**, *71*, 2332.
53. J. Gal, *Compt. Rend. Seances Acad. Sci.* **1892**, *114*, 1183; F. O. Rice, G. Sparrow, *J. Am. Chem. Soc.* **1953**, *75*, 848; F. O. Rice, J. Ditter, *J. Am. Chem. Soc.* **1953**, *75*, 6066.
54. A. Smith, W. B. Holmes, *Z. Phys. Chem.* **1903**, *42*, 469.
55. C. M. Carson, *J. Am. Chem. Soc.* **1907**, *29*, 499.
56. B. R. Currell, A. J. Williams, *Thermochim. Acta* **1974**, *9*, 255.
57. E. Beckmann, R. Paul, O. Liesche, *Z. Anorg. Allg. Chem.* **1918**, *103*, 189.
58. W. Klement, *J. Polym. Sci. (Polymer. Phys. Ed.)* **1974**, *12*, 815.
59. M. Schmidt, *Angew. Chem.* **1973**, *85*, 474.
60. R. Steudel, *Phosphorus Sulfur* **1983**, *16*, 251.
61. R. Steudel, Y. Steudel, M. W. Wong, *Top. Curr. Chem.* **2003**, in print.
62. J. A. Semlyen, *Trans. Faraday Soc.* **1968**, *64*, 1396.
63. J. A. Semlyen, *Polymer* **1971**, *12*, 383.
64. G. Gee, *Trans. Faraday Soc.* **1952**, *48*, 515.
65. E. Powell, H. Eyring, *J. Am. Chem. Soc.* **1943**, *65*, 648.
66. F. Fairbrother, G. Gee, G. T. Merrall, *J. Polymer Sci.* **1955**, *16*, 459.
67. A. V. Tobolsky, A. Eisenberg, *J. Am. Chem. Soc.* **1959**, *81*, 780.
68. A. V. Tobolsky, A. Eisenberg, *J. Am. Chem. Soc.* **1960**, *82*, 289.
69. D. C. Koningsberger, Doctoral Dissertation. Technische Hogeschool Eindhoven, The Netherlands, **1971**.
70. H. Radschait, J. A. Gardner, *J. Non-Cryst. Solids* **1980**, *35/36*, 1263.
71. For the preparation of high-purity sulfur and of particular sulfur allotropes, see review on solid sulfur allotropes by R. Steudel, B. Eckert, *Top. Curr. Chem.* **2003**, in print.
72. P. A. Rubero, *J. Chem. Eng. Data* **1974**, *9*, 481.
73. T. K. Wiewiorowski, F. J. Touro, *J. Chem. Phys.* **1966**, *70*, 234.
74. J. B. Hyne, E. Muller, T. K. Wiewiorowski, *J. Phys. Chem.* **1966**, *70*, 3733.
75. R. Fanelli, *Ind. Eng. Chem.* **1949**, *41*, 2031.
76. W. Woll, *Erdoel-Erdgas* **1983**, *99*, 297.
77. R. Steudel, R. Laitinen, *Top. Curr. Chem.* **1982**, *102*, 177.
78. K.-D. Pohl, R. Brückner, *Phys. Chem. Glasses* **1981**, *22*, 150.
79. H. Specker, *Kolloid-Z* **1952**, *125*, 106; *Angew. Chem.* **1953**, *65*, 299.
80. R. Steudel, H.-J. Mäusle, *Z. Anorg. Allg. Chem.* **1981**, *478*, 156.
81. H. Gerding, R. Westrick, *Rec. Trav. Chim. Pays-Bas* **1943**, *62*, 68.
82. I. Srb, A. Vasko, *Czech. J. Phys. B* **1963**, *13*, 827.
83. A. T. Ward, *J. Phys. Chem.* **1968**, *72*, 4133.

84. H. L. Strauss, J. A. Greenhouse, in: *Elemental sulfur*. (B. Meyer, ed.), Interscience, New York, 1965, p. 241.
85. K. Hattori, H. Kawamura, *J. Non-Cryst. Solids* **1983**, 59/60, 1063.
86. R. Steudel, *Spectrochim. Acta* **1975**, 31A, 1065.
87. J. Steidel, R. Steudel, A. Kutoglu, *Z. Anorg. Allg. Chem.* **1981**, 476, 171.
88. H.-J. Mäusle, R. Steudel, *Z. Anorg. Allg. Chem.* **1981**, 478, 177.
89. R. Steudel, H.-J. Mäusle, D. Rosenbauer, H. Möckel, T. Freyholdt, *Angew. Chem.* **1981**, 93, 402; *Angew. Chem. Int. Ed. Engl.* **1981**, 20, 394.
90. H. J. Möckel, *Fresenius' Z. Anal. Chem.* **1984**, 318, 327.
91. R. Steudel, R. Strauss, *Fresenius' Z. Anal. Chem.* **1987**, 326, 543.
92. R. Steudel, D. Jensen, P. Göbel, P. Hugo, *Ber. Bunsenges. Phys. Chem.* **1988**, 92, 119.
93. R. Steudel, R. Strauss, L. Koch, *Angew. Chem.* **1985**, 97, 58; *Angew. Chem. Int. Ed. Engl.* **1985**, 24, 59; R. Strauss, *Doctoral Dissertation*, Technische Universität Berlin **1987**.
94. H. Rau, T. R. N. Kutty, J. R. F. Guedes de Carvalho, *J. Chem. Thermod.* **1973**, 5, 833.
95. K. C. Mills, *Thermodynamic Data for Inorganic Sulfides, Selenides and Tellurides*. Butterworths, London, **1974**, p. 65.
96. R. O. Jones, P. Ballone, *J. Chem. Phys.* **2003**, 118, 9257.
97. R. Ludwig, J. Behler, B. Klink, F. Weinhold, *Angew. Chem.* **2002**, 114, 3331; *Angew. Chem. Int. Ed.* **2002**, 41, 3199.
98. H. P. Meissner, E. M. Redding, *Ind. Eng. Chem.* **1942**, 34, 521; H. Rau, T. R. N. Kutty, J. R. F. Guedes de Carvalho, *J. Chem. Thermodyn.* **1973**, 5, 291.
99. R. Fischer, R. W. Schmutzler, F. Hensel, *Ber. Bunsenges. Phys. Chem.* **1982**, 86, 546.
100. R. Steudel, B. Holz, *Z. Naturforsch. Part B* **1988**, 43, 581.
101. A. M. Bass, *J. Chem. Phys.* **1953**, 21, 80.
102. B. Meyer, T. V. Oommen, D. Jensen, *J. Phys. Chem.* **1971**, 75, 912; B. Meyer, T. Stroyer-Hansen, T. V. Oommen, *J. Mol. Spectrosc.* **1972**, 42, 335; B. Meyer, M. Gouterman, D. Jensen, T. V. Oommen, K. Spitzer, T. Stroyer-Hansen, *Adv. Chem. Ser.* **1972**, 110, 53.
103. G. Weser, F. Hensel, W. W. Warren, *Ber. Bunsenges. Phys. Chem.* **1978**, 82, 588; F. Hensel, *Angew. Chem.* **1980**, 92, 598.
104. K. Tamura, H. P. Seyer, F. Hensel, *Ber. Bunsenges. Phys. Chem.* **1986**, 90, 581.
105. S. Hosokawa, T. Matsuoka, K. Tamura, *J. Phys. Condens. Matter* **1994**, 6, 5273.
106. M. Zanini, J. Tauc, *J. Non-Cryst. Solids* **1977**, 23, 349.
107. R. I. Billmers, A. L. Smith, *J. Chem. Phys.* **1991**, 95, 4242-4245.
108. P. Lenain, E. Picquenard, J. Corset, D. Jensen, R. Steudel, *Ber. Bunsenges. Phys. Chem.* **1988**, 92, 859.
109. M. W. Wong, Y. Steudel, R. Steudel, *Chem. Phys. Lett.* **2002**, 364, 387.
110. R. O. Jones, D. Hohl, *Int. J. Quantum Chem. Quantum Chem. Symp.* **1990**, 110, 4703.
111. R. Steudel, R. Reinhardt, T. Sandow, *Angew. Chem.* **1977**, 89, 757; *Angew. Chem. Int. Ed. Engl.* **1977**, 16, 716. For reviews on homocyclic sulfur oxides, see R. Steudel, *Comments Inorg. Chem.* **1982**, 5, 313; *Top. Curr. Chem.* **2003**, in print.
112. D. B. Nash, *Icarus* **1987**, 72, 1.
113. http://dir.yahoo.com/Science/Astronomy/Solar_System/Planets/Jupiter/Moons/Io/
114. See the Section "Photochemical Behavior" in the review on solid sulfur allotropes by R. Steudel, B. Eckert, *Top. Curr. Chem.* **2003**, in print.
115. Y. Sakaguchi, K. Tamura, *J. Phys. Condens. Matter* **1995**, 7, 4787.
116. S. Munekiri, F. Shimojo, K. Hoshino, *J. Phys.: Condens. Matter* **2000**, 127999.
117. See the Section "High-Pressure Allotropes" in the review on solid sulfur allotropes by R. Steudel, B. Eckert, *Top. Curr. Chem.* **2003**, in print.
118. F. Fehér, H. D. Lutz, *Z. Anorg. Allg. Chem.* **1964**, 333, 216.
119. O. Watanabe, S. Tamaki, *Electrochim. Acta* **1968**, 13, 11.
120. J. A. Poullis, C. H. Massen, in *Elemental Sulfur*. (B. Meyer, ed.), Interscience, New York, **1965**, p.109.
121. R. K. Steunenberg, C. Trapp, R. M. Yonco, E. J. Cairns, *Adv. Chem. Ser.* **1972**, 110, 190.
122. E. H. Baker, T. G. Davey, *J. Mater. Sci.* **1978**, 13, 1951.
123. M. Edeling, R. W. Schmutzler, F. Hensel, *Phil. Mag. B.* **1979**, 39, 547.

124. R. Steudel, S. Passlack-Stephan, G. Holdt, *Z. Anorg. Allg. Chem.* **1984**, 517, 7.
125. R. Bellissent, L. Descotes, F. Boué, P. Pfeuty, *Phys. Rev. B* **1990**, 41, 2135.
126. F. H. Stillinger, T. A. Weber, *J. Chem. Phys.* **1987**, 91, 4899.
127. F. Shimojo, K. Hoshino, Y. Zempo, *J. Phys. Condens. Matter* **1998**, 10, L177.
128. J. S. Tse, D. D. Klug, *Phys. Rev. B* **1999**, 59, 34.
129. P. Ballone, R. O. Jones, *J. Chem. Phys.* **2001**, 115, 3895.
130. T. Doi, *Rev. Phys. Chem. Jpn.* **1965**, 35, 11.
131. J. A. Poulis, C. H. Massen, A. Eisenberg, A. V. Tobolski, *J. Am. Chem. Soc.* **1965**, 87, 413.
132. D. C. Koningsberger, T. DeNeef, *Chem. Phys. Lett.* **1972**, 14, 453.
133. G. Gee, *Chem. Soc. Spec. Publ.* **1963**, 15, 67.
134. B. Eichinger, E. Wimmer, J. Pretorius, *Macromol. Symp.* **2001**, 171, 45.
135. R. Steudel, *Top. Curr. Chem.* **1982**, 102, 149.
136. R. S. Laitinen, T. A. Pakkanen, R. Steudel, *J. Am. Chem. Soc.* **1987**, 109, 710.
137. R. Steudel, Y. Steudel, K. Miaskiewicz, *Chem. Eur. J.* **2001**, 7, 3281.

Speciation and Thermodynamics of Sulfur Vapor

Ralf Steudel¹ · Yana Steudel¹ · Ming Wah Wong²

¹ Institut für Chemie, Technische Universität Berlin, 10623 Berlin, Germany
E-mail: steudel@schwefel.chem.tu-berlin.de

² Department of Chemistry, National University of Singapore, Science Drive 3,
117543 Singapore
E-mail: chmwmw@nus.edu.sg

Abstract Sulfur vapor at temperatures of between 200 and 1000 °C consists of all molecules with 2–10 atoms, some of which exist as two or more isomers. Extensive mass spectrometric investigations and vapor pressure measurements provided reliable thermodynamic data for the various dissociation reactions $S_8 \rightleftharpoons {}^8/n S_n$. Earlier quantum-chemical calculations yielded data partly in conflict with these experimental findings, but the most recent high-level ab initio MO and DFT calculations confirmed more or less the best experimental results. These theoretical data may now be considered as the most trustworthy. At low temperatures S_8 , S_7 , and S_6 are dominating in saturated sulfur vapor, the concentration of S_4 passes through a maximum at 900 K, S_3 is always more abundant than S_4 , and S_2 is the dominating species above 1100 K. The S_4 molecule is of *cis*-planar geometry but under non-equilibrium conditions the *trans*-planar isomer has also been observed. Triplet chain molecules $S_n^{\cdot\cdot}$ as well as branched rings $S_n=S$ and other isomers are too unstable to contribute more than 1% in each group to the equilibrium vapor composition at any temperature.

Keywords Sulfur clusters · Quantum-chemical calculations · Stability · Isomers · Spectra

1	Introduction	118
2	Sulfur Vapor	118
2.1	General	118
2.2	Mass Spectrometry	119
2.3	Pressure and Density Measurements.	121
2.4	More Mass Spectrometry	122
2.5	Vibrational Spectra	122
2.6	UV-Vis Spectra	124
2.7	Quantum-Chemical Calculations	125
3	Summary	132
	References	132

1 Introduction

Elemental sulfur is produced on a huge scale, partly by mining (Frasch process) but mainly by desulfurization of “sour” natural gas (Claus process) and of crude oil (hydrodesulfurization in combination with the Claus process) [1]. Approximately 1000 Claus plants are operating worldwide. The total amount of elemental sulfur recovered annually from these three sources was 43 million tons in 1999 [2]. The sulfur is obtained in the liquid form and is often also shipped as a liquid. On the other hand, sulfur is the element with the largest number of solid allotropes. At least 30 *crystalline sulfur phases* have been prepared and characterized by X-ray diffraction [3]. Most of these allotropes consist of homocyclic molecules with ring sizes ranging from S_6 to S_{20} but in some allotropes polymeric chain-like molecules are present [3–5]. The molecular structures of the sulfur homocycles S_6 [6], S_7 [7], S_8 [8], S_9 [9], and S_{10} [10] are known from accurate X-ray diffraction studies on single crystals, usually carried out at low sample temperatures. At very high pressures three-dimensional networks are formed and the various phases of sulfur eventually become metallic conductors. Below 10–17 K sulfur is even superconducting under high pressure [3, 11, 12].

All sulfur rings from S_6 to S_{28} have been detected in *liquid sulfur* by high-pressure liquid chromatography of extracts of quenched sulfur melts which had been equilibrated before at temperatures of between 116 and 250 °C [13]. Raman spectra of hot sulfur melts also showed the presence of *cyclo- S_7* besides S_8 [14]. In addition, the sulfur melt contains varying concentrations of polymeric insoluble sulfur [13–15]. Above 150 °C trace amounts of sulfur radicals have been detected in liquid sulfur by ESR spectroscopy [16, 17] as well as by magnetic measurements [18]. It can be expected that the equilibrium sulfur vapor exhibits a similarly complex molecular composition as the melt although the smaller molecules will be enriched in the gas-phase, of course.

2 Sulfur Vapor

2.1 General

Sulfur vapor, saturated and unsaturated, has been investigated by UV-Vis spectroscopy [19], by mass spectrometry (see below), by resonance Raman spectroscopy [20–23], as well as by a sophisticated mathematical analysis [24] of carefully performed pressure measurements as a function of temperature and total sulfur concentration [25–27]. It was concluded that the vapor consists of all molecules from S_2 to S_8 in temperature- and pressure-dependent equilibria of the following type:

Table 1 Reaction enthalpies ΔH° (kJ mol⁻¹) for the equilibrium reactions $cyclo-S_8 \rightleftharpoons 8/n S_n$ in the gas-phase at selected temperatures according to various experimental investigations

Temperature	400 K	400 K	435–669 K	298 K	298 K (2nd law)	298 K (3rd law)
$S_8 \rightleftharpoons 4 S_2$	393	414	405±9	420	404	387
$S_8 \rightleftharpoons 8/3 S_3$	251	255	257±11	275	253	231
$S_8 \rightleftharpoons 2 S_4$	172	231	169±13	190	150	137
$S_8 \rightleftharpoons 8/5 S_5$	96	96	85±13	73	90	77
$S_8 \rightleftharpoons 4/3 S_6$	35	35	35±2	34	48	34
$S_8 \rightleftharpoons 8/7 S_7$	27	28	28±2	28	28	20
Reference	[28]	[30]	[31]	[24]	[32]	[32]



The presence of even larger molecules such as S_9 and S_{10} in equilibrium sulfur vapor has been suspected [20] but the mass spectroscopic evidence is weak. Sulfur atoms can be expected in sulfur vapor only at extremely high temperatures (>2000 K) owing to their high enthalpy of formation of 277 kJ mol⁻¹ [29].

Many authors have tried to derive the enthalpies of the gas-phase reactions (Eq. 1) as well as the entropies S° of the various S_n molecules for $n=2-8$ from the temperature dependence of the mass and Raman spectra in combination with the total pressure of saturated and unsaturated sulfur vapor. These results are summarized in Table 1 and will be commented on in detail in the following sections. Most authors assumed that only one species is present for each molecular size; in other words, possible isomers were neglected. It has later been found out that this is an oversimplification (see below).

2.2

Mass Spectrometry

The first reliable spectroscopic analysis of saturated sulfur vapor was published by Berkowitz and Marquart [28] who used a combination of a Knudsen effusion cell with a mass spectrometer and generated the sulfur vapor by evaporating either elemental sulfur (low temperature region) or certain metal sulfides such as HgS which decompose at high temperatures to sulfur and metal vapor. These authors observed ions for all molecules from S_2 to S_8 and even weak signals for S_9^+ and S_{10}^+ . From the temperature dependence of the ion intensities the reaction enthalpies for the various equilibria (1) were derived (see Table 1). Berkowitz and Marquart carefully analyzed their data to minimize the influence of fragmentation processes in the ion source of the spectrometer. They also calculated the total pressure of sulfur vapor from their data and compared the results with the vapor pressure measurements by Braune et al. [26]. The agreement is quite satisfactory but it probably

could have been even better if they had not used too high a value for the entropy of gaseous S_8 ($430 \text{ J mol}^{-1} \text{ K}^{-1}$ at 298 K). This entropy value had been published in 1954 by Guthrie et al. [33]. The latter authors had assigned the vibrational spectra of *cyclo*- S_8 and calculated the entropy by the methods of statistical thermodynamics. It was later shown by Steudel and Mäusle [34] that the earlier vibrational assignment of S_8 was partly in error. The new assignment based on the infrared and Raman spectra of $^{32}S_8$ and $^{34}S_8$ led to an entropy value for gaseous S_8 of $423 \text{ J mol}^{-1} \text{ K}^{-1}$ at 298 K. The outdated entropy value of Guthrie et al. has been used by many subsequent authors including so-called critical reviews of the thermodynamics of sulfur compounds [35, 36] and it is still listed in the thermodynamic data bank of the National Institute of Standards (NIST) [29].

In a subsequent publication Berkowitz and Chupka [37] investigated the fragmentation pattern of S_6 , S_7 , and S_8 and reached a somewhat better agreement than previously between their calculated total vapor pressures in the temperature region 350 to 1000 °C and the vapor pressure measurements of Braune et al. [26]. In a review article of 1965, Berkowitz published another set of enthalpy values [30] with the S_4 value considerably higher than his earlier data (see Table 1).

Another attempt to elucidate the thermodynamics of sulfur vapor was made by Detry et al. [31, 38] who used an electrochemical Knudsen cell built into a mass spectrometer. The elemental sulfur was generated by electrochemical decomposition of silver sulfide (Pt,Ag/AgI/Ag₂S,Pt cell) which allows the determination of the total amount of sulfur leaving the Knudsen cell. In this way it is possible to eliminate the contribution of the fragmentation processes to the various ion intensities in the mass spectrum. Therefore, the data obtained by Detry et al. for the temperature region 200–400 °C (Table 1) should be more accurate than the previous data obtained by Berkowitz et al. but the agreement of the two sets of data is astonishingly good (except the data on S_4). The ratio of the partial pressures calculated by Detry et al. for saturated sulfur vapor at a temperature of 300 °C is as follows: $S_8:S_7:S_6:S_5:S_4:S_3:S_2=1:0.35:0.44:0.026:0.001:0.001:0.007$. Note that the standard deviations given in Table 1 are lowest for the species which have the highest partial pressures. It should be pointed out, however, that the standard entropies S_T° used for these calculations are not in good agreement with the entropy data which later were derived from the experimental vibrational spectra of most of these molecules (see below).

Berkowitz and Lifshitz [39] determined the photoionization efficiencies for gaseous sulfur molecules and concluded that the species S_5 to S_8 must be cyclic molecules rather than chains. While the structure of S_4 was unknown at that time, the smaller molecules S_2 and S_3 were obviously treated as homologues of O_2 (symmetry $D_{\infty h}$) and O_3 (symmetry C_{2v}). The photoionization potentials were found to lie in the region 8.6–9.7 eV.

Table 2 Concentrations (c) of the various sulfur species (mmol l^{-1}) in the saturated vapor at $500\text{ }^\circ\text{C}$ [23], calculated from the thermodynamic data of Rau et al. [24]. Total pressure: 0.2 MPa. The molar ratio refers to $c(\text{S}_8)=100$

Species	Concentration	Molar ratio
S_2	1.58	15
S_3	0.41	4
S_4	0.34	3
S_5	0.91	9
S_6	8.13	77
S_7	9.58	91
S_8	10.5	100

2.3

Pressure and Density Measurements

The most elaborate analysis of the composition of sulfur vapor was published by Rau et al. in 1973. These authors first measured the pressure of saturated sulfur vapor up to 1273 K and estimated the critical temperature T_c as 1313 K ($p_c=182\text{ bar}$) [27]. The mean number of atoms per molecule at the critical point was calculated as 2.78. In a second publication [24] the densities of saturated and unsaturated sulfur vapor in the temperature range of 823–1273 K were reported. Using literature data for the entropy of S_8 a set of equations was derived which allow the partial pressures of the molecules S_2 to S_8 to be calculated as a function of total pressure and temperature (real gas corrections included). The obtained reaction enthalpies for the equilibria (Eq. 1) are listed in Table 1 (calculated from the data in Table 2 of [24]). Although one has to take into account that these data apply to 298 K, the agreement with the results of Berkowitz et al. and Detry et al. is rather poor except for the formation of the larger molecules S_6 and S_7 from S_8 . On the other hand, the ratio of the partial pressures calculated from Rau et al.'s enthalpies for the saturated vapor at $300\text{ }^\circ\text{C}$ ($\text{S}_8:\text{S}_7:\text{S}_6:\text{S}_5:\text{S}_4:\text{S}_3:\text{S}_2=1:0.36:0.43:0.024:0.001:0.001:0.005$) is in excellent agreement with the corresponding ratios calculated from the data of Detry et al. as given above. The absolute concentrations of the various sulfur species in the saturated vapor at $500\text{ }^\circ\text{C}$ (0.2 MPa) calculated from the data of Rau et al. [24] are given in Table 2.

It is not easy to locate the origin of the deviations between the various sets of thermodynamic data listed in Table 1. Rau et al. mentioned that the enthalpies of all reactions except for the formation of S_2 could be varied slightly without much effect on the total sulfur pressure which, on the other hand, was taken as the final proof of the consistency of the data set. In addition, the entropy of S_8 used by these authors ($430\text{ J mol}^{-1}\text{ K}^{-1}$ at 298 K) does not agree well with the experimental value of $423\text{ J mol}^{-1}\text{ K}^{-1}$ (298 K) derived from the geometrical data and the vibrational spectra [34].

2.4

More Mass Spectrometry

In 1983 another study of the thermodynamics of reactions (1) appeared. Rosinger et al. [32] also used a combination of a Knudsen cell with a mass spectrometer to study the composition of sulfur vapor generated by evaporation of either elemental sulfur or mercury sulfide (HgS). Using an electron beam energy of only 12 eV the authors tried to suppress fragmentation processes as much as possible. The equilibrium constants and reaction enthalpies for the equilibria (Eq. 1) were determined by the second and third law methods for the temperature range 430–490 K and were converted to 298 K using literature data for the entropies and heat capacities. The two sets of data obtained by Rosinger et al., given in Table 1, do not agree well with each other nor with the previously published reaction enthalpies, probably as a consequence of the small temperature range investigated. In particular, the enthalpies for $n=6$ and 7 deviate significantly from the values reported by the other authors. The previous values for S_6 and S_7 are supported by the corresponding reaction enthalpies derived for sulfur solutions and for liquid sulfur. In carbon disulfide solution 32 kJ mol⁻¹ are needed for the formation of S_6 from 1 mol of S_8 , and 24 kJ mol⁻¹ for S_7 [40]. In liquid sulfur at 116–159 °C, 30 kJ mol⁻¹ were obtained for the S_6 formation from S_8 and 24 kJ mol⁻¹ for S_7 [13].

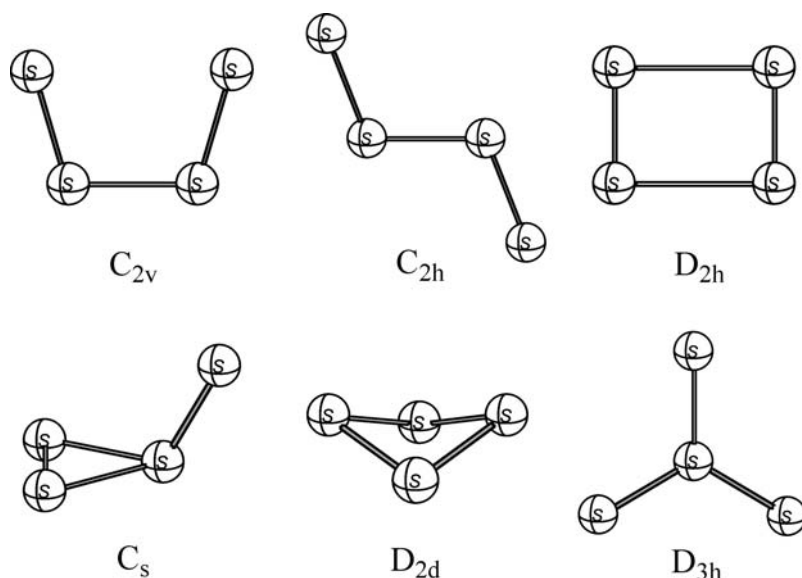
Thus, it is obvious that more work and new approaches are needed to establish finally reliable thermodynamic data for the various equilibrium reactions in sulfur vapor.

2.5

Vibrational Spectra

In 1988, it became obvious that the composition of sulfur vapor is even more complex than had been thought before: Lenain et al. published a Raman spectroscopic study of the sulfur vapor composition at temperatures of up to 700 °C [20]. Signals for the cyclic species S_8 , S_7 , and S_6 as well as for the acyclic molecules S_4 , S_3 , and S_2 were observed and spectroscopic evidence for the presence of two conformational isomers of S_4 and for either chain-like ($S_n^{\cdot\cdot}$) or branched-bonded species ($S_n=S$ with $n \geq 4$) was presented. These authors came to the conclusion that the thermodynamic data of Rau et al. [24] are reliable except for the enthalpy of S_7 formation from S_8 which was said to be too high.

The structure of S_4 has been a puzzling problem for a long time since the infrared spectra, recorded after matrix isolation of quenched sulfur vapor [41–43], did not allow a convincing assignment to just one particular molecular structure, and theoretical calculations yielded different results depending on the level of theory and the method applied. No fewer than six different structures have been reported by different authors to be the global minimum (see Scheme 1).



Scheme 1

Table 3 Relative energies or enthalpies (kJ mol^{-1}) calculated for various singlet isomers of S_4 since 1990 (ordered chronologically)

Method	C_{2v}	C_{2h}	D_{2h}	C_s	D_{2d}	D_{3h}	Reference
QCISD(T)/6-31G*	7	38	0		75	120	[47]
TC-CISD(Q)/TZ2P	0	24	(1) ^a	37 ^b	69	77 ^b	[44]
MRCI	0	41	(4) ^a	128	73	134	[48]
QCISD/6-311G(d)	0	37	(22) ^a	64 ^c	83 ^c		[49]
BLYP/CEP-121(BPF)	0		(1) ^a				[50]
B3LYP/6-31G*	0	29	(6) ^a	74	90	113	[51]
B3LYP/aug-cc-pVDZ	0	29	(9) ^a		75		[52]
CCSD(T)/aug-cc-pVDZ	1	39	(0) ^a	–	77		[52]
G3X(MP2)	0	41	^a	62	80	107	[53]
CCSD(T)/aug-cc-pVTZ	0	37	(4)	57	58	109	[53]
MD/DF	^a	32	0	–	112		[46]

^a Not a minimum but a transition state for the degenerate *cis-cis* interconversion

^b CISD(Q)/TZP value

^c G3(MP2) value

The S_4 structural problem was partly resolved in 1990 by Quelch et al. [44] who presented a high-level two-configuration CISD study of S_4 . They showed that the *cis*-planar C_{2v} singlet structure is the global minimum while the *trans*-planar C_{2h} isomer is by 24 kJ mol^{-1} less stable (ΔE) and a branched three-membered ring of C_s symmetry ($S_3=S$) is even less stable at the highest level of theory applied (Table 3). However, a planar rectangular S_4 structure

of D_{2h} symmetry (“ S_2 dimers”) may also be a minimum of comparable energy as was predicted by the density functional calculations published by Jones et al. [45, 46]; see Table 3.

In fact, matrix infrared spectra of quenched sulfur vapor originally provided some evidence for two planar chain structures of S_4 as well as for dimers of S_2 [42] but a subsequent reinvestigation of the spectra by Hassanzadeh and Andrews yielded a different assignment [43]. The latter authors identified two S_4 isomers: The *cis*-planar structure (absorbing green light near 520 nm) and the branched three-membered ring $S_3=S$ (absorbing red light in the 560–660 nm region). By proper illumination of the matrix-samples these two isomers could even be reversibly converted into each other [43]! However, Picquenard et al. assigned certain lines observed in the resonance Raman spectra of hot sulfur vapor also to two different isomers of S_4 . Saturated and unsaturated vapors were investigated and a strong dependence of the spectra on the laser power was observed and explained by a photothermic effect. In other words, the vapor was not always in the thermal equilibrium. On the basis of isotopic shifts and force constant calculations the species absorbing at 530 nm was now identified as the *trans*-planar structure of S_4 and the species absorbing at 620 nm was proposed to have the branched three-membered ring structure [23]; only the latter assignment is in agreement with the suggestions by Hassanzadeh and Andrews [43].

Despite much effort, the full set of the six fundamental vibrations of any S_4 isomer has not been observed yet. Most recent high-level G3X(MP2) and CCSD(T)/aug-cc-pVTZ [53] calculations confirmed the singlet planar C_{2v} structure as the global minimum with the C_{2h} isomer significantly higher in energy (see Table 3). The rectangular D_{2h} geometry is not a stable equilibrium structure at all. It corresponds to a transition state which interconverts two *cis*-planar forms. All calculations agree that the branched three-membered ring is considerably higher than the global minimum. The calculated order of stability of the various S_4 isomers is: $C_{2v} < C_{2h} < C_s < D_{2d} < D_{3h}$. These results are in sharp contrast to the spectroscopic work cited above which seem to indicate that the higher energy S_4 isomers of C_{2h} and C_s symmetry are also or even exclusively present in hot sulfur vapor which in the light of the data in Table 3 seems rather unlikely. As with the singlet, the lowest-energy triplet of S_4 has also a *cis*-planar geometry (3B_2 , C_{2v} symmetry). It lies ca. 40 kJ mol $^{-1}$ above the singlet ground state.

2.6

UV-Vis Spectra

Sulfur vapor exhibits three electronic absorption bands in the visible range at 400, 530, and 625 nm. Meyer et al. [54] first convincingly assigned the 400 nm band to S_3 and the 530 nm band to S_4 . Several authors confirmed this assignment [55–57]. The third band at 625 nm was suspected to originate from an isomer of S_4 [58] which was later confirmed [43]. High-temperature sulfur vapor at low pressure is said to be pale-violet due to the presence of S_2 [59].

Billmers and Smith [60] measured the UV-Vis absorption spectra of sulfur vapor at various pressures (9–320 Torr) and temperatures (670–900 K). They attempted to evaluate the thermodynamic data of the equilibrium between the molecules S_3 and S_4 using their broad absorption bands at 400 and 530 nm, respectively. The authors assumed that no other molecules contribute to these bands and that only one S_4 isomer is present in sulfur vapor. Their reaction enthalpy of 78 kJ mol^{-1} (at 800 K) for the conversion of 3 S_4 into 4 S_3 is in sharp contrast to the data in Table 1. For example, Rau et al. [24] determined this enthalpy as 128 kJ mol^{-1} (at 298 K) and Detry et al. [31] obtained a value of 132 kJ mol^{-1} . However, if the 530 nm band is to be assigned to just one of two isomers of S_4 , the enthalpy determined by Billmers and Smith applies only to the reaction $3 S_4(C_{2v}) \rightleftharpoons 4 S_3$ and not to the total amount of S_4 in the vapor as studied by all previous authors using mass spectrometry. Furthermore, the enthalpy of 78 kJ mol^{-1} is also not in agreement with the thermodynamic data obtained by high-level ab initio MO calculations which give a reaction enthalpy of 126 kJ mol^{-1} at 700 K for the conversion of 3 $S_4(C_{2v})$ into 4 S_3 (see Table 5). Hence, we conclude that the results of Billmers and Smith are seriously in error probably due to the higher concentration of S_3 compared to S_4 in sulfur vapor and due to the much higher molar extinction coefficient of S_3 which exceeds that of S_4 by more than one order of magnitude!

2.7

Quantum-Chemical Calculations

From the above discussion, it follows that the molecular composition of gaseous and liquid sulfur is too complex to be elucidated fully by experimental techniques alone. Fortunately, theoretical methods have now developed to such a high level that reliable thermodynamic and structural information on sulfur molecules with up to 10 atoms may be obtained by ab initio MO calculations. Numerous theoretical calculations on S_n molecules have already been published but most of them can be considered outdated. Recent studies have shown that inclusion of a considerable number of polarization functions in the basis set as well as correction for electron correlation effects are essential not only in the single-point energy calculation but also in geometry optimizations. For this reason most of the empirical, semiempirical and ab initio MO calculations published before 1990 resulted in either incorrect ground-state structures of some of the treated S_n molecules or in incorrect relative energies of the various isomers, especially for $n > 3$. These results will, therefore, not be discussed here. An exception is the theoretical treatment of the S_3 molecule where the lowest-energy structure was correctly predicted in 1986 to be of C_{2v} symmetry on the basis of CASSCF and MR-CISD calculations while SCF and CISD calculations resulted in a global minimum of D_{3h} symmetry [61]. This result was later confirmed by two other theoretical investigations [50, 62]. The D_{3h} structure is calculated to be 31–44 kJ mol^{-1} less stable than the bent open chain, depending on the method of calculation and the level of theory applied [46, 52].

Table 4 Gas-phase reaction energies (kJ mol^{-1}) for three equilibrium reactions $\text{cyclo-S}_8 \rightleftharpoons^8/n \text{ cyclo-S}_n$ calculated by different theoretical methods

Reaction	MP2/pDZ	MP4/6-31G**/HF/ 3-21G*	B3LYP/6-311G*	MP2/6-311G*
	ΔH°_{298}	ΔE_0^a	ΔH°_{298}	ΔH°_{298}
$\text{S}_8 \rightleftharpoons^8/5 \text{ S}_5$	122	127	119	122
$\text{S}_8 \rightleftharpoons^4/3 \text{ S}_6$	40	45	49	44
$\text{S}_8 \rightleftharpoons^8/7 \text{ S}_7$	31	34	30	32
Reference	[63]	[47]	[64]	[64]

^a Without zero-point energy correction

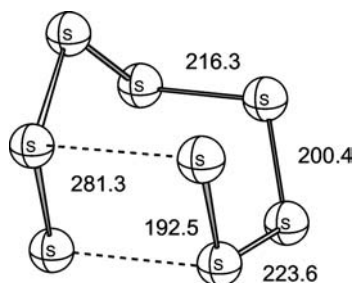
Table 4 summarizes ab initio results of the energetics of the reaction in Eq. 1 published by three different groups after 1989 [47, 63, 64]. While these data agree reasonably well with each other, the agreement with the experimental results in Table 1 is somewhat poor, especially in the case of S_5 . It, therefore, needs to be investigated whether this disagreement comes from deficiencies in the calculations or from errors in the experiments. In addition, density functional calculations of sulfur molecules have been carried out [65].

Very recently, high-level ab initio MO calculations on various isomers of homoatomic sulfur molecules S_n with $n=2-10$ have been carried out [53]. The results are given in Table 5. As can be seen, these computed data agree rather well with the experimental data by Rau et al. [24] shown in Table 1, with the exception of S_5 . This molecule is likely to undergo pseudorotation in the vapor phase resulting in an enhanced molecular entropy which is not taken into account in ab initio calculations. Furthermore, since S_5 is a minority species in sulfur vapor at all temperatures and pressures, it is possible that the data by Rau et al. are somewhat unreliable as far as this molecule is concerned.

The data in Table 5 may now be used to estimate very approximately the partial pressures of S_9 and S_{10} in saturated sulfur vapor at 300 °C (assuming a fugacity of 1 for all species). At this temperature the partial pressure of S_8 is 3.69 kPa [24] while for S_9 0.072 kPa and for S_{10} 0.014 kPa are obtained re-

Table 5 Calculated [G3X(MP2)] reaction energies (kJ mol^{-1}) for the equilibrium reactions $\text{cyclo-S}_8 \rightleftharpoons^8/n \text{ S}_n$ in the gas phase. All molecules are in their global minimum geometries; the species larger than S_4 are rings [53]

Reaction	ΔE_0	ΔH°_{298}	ΔG°_{298}	ΔH°_{700}	ΔG°_{700}
$\text{S}_8 \rightarrow 4 \text{ S}_2$	423	427	283	414	270
$\text{S}_8 \rightarrow^8/3 \text{ S}_3$	282	281	191	270	179
$\text{S}_8 \rightarrow 2 \text{ S}_4$	193	193	134	186	126
$\text{S}_8 \rightarrow^8/5 \text{ S}_5$	106	105	68	101	64
$\text{S}_8 \rightarrow^4/3 \text{ S}_6$	35	34	20	32	18
$\text{S}_8 \rightarrow^8/7 \text{ S}_7$	26	25	12	25	11
$\text{S}_8 \rightarrow^8/9 \text{ S}_9$	17	18	17	19	18
$\text{S}_8 \rightarrow^4/5 \text{ S}_{10}$	16	17	22	18	23



Scheme 2

sulting in a pressure ratio of $S_8:S_9:S_{10}=1:0.020:0.004$ (equal to the molar ratio). Lower fugacities will of course reduce the concentrations of S_9 and S_{10} in the vapor. This result is in fair agreement with the composition of the equilibrium sulfur melt which, after quenching in liquid nitrogen, extraction and HPLC analysis, contains ca. 54 mass % of S_8 , 0.6% of S_9 and 0.2% of S_{10} at 300 °C, equivalent to a molar ratio of 1:0.010:0.003 [13]. Thus, S_9 and probably also S_{10} should be detectable by mass spectrometry in saturated sulfur vapor, which has in fact been demonstrated [28].

The infrared spectra of quenched sulfur vapor exhibit an absorption at 683 cm^{-1} which has tentatively been assigned by several authors to a branched sulfur chain or a ring of the type $S_n=S$ ($n>4$) with one exocyclic atom [43, 66]. In search for plausible isomers of S_8 , molecular-dynamics density-functional calculations had shown that the energy of a cluster-like S_8 isomer of C_2 symmetry is only 42 kJ mol^{-1} higher than that of *cyclo*- S_8 [67]. This isomer has a bicyclic structure and is only loosely related to a branched ring; its structure is shown in Scheme 2 (bond lengths in pm).

Our recent high-level ab initio MO calculations by the G3X(MP2) method placed this isomer only 33 kJ mol^{-1} (ΔH_{298}°) higher than the crown-shaped S_8 ring [68]. This means that 1% of all S_8 molecules in sulfur vapor at the boiling point (445 °C) will be present as isomers of C_2 symmetry. Furthermore, these calculations demonstrated that several other isomers of S_8 exist with relative energies between those of the C_2 structure and the diradical chain which also has a C_2 symmetry. Some of these species exhibit SS stretching fundamentals in the $600\text{--}700\text{ cm}^{-1}$ region. For instance, the isomer $S_7=S$ with a structure similar to that of the related homocyclic oxide $S_7=O$ [69] is by 93 kJ mol^{-1} less stable than the S_8 crown if the exocyclic sulfur atom is in an axial position but by 96 kJ mol^{-1} if this atom is in an equatorial position with respect to the ring (ΔH_{298} values) [68].

The formation of an $S_7=S$ species was recently “observed” in a molecular-dynamics simulation of the reactions in liquid sulfur at 400 K [70]. It was found that some of the S_8 ring molecules homolytically open up on excitation of one electron from the HOMO to the LUMO. The chain-like diradicals $S_n^{\cdot\cdot}$ thus generated partly recombine intramolecularly with formation of $S_7=S$ rather than *cyclo*- S_8 . The $S_7=S$ molecule may then react with another $S_n^{\cdot\cdot}$ diradical to form a chain of 16 atoms. Such chains are, of course, also

formed by direct combination of two $S_n^{\cdot\cdot}$ diradicals. The conformation of this $S_7=S$ species observed after 933 fs is, however, different from the cluster structures mentioned above [67, 68]. Nevertheless, evidence is accumulating that branched sulfur rings and chains are present in liquid sulfur as well as in sulfur vapor at high temperatures [68].

The formation of chain-like sulfur diradicals by homolytic ring opening reactions of S_8 , S_7 , and S_6 in liquid sulfur requires enthalpies of 150, 127, and 124 kJ mol^{-1} , respectively ($\pm 5 \text{ kJ mol}^{-1}$ each; 298 K). While the S_8 value was obtained from temperature dependent ESR [16, 17] and magnetic susceptibility measurements [18], the data for S_6 and S_7 were estimated from the S_8 value using simple thermodynamic cycles and certain assumptions [71]. For comparison, the dissociation enthalpy of the central S-S bond of chain-like organic tetrasulfanes (e.g., Me_2S_4) amounts to $142 \pm 16 \text{ kJ mol}^{-1}$ in the gas phase [72]. Since the entropies of the chain-like sulfur molecules obtained by homolytic ring opening were not known until recently, the equilibrium concentration of such chains in liquid and gaseous sulfur could not be calculated accurately. However, it is generally believed [73] that their equilibrium concentration near 160 °C becomes high enough to trigger the well-known ring-opening polymerization of liquid sulfur which can best be recognized from the sudden increase of the viscosity by three orders of magnitude [74]. High-level ab initio MO calculations based on the G3X(MP2) method have now provided the Gibbs energy of the ring opening reaction of *cyclo*- S_8 at 298 K as 129 kJ mol^{-1} and $\Delta H_{298}^\circ = 154 \text{ kJ mol}^{-1}$ [68] in excellent agreement with the experimental data. If the temperature dependence of this enthalpy as well as mixing effects are neglected the molar ratio of *catena*- S_8 to *cyclo*- S_8 can be calculated as $7 \cdot 10^{-17}$ at 393 K (melting point of sulfur) and as $4 \cdot 10^{-10}$ at 718 K (boiling point) [68]. While the direct experimental evidence for such diradical-chains in liquid sulfur comes from the cited ESR spectroscopic and magnetic susceptibility measurements, no comparable investigations have been made in the case of sulfur vapor. Therefore, high-level ab initio MO calculations have been carried out to determine the relative energies and enthalpies of all triplet diradical chains of molecular size 2–10 [53]. These data are given in Table 6. As expected, the homolytic ring opening of the S_8 molecule requires the highest

Table 6 Calculated [G3X(MP2)] energy differences (kJ mol^{-1}) between the global minimum structures and the chain-like triplet diradicals of S_n molecules ($n=3-10$). All species are of C_2 symmetry except $S_3^{\cdot\cdot}$ and $S_4^{\cdot\cdot}$ which both are of C_{2v} symmetry [53]

$S_n^{\cdot\cdot}$ species	ΔE_0°	ΔH_{298}°	ΔG_{298}°
$S_3^{\cdot\cdot}$	96	96	92
$S_4^{\cdot\cdot}$	49	50	43
$S_5^{\cdot\cdot}$	109	111	99
$S_6^{\cdot\cdot}$	117	120	101
$S_7^{\cdot\cdot}$	135	138	121
$S_8^{\cdot\cdot}$	151	154	129
$S_9^{\cdot\cdot}$	134	137	115
$S_{10}^{\cdot\cdot}$	133	136	111

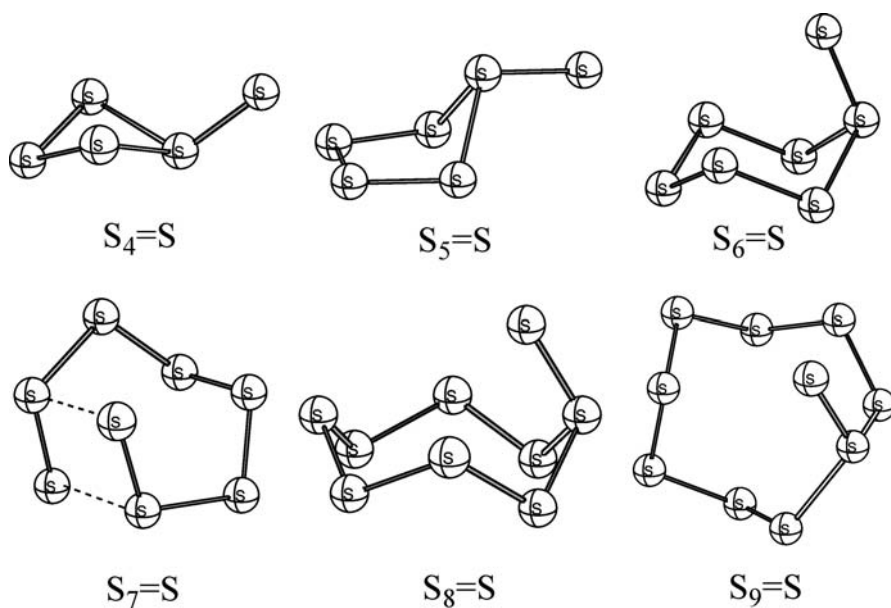


Fig. 1 Calculated structures of the lowest-energy branched ring molecules S_n of size $n=4-10$ [53]

reaction enthalpy (154 kJ mol^{-1}) while the transformation of the *cis*-planar S_4 structure into a triplet chain requires the lowest enthalpy (50 kJ mol^{-1}). It is, however, evident that all of these enthalpy values are too large for triplet molecules to substantially contribute to the molecular composition of equilibrium sulfur vapor except as reaction intermediates present in trace amounts.

As mentioned above, branched sulfur rings with one exocyclic atom are also potential isomers which may be present in hot sulfur vapor. Their relative energies and enthalpies with respect to the ground state structures have also been examined by the G3X(MP2) theory [53]. For the species with between 4 and 10 atoms these isomers are shown in Fig. 1, and their relative energies are given in Table 7. It follows that the ratio $S_8(D_{4d}):S_8(C_2)$ in sulfur vapor at the boiling point is 1.7×10^{-3} . For all other molecules, this ratio is much larger. Branched rings other than $S_8(C_2)$ will therefore hardly be detected.

There remains the unresolved problem of the isomeric S_4 structures (see Scheme 1 above). To provide a more definitive assignment of the various observed S_4 isomers, we have calculated their electronic and vibrational spectra. Table 8 summarizes the three strongest absorptions in the UV-Vis region and their transition probabilities obtained at the CIS/6-311+G(2df) level. As demonstrated by the computed transition energies, only the C_{2v} and C_{2h} isomers have UV absorptions at wavelengths above 400 nm. The branched ring $S_3=S$ is predicted to absorb at 240 nm. This is in agreement with the observed UV spectrum of $F_2S=S$, which is characterized by a peak at 244 nm

Table 7 Energy differences (kJ mol⁻¹) between the global minimum structures and the lowest-energy branched isomers of S_n molecules (n=4–10), calculated at the G3X(MP2) level of theory [53]

S _(n-1) =S species	ΔE° ₀	ΔH° ₂₉₈	ΔG° ₂₉₈
S ₃ =S	62	62	61
S ₄ =S	119	120	117
S ₅ =S _{eq} ^a	104	106	95
S ₆ =S	58	58	58
S ₇ =S	33	33	28
S ₈ =S	32	32	32
S ₉ =S	54	54	52

^a The S₅=S_{ax} species with the exocyclic atom in an axial position is not a stable equilibrium structure at this level of theory but collapses to the prismatic isomer of D_{3h} symmetry. On the other hand, S₅=S_{eq} with an equatorial exocyclic atom is a local energy minimum. All other species in this table have the exocyclic atom in the axial position

Table 8 The three strongest UV absorptions (T₁, T₂, and T₃, >200 nm) of various singlet S₄ isomers, calculated at the CIS/6-311+G(2df)//B3LYP/6-31G(2df) level. The computed transition energies are given in nm and the values of oscillator strength are in parenthesis [53]

Species	T ₁	T ₂	T ₃
C _{2v}	212 (0.063)	272 (0.056)	566 (0.192)
C _{2h}	201 (0.486)	227 (0.200)	634 (0.292)
C _s	203 (0.016)	211 (0.033)	241 (0.339)
D _{2d}	201 (0.018)	203 (0.006)	433 (0.004)
D _{3h}	213 (0.095)	320 (0.216)	^a

^a Only two UV absorptions above 200 nm

[75]. Thus, our calculated electronic spectra clearly indicate that the assignment of S₃=S as the red light absorbing isomer [23, 43] is incorrect. More importantly, the calculated transition energies of the C_{2v} and C_{2h} isomers (566 and 634 nm, respectively) match very well with the experimental results. We therefore conclude that the observed green and red absorbing S₄ isomers correspond to the C_{2v} and C_{2h} structures of S₄, respectively.

In Table 9 the calculated vibrational wavenumbers of the three most stable S₄ isomers are listed together with their infrared and Raman intensities. These data, obtained at the B3LYP/6-31G(2df) level of theory allow the reliable identification of two isomers observed in hot [23] and quenched [43] sulfur vapor.

Our assignment of the infrared and Raman spectra of the S₄ isomers is given in Table 9. The evidence for the *cis*-planar isomer is strong. In particular, the two calculated Raman lines at 373 and 674 cm⁻¹ of the C_{2v} isomer have also been observed in the spectrum of ultramarine red, the red color being caused by the 520 nm absorption band of S₄ [76]. The observed IR absorption at 642 cm⁻¹ and the Raman line at 635 cm⁻¹ can be assigned to the

Table 9 Harmonic fundamental modes of the three most stable isomers of S_4 with infrared and Raman intensities calculated at the B3LYP/6-31G(2df) level of theory (this work). Symmetrical modes (A symmetry) are shown in italics. For connectivities of the S_4 isomers, see Scheme 1 above. Experimental wavenumbers are given for comparison. Assignments made by the present authors using data from [23, 43]

Symmetry	C_{2v} ^a	C_{2h} ^a	C_s ^a	Matrix infrared spectra (12 K) [43]	Resonance Raman spectra (hot vapor) [23]
ν_1	674 w/76	649 0/100	665 vs/26	683 ($S_{n=S}$) ^d	678 (C_{2v}) ^b 635 (C_{2h}) ^c 601 (C_{2v} : 2×303) ^b
ν_2	649 vs/13	637 vs/0	541 m/100	662 (C_{2v}) 642 (C_{2h}) ^e	575 ^{b,c}
ν_3	373 w/100	471 0/51	390 s/50	–	400 (C_{2h} : $2 \times \nu_4$) ^c 375 (C_{2v}) ^b
ν_4	330 vw/35	225 0/55	308 m/27	–	322sh (C_{2v} : $\nu_5 + \nu_6$) ^b 303 (C_{2v}) ^b
ν_5	207 vw/1	124 w/0	215 w/52	–	–
ν_6	104 vw/33	93 vw/0	164 vw/41	–	–

^a Wavenumbers (unscaled; cm^{-1}) and relative infrared/Raman intensities as follows. Infrared intensities: very strong-strong-medium-weak-very weak-0. Raman intensities: 0–100 (sh: shoulder). In the case of the centrosymmetric point group C_{2h} the rule of mutual exclusion applies

^b Observed in the spectra excited with green light (488–530 nm)

^c Observed in the spectra excited with red light (647 nm)

^d Observed only after annealing of the matrix at 38 K; $n \geq 4$ [43]; may be assigned to the S_8 isomer of C_2 symmetry [68]

^e The other Raman lines calculated for this species at 471 and 225 cm^{-1} may have been obscured by the strong lines of S_8 , S_7 , and S_6 near 475 cm^{-1} (stretching) and 213/232/263 cm^{-1} (totally symmetrical bending) in the Raman spectra of sulfur vapor

trans-planar C_{2h} structure. Although there are a few Raman lines that may fit well to the calculated wavenumbers of $S_3=S$, we found no evidence for its presence based on the calculated electronic spectrum. Interestingly, we note that Andrews et al. [43] reported a new IR absorption at 635 cm^{-1} on annealing the argon matrix containing S_4 . This may, perhaps, be assigned to $S_3=S$ (calc. 665 cm^{-1}) or even more likely to the cluster-like isomer of S_8 shown in Scheme 2 (calc. 662 cm^{-1}) which may arise from the dimerization of S_4 .

We conclude that the *cis*-planar isomer is the dominating S_4 species in equilibrium sulfur vapor and the *trans*-planar isomer is generated by photo-thermal effects during laser irradiation [23] or by the microwave discharge applied to the sulfur vapor before matrix isolation [43].

For S_3 the vibrational wavenumbers are well established. The experimental values are: $\nu_{as}=674 \text{ cm}^{-1}$ (IR, Ar matrix [77]), $\nu_s=581 \text{ cm}^{-1}$ and $\delta=281 \text{ cm}^{-1}$ (both Raman vapor [78]). Our calculated wavenumbers are: 686 (vs/24), 594 (vw/100) and 261 cm^{-1} (vw/31) which agree within 20 cm^{-1} with the observed data (relative IR and Raman intensities in parentheses).

3 Summary

The molecular composition of sulfur vapor is much more complex than had been thought by all authors before the year 1990. Not only the molecular size can vary between 2 and—at least—10, but there are cyclic and chain-like isomers as well as branched rings and chains and even clusters to be taken into account. This makes experimental investigations rather difficult. However, the reaction enthalpies calculated by the most sophisticated ab initio MO methods (Table 5) are in good agreement with the most reliable experimental data obtained by mass spectrometry and vapor pressure measurements (Table 1, column 5).

While the structures of S_2 (D_{4h}) and S_3 (C_{2v}) are well known, there are at least two S_4 isomers in sulfur vapor: the green light absorbing ground state *cis*-planar structure of C_{2v} symmetry with a characteristic infrared absorption at 662 cm^{-1} and the red light absorbing isomer characterized by an infrared band at 642 cm^{-1} (both in Ar matrix) [43]. On the basis of recent high-level ab initio MO and DFT calculations (see Table 3), the latter isomer is reassigned as the *trans*-planar form with C_{2h} symmetry (see Scheme 1). Since these two isomers occur mainly under non-equilibrium conditions their energy difference of 41 kJ mol^{-1} may not be an obstacle. In equilibrium sulfur vapor, the absorption at 520 nm is much stronger than the absorption at 600 nm, i.e., the C_{2v} form of S_4 is the dominating isomer. This finding is also supported by the excellent agreement between the calculated and measured enthalpies of formation of S_4 from S_8 . The structures of all S_n species larger than S_4 are cyclic in sulfur vapor.

Acknowledgements This work has been supported by the Deutsche Forschungsgemeinschaft, the Verband der Chemischen Industrie and the National University of Singapore.

References

1. Review: R. Steudel, *Chemie unserer Zeit* **1996**, 30, 226.
2. M. Kitto, *Sulphur* **2001**, 275, 30.
3. Review: R. Steudel, B. Eckert, *Top Curr. Chem.* **2003**, 230, in print.
4. J. Donohue, *The Structures of the Elements*, Wiley, New York, **1974**, pp. 324.
5. Review: R. Steudel in: *Sulfur - Its Significance for Chemistry, for the Geo-, Bio- and Cosmosphere and Technology* (A. Müller, B. Krebs, Eds.), Elsevier, Amsterdam, **1984**, pp. 3–37.
6. J. Steidel, J. Pickardt, R. Steudel, *Z. Naturforsch. Part B* **1978**, 33, 1554.
7. R. Steudel, J. Steidel, J. Pickardt, F. Schuster, R. Reinhardt, *Z. Naturforsch. Part B* **1980**, 35, 1378.
8. P. Coppens, Y. W. Yang, R. H. Blessing, W. F. Cooper, F. K. Larsen, *J. Am. Chem. Soc.* **1977**, 99, 760; S. J. Rettig, J. Trotter, *Acta Cryst. C.* **1987**, 43, 2260.
9. R. Steudel, K. Bergemann, J. Buschmann, P. Luger, *Inorg. Chem.* **1996**, 35, 2184.
10. R. Steudel, J. Steidel, R. Reinhardt, *Z. Naturforsch. Part B* **1983**, 38, 1548.
11. H. Luo, R. G. Greene, A. L. Ruoff, *Phys. Rev. Lett.* **1993**, 71, 2943.
12. V. V. Struzkhin, R. J. Hemley, H. Mao, Y. A. Timofeev, *Nature* **1997**, 390, 382.

13. R. Steudel, R. Strauss, L. Koch, *Angew. Chem.* **1985**, *97*, 58; *Angew. Chem. Int. Ed. Engl.* **1985**, *24*, 59.
14. R. Steudel, H.-J. Mäusle, *Z. Anorg. Allg. Chem.* **1981**, *478*, 156; H.-J. Mäusle, R. Steudel, *Z. Anorg. Allg. Chem.* **1981**, *478*, 177.
15. J. C. Koh, W. Klement, *J. Chem. Phys.* **1970**, *74*, 4280.
16. D. M. Gardner, G. K. Fraenkel, *J. Am. Chem. Soc.* **1956**, *78*, 3279.
17. D. C. Koningsberger, T. De Neef, *Chem. Phys. Lett.* **1970**, *4*, 615.
18. J. A. Poullis, C. H. Massen, P. v. d. Leeden, *Trans. Faraday Soc.* **1962**, *58*, 474.
19. H. Braune, E. Steinbacher, *Z. Naturforsch. Part A* **1952**, *7*, 486.
20. P. Lenain, E. Picquenard, J. Corset, D. Jensen, R. Steudel, *Ber. Bunsenges. Phys. Chem.* **1988**, *92*, 859.
21. E. Picquenard, O. El Jaroudi, J. Corset, *J. Raman Spectrosc.* **1993**, *24*, 11.
22. E. Picquenard, M. S. Boumedien, J. Corset, *J. Mol. Struct.* **1993**, *293*, 63.
23. M. S. Boumedien, J. Corset, E. Picquenard, *J. Raman Spectrosc.* **1999**, *30*, 463; M. S. Boumedien, *Doctoral Dissertation, University of Paris 6, Paris 1995*.
24. H. Rau, T. R. N. Kutty, J. R. F. Guedes de Carvalho, *J. Thermodyn.* **1973**, *5*, 833.
25. G. Preuner, W. Schupp, *Z. Physik. Chem.* **1909**, *68*, 129.
26. H. Braune, S. Peter, V. Neveling, *Z. Naturforsch. Part A* **1951**, *6*, 32.
27. H. Rau, T. R. N. Kutty, J. R. F. Guedes de Carvalho, *J. Thermodyn.* **1973**, *5*, 291.
28. J. Berkowitz, J. R. Marquart, *J. Chem. Phys.* **1963**, *39*, 275.
29. <http://webbook.nist.gov/chemistry>.
30. J. Berkowitz in *Elemental Sulfur* (B. Meyer, ed.), Interscience Publ., New York; **1965**, pp. 125; data calculated from values in Table 7.8
31. D. Detry, J. Drowart, P. Goldfinger, H. Keller, H. Rickert, *Z. Physik. Chem. NF* **1967**, *55*, 314.
32. W. Rosinger, M. Grade, W. Hirschwald, *Ber. Bunsenges. Phys. Chem.* **1983**, *87*, 536.
33. G. B. Guthrie, D. W. Scott, G. Waddington, *J. Am. Chem. Soc.* **1954**, *76*, 1488.
34. R. Steudel, H.-J. Mäusle, *Z. Naturforsch. Part A* **1978**, *33*, 951.
35. S. W. Benson, *Chem. Rev.* **1978**, *78*, 23.
36. J. Chao, *Hydrocarbon Processing* **1980**, 217.
37. J. Berkowitz, W. A. Chupka, *J. Chem. Phys.* **1964**, *40*, 287.
38. J. Drowart, P. Goldfinger, D. Detry, H. Rickert, H. Keller, *Adv. Mass. Spectrom.* **1968**, *4*, 499.
39. J. Berkowitz, C. Lifshitz, *J. Chem. Phys.* **1968**, *48*, 4346.
40. R. Steudel, R. Strauss, *Z. Naturforsch. Part B* **1982**, *37*, 1219.
41. B. Meyer, T. Stroyer-Hansen, *J. Phys. Chem.* **1972**, *76*, 3968.
42. G. D. Brabson, Z. Mielke, L. Andrews, *J. Phys. Chem.* **1991**, *95*, 79.
43. P. Hassanzadeh, L. Andrews, *J. Phys. Chem.* **1992**, *96*, 6579.
44. G. E. Quelch, H. F. Schaefer III, C. J. Marsden, *J. Am. Chem. Soc.* **1990**, *112*, 8719.
45. S. Hunsicker, R. O. Jones, G. Ganteför, *J. Chem. Phys.* **1995**, *102*, 5917; D. Hohl, R. O. Jones, R. Car, M. Parrinello, *J. Chem. Phys.* **1988**, *89*, 6823.
46. R. O. Jones, P. Ballone, *J. Chem. Phys.* **2003**, *118*, 9257.
47. K. Raghavachari, C. M. Rohlfing, J. S. Binkley, *J. Chem. Phys.* **1990**, *93*, 5862.
48. W. von Niessen, *J. Chem. Phys.* **1991**, *95*, 8301.
49. J.-L. M. Abboud, M. Essefar, M. Herreros, O. Mó, M. T. Molina, R. Notario, M. Yáñez, *J. Phys. Chem. A* **1998**, *102*, 7996.
50. G. Orlova, J. D. Goddard, *J. Phys. Chem. A* **1999**, *103*, 6825.
51. M. D. Chen, M. L. Liu, H. B. Luo, Q. E. Zhang, C. T. Au, *J. Mol. Struct. (Theochem)* **2001**, *548*, 133.
52. S. Millefiori, A. Alparone, *J. Phys. Chem. A* **2001**, *105*, 9489.
53. M. W. Wong, R. Steudel, Unpublished results **2003**.
54. B. Meyer, T. Stroyer-Hansen, T. V. Oommen, *J. Mol. Spectrosc.* **1972**, *42*, 335.
55. G. Weser, F. Hensel, W. W. Warren, *Ber. Bunsenges. Phys. Chem.* **1978**, *82*, 588.
56. V. A. Krasnopolsky, *Adv. Space. Res.* **1987**, *7*, 25.
57. M. H. Moore, B. Donn, R. L. Hudson, *Icarus* **1988**, *74*, 399.

58. R. Steudel, J. Albertsen, K. Zink, *Ber. Bunsenges. Phys. Chem.* **1989**, 93, 502.
59. B. Meyer, *Chem. Rev.* **1976**, 76, 367.
60. R. I. Billmers, A. L. Smith, *J. Chem. Phys.* **1991**, 95, 4242.
61. J. R. Rice, R. D. Amos, N. C. Handy, T. J. Lee, H. F. Schaefer, *J. Chem. Phys.* **1986**, 85, 963.
62. A. S. Brown, V. H. Smith, *J. Chem. Phys.* **1993**, 99, 1837.
63. D. A. Dixon, E. Wasserman, *J. Phys. Chem.* **1990**, 94, 5772.
64. J. Cioslowski, A. Szarecka, D. Moncrieff, *J. Phys. Chem. A* **1990**, 105, 501.
65. L. Peter, *Phosphorus, Sulfur and Silicon* **2001**, 168, 287.
66. R. Steudel, *Z. Naturforsch. Part B* **1972**, 27, 469.
67. R. O. Jones, D. Hohl, *Int. J. Quantum Chem.: Quantum Chem. Symp.* **1990**, 24, 141.
68. M. W. Wong, Y. Steudel, R. Steudel, *Chem. Phys. Lett.* **2002**, 364, 387.
69. R. Steudel, R. Reinhardt, T. Sandow, *Angew. Chem.* **1977**, 89, 757; *Angew. Chem. Int. Ed. Engl.* **1977**, 16, 716.
70. S. Munejiri, F. Shimojo, K. Hoshino, *J. Phys. Condens. Matter* **2000**, 12, 7999.
71. R. Steudel, *Phosphorus and Sulfur* **1983**, 16, 251.
72. D. Griller, J. A. M. Simoes, D. D. M. Wayner, in: *Sulfur-Centered Reactive Intermediates in Chemistry and Biology* (C. Chatgililoglu, K.-D. Asmus, eds.), Plenum Press, New York, **1990**, p. 37.
73. R. Steudel, *Z. Anorg. Allg. Chem.* **1981**, 478, 139.
74. R. F. Bacon, R. Fanelli, *J. Am. Chem. Soc.* **1943**, 65, 639.
75. F. Fehér, *Z. Naturforsch. Part B* **1967**, 22, 221.
76. R. J. H. Clark, D. G. Cobbold, *Inorg. Chem.* **1978**, 17, 3169.
77. G. D. Brabson, Z. Mielke, L. Andrews, *J. Phys. Chem.* **1991**, 95, 79.
78. E. Picquenard, O. El Jaroudi, J. Corset, *J. Raman Spectrosc.* **1993**, 24, 11.

Homoatomic Sulfur Cations

Ingo Krossing

Institut für Anorganische Chemie der Universität, 76128 Karlsruhe, Germany
E-mail: krossing@chemie.uni-karlsruhe.de

Abstract This chapter gives an account on the recent achievements in an understanding of the synthesis, solution behavior, structure and bonding of the homopolyatomic sulfur cations. A focus is put on the developments aimed to understand experimental observations, i.e., quantum chemical calculations of these electronically delicate species. The synthesis of the highly electrophilic sulfur cations requires the use of very weakly basic conditions throughout, that is weakly coordinating counterions such as AsF_6^- , SbF_6^- , $\text{Sb}_2\text{F}_{11}^-$ as well as weakly basic solvents such as SO_2 , HF, HSO_3F . Structure and bonding of the currently structurally characterized S_4^{2+} , S_8^{2+} , and S_{19}^{2+} cations are governed by positive charge delocalization brought about by $3p_\pi-3p_\pi$, $\pi^*-\pi^*$ and $3p^2\rightarrow 3\sigma^*$ bonding interactions. The solution behavior of S_8^{2+} salts, which give rise to several sulfur radical cations such as S_5^+ , was analyzed in detail based on (calculated) thermodynamic as well as spectroscopic considerations and hitherto unknown D_{3d} symmetric S_6^{2+} and D_{4h} symmetric S_4^+ are likely players in SO_2 solutions of $\text{S}_8(\text{AsF}_6)_2$.

Keywords Sulfur · Cation · Ab initio · Bonding · DFT

1	Introduction	136
1.1	Historical Development	136
2	Synthesis of Sulfur Cations in Condensed Phases	137
3	Solid State Structures of Sulfur Cations	137
4	Sulfur Cations in Solution	138
5	Gaseous Sulfur Cations	139
5.1	Sulfur Monocations S_n^+	139
5.2	Sulfur Dications S_n^{2+}	140
5.2.1	Triplet S_3^{2+}	140
5.2.2	S_4^{2+} Isomers	141
5.2.3	Exo-Endo S_8^{2+}	141
5.2.4	Other S_n^{m+} Cations	142
6	Thermodynamics of the Sulfur Cations	143
6.1	Basic Thermochemical Data	143
6.2	The Preference of S_4^{2+} Over 2 S_2^{++} in the Solid State	143
6.3	Dissociation of S_n^{2+} ($n=4, 6, 8, 10$) in the Gas Phase and in Solution	144

7	Bonding	146
7.1	Bonding in S_4^{2+} with 6π electrons	147
7.2	Bonding in S_6^{2+} with 10π Electrons	147
7.3	Bonding in S_8^{2+}	148
7.4	Bonding in S_{19}^{2+}	150
8	Summary, Conclusion, and Outlook	150
References		151

1

Introduction

Elemental sulfur with its relatively high electronegativity of 2.4 (Allred-Rochow) is commonly used as an electron acceptor and thus as an oxidizing agent. Accordingly a plethora of structures of homoatomic sulfur anions S_n^- and S_n^{2-} ($n \geq 2$) and derivatives thereof is known but only three sulfur cations S_n^{m+} ($n \geq 2$, $m=1, 2$) were characterized in the solid state and a few more are known in solution and in the gas phase. This is in part due to the high 1st and 2nd ionization energies of the sulfur homocycles that required the development of special experimental techniques to handle the thermodynamically stable but very reactive polysulfur cation salts in condensed phases. Notwithstanding these problems, the chemistry of the homoatomic sulfur cations emerged from being poorly understood laboratory curiosities to fully understood and thoroughly examined textbook examples of fundamental interest to the chemistry of the elements [1].

1.1

Historical Development

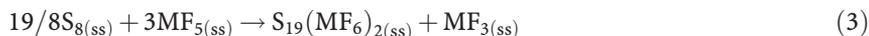
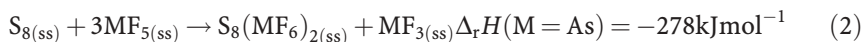
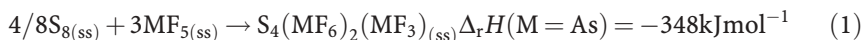
The first written account of species which now have been accepted to be sulfur cations dates back to 1804 when Bucholz [2] reported on the blue color obtained upon addition of elemental sulfur to freshly distilled oleum. The nature of these blue species gave rise to much speculation and is currently—almost 200 years later—still under investigation [3]. Considerable progress was made in sulfur cation chemistry in the late 1960s until the early 1980s. This was connected to the development of a facile synthesis of salts of sulfur cations with weakly basic (mainly) fluoroarsenate(V) and -antimonate(V) anions and the use of weakly basic solvents such as HF, HSO_3F , oleum, SO_2 , and AsF_3 . The first structural information on sulfur cations dates back to 1971 when the solid state structure of $S_8(AsF_6)_2$ containing the weakly transannularly bonded C_s symmetric S_8^{2+} dication was determined [4]. In 1980 the structures of square planar S_4^{2+} and irregular S_{19}^{2+} cations were elucidated by single crystal X-ray diffraction methods [5, 6]. However, the situation is less clear in solution and already 45 years ago it was noticed that

sulfur cation solutions contain larger quantities of at least two (radical-)cations S_n^{+} ($n \geq 4$). Only the existence of dissolved S_5^{+} was established in 1976 with great certainty [7] while another cation was tentatively assigned as S_7^{+} [8]. The driving force for the formation of less charged (radical-)monocations in solutions presumably is due to electrostatics and a “coulomb explosion” of the in the solid state lattice stabilized S_n^{2+} dications. Other than the above-mentioned five species no further sulfur cations were identified with confidence in condensed phases. However, very recently evidence for the existence of D_{3d} symmetric S_6^{2+} and square planar S_4^{+} was presented [3].

2

Synthesis of Sulfur Cations in Condensed Phases

The synthesis of the highly electrophilic sulfur cation salts requires the use of strong one or two electron oxidizing agents such as SO_3 , $S_2O_6F_2$, or MF_5 ($M=As, Sb$) in weakly basic and oxidation resistant solvents. From all reported synthetic procedures (see [1a] for an overview) the oxidation using MF_5 in a suitable solvent (such as SO_2 emerged as the most straight forward method, i.e., Eqs. (1–3) [(ss)=standard state]:



The synthesis of the highest oxidized S_4^{2+} salt in Eq. (1) necessitates the presence of a trace amount of halogen (=“facilitator”).[9] Salts containing the S_4^{2+} cation are colorless, while those of S_8^{2+} appear to be blue [10] and S_{19}^{2+} salts are orange-red. Crystalline samples of all three sulfur cation salts were characterized by a variety of experimental techniques including vibrational and UV-Vis spectroscopy as well as X-ray diffraction (see [1a] for a detailed overview on the physical characterization of sulfur cation salts in condensed phases).

3

Solid State Structures of Sulfur Cations

The solid state structures of the known S_n^{2+} ($n=4, 8, 19$) dications including their basic structural parameters are collected in Fig. 1.

All known solid state structures shown in Fig. 1 contain sulfur homocycles. While the S_4^{2+} cation is a regular square, the S_8^{2+} cation adopts an approximately C_s symmetric exo-endo conformation with three transannular contacts and S_{19}^{2+} consists of two seven membered rings linked by a penta-sulfur chain and incorporates two tricoordinate sulfur atoms. An analysis of the solid state anion contacts of the S_4^{2+} and S_8^{2+} cations showed that the positive charge is delocalized almost equally over the entire cations [11, 23].

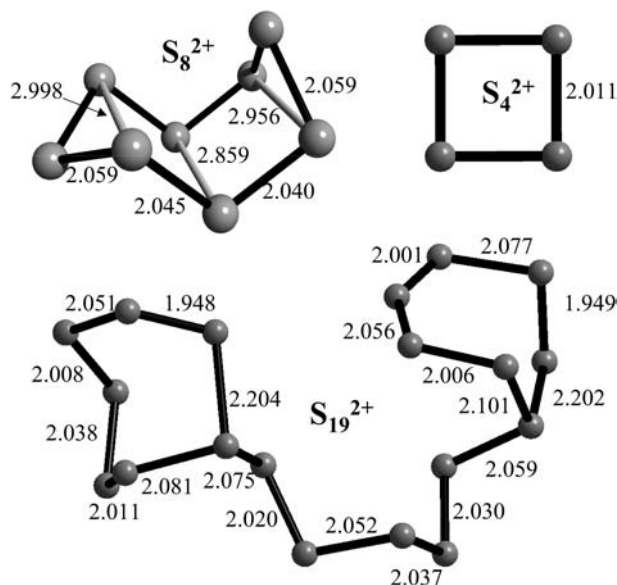


Fig. 1 The solid state structures of all currently known structurally characterized sulfur cations S_n^{2+} ($n=4, 8, 19$). Distances within the figure are given in Å. They originate from the crystal structures of $S_4(AsF_6)_2(AsF_3)$ [11] (averaged according to local D_{4h} symmetry), $S_8(AsF_6)_2$ [23] (averaged assuming local C_s symmetry) and $S_{19}(SbF_6)_2$ [12]. For comparison: the S-S distance of neutral S_8 corrected for librational motion is 2.060 Å [13]

From the structural data collected in Fig. 1 we note the following: (i) most of the S-S bond distances between the dicoordinate sulfur atoms are slightly shorter than those in neutral S_8 [$d(S-S)=2.060$ Å [13], corrected for librational motion]; (ii) the S-S bond lengths around the truly tricoordinate sulfur atoms in S_{19}^{2+} are the longest of all S-S bond lengths in Fig. 1; (iii) in both, S_8^{2+} and S_{19}^{2+} , a small bond lengths alternation is evident; (iv) in S_8^{2+} three rather odd weakly bonded transannular contacts occur at $d(S-S)=2.85$ to 3.00 Å.

4 Sulfur Cations in Solution

The successive oxidation of sulfur by $S_2O_6F_2$, oleum or AsF_5 was monitored with several experimental techniques such as Magnetic Circular Dichroism (MCD) [14], UV/Vis spectroscopy [6], ESR spectroscopy [7], and magnetic measurements [4]. The last two methods pointed out the existence of singly charged radical cations $S_n^{\cdot+}$ ($n \geq 4$) in equilibrium with the diamagnetic solid state cations S_8^{2+} and S_{19}^{2+} , while pure S_4^{2+} solutions are ESR-silent. Of the detected radical(mono-)cations only $S_5^{\cdot+}$ was unambiguously characterized on experimental grounds [7]. The lower the polarity of the solvent used to

examine the properties of the dissolved sulfur dication salts, the higher was the concentration of radical cations present, i.e., the radical concentration in relatively less polar SO_2 with a dielectric constant (DC) of 14 was much higher than in the strong acid HSO_3F (DC=110). Based on a joined ESR and UV-Vis spectroscopic study the very intense blue color of solutions of S_8^{2+} salts with a broad absorption at 585 nm was attributed to the S_5^+ cation [8]. However, recently evidence was presented [3] that this blue color is almost entirely due to the $\pi^*-\pi^*$ transition of a hitherto unknown cation: the D_{3d} symmetric S_6^{2+} dication with 10π electrons (see below).

The above may be summarized as follows: it is clear from MCD and Raman studies that S_4^{2+} occurs as such in solution in various solvents. Whether the dications S_8^{2+} or S_{19}^{2+} also exist as such in solution may depend on the solvent with polar solvents favoring the dications over their dissociation products. However, this is far from being fully understood and subject to ongoing research.

5 Gaseous Sulfur Cations

5.1 Sulfur Monocations S_n^+

In the gas phase sulfur (radical-)cations S_n^+ ($n=2-8$) are well known and their basic thermodynamic (see section below) and for S_2^+ also the structural properties were determined (i.e., by mass spectrometry and/or photo ionization) [15]. It was shown [16] that the simplest homopolyatomic sulfur cation S_2^+ is highly π bonded as evident from the short S-S distance of 1.825 Å corresponding to a bond order of 2.5 (cf. the MO treatment of the lighter homologue O_2^+). However, no structural information based on experimental data is available for the larger cations S_n^+ with $n \geq 3$ but some gas phase reactions of S_n^+ were assessed [17]. With the advent of easy to use quantum chemical program codes, powerful computers and advanced ab initio or DFT methods it is nowadays possible to reliably assess the structural properties of these species by calculations. Figure 2 shows the most recently at the B3PW91/6-311+G* level calculated minimum structures of the S_n^+ ($n=3-7$) cations [3, 18].

All radical cations S_n^+ in Fig. 2, with the exception of S_3^+ , form homocycles in which the positive charges as well as the spin densities are delocalized over at least four to five atoms. Within the structures of the less regular uneven S_5^+ and S_7^+ cations a small bond lengths alternation is evident similar to the situation in S_8^{2+} and S_{19}^{2+} above or in neutral S_7 .

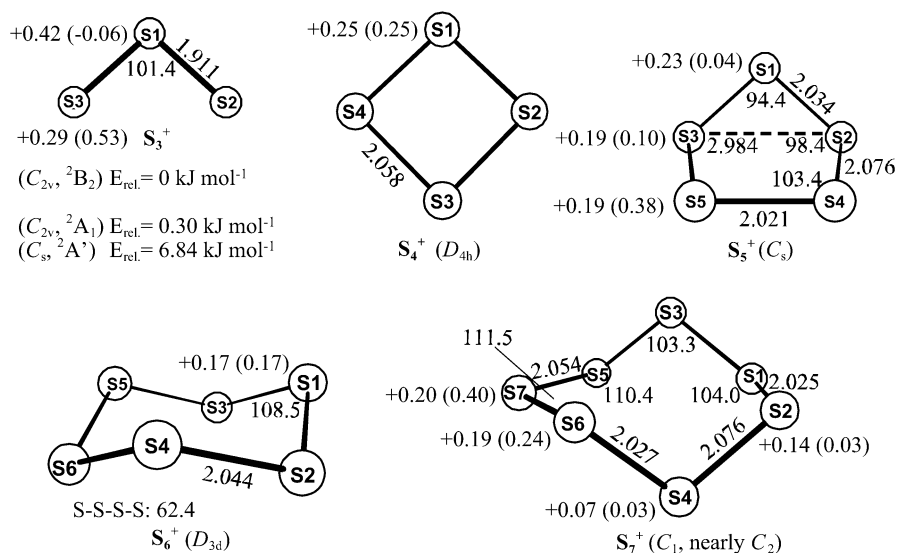


Fig. 2 Optimized geometries, calculated Mulliken charges (spin densities) of the true S_n^{2+} ($n=3-7$) minima at the B3PW91/6-311+G* level of theory

5.2

Sulfur Dications S_n^{2+}

Gaseous dications S_n^{2+} reduce the unfavorable Coulomb repulsion of the two positive charges in close proximity and dissociate with formation of two monocations S_x^+ and S_y^+ with $x+y=n$. This is called a ‘‘Coulomb Explosion’’. For the same reason classical solid state ions like sulfate SO_4^{2-} are unstable in the gas phase. This instability of gaseous S_n^{2+} cations makes quantum chemical calculations of sulfur cations delicate and requires the use of flexible basis sets and highly correlated methods. The consequences of this behavior for the chemistry of the sulfur cations are discussed below in the thermodynamics section.

5.2.1

Triplet S_3^{2+}

The S_3^{2+} dication was the subject of extensive investigations, since it appeared likely that it has a triplet ground state. A detailed CI study on the geometry, bonding and energetics of several S_3^{2+} isomers and electronic states showed that the triplet is the ground state. The global minimum is a regular D_{3h} symmetric S_3^{2+} triangle with a $^3A_1'$ electronic state and a relatively short ‘‘best’’ S-S bond length of about 2.03 \AA [19].

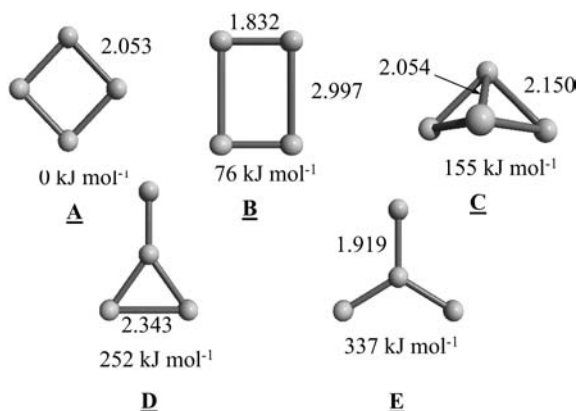


Fig. 3 Optimized geometries and relative energies of all true S_4^{2+} minima at the B3PW91 level of theory [21]

5.2.2

S_4^{2+} Isomers

Due to the high local D_{4h} symmetry it appeared simple to obtain reliable quantum chemical results not only on the structure but also on the energetics of the S_4^{2+} dication. It was shown, however, that especially the calculation of S_4^{2+} required great care and the highest level of theory available in order to obtain reliable results (see thermodynamics section) [20]. From this publication also followed that the only affordable and comparably fast computational technique for the correct structural and energetic description of sulfur homopolyatomic cations is the hybrid HF-DFT level B3PW91 and its newer modified version MPW1PW91. In the following, therefore, the potential energy surface of the gaseous S_4^{2+} dication was examined with the B3PW91 method and this investigation revealed the presence of at least five local minima (Fig. 3) [21].

From Fig. 3 it is clear that, as in the solid state, square planar S_4^{2+} (**A**) is the global minimum of all assessed isomers. It should be noted though that the second favorable isomer **B** has an unexpected non-classical highly π and π^* - π^* bonded structure and only the next all σ bonded isomer **C** with a high relative energy of +155 kJ mol⁻¹ has a classically expected geometry with the tricoordinate sulfur atoms formally bearing the positive charge.

5.2.3

Exo-Endo S_8^{2+}

MP2, B3LYP, BLYP, BP86, and HF levels were unsuccessfully [22] employed to optimize the geometry of isolated S_8^{2+} dication. By contrast, the B3PW91 and MPW1PW91 levels for the first time led to a geometry of gaseous S_8^{2+} similar to solid S_8^{2+} in $S_8(\text{AsF}_6)_2$ including the three long transannular con-

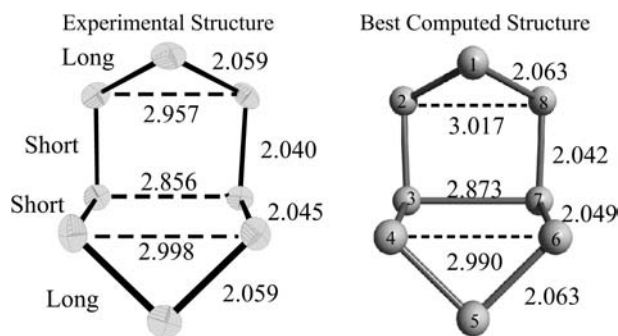


Fig. 4 Comparison of experimental and computed structure of the S_8^{2+} dication (inter-nuclear distances in Å) [23]

tacts at 2.85 to 3.00 Å (see Fig. 4) [23]. This again demonstrated the special usefulness of the B3PW91 and MPW1PW91 levels for quantum chemical investigations of sulfur cations.

5.2.4

Other S_n^{m+} Cations

After it had become evident that the electronically delicate geometry optimization of S_8^{2+} was successfully achieved by the B3PW91 method, the hitherto unknown dications S_6^{2+} , S_6^{4+} and S_{10}^{2+} were also calculated (see Fig. 5, cf. experimentally found Te_6^{2+} , Te_6^{4+} and Se_{10}^{2+}) [1].

It should be noted that a D_{3d} symmetric S_6^{2+} cation is considerably favored over a C_{2v} symmetric boat structure that was observed in several Te_6^{2+} salts [1]. The structures of the S_6^{4+} and S_{10}^{2+} dications are in good qualitative agreement with their heavier homologues and the optimized geometry

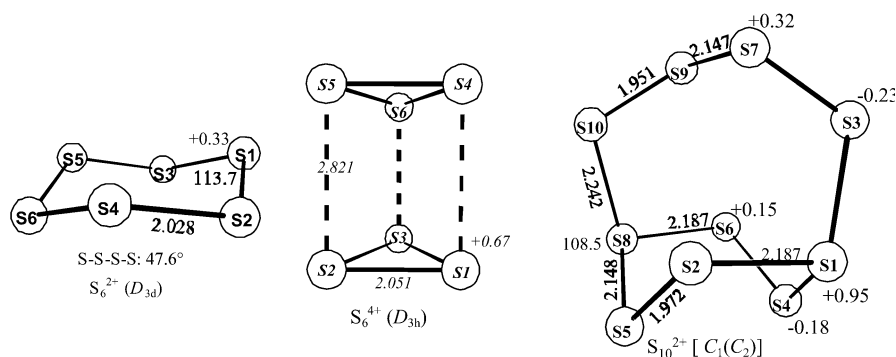


Fig. 5 Fully optimized geometries and calculated partial charges of S_6^{2+} , S_6^{4+} , and S_{10}^{2+} at the B3PW91 level (distances in Å) [3]

Table 1 Enthalpies of formation of gaseous and solid sulfur cations in kJ mol⁻¹ at 298 K

Cation	S ₂ ⁺	S ₃ ⁺	S ₄ ⁺	S ₅ ⁺	S ₆ ⁺	S ₇ ⁺	S ₈ ⁺	–
Δ _f H ₂₉₈ (g)	1031 [15]	1076 [15]	972 [21]	939 [15]	971 [15]	951 [15]	976 [15]	–
Dication	–	S ₃ ²⁺	S ₄ ²⁺	–	S ₆ ²⁺	–	S ₈ ²⁺	S ₁₀ ²⁺
Δ _f H ₂₉₈ (g)	–	2538 [3]	2318 [21]	–	2238 [3]	–	2151 [23]	2146 [3]
Salt	–	–	S ₄ (AsF ₆) ₂ ^a	–	S ₆ (AsF ₆) ₂	–	S ₈ (AsF ₆) ₂	–
Δ _f H ₂₉₈ (s)	–	–	–3104 [11]	–	–3103 [3]	–	–3122 [23]	–

^a S₄(AsF₆)₂(AsF₃): –4050 [11]

of S₁₀²⁺ shows a similar bond length alternation as observed in S₁₉²⁺ with similarly long S-S distances around the two tricoordinate sulfur atoms.

6 Thermodynamics of the Sulfur Cations

6.1

Basic Thermochemical Data

The enthalpies of formation of several gaseous and solid sulfur cations were experimentally determined or computationally assessed. Table 1 summarizes the currently established “best” values.

6.2

The Preference of S₄²⁺ Over 2 S₂⁺ in the Solid State

In order to understand the observation that oxygen in the oxidation state +0.5 forms salts that contain the O₂⁺ cation with a variety of anions while sulfur in the same oxidation state forms a dimer of the composition S₄²⁺[(S₂⁺)₂], the gas phase dissociation enthalpy of S₄²⁺ giving two S₂⁺ was assessed by quantum chemical calculations [20, 21], i.e. [(g)=gaseous]:



Initial results gave dissociation enthalpies that ranged from –200 to –530 kJ mol⁻¹ with a rather erratic behavior within all methods employed [20]. A systematic investigation of correlation and basis set effects on this reaction enthalpy finally revealed a dissociation enthalpy of –257 kJ mol⁻¹ obtained at the extremely expensive CCSD(T)/cc-pV5Z level of theory, while the B3PW91/6–311+G(3df) level was the only affordable energy calculation that systematically gave the same result [20]. Using this reaction enthalpy, a suitable Born-Haber cycle and estimation of the lattice potential enthalpies of the respective salts eventually showed that the preparation of solid S₂⁺ salts is impossible with all currently available anions and that S₄²⁺, although

unstable in the gas phase with respect to two S_2^+ ions, is lattice stabilized in the solid state by the much higher lattice potential enthalpies of a 2:1 vs a 1:1 salt [11]. For example, solid $S_4(AsF_6)_2$ is by 362 kJ mol⁻¹ favored over 2 $S_2(AsF_6)$. In order to overcompensate the lattice enthalpy gain of S_4^{2+} salts and stabilize a S_2^+ salt, anions with a thermochemical volume of at least 5000 Å³ would be needed [11]. Given the thermochemical volume of the AsF_6^- anion of 110 Å³ this appears unlikely to be achieved in the future!

6.3

Dissociation of S_n^{2+} ($n=4, 6, 8, 10$) in the Gas Phase and in Solution

The S_8^{2+} dication is also lattice stabilized in the solid state [1a, 23, 24]. In 1994 [24] it was shown that isolated gaseous S_8^{2+} is unstable with respect to a stoichiometric dissociation into various monocations S_n^+ ($n=2-7$) and by analogy one expects the same to hold for S_{19}^{2+} . However, due to the great difficulties in obtaining a good quantum chemical calculation of the gaseous S_8^{2+} cation, it was not before the year 2000 that reliable numbers could be put on the various dissociation equilibria [23]. Moreover, the puzzling fact that solutions of S_n^{2+} ($n=8, 19$) salts in several solvents also contain varying amounts of sulfur radical cations S_n^+ ($n \geq 4$) sparked additional quantum chemical calculations which included approximate solvation energies [3] as calculated by one of the modern PCM models (=Polarizable Continuum Model) developed by Tomasi et al. [25]. Other recent publications on the use of PCM solvation models established the quality of this method [26]. The results of these calculations are collected in Table 2.

From the energetics summarized in Table 2 it is evident that all doubly charged gaseous sulfur cations are unstable with respect to a dissociation into monocations due to a relief of electrostatic repulsion upon dissociation (i.e., a Coulomb explosion). However, the solvation energies of dications are much higher than those of monocations and, consistently, none of the dissociation reactions in Table 2 giving only monocations is exergonic in solution. But how are the monocations in solutions of S_8^{2+} and S_{19}^{2+} salts then formed? Especially bearing in mind that both observed or tentatively assigned monocations S_5^+ and S_7^+ have a lower average oxidation state than S_8^{2+} . This then pointed out that in dissociation reactions of S_8^{2+} another species with a higher average oxidation state than S_8^{2+} must form. S_4^{2+} could be a player; however, it was convincingly shown that in the absence of halogen facilitator the S_4^{2+} oxidation stage was never reached [9] for kinetic reasons and therefore this dication, although thermochemically possible, is no player in equilibria of dissolved S_8^{2+} . Eventually and in agreement with a reinterpretation of earlier experimental work it was concluded that the higher oxidized species necessary to account for the observation of reduced S_5^+ and S_7^+ is the D_{3d} symmetric S_6^{2+} dication (=dimer of S_3^+). The S_6^{2+} dication with 10π electrons shown in Fig. 5 is apparently also responsible for the intense blue color of solutions of S_8^{2+} salts (see below) and the most favored dissociation reaction of S_8^{2+} , excluding S_4^{2+} , is Eq. (g) in Table 2. The picture changes when a small amount of halogen facilitator is added: the formation

Table 2 Selected reaction enthalpies and free energies of dissociation reactions of S_n^{2+} ($n=4, 6, 8, 10$) in the gas phase and in SO_2 solution at 298 K [in kJ mol^{-1}]. Some equilibria were also assessed using HF (DC=83) or oleum (DC=110) as solvent. Exergonic Gibbs energies of reaction in solution are printed in bold

Eq.	Dissociation reactions of S_n^{2+} [kJ/mol]	$\Delta_r H_{298}$	$\Delta_r G_{298}$ (SO_2)	$\Delta_r G_{298}$ (HF)	$\Delta_r G_{298}$ (Oleum)
(a)	$S_4^{2+}(\text{g}) \rightarrow 2 S_2^{+}(\text{g})$	-257	-308	-	-
(b)	$S_6^{2+}(\text{g}) \rightarrow 2 S_3^{+}(\text{g})$	-93	-157	-	-
(c)	$S_6^{2+}(\text{g}) \rightarrow 1/2 S_4^{2+}(\text{g}) + S_4^{+}(\text{g})$	-84	-110	-	-
(d)	$S_6^{2+}(\text{g}) \rightarrow 2/3 S_4^{2+}(\text{g}) + 2/3 S_5^{+}(\text{g})$	-58	-78	-	-
(e)	$S_8^{2+}(\text{g}) \rightarrow 2 S_4^{+}(\text{g})$	-170	-224	+41	+42
(f)	$S_8^{2+}(\text{g}) \rightarrow S_3^{+}(\text{g}) + S_5^{+}(\text{g})$	-135	-200	-	-
(g)	$S_8^{2+}(\text{g}) \rightarrow 1/2 S_6^{2+}(\text{g}) + S_5^{+}(\text{g})$	-89	-121	+2.18	+2.22
(h)	$S_8^{2+}(\text{g}) \rightarrow 2/3 S_6^{2+}(\text{g}) + 1/3 S_5^{+}(\text{g}) + 1/3 S_7^{+}(\text{g})$	-30	-51	+17	+17
(i)	$S_8^{2+}(\text{g}) \rightarrow 3/4 S_6^{2+}(\text{g}) + 1/2 S_7^{+}(\text{g})$	0	-15	+24	+24
(j)	$S_8^{2+}(\text{g}) \rightarrow 0.5 [S_4^{2+}(\text{g}) + S_5^{+}(\text{g}) + S_7^{+}(\text{g})]$	-43	-74	-	-
(k)	$S_{10}^{2+}(\text{g}) \rightarrow 2 S_5^{+}(\text{g})$	-268	-337	-	-

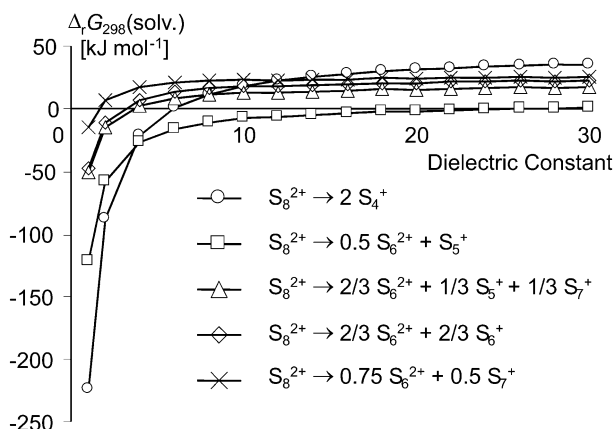


Fig. 6 Solvent dependence of the calculated free energies of the dissociation of selected equilibria of S_8^{2+} giving S_6^{2+} and radical cations S_n^+ ($n=4-7$) [in kJ mol^{-1} at 298 K. [3]

of S_4^{2+} in solution is no longer *kinetically* hindered and, therefore, S_4^{2+} is in equilibrium with S_8^{2+} and the most favored equilibria include the formation of the hitherto unknown S_4^+ radical cation in addition to the established S_5^+ (Eqs. c, d, and j in Table 2). This is in agreement with preliminary temperature and concentration dependent ESR and magnetic measurements [27].

The quantity of radical cations formed by dissociation of S_8^{2+} is dependent on the polarity of the solvent with less polar solvents such as SO_2 or SO_2ClF favoring the formation of radical (mono-)cations if compared to polar solvents like HF or oleum. This can be understood by quantum chemical calculations with inclusion of solvation energies that approximate solvents of different polarities. A measure for the polarity of a solvent is the dielectric constant (DC) and a graphic representation of the calculated Gibbs energies of selected dissociation equilibria of S_8^{2+} in solvents with dielectric constants between 1 and 30 is given in Fig. 6 [3]. For comparison: the DC of SO_2 at 298 K is 14 and that of HF is 83.

Analysis of the data in Fig. 6 shows that, in agreement with the experiment, non-polar solvents favor the dissociation of S_8^{2+} to sulfur monocations as the overall solvation energies decrease with decreasing dielectric constant.

7 Bonding

The structure and bonding of the sulfur cations has been the focus of recent work and revealed the presence of non-classical $3p_\pi-3p_\pi$, $\pi^*-\pi^*$, and $3p^2\rightarrow 3\sigma^*$ bonding interactions as a means to delocalize the unfavorable localized positive charges expected from classical electron precise structures [1a].

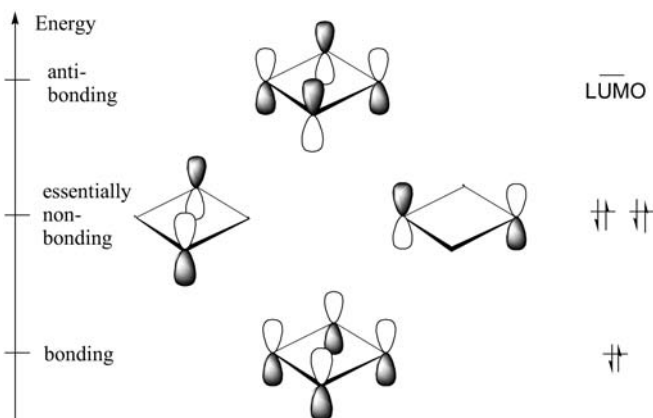


Fig. 7 Molecular orbitals of π symmetry in S_4^{2+}

7.1

Bonding in S_4^{2+} with 6π electrons

The square planar S_4^{2+} dication (as well as its heavier homologues E_4^{2+} with $E=Se$ and Te) was shown to be an inorganic 6π Hückel aromatic; the S_4^{2+} molecular orbitals of π symmetry are shown in Fig. 7.

Overall the four atomic $3p_z$ orbitals combine to one π bonding, two non-bonding and one anti bonding empty π^* MO and in total one π bond is delocalized over all four atoms giving a bond order of 1.25 which is in agreement with the by 5 pm shortened S-S distance in S_4^{2+} salts [5, 11] as well as with recent calculations [21].

7.2

Bonding in S_6^{2+} with 10π Electrons

The recently suggested D_{3d} symmetric S_6^{2+} cation is also π bonded. Albeit not being completely planar, the 10π electrons reside in orbitals of local π symmetry and S_6^{2+} may be viewed as being a Hückel aromatic with 10π electrons, although a strict differentiation between σ - and π -MOs is impossible [3]. Removal of two electrons from the occupied $3p^2$ lone pair orbitals of the neutral S_6 molecule with formally 12π electrons leads to one π bond delocalized over all six sulfur atoms. In agreement with this the S_6^{2+} dication exhibits an increased S-S-S bond angle α of 113.7° and a smaller S-S-S-S torsion angle τ of 47.6° compared to S_6 and S_6^+ (cf. S_6 : $\alpha=103.0^\circ$, $\tau=73.1^\circ$; S_6^+ : $\alpha=108.5^\circ$, $\tau=62.4^\circ$; calculated values throughout for consistency; see Fig. 8a). The (calculated) S-S distance in S_6^{2+} is shortened from 2.050 Å in the clearly all σ -bonded S_8 molecule to 2.028 Å in $10\pi S_6^{2+}$. The electronic transition responsible for the blue color of S_6^{2+} is of $\pi^*-\pi^*$ nature and the S_6^{2+} molecular orbitals of π and π^* symmetry are shown in Fig. 8b [28].

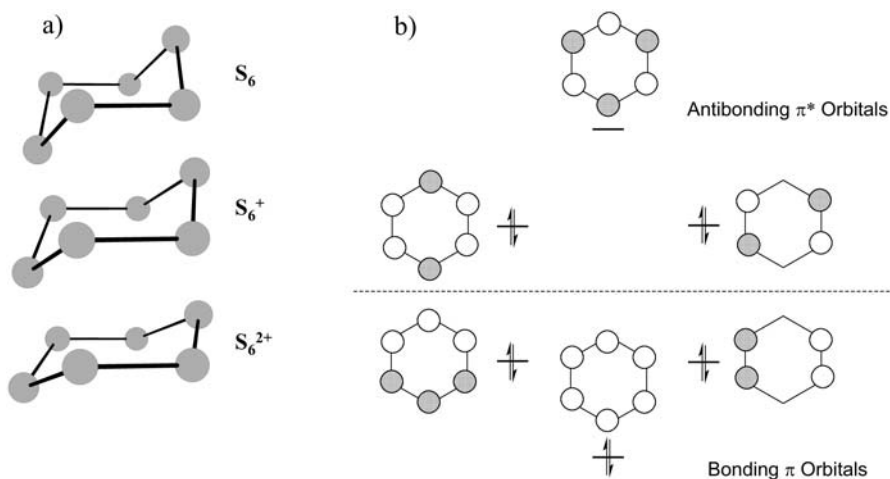


Fig. 8 a Structural changes upon oxidation of S_6 to S_6^{2+} . b Top view of the S_6^{2+} molecular orbitals of local π and π^* symmetry with the HOMO-LUMO transition of $\pi^*-\pi^*$ symmetry being the reason for the intense blue color of S_6^{2+} in solution

7.3

Bonding in S_8^{2+}

The overall structure of exo-endo S_8^{2+} was not unexpected since it is intermediate between the structure of crown (exo-exo) S_8 and endo-endo S_4N_4 (isoelectronic with S_8^{4+}) as shown in Fig. 9:

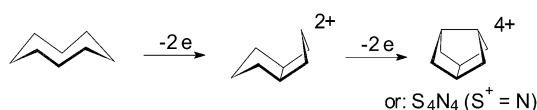


Fig. 9 Structural relationships between S_8 , S_8^{2+} and S_8^{4+}

However, the long transannular bonds at 2.85 to 3.00 Å and the entirely delocalized charges are not accounted for by this model. Since the central six atoms of S_8^{2+} have a similar structural arrangement as the six atoms of $Se_2I_4^{2+}=(SeI_2^+)_2$ it was postulated that the bonding in S_8^{2+} should be related and due to a $\pi^*-\pi^*$ interaction; see Fig. 10a. Later [23] it was verified that the weak cross ring bonds are due to a weakly bonding $\pi^*-\pi^*$ interaction [29] of the partially occupied 3p orbitals of the six central sulfur atoms of the S_8^{2+} dication (HOMO in Fig. 10b).

An interaction as shown in Fig. 10b leads to a delocalization of one π bond over the central six sulfur atoms and the two halves of the HOMO, which is best described as being of π^* nature, provide a non-cancelled weakly bonding interaction between the three transannular pairs of sulfur atoms.

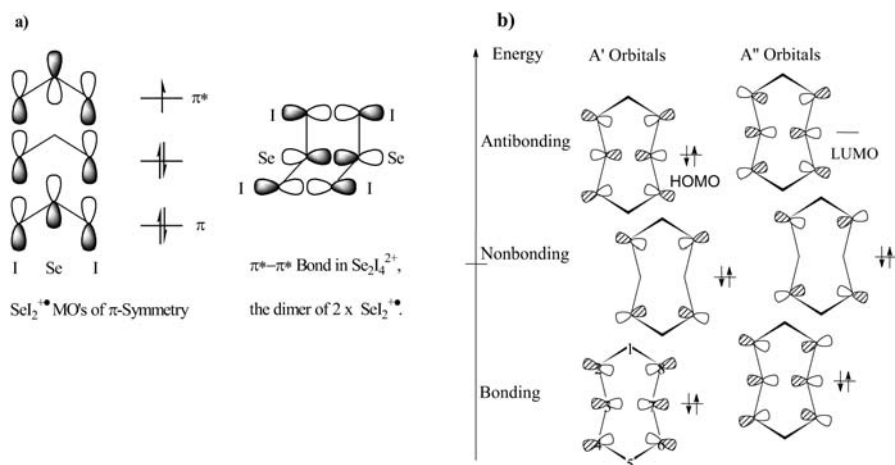


Fig. 10a,b π and $\pi^*-\pi^*$ bonding molecular orbitals in: **a** $\text{Se}_2\text{I}_4^{2+}=(\text{SeI}_2^+)_2$; **b** the structurally similar S_8^{2+}

A further interaction that allows to delocalize the positive charge also onto the two apical sulfur atoms was found to be the $3p^2 \rightarrow 3\sigma^*$ hyperconjugation as shown in Fig. 11.

With this interaction, initially suggested by Steudel et al. [30] to explain the bond length alternation in neutral S_7 , electron density from the occupied apical $3p^2$ lone pair orbitals is transferred into the empty $3\sigma^*$ orbitals of the vicinal S-S bonds. The overall process can be summarized as shown in Fig. 12.

Starting from the classically expected structure with a short transannular bond and localized charges residing on the tricoordinate atoms the positive charges are delocalized over the central six sulfur atoms by a $\pi^*-\pi^*$ interaction which is further responsible for the three weak transannular bonds. Additionally the positive charge is delocalized onto all atoms—as found in the experiment—by a further $3p^2 \rightarrow 3\sigma^*$ interaction. The combination of both in-

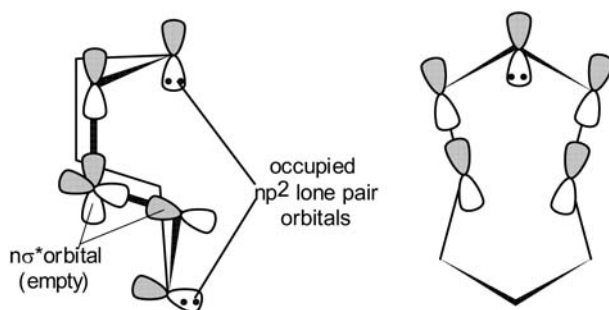


Fig. 11 Further charge delocalization in S_8^{2+} by a $3p^2 \rightarrow 3\sigma^*$ interaction

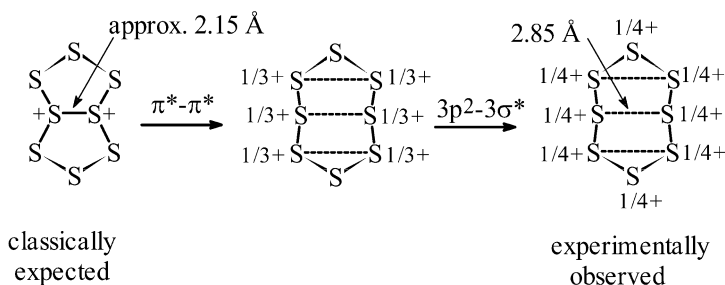


Fig. 12 Charge delocalization in S_8^{2+}

teractions leads to the observed slightly shortened S-S bond lengths and the small long-short-short-long bond lengths alternation starting from the apical sulfur atom [23].

7.4

Bonding in S_{19}^{2+}

Little is known about the S_{19}^{2+} dication and no quantum chemical calculation of this species has been reported to date. However, by analogy to the bonding modes established for S_8^{2+} it was suggested that the marked bond length alternation within the two seven membered rings, which decreases with increasing distance from the tricoordinate sulfur atoms, is due to multiple $3p^2 \rightarrow 3\sigma^*$ interactions. The tricoordinate sulfur atoms in S_{19}^{2+} are, presumably, the only atoms that only possess a $3s^2$ lone pair, but no $3p^2$ lone pair orbital. The unfavorable localized positive charge formally residing on the two tricoordinate chalcogen atoms is then delocalized by several $3p^2 \rightarrow 3\sigma^*$ interactions, which transfer electron density from the vicinal $3p^2$ lone pair orbitals into the empty, antibonding $3\sigma^*$ orbital of the bonds adjacent to the tricoordinate atoms. Therefore the bonds around the tricoordinate chalcogen atoms are relatively long. Strong interactions around the tricoordinate sulfur atoms, in turn, induce a positive charge to reside on the vicinal sulfur atoms which is then subsequently delocalized by the formation of further $3p^2 \rightarrow 3\sigma^*$ interactions. This and the bond lengths alternation inherent in an S_7 ring [30, 31] lead to the bond lengths alternation observed throughout the seven membered rings.

8

Summary, Conclusion, and Outlook

Homoatomic sulfur cation are a fascinating class of compounds that maximize non-classical bonding in their solid state structures. Synthesis as well as quantum chemical calculations of these species are difficult but yet possible tasks and their structures and bonding interactions are now well understood. Structure and bonding of the in the solid state characterized sulfur

cations is governed by positive charge delocalization which enforces the formation of thermodynamically stable $3p_{\pi}-3p_{\pi}$, $\pi^*-\pi^*$, and $3p^2\rightarrow 3\sigma^*$ bonded species. In the gas phase and in solution the higher charged and in the solid state lattice stabilized S_n^{2+} dications ($n=4, 8, 19$) are unstable with respect to a dissociation into smaller cations, and recently it has been concluded that solutions of S_8^{2+} salts contain at least S_6^{2+} , S_5^+ , and S_7^+ or S_4^{2+} , S_4^+ , S_5^+ , and S_7^+ depending on whether halogen facilitator is present or not. With the help of quantum chemical calculations, which now already have predictive power, the experimental access to new sulfur cations in condensed phases is only a matter of time. Promising new preparative routes to salts of these new mono- or dications include the use of large and weakly coordinating anions, i.e., $Al(OR)_4^-$ ($R=C(CF_3)_3$) [32, 33], that drastically change the lattice energies of all species in question and, therefore, should allow the synthesis of crystalline samples of hitherto in the solid state unknown sulfur cations.

Acknowledgement This chapter is dedicated to Jack Passmore with whom I had the honor to spend my postdoctoral fellowship and who introduced me to the fascinating world of small but electronically delicate main group cations such as the homopolyatomic sulfur cations. Thank you! This would have been impossible without the fine and bureaucracy-free sponsorship of the *Alexander von Humboldt Stiftung* in Bonn, Germany.

References

- [1]. For reviews on sulfur and other chalcogen cations see: a) S. Brownridge, I. Crossing, J. Passmore, H. D. B. Jenkins, H. K. Roobottom, *Coord. Chem. Rev.* **2000**, *197*, 397; b) N. Burford, J. Passmore, J. C. P. Sanders, *From Atoms to Polymers, Isoelectronic Analogies*, **1989**, pp. 53-108, Eds. J. F. Liebman and A. Greenburg, VCH; c) R. J. Gillespie, J. Passmore, *Adv. Inorg. Radiochem.* **1975**, *17*, 49; d) R. J. Gillespie, *J. Chem. Soc. Rev.* **1979**, *8*, 315; e) J. Beck, *Angew. Chem. Int. Ed. Eng.* **1994**, *33*, 163; f) J. Beck, *Angew. Chem. Rev.* **1997**, *163*, 55-70; g) S. Ulvenlund, L. Bengtsson-Kloo, in *Metal Clusters in Chemistry I*, ed.: P. Braunstein, L. A. Oro, P. R. Raithby, Wiley-VCH, Weinheim, Germany, **1999**, 561.
- [2]. C. F. Bucholz, *Gehlen's neues J. Chem.* **1804**, *3*, 7.
- [3]. I. Crossing, J. Passmore, *Inorg. Chem.* (accepted).
- [4]. a) R. J. Gillespie, J. Passmore, *Chem. Comm.* **1969**, 1333; b) R. J. Gillespie, J. Passmore, P. K. Ummat, O. C. Vaidya, *Inorg. Chem.* **1971**, *10*, 1327; c) C. G. Davies, R. J. Gillespie, J. J. Park, J. Passmore, *Inorg. Chem.* **1971**, *10*, 2781.
- [5]. a) J. Passmore, G. Sutherland, P. S. White, *J. Chem. Soc., Chem. Commun.* **1980**, 330; b) J. Passmore, G. W. Sutherland, P. S. White, *Inorg. Chem.* **1982**, *21*, 2717.
- [6]. R. C. Burns, R. J. Gillespie, J. F. Sawyer, *Inorg. Chem.* **1980**, *19*, 1423.
- [7]. I.e. by ESR-spectroscopy using 92% ^{33}S enriched sulfur; see: H. S. Low, R. A. Beaudet, *J. Am. Chem. Soc.* **1976**, *98*, 3849.
- [8]. a) R. C. Burns, R. J. Gillespie, J. F. Sawyer, *Inorg. Chem.* **1980**, *19*, 1423; b) J. Passmore, G. Sutherland, P. Taylor, T. K. Whidden, P. S. White, *Inorg. Chem.* **1981**, *20*, 3839.
- [9]. M. P. Murchie, J. Passmore, G. W. Sutherland, R. Kapoor, *Dalton Trans.* **1992**, 503.
- [10]. However, recently a sample of crystalline $S_8(AsF_6)_2$ was prepared that was red in transmitted but blue in reflected light.[23] The colors and UV-Vis spectra of sulfur cations were also the focus of much recent work; see [3].
- [11]. T. S. Cameron, H. K. Roobottom, I. Dionne, J. Passmore, H. D. B. Jenkins, *Inorg. Chem.* **2000**, *39*, 2042.
- [12]. R. Faggiani, R. J. Gillespie, J. F. Sawyer, J. E. Vekris, *Acta Cryst.* **1989**, *C45*, 1847.

- [13]. R. Steudel, *Angew. Chem. Int. Ed. Engl.* **1975**, *10*, 655.
- [14]. P. J. Stevens, *Chem. Comm.* **1969**, 1496.
- [15]. A wealth of thermodynamic data is now available online at the website of the National Institute of Standards and Technology NIST: <http://www.nist.gov/chemistry> or as hard-copy: a) Wagman, D. D.; Evans, W.H.; Parker, V. B.; Schumm, R. H.; Halow, I.; Bailey; Churney, K.L.; Nuttal, R. L. *J. Phys. Chem. Ref. Data*, **1982**, *11*, Suppl. 2. b) Lias, S. G.; Bartmess, J. E.; Liebman, J. F.; Holmes, J. L.; Levin, R. D.; Mallard, W. G. *J. Phys. Chem. Ref. Data* **1988**, *17*, Suppl. 1.
- [16]. K. Brabaharan, J. A. Coxon, *J. Phys. Chem. Ref.* **1988**, *128*, 540.
- [17]. a) G. Niedner-Schattenburg, J. Silha, T. Schindler, V. E. Bondybey, *Chem. Phys. Lett.* **1991**, *187*, 60; b) *J. Chem. Phys.* **1993**, *99*, 9664.
- [18]. see also: M. D. Chen, M. Liu, J. W. Liu, Q. E. Zhang, C. T. Au, *J. Mol. Struct. Theochem.* **2002**, *582*, 205.
- [19]. C. J. Marsden, G. E. Quelch, H. F. Schaefer, *J. Am. Chem. Soc.* **1992**, *114*, 6802.
- [20]. H. D. B. Jenkins, L. C. Jitariu, I. Crossing, J. Passmore, R. Suontamo, *J. Comp. Chem.* **2000**, *21*, 218.
- [21]. I. Crossing, J. Passmore, *Inorg. Chem.* **1999**, *38*, 5203.
- [22]. Either the strengths of the transannular bonds were overestimated (HF: 205 to 220 Å) or not at all present (all correlated methods): a) HF, BLYP and MP2: J. Cioslowski, X. Gao, *Int. J. Quant. Chem.* **1997**, *65*, 609; b) T. H. Tang, R. F. W. Bader, P. J. MacDougall, *Inorg. Chem.* **1985**, *24*, 2047; c) BP86 and B3LYP: I. Crossing, unpublished results using Turbomole and the TZVPP basis set.
- [23]. T. S. Cameron, R. J. Deeth, I. Dionne, H. D. B. Jenkins, I. Crossing, J. Passmore, H. Roobottom, *Inorg. Chem.* **2000**, *39*, 5614.
- [24]. I. Thomaskiewicz, J. Passmore, G. Schatte, G. W. Sutherland, P. A. G. O'Hare, *J. Chem. Thermodynamics* **1994**, *26*, 299.
- [25]. J. Thomasi, M. Persico, *Chem. Rev.* **1994**, *84*, 2027.
- [26]. A literature search with the program Scifinder (CAS database) gave 694 hits for the term "polarizable continuum model" mainly originating from the last few years. This shows the now widely accepted use of these models. Some selected successful (inorganic) applications of the PCM models approximating non-aqueous solvents are found in: a) G. Lanza, I. L. Fragala, T. J. Marks, *J. Am. Chem. Soc.* **2000**, *122*, 12764; b) P. Perez, A. Torre-Labbe, R. Contreras, *J. Am. Chem. Soc.* **2001**, *123*, 5527; c) H. Saint-Martin, L. E. Vicent, *J. Phys. Chem. A* **1999**, *103*, 6862.
- [27]. J. Passmore, D. Wood, to be published (cited in Ref. [3]).
- [28]. Our calculated π MOs of S_6^{2+} are in agreement with those calculated earlier for $C_6H_6^{4-}$, N_6^{4-} , P_6^{4-} , S_6^{2+} , Te_6^{2+} , and $S_3N_3^-$ by: J. Li, C. -W. Liu, J. -X. Lu, *J. Mol. Struct. Theochem.* **1993**, 223.
- [29]. The $\pi^*-\pi^*$ interaction was first established two account for the weak bonding between the two I_2^+ halves in $I_4(AsF_6)_2$ and the two SeI_2^+ moieties in $Se_2I_4(MF_6)_2$ (M=As, Sb); see: a) J. Passmore, G. Sutherland, T. Whidden, P. S. White, C. -M. Wong, *J. Chem. Soc. Chem. Comm.* **1982**, 1098; b) WAS Nandana, J. Passmore, P. S. White, C. -M. Wong, *Inorg. Chem.* **1990**, *29*, 3529.
- [30]. a) R. Steudel, *Top. Curr. Chem.* **1981**, *102*, 149; b) R. Steudel, R. Reinhard, F. Schuster, *Angew. Chem. Int. Ed. Engl.* **1977**, *16*, 715; c) R. Steudel, F. Schuster, *J. Mol. Struct.* **1978**, 143; d) R. Steudel, Steidel J, Pickard J, R. Reinhard, F. Schuster, *Z. Naturforsch.* **1980**, *B35*, 1378.
- [31]. W. A. Shantha Nandana, J. Passmore, P. S. White, C. -W. Wong, *Inorg. Chem.* **1989**, *28*, 3320.
- [32]. I. Crossing, *Chem. Eur. J.* **2001**, *7*, 490.
- [33]. S. M. Ivanova, B. G. Nolan, Y. Kobayashi, S. M. Miller, O. P. Anderson, S. H. Strauss, *Chem. Eur. J.* **2001**, *7*, 503.

Aqueous Sulfur Sols

Ralf Steudel

Institut für Chemie, Sekr. C2, Technische Universität Berlin, 10623 Berlin, Germany
E-mail: steudel@schwefel.chem.tu-berlin.de

Abstract Sulfur sols are colloidal solutions of elemental sulfur or of sulfur-rich compounds. The particles in these solutions have diameters of 0.1–1.0 μm and consist either of S_8 molecules (hydrophobic sulfur sols) or of chain-like sulfur compounds with hydrophilic end groups like sulfonate or functionalized organic groups (hydrophilic sulfur sols). Both types of sols are stabilized by the negative charge of the particles which results in mutual repulsion. Therefore, cations and especially multivalent cations are able to precipitate the sol particles. While hydrophilic sulfur sols can be prepared with sulfur concentrations of up to 600 g l^{-1} , hydrophobic sols are much more dilute ($<0.1 \text{ g l}^{-1}$). Sols of these types occur both in industrial desulfurization plants where sulfide is oxidized to elemental sulfur as well as in cultures of certain oxidizing sulfur bacteria.

Keywords Hydrophilic sulfur · Hydrophobic sol · Polythionates · Micelles · Colloidal solution · Stabilization · Precipitation · Coagulation

1	Introduction	153
2	Hydrophobic Sulfur Sols	154
3	Hydrophilic Sulfur Sols	156
3.1	General	156
3.2	Raffo Sols	157
3.3	Selmi Sols	161
4	Sulfur Sols by Oxidation of Hydrogen Sulfide	163
5	Sulfur Sols Produced by Bacteria	163
	References	164

1 Introduction

Emulsions of very small droplets of liquid sulfur or of sulfur-rich compounds (e.g., polythionates) in water are called “sulfur sols”. Such mixtures can be prepared by a variety of methods. *Hydrophobic sulfur sols* are obtained on dilution of saturated solutions of elemental sulfur in organic solvents like ethanol or acetone with a large excess of water. These preparations are usually called Weimarn sols honoring the principal author who first re-

ported this method [1]. *Hydrophilic sulfur sols* are obtained by decomposition of aqueous thiosulfate solutions with strong mineral acids (Raffo sols [2]) or by reaction of aqueous sulfite ions with sulfide ions at acidic pH values (Selmi sols [3]). Similar sols are obtained by hydrolysis of S_2Cl_2 with cold water. Collectively, the hydrophilic sulfur sols are sometimes termed Odén sols [4].

Weimarn sols are metastable but exist only at rather low sulfur concentrations ($<0.1 \text{ g l}^{-1}$) while stable Raffo sols with up to 600 g l^{-1} have been prepared. Thermodynamically, all sulfur sols are unstable with respect to transformation into orthorhombic sulfur S_8 which is water-insoluble and precipitates from the solution.

Sulfur sols play an important role in certain industrial desulfurization processes where elemental sulfur is formed [5]. This sulfur sometimes stays in the liquid state for several days creating separation and clogging problems. Furthermore, certain sulfur bacteria produce so-called “globules” of liquid sulfur or sulfur-rich compounds by oxidation of sulfide HS^- , thiosulfate $S_2O_3^{2-}$ or polythionate ions $S_nO_3^{2-}$ (see later). The characterization of these globules has considerably stimulated the interest in sulfur sols in recent years.

Historically, aqueous sulfur sols are related to the so-called “Wackenroder’s solution” which is obtained by reaction of H_2S with SO_2 in water at 0°C and which contains polythionic acids as well as elemental sulfur besides other sulfur compounds (e.g., sulfate). For a detailed early investigation and vivid description of this mixture, see ref. [6]; for more recent studies, see later. A compilation of 23 patents for the preparation of colloidal sulfur mixtures from the years 1931–1948 has been published by Meyer [7].

2 Hydrophobic Sulfur Sols

Weimarn sols can be obtained by dilution of an S_8 solution in a solvent which is indefinitely miscible with water [4, 8]. Most often ethanol or acetone is used to dissolve the sulfur and this mixture is then poured into a large excess of water (>35 times the volume of the S_8 solution). Since the solubility of S_8 in water at 25°C is only $5 \times 10^{-6} \text{ g l}^{-1}$ [9] the sulfur precipitates practically quantitatively, but not necessarily in the solid form. At sulfur concentrations of $<100 \text{ mg l}^{-1}$ the freshly prepared sol shows initially a bluish-white opalescence which after ca. 10 min changes to a reddish-violet hue. One hour after preparation the sol is of white, milk-like appearance. Under a microscope spherical particles with diameters of up to $0.8 \mu\text{m}$ can be recognized (magnification 1000 \times). Using polarizers the particles exhibit the typical Malteser cross pattern which is known from lamellar phases of amphiphilic substances [10]. In other words, the particles are composed of liquid rather than crystalline sulfur. Such a sol is metastable at 20°C for a few days but since liquid sulfur is thermodynamically unstable at 20°C , the sulfur eventually crystallizes and the small crystals of α - S_8 form aggregates of up to $50 \mu\text{m}$ diameter which settle to the bottom of the flask. This process

takes about 1 week to be completed and can be accelerated by centrifugation [4, 10].

To obtain a monodispersed sol it is necessary to add the water to the organic sulfur solution and not the other way round. The observed particle size, derived from higher order Tyndall spectra, ranges from 0.20 to 0.45 μm if the initial sulfur concentration in ethanol is between 0.25 and 2.9 mg l^{-1} [8].

The pH value of a freshly prepared Weimarn sol, obtained from ethanolic solutions of recrystallized S_8 and deionized and doubly distilled water, was 5.4 and this value remained practically constant when the sol was stored under nitrogen. However, in the presence of air the pH slowly decreased to 5.2 after 7 days and to 4.3 after 17 days. The most likely explanation is the following disproportionation reaction:



Since both H_2S and SO_2 are weak acids in water the drop in pH can be understood by the following reactions:



The driving force of the reaction at Eq. (1) comes from the thermodynamic instability of elemental sulfur in water. The Pourbaix diagram of the $\text{S}_8/\text{H}_2\text{O}$ system at 20 °C shows elemental sulfur to exist as a separate phase only at very low pH values and redox potentials in the range 0.1–0.3 V [11].

Electrophoretic measurements have demonstrated that the particles of Weimarn sols are negatively charged. This charge originates from the adsorption of anions. Therefore, the charge can be increased by adding OH^- ions to the aqueous phase [4]. The anions HS^- and HSO_3^- resulting from the reactions at Eqs. (2) and (3) will also be partly adsorbed by the liquid S_8 particles and in this way contribute to their negative charge.

As a consequence of the negative charge of the sol particles they can be precipitated by cations the efficiency of which increases in the order H_3O^+ , K^+ , Na^+ , $\text{Li}^+ < \text{Be}^{2+}$, Ca^{2+} , Zn^{2+} , Mg^{2+} , $\text{Ba}^{2+} < \text{Ce}^{3+}$. In the case of Ce^{3+} approximately 0.2 mmol l^{-1} are sufficient while 2–4 mmol l^{-1} are needed for the two-valent ions and 10–35 mmol l^{-1} for the univalent cations. The obtained precipitate dissolves in CS_2 but cannot be peptized in water [4]. If two types of cations are used their action works in the same direction: Less of the second cation is needed for precipitation if there is already another ion present [12].

The most interesting property of Weimarn sols is their stabilization by surfactants as well as by certain biopolymers. Most effective seems to be gelatine of which only 0.025 μg are needed to prevent the precipitation of 2 ml sol by aqueous NaCl (10%) within 5 min. The same result is obtained by 3 μg of saponin, by 5 μg each of egg albumin, gum arabic or sodium stearate, by 25 μg of dextrin, or by 500 μg of sodium cholate [13–15]. It can be assumed that the biopolymer molecules are adsorbed by their hydropho-

bic parts on the surface of the sulfur particles and that the hydrophilic parts face the aqueous phase. In this way the fusion of the sol particles is suppressed. This fusion process is to some extent a prerequisite for the crystallization and the following sedimentation.

In the case of surfactants it has been observed that sodium dodecylsulfate (SDS), Tergitol 7 [sodium 4-ethyl-1(3-ethylpentyl)octyl sulfate], and CTAB [hexadecyl(trimethyl)ammonium bromide] increase the solubility of S_8 in water dramatically, provided the critical concentration for micelle formation is exceeded. For instance, 50 g l^{-1} SDS enhance the solubility of S_8 at $20 \text{ }^\circ\text{C}$ from $5 \text{ } \mu\text{g l}^{-1}$ to 20 mg l^{-1} , i.e., by a factor of 4000. This enhanced solubility increases further with increasing temperature. It is believed that the surfactant molecules form micelles and that the S_8 molecules dissolve in the hydrophobic interior of these micelles in a similar fashion as in a liquid hydrocarbon solvent [16].

The stability of freshly prepared Weimarn sols towards crystallization and sedimentation can be increased by addition of surfactants at concentrations below the critical concentration for micelle formation [10]. At a molar ratio S_8 :surfactant of 1:1 the commercial surfactant Triton X-100 was most effective followed by CTAB and SDS. After storage for seven days, a Triton stabilized sol contained about twice as much sulfur as an unstabilized but otherwise identical Weimarn sol. The stabilizing effect of Triton X-100 can also be observed if the aqueous phase contains Ca^{2+} or Mg^{2+} ions at a concentration of $1\text{--}2 \text{ mmol l}^{-1}$ [10].

Hydrophobic sulfur sols can also be prepared by blowing sulfur vapor into cold water where it immediately condenses [17]. After filtration these sols are polydisperse, exhibit a strong Tyndall phenomenon, and can be kept for two to six weeks at $20 \text{ }^\circ\text{C}$ before the sulfur starts to settle to the bottom of the flask. The crystalline precipitate obtained in this way cannot be peptized in water but dissolves quantitatively in carbon disulfide. The sulfur content of the original but filtrated sol was between 0.01 and 0.08 mass %; the particles are negatively charged and move in an electrical field to the anode.

3 Hydrophilic Sulfur Sols

3.1 General

Elemental sulfur is an extremely hydrophobic material and the same holds for sulfur-rich compounds $\text{R-S}_n\text{-R}$ with hydrophobic organic terminal groups R like alkyl or aryl. However, strongly hydrophilic groups like $-\text{SO}_3^-$ are able to turn these hydrophobic substances into hydrophilic materials even at very high sulfur contents. Sulfane disulfonate anions $\text{S}_n(\text{SO}_3)_2^{2-}$, better known as polythionate anions, are such species which qualify for amphiphilic behavior in water. These ions exist as a long homologous series with n

ranging from 1 (trithionate) via 2 (tetrathionate) to probably more than 50 (polythionates) [18]. On the other hand, the free polythionic acids are unstable and subject to slow disproportionation on attempts to prepare them from their salts by ion exchange, for instance. Therefore, the structures of these species have not been determined experimentally but the lower members as well as their monoanions have been studied by ab initio MO calculations (for $n=2-4$) [19]. The structures of the corresponding dianions are known from the X-ray structural analyses of a number of salts [20].

Long-chain polythionate anions can be dispersed in water to form emulsions called hydrophilic sulfur sols [21]. Depending on how these anions are synthesized from small precursors two types of sols are known. Raffo sols result from the acid decomposition of sodium thiosulfate by concentrated sulfuric acid, while Selmi sols are obtained by comproportionation of sulfide and sulfite ions in acidic solution or by the reaction of H_2S with an excess of SO_2 in water, respectively. Bassett and Durrant [22] have been the first to recognize "Odén's colloidal sulfur" (hydrophilic sulfur sol) as the "soluble sodium salt of a sulfur-polythionate complex" although these authors believed that only *one* polythionate, namely hexathionate, was present which they thought to be "the highest polythionate capable of existence" at that time. More recent analyses using modern chromatographic techniques have shown that the sulfur is present as a number of different homocycles and a mixture of many different long-chain polythionate ions (or their sodium salts). The latter can be separated by ion-pair chromatography [23], while the sulfur rings may be analyzed and determined using reversed-phase HPLC [24, 25]. UV absorbance detectors are employed in both cases since all compounds containing bonds between two-valent sulfur atoms show a strong absorption near 230 nm. Linear calibration functions have been obtained for the concentration dependence of the UV absorption of polythionates and of sulfur homocycles allowing quantitative analyses.

3.2

Raffo Sols

So-called Raffo or LaMer sulfur sols are used most frequently. These can be prepared by dropwise addition of aqueous sodium thiosulfate to concentrated sulfuric acid followed by cooling and precipitation of the hydrophilic sol by a saturated solution of sodium chloride. The sol originates from the spontaneous decomposition of the primary product thiosulfuric acid ($H_2S_2O_3$) which disproportionates in a series of complex redox reactions producing elemental sulfur, hydrogen sulfide, sulfur dioxide and polythionic acids:



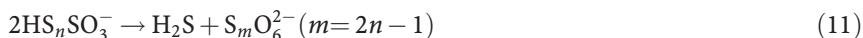
Sulfane monosulfonic acids $\text{H-S}_x\text{-SO}_3\text{H}$ are intermediates in the reaction at Eq. (5); see below. As indicated by Eq. (6) the elemental sulfur formed will be a mixture of homocycles S_x from S_6 via S_7 and the main product S_8 up to traces of larger rings.

To purify the sol the mixture is first separated by centrifugation and decantation from the mother liquor which is discarded. The solid sol is then peptized ("dissolved") in water and precipitated again by aqueous sodium chloride followed by filtration. This procedure is repeated ten times to obtain a sol free of sulfate ions, SO_2 , H_2S , and lower polythionates [22, 26]. After this procedure the average composition of the precipitated sol has been determined as $\text{Na}_{1.64}\text{S}_{28.6}\text{O}_{6.6}/n \text{ S}_n \cdot 1.0 \text{ NaCl}$ with the relative amounts of sulfur rings decreasing in the order $\text{S}_8 > \text{S}_7 > \text{S}_6 > \text{S}_{10} > \text{S}_{11} > \text{S}_{12} > \text{S}_{13} > \text{S}_{14}$ [26]. The missing cations will be present as H_3O^+ . In other words, the sol basically consists of sodium salts of higher polythionate anions which in water are expected to form micelles and maybe even vesicles. Earlier analyses of freshly prepared Raffo sols showed compositions like $\text{Na}_2\text{S}_{55}\text{O}_6$ but the analytical data for a number of different sols varied considerably and compositions with more than 100 sulfur atoms in the formula have been reported [21, 22].

The reaction mechanism for the formation of sulfur sols can be understood on the basis of the following sulfur-transfer reactions. While thiosulfate ions are stable in water at 20 °C, the protonated anion will be attacked by the more nucleophilic dianion resulting in a growth of the sulfur chain [27]:



This process continues until long-chain sulfane monosulfonate ions HS_nSO_3^- ($n > 5$) have been formed from which both sulfur homocycles S_n as well as higher polythionate ions can be generated:



The reactions at Eqs. (7)–(10) are reversible: At pH values above 7 elemental sulfur dissolves in aqueous sulfite solutions and thiosulfate is obtained [28] which is produced industrially in this manner.

In the concentration range of up to 15 g sulfur in 100 ml of the sol the density and the refraction index of Raffo sols increase first linearly (up to 10 g/100 ml) and at higher concentrations more or less linearly with the sulfur content [29, 30]. The density of the dissolved particles was calculated as 1.9–2.1 g cm⁻³ which is roughly identical to the density of liquid sulfur at 20 °C. The thermal expansion coefficient, the viscosity as well as the surface tension of Raffo sols have also been studied in detail [30].

After aging at 20 °C for some hours the aqueous phase of Raffo sols contains lower polythionate anions and the amount of elemental sulfur increases resulting eventually in the crystallization and precipitation of α -S₈ [26]; see Eq. (12):



Nucleophiles like alkali hydroxides, ammonia, H₂S, sulfide, and thiosulfate anions destroy the long-chain polythionates and the Raffo sol decomposes with precipitation of crystalline S₈ [14, 31]. Therefore, Raffo sols are metastable only at pH values below 7.

The particle diameters of some dilute Raffo sols have been determined as 0.1–0.5 μm [31, 32]. The densities of Raffo sols increase linearly with the sulfur content and reach a value of 1.24 g cm⁻³ at 16 °C for a sulfur content of 450 g l⁻¹ [30]. After evaporation of some of the water sulfur contents of up to 600 g l⁻¹ have been obtained! Such sols are of oily or honey-like viscosity [30]. More dilute sols are clear yellow liquids stable for several weeks and undecomposed even when heated to 100 °C, provided all salts have been carefully removed. No phase transition occurs on heating up to 150 °C [30] which indicates that the sulfur and the polythionates of the sol are in a liquid-like state.

It is believed that the long-chain polythionate ions of Raffo sols aggregate in water by self-organization in such a way that the hydrophobic sulfur chains stick together forming a core the structure of which must resemble the structure of liquid sulfur at higher temperatures [33]. These particles obviously are able to dissolve small sulfur homocycles to some extent. From the hydrophobic core the sulfonate groups will be sticking out making the particles hydrophilic at the outside; see Fig. 1. In other words, the sol particles are giant multivalent anions which will bind some cations and probably many water molecules on their surface. Their negative charge results in a certain stabilization due to the Coulomb repulsion between single particles.

This Coulomb repulsion can however be overcome by addition of multivalent cations which are attracted more efficiently than univalent ions and therefore stimulate further aggregation, fusion and precipitation. The cations then become part of the coagulated sol particles. The efficiency of the coagulation by various cations decreases in the order Nd³⁺ > Th⁴⁺ > Al³⁺ > Ba²⁺ > Sr²⁺ > Ca²⁺ > Mg²⁺ > Zn²⁺ [8, 31, 34]. In contrast to the precipitation by NaCl, LiCl, or HCl, the coagulation by multivalent cations is irreversible, and the univalent ions H⁺ and Li⁺ act antagonistically to the multivalent cations. This not only means that a higher concentration of multivalent cations is needed for precipitation if Li⁺ or H⁺ are present, but the precipitation by multivalent cations can even be reversed by the subsequent addition of H⁺ or Li⁺ [8, 12, 22]! The charge of the anions also affects the coagulation process: Compared to chloride ions, sulfate ions enhance the antagonistic action of univalent cations, evidently by increasing the negative particle charge [12, 35]. These observations also hold for Selmi sols (see below).

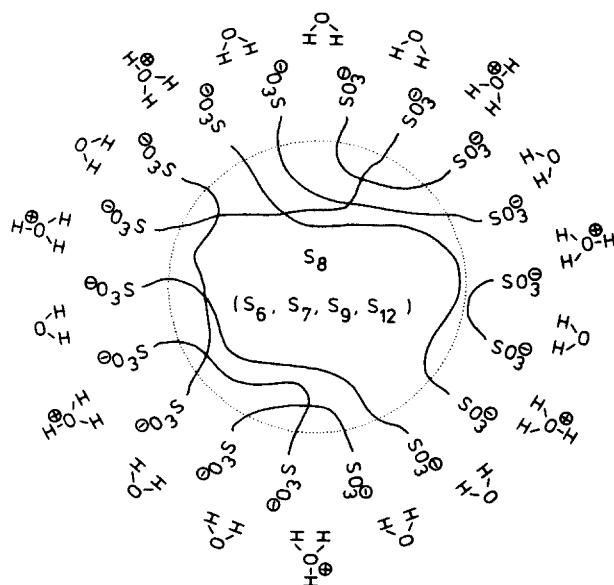


Fig. 1 Schematic model for the composition of the particles in hydrophilic sulfur sols consisting of long-chain polythionates $S_n(\text{SO}_3^-)_2$ and sulfur homocycles S_n

The average density of the sol particles has been determined both before and after precipitation. For the dissolved particles a value of 1.92 g cm^{-3} has been found at 16°C [30, 36] which is close to the density of liquid sulfur when extrapolated to 16°C [37]. A value of 1.9 g cm^{-3} was obtained for sol particles precipitated by K^+ or Ba^{2+} ions, while coagulation by Na^+ ions yields particles with densities of between 1.2 and 1.4 g cm^{-3} [36]. Evidently, the sodium salts of Raffa sol particles contain considerable amounts of H_2O molecules and therefore can be peptized in water while the more or less water-free potassium and barium salts do not re-dissolve in water.

The reversible coagulation of Raffa sols is strongly temperature dependent. The higher the temperature the more "soluble" the particles are. In other words, peptization is promoted by increasing temperatures, and since this dependence is exponential an increase in temperature T from 10°C to just 17°C may result in an increase in sulfur concentration c in the aqueous phase by a factor of 1000 (at a NaCl concentration of 0.101 mol l^{-1}) [14].

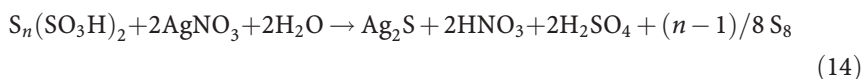
Odén has shown that Raffa sols can be separated into fractions of differing particle size by fractional precipitation with increasing concentrations of NaCl . As larger the particles as less NaCl is needed for precipitation [38]. Under special conditions monodispersed Raffa sols of particle size between 0.1 and $1.0 \mu\text{m}$ can be prepared directly from very dilute aqueous thiosulfate and sulfuric acid or hydrochloric acid without fractionation. These sols are characterized by higher order Tyndall spectra [39].

Several authors [12, 40] prepared Raffa sols free of cations other than H_3O^+ by removing the sodium ions by electro dialysis and studied the prop-

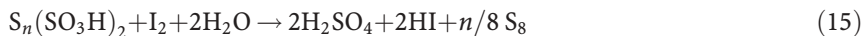
erties and composition of the resulting “acidoid” sols. Pauli et al. [40] performed electric conductivity measurements, titrations with NaOH, Ba(OH)₂, BaCl₂, AgNO₃, and HgNO₃, reactions with I₂ and NaOH as well as heating, freezing and coagulation of the sol with salts. All reported observations can be explained by the model described above, i.e., with particles consisting mainly of long-chain polythionic acids (as oxonium salts) with a certain amount of sulfur homocycles, but the original authors came to a totally different conclusions and proposed a model in which elemental sulfur is the main component and adsorbed thiosulfuric acid as well as traces of polythionic acids were assumed to make these particles hydrophilic. The acidoid sol may be titrated with NaOH or Ba(OH)₂ like a normal mineral acid, the endpoint can be observed conductometrically. Addition of BaCl₂ sets the hydrogen ions free (by ion exchange) which then can be titrated acidimetrically with NaOH:



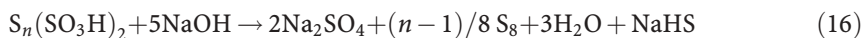
The reaction with AgNO₃ (or HgNO₃) is slow and proceeds according to Eq. (14):



The freshly prepared sol did not react with iodine which indicates that no -SH groups and therefore no sulfane monosulfonic acids HS_nSO₃H are present. However, the following reaction takes place slowly:



In the reactions at Eqs. (14) and (15) the S–SO₃ bonds are hydrolytically cleaved because these are the longest and obviously weakest SS bonds in polythionate anions [41]. Sodium hydroxide destroys polythionic acids in a similar reaction:



Pauli et al. studied all of these reactions quantitatively but interpreted the results erroneously in terms of the presence of H₂S₂O₃ [40]. They also observed that the conductivity of the acidoid sol increased with aging which can be understood in terms of the reaction at Eq. (6) in which lower polythionate anions are formed which are soluble in water in contrast to the very long-chain anions in the sol particles. Coagulation by electrolytes was most efficient with AgNO₃ and La(NO₃)₃ followed by BaCl₂.

3.3

Selmi Sols

Selmi sols are obtained either by reaction of gaseous H₂S with aqueous SO₂ [4] or by reaction of aqueous Na₂S with aqueous Na₂SO₃, if both solutions

have previously been acidified with sulfuric acid [42]. In the first case, H₂S is slowly bubbled into a concentrated cold solution of SO₂ in water until no SO₂ can be detected any longer in the headspace [4, 43]. The reactions taking place are not completely understood [44] but polythionates and elemental sulfur are formed in a series of redox reactions, e.g.:



Other lower oxoacids of sulfur including sulfane monosulfonic acids must be intermediates which then undergo reactions according to Eqs. (7)–(12). The freshly prepared sol is purified by precipitation with saturated aqueous NaCl, isolated by centrifugation, peptized in water and precipitated again. This procedure is repeated several times until no sulfate ions can be detected in the aqueous phase any longer.

Selmi sols are yellow and clear at low concentrations but turbid at higher concentrations. They have properties very similar to those of Raffo sols and sometimes these two types of hydrophilic sulfur sols are summarized as Odén sols [4]. Sols prepared by hydrolysis of S₂Cl₂ also resemble Raffo sols since the hydrolysis in cold water produces H₂S, SO₂, HCl and polythionic acids in the first place [4].

The particles of Selmi sols prepared by the method of Janek [42] have been investigated by infrared and Raman spectroscopy as well as by ion-pair chromatography. They consist of polythionates S_mO₆²⁻ with *m*=4–16 as well as of sulfur homocycles S_{*n*} (*n*=6–10), but depending on the method of preparation and purification a certain amount of salts (Na₂SO₄, NaCl) will be present in addition. The sulfur atoms in the zero oxidation state are distributed between elemental sulfur and polythionates in an approximate ratio of 2:1 [45].

Sols obtained from H₂S and aqueous SO₂ and purified by repeated precipitation with saturated aqueous NaCl are polydispersed and metastable at 20 °C for a long time but are decomposed by NaOH, NH₃, or H₂S. They consist of negatively charged particles of ca. 0.2 μm diameter which can be precipitated by cations. Most effective in this respect are the chlorides of Ce³⁺, Al³⁺, Sm³⁺, and Th⁴⁺ followed by Ba²⁺, Sr²⁺, and Ca²⁺ [4, 31]. If H₃O⁺, Li⁺, or Na⁺ ions are present higher concentrations of the precipitating agents are necessary. For this antagonistic effects of these and other cations, see [46] and also the analogous behavior of Raffo sols above.

Odén has shown that Selmi sols can be separated into fractions of differing particle size by fractional precipitation with increasing concentrations of NaCl. The larger the particles the less NaCl is needed for precipitation [38].

Selmi sols are metastable for many weeks [4], but on aging the sol slowly decomposes to elemental sulfur (which precipitates as S₈ crystals) and lower polythionates (which remain dissolved in water) in a similar fashion as Raffo sols do, but it should be pointed out that the relative content of elemental sulfur in Selmi sols is higher from the beginning compared to Raffo sols [4].

Verstraete [31] prepared Selmi sols free of cations other than H_3O^+ by removing the sodium ions by electro dialysis and studied the properties and composition of the “acidoid” or “ash-free” sols. Conventional dialysis also yields sols free of an evaporation residue and of chloride [47].

4

Sulfur Sols by Oxidation of Hydrogen Sulfide

Autoxidation of aqueous H_2S solutions results in elemental sulfur, sulfite, thiosulfate, and eventually sulfate. However, under certain conditions monodispersed sulfur sols with particle diameters of between 0.2 and 1.2 μm are obtained [48]. For example, a solution of H_2S of concentration 46 mmol l^{-1} in pure H_2O exposed to air at 25 °C became turbid after an induction period of ca. 8 h and then showed brilliant higher-order Tyndall spectra. A solution saturated in H_2S exhibited a pH value of 4.1 and was rapidly oxidized in an atmosphere of pure O_2 . At pH values >8 no elemental sulfur was formed (clear colorless solution), in the range $\text{pH}=7\text{--}8$ yellow solutions were obtained (polysulfide anions), while at $\text{pH}<7$ turbid solutions were produced but the induction period was as longer as lower the pH value [48]:



At pH values around 6 the formation of sulfur was most rapid. Several metal salts like AlCl_3 , $\text{Fe}(\text{NH}_4)_2(\text{SO}_4)_2$ and $\text{K}_4[\text{Fe}(\text{CN})_6]$ decreased the induction period considerably while KCl , K_2SO_4 , and MgCl_2 had no effect. The growth of the sulfur particles was found to be diffusion controlled but the molecular nature of the particles was not investigated [48].

5

Sulfur Sols Produced by Bacteria

Numerous so-called sulfur bacteria produce sulfur sols which are similar in their chemical and physical properties to the above described Weimarn, Raffo, or Selmi sols. Such bacteria live in all wet environments from soils, ponds, creeks, rivers, and lakes to seashores [49]. The oxidizing sulfur bacteria oxidize reduced sulfur compounds like sulfide ions either by molecular oxygen or, using sunlight as an energy source, by carbon dioxide to the level of S^0 , i.e., sulfur in the zero oxidation state:



This sulfur is excreted as a globule, i.e., a tiny droplet of spherical or ellipsoidal shape of up to 1 μm in diameter and consisting of a non-crystalline sulfur-rich material [50]. Depending on the organism the globules are produced either inside or outside the bacterial cells, and different organism produce sulfur globules of differing molecular composition [49, 51, 52]. Except from sulfide ions the sulfur globules can also be produced from other re-

duced compounds like thiosulfate and tetrathionate, probably via the following reactions:



In cultures of sulfur bacteria the reactions at Eqs. (20)–(22) are catalyzed by appropriate enzymes. The sulfane monosulfonate formed in the reaction at Eq. (22) is unstable and decomposes to polythionate anions and elemental sulfur which are the components of Raffo and Selmi sols as shown above; see Eqs. (10) and (11). These reactions take place, for example, if cultures of *Acidithiobacillus ferrooxidans* (formerly *Thiobacillus ferrooxidans*) are “incubated” (mixed) with tetra- or pentathionate at 30 °C in air. After some time all polythionate anions with up to 17 sulfur atoms could be detected by ion-pair chromatography in the filtrated aqueous phase while the sulfur globules excreted extracellularly were isolated and extracted by CS₂. According to a HPLC analysis this extract contained S₈ and small amounts of the homocycles S₆, S₇, and S₁₂ [53].

Other types of sulfur bacteria produce globules which seem to consist of organic polysulfanes R-S_n-R although the chain-terminating groups have not been identified yet [54, 55].

Many times it has been observed that sulfur bacteria enter chemical plants in which sulfur compounds are treated. Sulfate reducing bacteria (SRB) produce sulfide ions which may then be used by oxidizing bacteria like thiobacilli to generate sulfur sols consisting of polythionates. In this way, serious disturbances of the production conditions may occur. This holds in particular for desulfurization plants of the Stretford and Sulfolin type in which hydrogen sulfide is oxidized to elemental sulfur which is supposed to crystallize rapidly to be separated by flotation [5].

Mixed cultures of sulfur bacteria are used industrially for the desulfurization of wastewater and waste gases by biological conversion to elemental sulfur which has colloidal properties [56, 57].

References

1. P. P. von Weimarn, B. W. Malyschew, *Kolloid-Z* **1911**, 8, 216; P. P. von Weimarn, *Kolloidchem. Beihefte* **1926**, 22, 38.
2. M. Raffo, *Kolloid-Z.* **1908**, 2, 358.
3. F. Selmi, *J. Prakt. Chem.* **1852**, 57, 49 and references cited therein.
4. H. Freundlich, P. Scholz, *Kolloidchem. Beihefte* **1922**, 16, 234.
5. R. Steudel, *Ind. Eng. Chem. Res.* **1996**, 35, 1417.
6. H. Debus, *J. Chem. Soc.* **1888**, 53, 278. The “new allotropic d-sulfur” proposed in this publication is in reality a mixture of long-chain polythionic acids (see the Section 3.3: Selmi Sols).
7. B. Meyer, *Sulfur, Energy, and Environment*, Elsevier, Amsterdam, **1977**, p. 63.
8. V. K. LaMer, R. H. Dinegar, *J. Am. Chem. Soc.* **1950**, 72, 4847.
9. J. Boulege, *Phosphorus Sulfur* **1978**, 5, 127; see also ref. [8].

10. R. Steudel, A. Albertsen, in *Biochemical Principles and Mechanisms of Biosynthesis and Biodegradation of Polymers*. (A. Steinbüchel, ed.), Wiley-VCH, Weinheim, 1999, p. 17.
11. R. M. Garrels, C. R. Naeser, *Geochim. Cosmochim. Acta* 1958, 15, 113.
12. H. Freundlich, P. Scholz, *Kolloidchem. Beihefte* 1922, 16, 267.
13. J. Traube, E. Rackwitz, *Kolloid-Z.* 1925, 37, 131.
14. H. Freundlich, *Kapillarchemie*, Vol. II, 4th ed. Akademische Verlagsgesellschaft, Leipzig, 1932, p. 382.
15. H.-D. Dörfler, *Grenzflächen- und Kolloidchemie*, VCH, Weinheim, 1994, p. 339.
16. R. Steudel, G. Holdt, *Angew. Chem.* 1988, 100, 1409; *Angew. Chem. Int. Ed. Engl.* 1988, 27, 1358.
17. A. Gutbier, *Z. Anorg. Allg. Chem.* 1926, 152, 163.
18. E. Weitz, K. Spohn, *Chem. Ber.* 1956, 89, 2332; E. Weitz, F. Becker, *Chem. Ber.* 1956, 89, 2345; E. Weitz, F. Becker, K. Gieles, B. Alt, *Chem. Ber.* 1956, 89, 2353.
19. A. H. Otto, R. Steudel, *Eur. J. Inorg. Chem.* 2001, 3047.
20. A. F. Wells, *Structural Inorganic Chemistry*, 5th ed., Clarendon Press, Oxford, 1984, p. 732.
21. E. Weitz, K. Gieles, J. Singer, B. Alt, *Chem. Ber.* 1956, 89, 2365.
22. H. Bassettt, R. G. Durrant, *J. Chem. Soc.* 1931, 2919.
23. R. Steudel, G. Holdt, *J. Chromatogr.* 1986, 361, 379.
24. R. Steudel, H.-J. Mäusle, D. Rosenbauer, H. Möckel, T. Freyholdt, *Angew. Chem.* 1981, 93, 402; *Angew. Chem. Int. Ed. Engl.* 1981, 20, 394.
25. R. Steudel, R. Strauss, *Fresenius Z. Anal. Chem.* 1987, 326, 543.
26. R. Steudel, T. Göbel, G. Holdt, *Z. Naturforsch. Part B* 1988, 43, 203.
27. R. Steudel, A. Prenzel, *Z. Naturforsch. Part B* 1989, 44, 1499.
28. R. H. Dinigar, R. H. Smellie, *J. Colloid. Sci.* 1952, 7, 370. The quantitative data in this publication are out of date since too simple a model for the molecular composition of Raffo sols has been used.
29. J. Lifschitz, J. Brandt, *Kolloid-Z* 1918, 22, 133.
30. S. Odén, *Z. Phys. Chem.* 1912, 80, 709.
31. E. O. K. Verstraete, *Kolloid-Z.* 1943, 102, 251 and 1943, 103, 25.
32. M. Kerker, E. Daby, G. L. Cohen, J. P. Kratochvil, E. Matijevic, *J. Phys. Chem.* 1963, 67, 2105.
33. See the Chapter on Liquid Sulfur by R. Steudel in this Volume.
34. H. B. Weiser, G. R. Gray, *J. Phys. Chem.* 1935, 39, 1163.
35. W. Dorfman, D. Scerbacewa, *Kolloid-Z.* 1930, 52, 289.
36. T. R. Bolam, A. K. M. Trivedi, *Trans. Faraday Soc.* 1942, 38, 140.
37. S. Rosental, *Z. Phys.* 1930, 66, 652.
38. S. Odén, *Z. Phys. Chem.* 1912, 78, 682.
39. V. K. LaMer, M. D. Barnes, *J. Colloid Sci.* 1946, 1, 71; I. Johnson, V. K. LaMer, *J. Am. Chem. Soc.* 1947, 69, 1184; E. M. Zaiser, V. K. LaMer, *J. Colloid Sci.* 1948, 3, 571.
40. W. Pauli, E. Russer, P. Balog, *Helv. Chim. Acta* 1944, 27, 585.
41. R. Steudel, *Angew. Chem.* 1975, 87, 683; *Angew. Chem. Int. Ed. Engl.* 1975, 14, 655.
42. A. Janek, *Kolloid-Z.* 1933, 64, 31.
43. S. Odén, *Der Kolloide Schwefel*, Akademische Buchdruckerei, Upsala 1913.
44. E. Blasius, R. Krämer, *J. Chromatogr.* 1965, 20, 367; E. Blasius, W. Burmeister, *Z. Anal. Chem.* 1959, 168, 1; E. Blasius, H. Thiele, *Z. Anal. Chem.* 1963, 197, 347; P. W. Schenk, W. Kretschmer, *Angew. Chem.* 1962, 74, 695; P. W. Schenk, R. Steudel, *Angew. Chem.* 1965, 77, 437; *Angew. Chem. Int. Ed. Engl.* 1965, 4, 402.
45. R. Steudel, T. Göbel, G. Holdt, *Z. Naturforsch. Part B* 1989, 44, 526.
46. W. A. Dorfman, *Kolloid-Z.* 1928, 46, 186, 198.
47. H. B. Weiser, G. E. Cunningham, *J. Phys. Chem.* 1929, 33, 301.
48. G. Chiu, E. J. Meehan, *J. Colloid. Interface Sci.* 1977, 62, 1.
49. C. Dahl, A. Prange, R. Steudel, Chapter 2 in *Biopolymers*, Vol. 9. (A. Steinbüchel, S. Matsumura, eds.), Wiley-VCH, Weinheim, 2002, p. 35.

50. R. Steudel, in *Biology of Autotrophic Bacteria* (H. G. Schlegel, B. Bowien, eds.), Chapter 16, Sci. Tech. Publ. Madison (USA), 1988, p. 289.
51. I. J. Pickering, G. N. George, E. Y. Yu, D. C. Brune, C. Tuschak, J. Overmann, J. T. Beatty, R. C. Prince, *Biochemistry* 2001, 40, 8138.
52. A. Prange, R. Chauvistré, H. Modrow, J. Hormes, H. G. Trüper, C. Dahl, *Microbiology* 2002, 148, 267.
53. R. Steudel, G. Holdt, T. Göbel, W. Hazeu, *Angew. Chem.* 1987, 99, 143; *Angew. Chem. Int. Ed. Engl.* 1987, 26, 151.
54. A. Prange, I. Arzberger, C. Engemann, H. Modrow, O. Schumann, H. G. Trüper, R. Steudel, C. Dahl, J. Hormes, *Biochim. Biophys. Acta* 1999, 1428, 446; A. Prange, R. Chauvistré, H. Modrow, J. Hormes, H. G. Trüper, C. Dahl, *Microbiology* 2002, 148, 167.
55. I. J. Pickering, G. N. George, E. Y. Yu, D. C. Brune, C. Tuschak, J. Overmann, J. T. Beatty, R. C. Prince, *Biochemistry* 2001, 40, 8138.
56. J. G. Kuenen, L. A. Robertson, *Biodegradation* 1992, 3, 239.
57. See the Chapter on Biologically Produced Sulfur by A. Janssen et al. in this Volume. A. J. H. Janssen, A. de Keizer, G. Lettinga, *Colloids and Surfaces A: Physicochemical and Engineering Aspects* 1999, 151, 389; A. Janssen, A. de Keizer, A. van Aelst, R. Fokking, H. Yangling, G. Lettinga, *Colloids and Surfaces B: Biointerfaces* 1996, 6, 115. A. J. H. Janssen, A. de Keizer, G. Lettinga, *Colloids and Surfaces B: Biointerfaces* 1994, 3, 111.

Biologically Produced Sulfur

Wilfred E. Kleinjan¹ · Arie de Keizer¹ · Albert J. H. Janssen²

¹ Laboratory of Physical Chemistry and Colloid Science, Wageningen University,
P.O. Box 8083, 6700 EK Wageningen, The Netherlands

E-mail: wilfred.kleinjan@wur.nl

E-mail: arie.dekeizer@wur.nl

² Shell Global Solutions International B.V., P.O. Box 38 000, 1030 BN Amsterdam,
The Netherlands

E-mail: a.janssen@paques.nl

Abstract Sulfur compound oxidizing bacteria produce sulfur as an intermediate in the oxidation of hydrogen sulfide to sulfate. Sulfur produced by these microorganisms can be stored in sulfur globules, located either inside or outside the cell. Excreted sulfur globules are colloidal particles which are stabilized against aggregation by electrostatic repulsion or steric stabilization. The formed elemental sulfur has some distinctly different properties as compared to “normal” inorganic sulfur. The density of the particles is for instance lower than the density of orthorhombic sulfur, and the biologically produced sulfur particles have hydrophilic properties whereas orthorhombic sulfur is known to be hydrophobic. The nature of the sulfur and the surface properties of the globules are however not the same for sulfur produced by different bacteria. The globules produced by phototrophic bacteria appear to consist of long sulfur chains terminated with organic groups, whereas chemotrophic bacteria produce globules consisting of sulfur rings (S₈). Adsorbed organic polymers such as proteins cause the hydrophilic properties of sulfur produced by a mixed culture of *Thiobacilli*. The hydrophilicity of extracellularly stored sulfur globules produced by *Acidithiobacillus ferrooxidans* can probably be explained by the vesicle structure consisting mainly of polythionates (⁻O₃S-S_n-SO₃⁻). Sulfur compound oxidizing bacteria, especially *Thiobacilli*, can be applied in biotechnological sulfide oxidation installations for the removal of hydrogen sulfide from gas streams and the subsequent oxidation of sulfide to sulfur. Due to the small particle size and hydrophilic surface, biologically produced sulfur has advantages over sulfur flower in bioleaching and fertilizer applications.

Keywords Sulfur bacteria · Colloidal stability · Sulfur globules · Hydrogen sulfide · Biotechnology

1	Introduction	168
1.1	Biological Sulfur Cycle.	168
1.2	Sulfur Compound Oxidizing Bacteria	169
2	Colloidal Stability of Sulfur Particles	172
3	Properties of Biologically Produced Sulfur	174
3.1	Intracellularly Stored Sulfur	175
3.2	Extracellularly Stored Sulfur	177
3.3	Formation of Biologically Produced Sulfur	179

4	Sulfur Compound Oxidizing Bacteria in Industrial Applications.	181
4.1	Removal of Hydrogen Sulfide From Gas Streams.	181
4.2	Biotechnological Removal of Hydrogen Sulfide from Gas Streams	182
5	Applications of Biologically Produced Sulfur.	184
6	Conclusions	185
	References	186

List of Abbreviations

Ac.	<i>Acidithiobacillus</i>
Al.	<i>Allochromatium</i>
B.	<i>Beggiatoa</i>
HPLC	High pressure liquid chromatography
SB	Sulfur compound oxidizing bacteria
SRB	Sulfate reducing bacteria
XANES	X-ray absorption near-edge spectroscopy
XRD	X-ray diffraction

1

Introduction

1.1

Biological Sulfur Cycle

Biologically produced sulfur (often termed biosulfur, elemental sulfur, or S^0) is a form of sulfur of oxidation state zero that is produced by microorganisms. At the end of the nineteenth century, first reports on the formation and the identification of sulfur globules were published with *Beggiatoa* bacteria fed with a solution containing hydrogen sulfide [1]. Since then, a large variety of bacteria that are capable of sulfur formation have been reported [2–4]. The sulfur formed by these bacteria is an intermediate in the oxidation of sulfide or thiosulfate to sulfate and the bacteria are sulfur compound oxidizing bacteria, often called sulfur bacteria (SB). In Fig. 1 the role of these sulfur compound oxidizing bacteria in the biological sulfur cycle is pointed out.

The biological sulfur cycle consists of a continuous oxidation and reduction of sulfur compounds by microorganisms or plants. On the left hand side of the cycle in Fig. 1 the most reduced sulfur compound is shown (sulfide) and on the right hand side the most oxidized form of sulfur (sulfate).

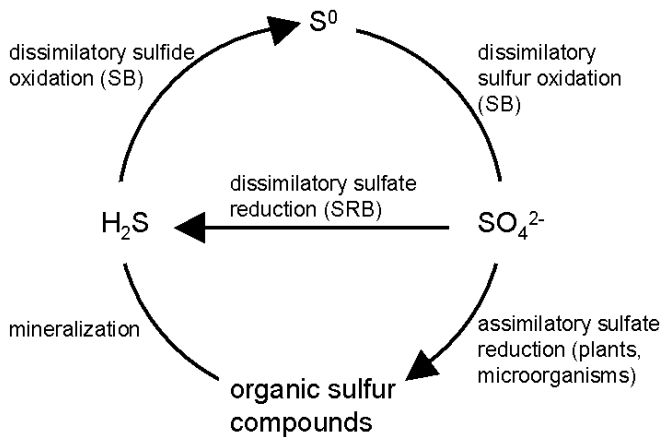


Fig. 1 The biological sulfur cycle. SB: sulfur compound oxidizing bacteria; SRB: sulfate reducing bacteria

Sulfur compound oxidizing bacteria cover the oxidation of sulfide to sulfate with reduced sulfur compounds such as sulfur, thiosulfate, and tetrathionate as intermediates. It should be noted that there is a large variety in sulfur compound oxidizing bacteria of which some species are only capable of covering a specific step in the oxidation of sulfide to sulfate (e.g., oxidation of thiosulfate to sulfate). Also the pathways in which the oxidation takes place may vary so that not always the same intermediates are formed. The reduction of sulfate back to sulfide takes place in two ways. In the first way, sulfate reducing bacteria (SRB) reduce sulfate via dissimilatory reduction (inorganic compounds reduced to other inorganic compounds). Second, inorganic sulfur compounds can be incorporated into organic substrates, such as proteins, by plants or other microorganisms (assimilatory reduction). Sulfide is then formed by mineralization of the organic matter.

In natural ecosystems the sulfur cycle should be in balance, meaning that the amount of sulfide that is oxidized should correspond to the amount of sulfate that is reduced. Such a balance can be found in a 'sulfuretum'. This is a syntrophical community of bacteria in which H_2S produced by sulfate reducing bacteria is reoxidized by the sulfur compound oxidizing bacteria.

1.2

Sulfur Compound Oxidizing Bacteria

Sulfur compound oxidizing bacteria were often called 'sulfur bacteria', which was used to indicate autolithotrophic (using inorganic compounds to obtain carbon and hydrogen) sulfur compound oxidizing bacteria. These sulfur bacteria consisted of phototrophic (purple and green) and chemotrophic (colorless) bacteria. A number of sulfur bacteria were however found to be able to grow organoheterotrophically (using organic compounds as car-

Table 1 Properties of some sulfur compound oxidizing bacteria

Organism	Energy	Carbon source	Sulfur globules	pH of growth	Ref.
Chlorobiaceae β -Proteobacteria	Phototrophic	Autotrophic	Extracellular		[3]
Thiobacillus thioparus	Chemotrophic	Autotrophic	Extracellular	6–8	[5]
Thiobacillus denitrificans	Chemotrophic	Autotrophic	Extracellular	6–8	[5]
Thiobacillus sp. W5 γ -Proteobacteria	Chemotrophic	Autotrophic	Extracellular	7–9	[6]
Allochromatium vinosum ^a	Phototrophic	Mixotrophic	Intracellular	7.5	[3, 7]
Halorhodospira abdelmalekii ^b	Phototrophic	Mixotrophic	Extracellular	8.4	[3, 8]
Beggiatoa alba	Chemotrophic	Mixotrophic	Intracellular		[4, 9]
Acidithiobacillus thiooxidans ^c	Chemotrophic	Autotrophic	Extracellular	2–5	[5]
Acidithiobacillus ferrooxidans ^c	Chemotrophic	Mixotrophic	Extracellular	2–6	[5]
Thioalkalivibrio denitrificans	Chemotrophic	Autotrophic	Extracellular	7.5–10.5	[10]
Thioalkalimicrobium cyclicum	Chemotrophic	Autotrophic	Extracellular	7.5–10.5	[10]
Xanthomonas Cyanobacteria	Chemotrophic	Heterotrophic		7	[11]
Oscillatoria limnetica	Phototrophic	Autotrophic	Extracellular	6.8	[12]

^a *Allochromatium vinosum* was formerly known as *Chromatium vinosum* [13]

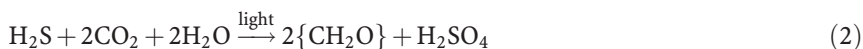
^b *Halorhodospira abdelmalekii* was formerly known as *Ectothiorhodospira abdelmalekii* [14]

bon and hydrogen source) and other bacteria than the sulfur bacteria were found to be able to grow autotrophically. The term ‘sulfur bacteria’ is therefore not used, but sulfur compound oxidizing bacteria is used instead.

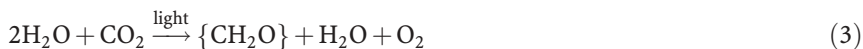
There is a wide variety of sulfur compound oxidizing bacteria consisting of different groups and genera. Each of the bacteria has its own specific properties, such as the source for energy, carbon or hydrogen, the sulfide oxidizing pathway, the size and shape of the bacteria and location of storing intermediate sulfur. In Table 1 a number of sulfur compound oxidizing bacteria are listed with some of their distinctive properties. Classification of sulfur compound oxidizing bacteria is however not straightforward. Different bacteria of the same bacterial family can have different properties. Each family consists of a wide variety of genera and strains, which can differ substantially in sulfur-oxidizing capacities or other properties. Therefore, the

data in Table 1 should be seen only as a list of properties of some sulfur compound oxidizing bacteria.

Most important in the classification of sulfur bacteria is the distinction between phototrophic and chemotrophic sulfur bacteria. Phototrophic (purple or green) bacteria use light as energy source to reduce CO_2 to carbohydrates. Reduced sulfur compounds are used as an electron donor for this reduction, which takes place under anaerobic conditions. The oxidation reactions of sulfide to sulfur and sulfate by phototrophic bacteria are called the Van Niel reactions:



The first Van Niel reaction Eq. (1) has a strong parallel with the photosynthesis in plants [3]:



In fact, cyanobacteria are capable of both ways of photosynthesis, which is why it was found difficult to place them in the group of plants (prokaryotes) or bacteria (eukaryotes) [12].

The chemotrophic (colorless) sulfur bacteria obtain energy from the chemical aerobic oxidation of reduced sulfur compounds. The overall reactions occurring, concerning the biological oxidation of sulfide, are the formation of sulfur (at low oxygen concentrations) and the formation of sulfate (when there is an excess of oxygen):



Apart from the above sulfide oxidation reactions, other sulfur compounds, such as sulfur and thiosulfate, can be oxidized by sulfur compound oxidizers. Furthermore, nitrate can be used as oxidant instead of oxygen. In Table 2 a list is shown of some other sulfur compound oxidation reactions occurring in chemotrophic sulfur compound oxidizing bacteria. It should be

Table 2 Overall reactions occurring in sulfur compound oxidizing bacteria (after [5])

Overall reactions	
$\text{S}^0 + 3/2\text{O}_2 + \text{H}_2\text{O} \rightarrow \text{H}_2\text{SO}_4$	(6)
$\text{S}_2\text{O}_3^{2-} + 2\text{O}_2 + \text{H}_2\text{O} \rightarrow \text{H}_2\text{SO}_4 + \text{SO}_4^{2-}$	(7)
$\text{S}_2\text{O}_3^{2-} + 1/4\text{O}_2 + 1/2\text{H}_2\text{O} \rightarrow 1/2\text{S}_4\text{O}_6^{2-} + \text{OH}^-$	(8)
$2\text{S}_4\text{O}_6^{2-} + 7\text{O}_2 + 6\text{H}_2\text{O} \rightarrow 6\text{H}_2\text{SO}_4 + 2\text{SO}_4^{2-}$	(9)
$5\text{H}_2\text{S} + 2\text{HNO}_3 \rightarrow 5\text{S}^0 + \text{N}_2 + 6\text{H}_2\text{O}$	(10)
$5\text{H}_2\text{S} + 8\text{HNO}_3 \rightarrow 5\text{H}_2\text{SO}_4 + 4\text{N}_2 + 4\text{H}_2\text{O}$	(11)

noted that not all sulfur compound oxidizing bacteria are capable of all the reactions listed in this table.

With respect to the carbon source, the sulfur compound oxidizing bacteria can be classified as heterotrophs, autotrophs, or mixotrophs. Autotrophic bacteria use CO_2 as the major carbon source for production of organic molecules. Heterotrophic bacteria use organic material as carbon source. Obligate autotrophs strictly need CO_2 as carbon source and facultative autotrophs (or mixotrophs) can also grow heterotrophically. Heterotrophic sulfur compound oxidizing microorganisms need a nutrient feed containing organic substrates (e.g., meat or yeast extracts [11]). Sulfur compound oxidizing bacteria can also be classified according to the nature of the hydrogen source. Lithotrophic bacteria use inorganic substrates (e.g., NH_3 , H_2S) as a source for hydrogen atoms. Organotrophic bacteria obtain hydrogen from organic molecules. In most organisms lithotrophy is linked to autotrophy, which means that for instance obligate autotrophic *Thiobacillus* bacteria are also called chemolithotrophic.

Elemental sulfur is often observed as an intermediate product in the oxidation of sulfide to sulfate in sulfur compound oxidizing bacteria. It can be present in considerable concentrations but will eventually be further oxidized to sulfate. The elemental sulfur is stored in sulfur globules, which some bacteria deposit inside the cell membrane and others outside the cell membrane. Later in this chapter the properties of these sulfur globules are discussed.

The optimum pH of growth of the bacteria differs per species. Neutral and acidiphilic sulfur compound oxidizing bacteria have been long known, mostly isolated from marine or freshwater sediments (e.g., [2, 5]). From highly alkaline salt lakes a number of alkaliphilic sulfur compound oxidizing bacteria have been isolated, both phototrophic [8] and chemotrophic [10, 16]. The technological relevance of alkaliphilic sulfur compound oxidizers is discussed later in this chapter.

2 Colloidal Stability of Sulfur Particles

Sulfur particles formed by sulfur compound oxidizing bacteria have particle sizes that fall in the range of the colloidal domain (approximately up to $1.0\ \mu\text{m}$). The internally stored sulfur particles produced by four different chemotrophic *Beggiatoas* as well as by a phototrophic *Allochromatium* bacterium have a particle diameter around 250 nm (both observed with electron microscopy) [17, 18] but the diameter of internally stored sulfur globules can reach up to $1\ \mu\text{m}$. Extracellularly stored sulfur globules produced by *Thiobacillus* bacteria in a sulfide-oxidizing reactor initially have approximately the same diameter (observed with electron microscopy and size distribution measured with Single Particle Optical Sizing) [19].

The balance between attractive and repulsive forces governs stability of colloidal sulfur particles. The most important forces are the van der Waals attraction and electrostatic repulsion, on which the DLVO-theory of colloidal

stability is based. The attractive van der Waals force depends on the size of and the distance between two bodies. The repulsive electrostatic force originates from the surface charge of the colloidal particles. Apart from this, structural forces (e.g., hydrogen bonding) can stabilize or destabilize colloidal particles depending on the nature of the particles, and adsorption of polymer material at the sulfur-solvent interface can cause steric stabilization.

The origin of charge can be the presence of surface functional groups, such as carboxylic acid or amino groups. Surfaces on which proteins are adsorbed show a dependency of the surface charge on the pH value due to the presence of carboxylic acid and amino groups. At high pH a protein-covered surface will be negatively charged ($-\text{COO}^-$ and $-\text{NH}_2$ groups) and at low pH the surface will show an overall positive charge ($-\text{COOH}$ and $-\text{NH}_3^+$ groups). The pH at which the overall surface charge is zero is called the point of zero charge. In the absence of specific adsorption it coincides with the iso-electric point.

This surface charge attracts oppositely charged ions to the surface and equally charged ions are repelled from the surface. This results in an ion concentration profile as is represented in Fig. 2, which is called the diffuse electric double layer. Presence of salt causes a screening of the electric double layer.

The repulsive and attractive energies of two interfaces can be calculated as a function of their distance (Fig. 3). When salt is added to a colloidal solution the electrostatic repulsion can be screened, resulting in a destabilization of the colloids.

Long chain polymers, such as proteins, can often adsorb to the surface of colloidal particles (because they gain adsorption energy), which can have a significant influence on colloidal stability. Adsorption of polymeric material at an interface takes place in such a way that the chains can extend from the

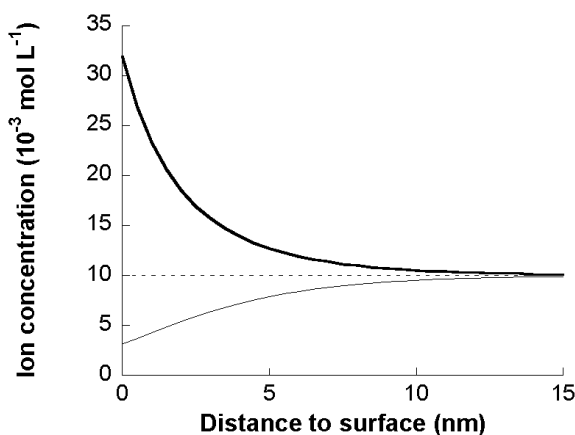


Fig. 2 Concentration profile of positive (*thick line*) and negative (*thin line*) ions in a diffuse electrical double layer near a negatively charged surface. $[\text{NaCl}] = 0.01 \text{ mol l}^{-1}$

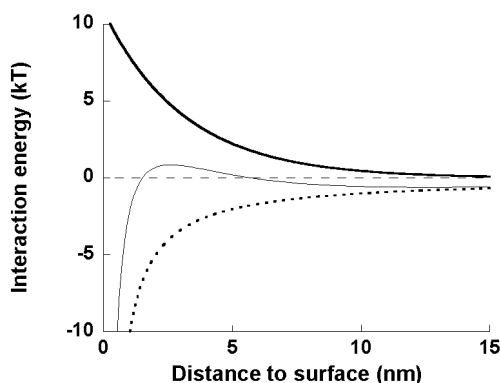


Fig. 3 Electrostatic repulsive (*thick line*), van der Waals attractive (*dotted line*) and total (*thin line*) interaction energies of two approaching spherical particles. Particle radius, $R=100$ nm; Stern potential, $\Psi_d=10$ mV; Hamaker constant, $A=0.5\times 10^{-20}$ J

surface into the solution and can rearrange their position and orientation. The effect of polymer adsorption can be both attractive and repulsive but in most cases the effect is repulsive.

Stabilization of colloidal particles by adsorption of an uncharged polymer is called steric stabilization. The two main contributions to this influence are a volume restriction effect and an osmotic effect. The volume restriction effect is caused by the loss of configurational entropy if the adsorbed polymer chain is compressed (less possible configurations of the flexible part of the polymer). The osmotic effect is caused by the increase in osmotic pressure between two particles if the polymer layers of two particles overlap. This effect depends on the quality of the solvent. In a good solvent polymer segments favor contact with the solvent over contact with other polymer segments which causes repulsion. In a poor solvent, polymer segments favor contact with other polymer segments over contact with the solvent.

Apart from polymer adsorption for uncharged macromolecules, charged macromolecules (polyelectrolytes), such as proteins can also adsorb at surfaces [20, 21]. Adsorption of a charged macromolecule is different from adsorption of an uncharged polymer in that there is a high dependency on the salt concentration. At a low salt concentration, repulsive electrostatic forces between charged polymer chains will inhibit formation of loops and tails (Fig. 4). This has been predicted and confirmed, for instance for adsorption of humic acids on iron-oxide particles [22].

3 Properties of Biologically Produced Sulfur

In the last 30 years a significant amount of research has been done on sulfur globules that are stored intracellularly (especially sulfur globules of *Al. vinosum* and *Beggiatoa alba*) and that are excreted outside the cell membrane

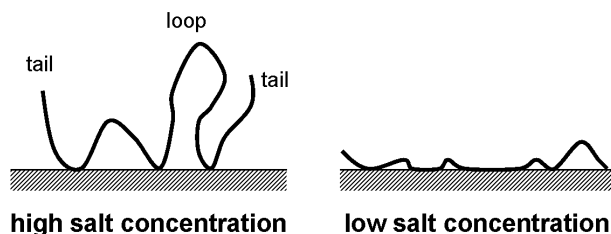


Fig. 4 The effect of salt concentration on the adsorption of charged polymers at a surface

(especially *Thiobacillus* sp.). This section is about the physico-chemical properties of those biologically produced sulfur globules stored intracellularly and extracellularly.

Research by Vetter [23] on externally excreted sulfur globules suggested that sulfur is stored as an energy reservoir rather than as a way of detoxification of excess hydrogen sulfide. As long as dissolved sulfide is available, sulfur is stored in globules. When sulfide is depleted, the stored sulfur is oxidized.

The identification of the nature of elemental sulfur in globules produced by sulfur compound oxidizing bacteria is not straightforward. Several studies have been performed with several different techniques but unfortunately the interpretation of the results sometimes seems to be contradictory. Although several studies propose models for the nature of sulfur globules produced by all sulfur compound oxidizing bacteria [24–26] it is safer to distinguish between sulfur globules produced by different bacteria because there are indications that not all sulfur globules are comparable [27, 28]. To give a clear overview of what is known about the nature of sulfur in globules, studies on sulfur globules from each organism are discussed separately.

3.1

Intracellularly Stored Sulfur

Several sulfide-oxidizing bacteria contain globules inside the cell membrane. The globules are membrane-limited and extracytoplasmic [17, 29]. In that way these globules could also be called extracellular, however we will call them intracellular because the globules are stored within the cell membrane.

In 1887 Winogradsky had already stated that living cells would contain globules of amorphous sulfur while in dead cells the sulfur would crystallize (ref. in [1]). X-ray diffraction (XRD) on intracellularly produced sulfur globules (among which *Allochromatium* sp.) has shown a difference between the isolated sulfur structure of fresh globules in the wet-state and the dried sulfur globules. The XRD pattern for fresh globules resembled the pattern of liquid sulfur whereas the pattern for dried globules and globules that were kept in a wet-state for several days, resembled the pattern of crystalline orthorhombic sulfur [1, 30]. This indicated that the structure of fresh sulfur

globules is not crystalline orthorhombic sulfur, but rather a liquid or amorphous form of sulfur, which converts into crystalline orthorhombic sulfur on drying or aging. After this, it was shown that the density of the sulfur globules produced by two *Allochromatium* species is 1.31 g cm^{-3} [31, 32]. This is considerably lower than the density of liquid sulfur (1.89 g cm^{-3}) or that of any form of crystalline sulfur ($1.9\text{--}2.2 \text{ g cm}^{-3}$) [33], indicating that the globules did not consist of pure liquid sulfur either. The suggestion was made that sulfur globules consist of sulfur and an unidentified moiety, which is probably water. In a model proposed by Steudel et al. [34] the globules consist of a nucleus of sulfur rings (S_8) with water around it and long-chain sulfur compounds such as polysulfides or polythionates as amphiphilic compounds at the interface. Polythionate chains were however not detected in cultures of *Al. vinosum* storing sulfur globules inside the bacterial cell, thereby limiting the possible amphiphilic compound in the model to long-chain polysulfides or sulfanemonosulfonates [32]. Polythionates in sulfur globules of *Al. vinosum* were also not detected by Prange et al. [28] who used X-ray absorption near-edge spectroscopy (XANES) [27]. Moreover, they ruled out the presence of sulfur rings and found the globules to consist of long sulfur chains terminated by organic groups ($\text{R-S}_n\text{-R}$), indicating the inapplicability of Steudel's model of a core of sulfur rings surrounded with water and polythionates or polysulfides for *Al. vinosum* sulfur globules. Some controversy has however arisen around these XANES measurements since Pickering et al. [25] claimed that the experimental results were misinterpreted due to artifacts and that sulfur globules of *Al. vinosum* consisted of 'simple, solid sulfur'. The discussion around this topic focuses on the measurement mode, with each mode having its own problem (electron yield mode with a sample charging effect; fluorescence mode with a self-absorption effect; transmittance mode with a 'pinhole' effect) [35, 36]. The model for sulfur globules of *Al. vinosum* that corresponds best with the available experimental data consists of long sulfur chains terminated by organic groups as was suggested by Prange et al. [28]. This can account for the observed low density and does not need to assume that the observed density is erroneously low.

XANES seems to be a useful technique because it can give information on the structure of sulfur globules in situ. Prange et al. showed that isolation of sulfur globules from the bacteria affects the structure of the sulfur [28], thereby limiting the value of studies with experimental techniques which do require isolation of the sulfur globules (e.g., XRD). There are however also certain limitations of the technique concerning interpretation of the data and availability of reference compounds, such as long chain organic sulfur compounds.

The sulfur globules of the chemotrophic bacteria *B. alba* have also been studied quite extensively. The density of the globules has not been determined but energy-dispersive X-ray microanalysis showed that the globules consisted almost entirely of sulfur [9]. XANES [28] and Raman spectroscopy [26] confirmed that the sulfur globules of *B. alba* consist of S_8 sulfur rings.

Apart from the nature of the sulfur in the globules, the surface of these globules has been studied as well. Studies on sulfur globules produced by *Al. vinosum* showed that the sulfur particle is bounded by a protein membrane, which appears to be sulfur-free [7, 18]. The proteins of the membrane were isolated by extraction and separated by reversed-phase HPLC, revealing three major proteins [37]. Proteins associated with sulfur globules of *Thiocapsa roseopersicina* appeared to correspond to the proteins on the sulfur globules of *Al. vinosum*. Later research was able to locate the genes responsible for the production of these proteins and it was concluded that sulfur globules in *Al. vinosum* are extracytoplasmic due to the presence of this protein cell membrane [27]. Such a cell membrane was also found for sulfur globules in *B. alba*, where it was called sulfur inclusion envelope [17]. The exact function of the protein is still not clear. Because of the similarity to proteins such as keratin or plant cell wall it has been suggested that the proteins have a structural rather than an enzymatic function [29]. The proteins might also prevent the crystallization of the sulfur in the globule [38].

3.2

Extracellularly Stored Sulfur

Sulfur globules produced by bacteria excreting the globules outside the cell membrane have also been studied. Especially for biotechnological applications these sulfur compound oxidizing bacteria are interesting since they allow an easy separation of the sulfur from the bacteria. In Fig. 5 sulfur globules can be seen which have been excreted by a *Thiobacillus* bacterium.

Steudel proposed a number of models for the composition of bacterial sulfur globules in which he did not always distinguish between intracellularly and extracellularly stored sulfur. In a model proposed for sulfur globules excreted by *Acidithiobacillus ferrooxidans* [39] the globules consist of a sulfur nucleus (mainly S_8 rings and small amounts of other sulfur rings) and

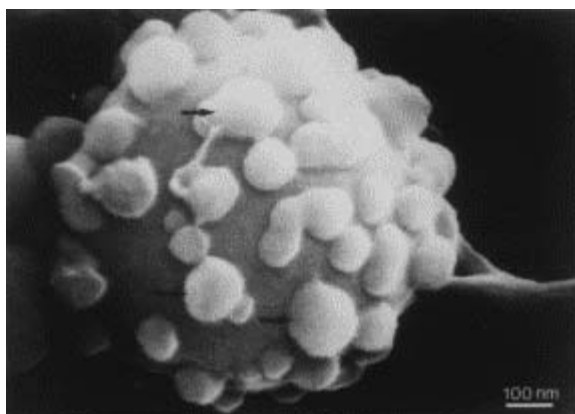


Fig. 5 Scanning electron micrograph of sulfur excreting *Thiobacillus* [40]

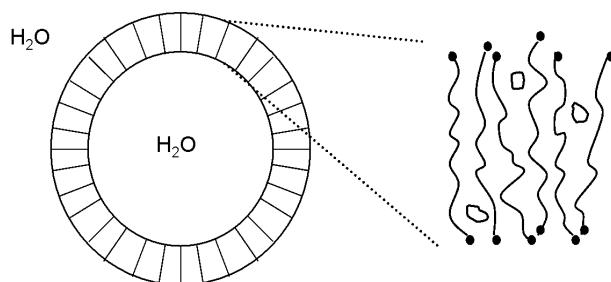


Fig. 6 Vesicle model proposed by Steudel for sulfur globules excreted by *Ac. ferrooxidans*. Vesicles are composed of long chain polythionates ($^-\text{O}_3\text{S-S}_n\text{-SO}_3^-$) in which small amounts of sulfur rings can be present (after [24])

long-chain polythionates present on the surface. Indeed HPLC [39] and XANES [28] analysis showed the presence of polythionates in the cultures of *Ac. ferrooxidans* excreting sulfur globules. XANES analysis did however also show that S_8 rings were not present. Another model proposed by Steudel [24] consists of vesicles composed of a polythionate membrane. The inside of the vesicle may contain water, and sulfur rings are only present in low concentrations in the membrane part of the vesicle. This model is in accordance with the observed experimental data obtained by XANES analysis and therefore seems suitable for globules produced by *Ac. ferrooxidans*.

It should be noted that polythionates are only stable at low pH [33] and it is therefore unlikely that the polythionate vesicle model is applicable to sulfur globules produced by bacteria growing at another pH than the acidic conditions at which *Ac. ferrooxidans* grows [5] (see Fig. 6).

Janssen et al. have studied the properties of sulfur produced by bacteria of the genus *Thiobacillus* grown at neutral to alkaline pH [19, 40, 41]. The sulfur was produced in a bioreactor in which a mixed culture of *Thiobacilli* was present.

X-ray diffraction of sulfur particles excreted by *Thiobacillus* sp. showed the presence of orthorhombic sulfur crystals. The solubility of crystalline orthorhombic sulfur in water is known to be only $5 \mu\text{g l}^{-1}$ [42]. In the solubility test shown in Fig. 7 it was seen that the biologically produced sulfur particles can be dispersed in water but not in hexadecane, whereas crystalline orthorhombic sulfur is soluble in hexadecane but not in water. The reason for the observed hydrophilicity of the biologically produced sulfur particles has to be attributed to the hydrophilic properties of the surface of the sulfur particles. Because of the relatively high stability of the biologically produced sulfur particles at high salt concentrations, it is concluded that the colloidal stability is not merely based on electrostatic repulsion. It is known that hydrophobic sulfur can be wetted by *Thiobacillus thiooxidans* bacteria due to formation of organic surface-active substances [43, 44].

It was concluded that the particles are stabilized by long chain polymers, most probably proteins. Indeed, measurements with dynamic light scattering showed a relatively high variation of the determined hydrodynamic radi-

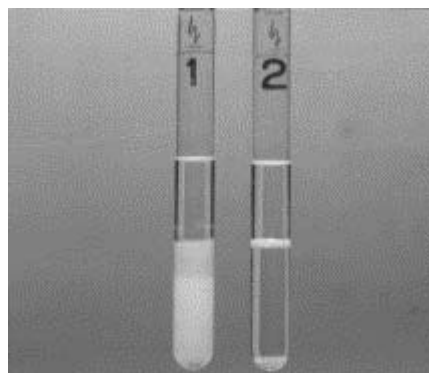


Fig. 7 Hexadecane-water partition test. Biologically produced sulfur remains in the lower water phase (1) whereas crystalline sulfur remains in the upper hexadecane-phase (2) [40]

us with changing salt concentration, indicating the presence of relatively thick adsorbed layers on the sulfur particles (see Fig. 4). This, as well as surface charge density measurements showing values comparable to surface charge densities of bacterial cell walls and humic acids, support the suggestion of proteins adsorbed on the particles. In addition, electrophoretic mobility experiments showed an iso-electric point comparable to the pK_a -value of carboxylic acid groups in proteins ($pK_a=2.3$) [45].

As stated above, the presence of proteins on the surface of sulfur globules stored intracellularly has been demonstrated [8, 37]. These well-defined proteins act as a membrane between the cytoplasm and the intracellular sulfur particle. It is not known whether the proteins associated with the sulfur particles excreted by *Thiobacillus* bacteria are well-defined proteins synthesized by the bacterium or if they are originating from organic compounds already present in the liquid reactor system.

3.3

Formation of Biologically Produced Sulfur

Biologically produced sulfur is often written as ' S^0 ', which only indicates that a large part of the sulfur in the sulfur globules is present in oxidation state zero. It should not be mistaken for atomic sulfur, which has a very high enthalpy of formation and therefore cannot exist at ambient temperature [33]. In the previous sections it has been shown that the sulfur in globules can be present as sulfur rings, long-chain polythionates and long sulfur chains terminated by organic groups. The mechanisms in which these forms of sulfur are formed are not known but the formation of sulfur rings is assumed to proceed through the formation of polysulfides [3].

Stuedel [38] proposed a reaction mechanism for the chemical oxidation of sulfide to sulfur rings (S_8), which should take place in a similar way in

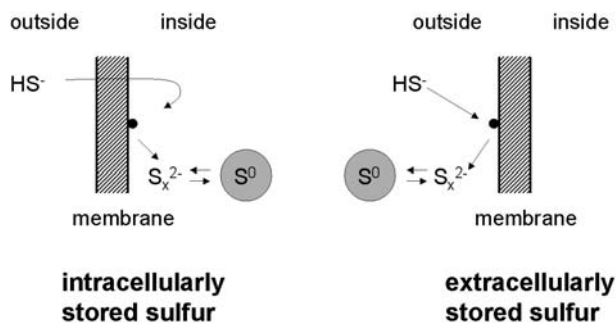
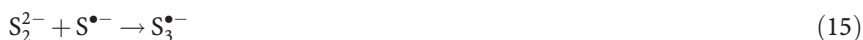


Fig. 8 Model for the deposition of sulfur inside or outside the cells in which the position of the electron acceptor on the membrane (●) determines the location of sulfur storage (after [46])

sulfur compound oxidizing bacteria. In this mechanism HS⁻ anions are oxidized forming sulfide radicals (HS[•] or S^{•-}):



These radicals are the basis for a complex sequence of reactions involving radicalization of ions and dimerization of radical ions, resulting in polysulfide anions (S_x²⁻), e.g.:



etc.

Upon acidification of long chain polysulfide anions, elemental sulfur rings are formed:



In chemical oxidation reactions, the first oxidation step (forming of sulfide radicals) is catalyzed by metal-ions like V⁵⁺, Fe³⁺, and Cu²⁺. In most sulfur compound oxidizing bacteria, the first step in the oxidation of sulfide to sulfur is catalyzed by the enzyme flavocytochrome c [3]. In a number of bacteria with the capacity to oxidize sulfide to sulfur, flavocytochrome c has not been found and other cytochromes or quinones are believed to catalyze the oxidation of sulfide in these organisms.

Brune [3] has suggested that the location of the catalyst for the acidification of polysulfide anions to elemental sulfur determines whether sulfur is

stored extracellularly or intracellularly. Van Gernerden however suggested that the location of the electron acceptor in the HS^- oxidation step determines whether sulfur is stored extracellularly or intracellularly [46] as is explained in Fig. 8. This is supported by research of Then and Trüper [8] on sulfide oxidation in *Halorhodospira abdelmalekii*, excreting sulfur globules extracellularly. They showed the cytochrome c-551 to have a catalytic effect on the oxidation of sulfide and to be located on the outside of the cell membrane. In *Al. vinosum* cytochrome c-551 is located in the periplasmic space, the space between the outer cell wall and the cytoplasmic membrane, which is also the location of storage of sulfur globules [47].

4

Sulfur Compound Oxidizing Bacteria in Industrial Applications

4.1

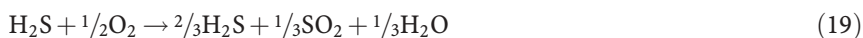
Removal of Hydrogen Sulfide From Gas Streams

A number of environmental problems are strongly related to the emission of sulfur compounds, such as SO_2 , in the atmosphere. SO_2 emission is mainly due to combustion of fossil fuels containing H_2S or organic S-compounds. In the atmosphere, SO_2 is oxidized forming sulfuric acid resulting in acid rain. Fortunately, the emission of SO_2 has decreased considerably since the 1970s due to selection of low sulfur-content fuels, waste gas treatment and specialized combustion processes.

In order to prevent SO_2 emission, H_2S has to be removed from gas streams prior to combustion. Apart from environmental reasons, removal of H_2S from waste gas streams is also required for health reasons (H_2S is a toxic gas, lethal at concentrations exceeding 600 ppm) and to prevent corrosion of equipment. Gases that can contain H_2S and need treatment are, for instance, natural gas, syngas and biogas (formed in anaerobic wastewater treatment).

Removal of H_2S from gas streams is generally done in two steps. In the first step, H_2S is separated from the gas stream and in the second step, the removed H_2S (dissolved in liquid or as concentrated gas) is converted into elemental sulfur. Several processes exist that purify gases according to these two steps.

The method most commonly used is based on absorption of H_2S in an amine solution and the subsequent stripping of the dissolved H_2S from this solution forming a concentrated gas ('Claus gas') which is then converted into elemental sulfur in the Claus process. In the Claus process, a third of the H_2S gas is first burned to SO_2 after which the remaining H_2S reacts with the formed SO_2 to elemental sulfur:



In other methods H_2S is absorbed in a solution after which the dissolved H_2S is converted to elemental sulfur without stripping the gas from the solution. Differences between different methods basically consist of a different absorption solution or a different oxidation catalyst.

Disadvantages are the high operational costs due to high pressures and high temperatures and the need of special chemicals (catalysts).

4.2

Biotechnological Removal of Hydrogen Sulfide from Gas Streams

To overcome the disadvantages of physico-chemical processes for H_2S removal, the use of microorganisms can be an interesting alternative. Several microorganisms are capable of the oxidation of H_2S at ambient temperatures and pressures, and both phototrophic and chemotrophic organisms have been studied for their industrial application. The phototrophic sulfur oxidizing bacteria *Chlorobium limicola* forma *thiosulfatophilum* has been studied [48, 49] but phototrophic bacteria have the disadvantage of the requirement of light and therefore the need of a transparent reactor surface and reaction solutions. Of the chemotrophic bacteria, heterotrophs as well as autotrophs have been studied. The heterotrophic *Xanthomonas* bacterium has been studied for H_2S removal [11] but showed lower removal rates than other autotrophic bacteria and, in addition, heterotrophic organisms have the disadvantage of the requirement of organic compounds. Chemoautotrophic bacteria (especially *Thiobacilli*) are the types of sulfur oxidizing bacteria that have been studied and used mostly in H_2S removal processes.

The use of *Thiobacillus* species has been studied quite extensively. Sublette and Sylvester especially focused on the use of *Thiobacillus denitrificans* [50–52] for aerobic or anaerobic oxidation of sulfide to sulfate. In the anaerobic oxidation NO_3^- was used as an oxidant instead of oxygen (confirm Table 2). Buisman used a mixed culture of *Thiobacilli* for the aerobic oxidation of sulfide to elemental sulfur and studied technological applications [53–55]. Visser showed the dominant organism in this mixed culture to be a new organism named *Thiobacillus* sp. W5 [6].

The production of sulfur from sulfide has some distinct advantages over the production of sulfate. First, elemental sulfur is seen as a less harmful form of sulfur than sulfate. Secondly, the separation of the insoluble sulfur from aqueous streams is easier than separation of sulfate and thirdly less oxygen is needed for the oxidation, which saves energy costs for aeration:



According to Kuenen, the formation of sulfate yields more energy than the formation of sulfur [2]. To stimulate formation of sulfur, the oxygen concentration should be limited [56, 57].

Several reactor systems possible for the biotechnological removal of H_2S from a gas exist. Currently, three types of biotechnological process systems

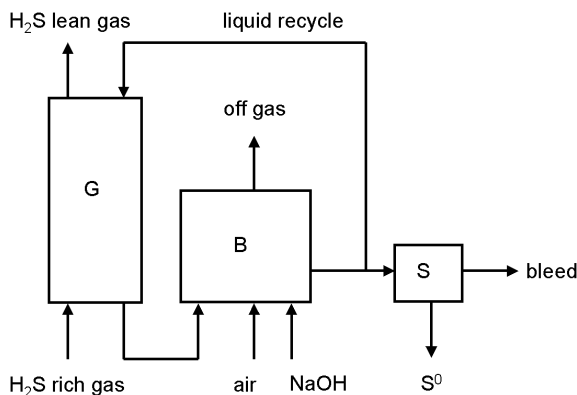


Fig. 9 Scheme of the process for the biotechnological removal of H_2S from gas streams. G=Gas absorber; B=Bioreactor; S=Settler

are being used; bioscrubber, biotrickling filter, and biofilter. Since in the last two processes, sulfate is produced and not elemental sulfur, it is not within the scope of this chapter to elaborate on this (see [58]). The technology of the bioscrubber is however relevant since it is used in practice for the production of “biosulfur”.

The principle of a bioscrubber system is explained in Fig. 9. It consists of a bioscrubber or gas absorber (G) and a bioreactor (B). In the gas absorber H_2S is scrubbed from a gas stream by an alkaline solution:



After this the dissolved hydrogen sulfide is oxidized to elemental sulfur in a bioreactor:



The formed elemental sulfur is then separated from the liquid by sedimentation in a settler (S). Here, aggregates of sulfur are formed, which can grow to particles with a diameter of up to 3 mm but which can also be easily ground down [40].

A limitation to the alkalinity of the liquid recycle is the optimum pH of growth of the bacteria in the bioreactor. Use of alkaliphilic sulfur compound oxidizing bacteria is therefore very interesting from a technological point of view.

Apart from this, a number of side reactions take place. In the gas absorber polysulfides (S_x^{2-} , with $x \leq 6$) can be formed by reaction of hydrogen sulfide with sulfur:



The sulfur particles are fed to the gas absorber by the liquid recycle due to an incomplete separation of solid sulfur in the separation step of the process. In the bioreactor, the polysulfide anions either decompose into sulfide and sulfur (Eq. 28), or are oxidized to thiosulfate (Eq. 29). Sulfate can also be formed by oxidation of HS^- (Eq. 30):



In principal, oxygen from air is the only reagent needed for this process. However, due to the occurrence of sulfate and thiosulfate formation, extra sodium hydroxide has to be dosed to the bioreactor and a bleed stream is necessary to prevent accumulation of sodium salts. The amount of NaOH that has to be added to the bioreactor can be minimized if the occurrence of (thio)sulfate formation is minimized. Previous research showed that sulfide oxidation to sulfate can be selectively prevented by applying a low oxygen concentration [56]. The oxidation of anionic polysulfides, however, cannot easily be prevented by controlling of the oxygen concentration because the oxidation rate of polysulfides is higher than the oxidation rate of sulfide, as was suggested by Chen and Morris [59]. In order to determine the best way to prevent the thiosulfate formation, more should be known about the role of the polysulfide anions and their specific interaction with the biologically produced sulfur particles.

5 Applications of Biologically Produced Sulfur

Sulfur produced by microorganisms in H_2S removal plants such as described in the previous section, can be handled in a number of ways. Dried sulfur solids can be used in sulfuric acid production (99% sulfur purity needed) or the formed sulfur sludge can be directed to a smelter where it is converted into high purity sulfur (>99.9%). Unfortunately, currently more sulfur is produced worldwide than is needed as pure chemical and therefore sulfur is also stored in landfill (95–98% sulfur purity needed). Although solid sulfur is considered as a non-hazardous refinery waste, landfill is an undesirable option, partly because acidification by oxidation has to be prevented.

To avoid the landfill, possible applications of the biologically produced sulfur have been investigated. In bioleaching and in agriculture, it was found that the specific properties of biologically produced sulfur (small particle size, hydrophilic surface) have clear advantages over the use of inorganic sulfur.

Bioleaching is used in mining to dissolve metals from sulfide-ores. The aim of bioleaching is to achieve pH values that are low enough to solubilize a maximum of metals. In some cases additional elemental sulfur is added as

Table 3 Grain yield of Breton Canola for different sulfur sources

Sulfur source	Grain yield (kg/ha)
None	14.6
K ₂ SO ₄	15.9
T90CR	17.4
S95	18.0
Claus sulfur	17.1
Biosulfur paste	22.3
Biosulfur powder	19.8

substrate for bacteria [60], which oxidize the sulfur forming sulfuric acid, and thereby decrease the pH. Tichý compared the use of sulfur flower with biologically produced sulfur, produced by sulfide oxidation of *Thiobacilli* under oxygen limitation [61]. He concluded that the hydrophilic properties of biologically produced sulfur have a positive effect in bioleaching because they cause an increase of the rate of sulfuric acid production.

Another field in which biologically produced sulfur can be used is in agriculture. Sulfur is an important nutrient for plants, which can take up sulfur by their leaves from the atmosphere as very reduced (COS, CS₂, and H₂S) up to highly oxidized compounds (SO₂). Most of the sulfur, however, is taken up by plant roots as water-soluble sulfate. Partly due to the decrease in SO₂ emissions since the 1970s, there is a widespread sulfur deficiency in soils that are used for cultivation of several highly S-demanding crops, especially oilseed rape and cereals in Denmark, England, F.R.G. and Scotland. In those circumstances additional S feeding is required.

First results of studies [62] on the yield of canola showed that the grain yield is higher when biologically produced sulfur is used than when other commercially available sulfur sources were used (Table 3).

6 Conclusions

Elemental sulfur produced by sulfur compound oxidizing bacteria (“biosulfur”) has distinctly different properties than crystalline elemental sulfur. The hydrophilic properties of “biosulfur” are the most striking of these differences. As a result of this, biologically produced sulfur can be dispersed in aqueous solutions, whereas crystalline inorganic sulfur is hydrophobic and will not be wetted by an aqueous solution.

The origin of the hydrophilicity of biologically produced sulfur is however not the same for sulfur produced by different bacteria. Intracellularly stored sulfur globules produced by *Al. vinosum* consist of long sulfur chains terminated with organic groups. These organic end groups are likely to be responsible for the hydrophilic character of the sulfur globules. The hydrophilicity of extracellularly stored sulfur globules produced by *Ac. ferrooxidans* probably can be explained by the vesicle structure consisting mainly of poly-

thionates ($^-O_3S-S_n-SO_3^-$). Adsorbed organic polymers such as proteins cause the hydrophilic properties of sulfur produced in biotechnological sulfide oxidation installations by a mixed culture of *Thiobacilli*.

Due to the small particle size and hydrophilic surface, biologically produced sulfur has advantages over other available sulfur sources in bioleaching and fertilizer applications.

References

1. H. G. Trüper, J. C. Hathaway, *Nature* **1967**, *215*, 435-436.
2. J. G. Kuenen, *Plant Soil* **1975**, *43*, 49-76.
3. D. C. Brune, *Biochim. Biophys. Acta* **1989**, *975*, 189-221.
4. T. Brüser, P. N. L. Lens, H. G. Trüper in *Environmental technologies to treat sulfur pollution-principles and engineering* (Eds.: P.N. L. Lens, L. Hulshoff Pol), IWA Publishing, London, **2000**, pp. 47-85.
5. H. G. Schlegel, *General Microbiology*, 7th ed. Cambridge University Press, Cambridge, **1995**, p. 390.
6. J. M. Visser, G. C. Stefess, L. A. Robertson, J. G. Kuenen, *Antonie Van Leeuwenhoek* **1997**, *72*, 127-134.
7. G. L. Schmidt, G. L. Nicolson, M. D. Kamen, *J. Bacteriol.* **1971**, *105*, 1137-1141.
8. J. Then, H. G. Trüper, *Arch. Microbiol.* **1983**, *135*, 254-258.
9. N. H. Lawry, V. Jani, T. E. Jensen, *Curr. Microbiol.* **1981**, *6*, 71-74.
10. D. Y. Sorokin, J. G. Kuenen, M. S. M. Jetten, *Arch. Microbiol.* **2001**, *175*, 94-101.
11. K. S. Cho, M. Hirai, M. Shoda, *Appl. Environ. Microbiol.* **1992**, *58*, 1183-1189.
12. Y. Cohen, E. Padan, M. Shilo, *J. Bacteriol.* **1975**, *123*, 855-861.
13. J. F. Imhoff, J. Suling, R. Petri, *Int. J. Syst. Bacteriol.* **1998**, *48*, 1129-1143.
14. J. F. Imhoff, J. Suling, *Arch. Microbiol.* **1996**, *165*, 106-113.
15. D. P. Kelly, A. P. Wood, *Int. J. Syst. Evol. Microbiol.* **2000**, *50*, 511-516.
16. D. Y. Sorokin, L. A. Robertson, J. G. Kuenen, *Antonie Van Leeuwenhoek* **2000**, *77*, 251-262.
17. W. R. Strohl, I. Geffers, J. M. Larkins, *Curr. Microbiol.* **1981**, *6*, 75-79.
18. G. L. Nicolson, G. L. Schmidt, *J. Bacteriol.* **1971**, *105*, 1142-1148.
19. A. Janssen, A. de Keizer, A. van Aelst, R. Fokkink, H. Yangling, G. Lettinga, *Colloid Surf. B-Biointerfaces* **1996**, *6*, 115-129.
20. J. Lyklema, *Pure Appl. Chem.* **1976**, *46*, 149-156.
21. J. Lyklema, G. J. Fleer, *Colloids Surfaces* **1987**, *25*, 357-368.
22. C. L. Tiller, C. R. O'Melia, *Colloid Surf. A-Physicochem. Eng. Asp.* **1993**, *73*, 89-102.
23. R. D. Vetter, *Mar. Biol.* **1985**, *88*, 33-42.
24. R. Steudel in *Autotrophic bacteria* (Eds.: H. G. Schlegel, B. Bowien), Science Technology Publishers, Madison, WI, **1989**, pp. 289-303.
25. I. J. Pickering, G. N. George, E. Y. Yu, D. C. Brune, C. Tuschak, J. Overmann, J. T. Beatty, R. C. Prince, *Biochemistry* **2001**, *40*, 8138-8145.
26. J. D. Pasteris, J. J. Freeman, S. K. Goffredi, K. R. Buck, *Chem. Geol.* **2001**, *180*, 3-18.
27. A. Prange, I. Arzberger, C. Engemann, H. Modrow, O. Schumann, H. G. Trüper, R. Steudel, C. Dahl, J. Hormes, *Biochim. Biophys. Acta* **1999**, *1428*, 446-454.
28. A. Prange, R. Chauvistre, H. Modrow, J. Hormes, H. G. Trüper, C. Dahl, *Microbiology-(UK)* **2002**, *148*, 267-276.
29. K. Pattaragulwanit, D. C. Brune, H. G. Trüper, C. Dahl, *Arch. Microbiol.* **1998**, *169*, 434-444.
30. G. J. Hageage, E. D. Eanes, R. L. Gherna, *J. Bacteriol.* **1970**, *101*, 464-469.
31. R. Guerrero, J. Mas, C. Pedrós-Alió, *Arch. Microbiol.* **1984**, *137*, 350-356.
32. J. Mas, H. van Gernerden, *Arch. Microbiol.* **1987**, *146*, 362-369.

33. R. Steudel in *Environmental technologies to treat sulfur pollution—principles and engineering* (Eds.: P.N. L. Lens, L. Hulshoff Pol), IWA Publishing, London, **2000**, pp. 1-31.
34. R. Steudel, G. Holdt, P. T. Visscher, H. van Gernerden, *Arch. Microbiol.* **1990**, *153*, 432-437.
35. G. N. George, I. J. Pickering, E. Y. Yu, R. C. Prince, *Microbiology-(UK)* **2002**, *148*, 2267-2268.
36. A. Prange, C. Dahl, H. G. Trüper, R. Chauvistre, H. Modrow, J. Hormes, *Microbiology-(UK)* **2002**, *148*, 2268-2270.
37. D. C. Brune, *Arch. Microbiol.* **1995**, *163*, 391-399.
38. R. Steudel, *Ind. Eng. Chem. Res.* **1996**, *35*, 1417-1423.
39. R. Steudel, G. Holdt, T. Goebel, W. Hazeu, *Angew. Chem. Int. Ed. Eng.* **1987**, *26*, 151-152.
40. A. J. H. Janssen, G. Lettinga, A. de Keizer, *Colloid Surf. A-Physicochem. Eng. Asp.* **1999**, *151*, 389-397.
41. A. J. H. Janssen, A. de Keizer, G. Lettinga, *Colloid Surf B-Biointerfaces* **1994**, *3*, 111-117.
42. J. Boulègue, *Phosphorus Sulfur Silicon Relat. Elem.* **1978**, *5*, 127-128.
43. G. E. Jones, R. L. Starkey, *J. Bacteriol.* **1961**, *82*, 788-789.
44. G. E. Jones, A. A. Benson, *J. Bacteriol.* **1965**, *89*, 260-261.
45. W. E. Kleinjan (Unpublished Results).
46. H. van Gernerden, *Arch. Microbiol.* **1984**, *139*, 289-294.
47. G. O. Gray, D. B. Knaff, *Biochim. Biophys. Acta* **1982**, *680*, 290-296.
48. B. W. Kim, H. N. Chang, *Biotechnol. Prog.* **1991**, *7*, 495-500.
49. D. J. Cork, R. Garunas, A. Sajjad, *Appl. Environ. Microbiol.* **1983**, *45*, 913-918.
50. K. L. Sublette, N. D. Sylvester, *Biotechnol. Bioeng.* **1987**, *24*, 759-761.
51. K. L. Sublette, N. D. Sylvester, *Biotechnol. Bioeng.* **1987**, *24*, 753-758.
52. K. L. Sublette, N. D. Sylvester, *Biotechnol. Bioeng.* **1987**, *24*, 249-257.
53. C. J. N. Buisman, B. G. Geraarts, P. IJspeert, G. Lettinga, *Biotechnol. Bioeng.* **1990**, *35*, 50-56.
54. C. J. N. Buisman, P. IJspeert, A. Hof, A. J. H. Janssen, R. ten Hagen, G. Lettinga, *Biotechnol. Bioeng.* **1991**, *38*, 813-820.
55. C. J. N. Buisman, G. Lettinga, C. W. M. Paasschens, L. H. A. Habets, *Water Sci. Technol.* **1991**, *24*, 347-356.
56. A. J. H. Janssen, S. Meijer, J. Bontsema, G. Lettinga, *Biotechnol. Bioeng.* **1998**, *60*, 147-155.
57. R. V. Gadre, *Biotechnol. Bioeng.* **1989**, *34*, 410-414.
58. V. Herrygers, H. van Langenhove, E. Smet in *Environmental technologies to treat sulfur pollution—principles and engineering* (Eds.: P. N. L. Lens, L. Hulshoff Pol), IWA Publishing, London, **2000**, pp. 281-304.
59. K. Y. Chen, J. C. Morris, *Environ. Sci. Technol.* **1972**, *6*, 529-537.
60. R. Tichý in *Environmental technologies to treat sulfur pollution—principles and engineering* (Eds.: P.N. L. Lens, L. Hulshoff Pol), IWA Publishing, London, **2000**, pp. 329-354.
61. R. Tichý, A. Janssen, J. T. C. Grotenhuis, G. Lettinga, W. H. Rulkens, *Bioresour. Technol.* **1994**, *48*, 221-227.
62. S. W. S. Kijlstra, A. J. H. Janssen, B. Arena, *Proceedings of the Laurance Reid gas conditioning conference* **2001**.

Author Index Volumes 201–230

Author Index Vols. 26–50 see Vol. 50

Author Index Vols. 51–100 see Vol. 100

Author Index Vols. 101–150 see Vol. 150

Author Index Vols. 151–200 see Vol. 200

The volume numbers are printed in italics

- Achilefu S, Dorshow RB (2002) Dynamic and Continuous Monitoring of Renal and Hepatic Functions with Exogenous Markers. *222*: 31–72
- Albert M, see Dax K (2001) *215*: 193–275
- Angyal SJ (2001) The Lobry de Bruyn-Alberda van Ekenstein Transformation and Related Reactions. *215*: 1–14
- Armentrout PB (2003) Threshold Collision-Induced Dissociations for the Determination of Accurate Gas-Phase Binding Energies and Reaction Barriers. *225*: 227–256
- Astruc D, Blais J-C, Cloutet E, Djakovitch L, Rigaut S, Ruiz J, Sartor V, Valério C (2000) The First Organometallic Dendrimers: Design and Redox Functions. *210*: 229–259
- Augé J, see Lubineau A (1999) *206*: 1–39
- Baars MWPL, Meijer EW (2000) Host-Guest Chemistry of Dendritic Molecules. *210*: 131–182
- Balczewski P, see Mikolajczyk M (2003) *223*: 161–214
- Ballauff M (2001) Structure of Dendrimers in Dilute Solution. *212*: 177–194
- Baltzer L (1999) Functionalization and Properties of Designed Folded Polypeptides. *202*: 39–76
- Balzani V, Ceroni P, Maestri M, Saudan C, Vicinelli V (2003) Luminescent Dendrimers. *Recent Advances*. *228*: 159–191
- Barré L, see Lasne M-C (2002) *222*: 201–258
- Bartlett RJ, see Sun J-Q (1999) *203*: 121–145
- Bertrand G, Bourissou D (2002) Diphosphorus-Containing Unsaturated Three-Membered Rings: Comparison of Carbon, Nitrogen, and Phosphorus Chemistry. *220*: 1–25
- Betzemeier B, Knochel P (1999) Perfluorinated Solvents – a Novel Reaction Medium in Organic Chemistry. *206*: 61–78
- Bibette J, see Schmitt V (2003) *227*: 195–215
- Blais J-C, see Astruc D (2000) *210*: 229–259
- Bogár F, see Pipek J (1999) *203*: 43–61
- Bohme DK, see Petrie S (2003) *225*: 35–73
- Bourissou D, see Bertrand G (2002) *220*: 1–25
- Bowers MT, see Wyttenbach T (2003) *225*: 201–226
- Brand SC, see Haley MM (1999) *201*: 81–129
- Bray KL (2001) High Pressure Probes of Electronic Structure and Luminescence Properties of Transition Metal and Lanthanide Systems. *213*: 1–94
- Bronstein LM (2003) Nanoparticles Made in Mesoporous Solids. *226*: 55–89
- Brönstrup M (2003) High Throughput Mass Spectrometry for Compound Characterization in Drug Discovery. *225*: 275–294
- Brücher E (2002) Kinetic Stabilities of Gadolinium(III) Chelates Used as MRI Contrast Agents. *221*: 103–122
- Brunel JM, Buono G (2002) New Chiral Organophosphorus catalysts in Asymmetric Synthesis. *220*: 79–106
- Buchwald SL, see Muci A R (2002) *219*: 131–209
- Bunz UHF (1999) Carbon-Rich Molecular Objects from Multiply Ethynylated *p*-Complexes. *201*: 131–161
- Buono G, see Brunel JM (2002) *220*: 79–106

- Cadierno V, see Majoral J-P (2002) 220: 53–77
- Caminade A-M, see Majoral J-P (2003) 223: 111–159
- Carmichael D, Mathey F (2002) New Trends in Phosphametalocene Chemistry. 220: 27–51
- Caruso F (2003) Hollow Inorganic Capsules via Colloid-Templated Layer-by-Layer Electrostatic Assembly. 227: 145–168
- Caruso RA (2003) Nanocasting and Nanocoating. 226: 91–118
- Ceroni P, see Balzani V (2003) 228: 159–191
- Chamberlin AR, see Gilmore MA (1999) 202: 77–99
- Chivers T (2003) Imido Analogues of Phosphorus Oxo and Chalcogenido Anions. 229: 143–159
- Chow H-F, Leung C-F, Wang G-X, Zhang J (2001) Dendritic Oligoethers. 217: 1–50
- Clarkson RB (2002) Blood-Pool MRI Contrast Agents: Properties and Characterization. 221: 201–235
- Cloutet E, see Astruc D (2000) 210: 229–259
- Co CC, see Hentze H-P (2003) 226: 197–223
- Cooper DL, see Raimondi M (1999) 203: 105–120
- Cornils B (1999) Modern Solvent Systems in Industrial Homogeneous Catalysis. 206: 133–152
- Corot C, see Idee J-M (2002) 222: 151–171
- Crépy KVL, Imamoto T (2003) New P-Chirogenic Phosphine Ligands and Their Use in Catalytic Asymmetric Reactions. 229: 1–40
- Cristau H-J, see Taillefer M (2003) 229: 41–73
- Crooks RM, Lemon III BI, Yeung LK, Zhao M (2001) Dendrimer-Encapsulated Metals and Semiconductors: Synthesis, Characterization, and Applications. 212: 81–135
- Croteau R, see Davis EM (2000) 209: 53–95
- Crouzel C, see Lasne M-C (2002) 222: 201–258
- Curran DP, see Maul JJ (1999) 206: 79–105
- Currie F, see Häger M (2003) 227: 53–74
- Davidson P, see Gabriel J-C P (2003) 226: 119–172
- Davis EM, Croteau R (2000) Cyclization Enzymes in the Biosynthesis of Monoterpenes, Sesquiterpenes and Diterpenes. 209: 53–95
- Davies JA, see Schwert DD (2002) 221: 165–200
- Dax K, Albert M (2001) Rearrangements in the Course of Nucleophilic Substitution Reactions. 215: 193–275
- de Keizer A, see Kleinjan WE (2003) 230: 167–188
- de la Plata BC, see Ruano JLG (1999) 204: 1–126
- de Meijere A, Kozhushkov SI (1999) Macrocyclic Structurally Homoconjugated Oligoacetylenes: Acetylene- and Diacetylene-Expanded Cycloalkanes and Rotanes. 201: 1–42
- de Meijere A, Kozhushkov SI, Khlebnikov AF (2000) Bicyclopropylidene – A Unique Tetra-substituted Alkene and a Versatile C₆-Building Block. 207: 89–147
- de Meijere A, Kozhushkov SI, Hadjiaraoglou LP (2000) Alkyl 2-Chloro-2-cyclopropylideneacetates – Remarkably Versatile Building Blocks for Organic Synthesis. 207: 149–227
- Dennig J (2003) Gene Transfer in Eukaryotic Cells Using Activated Dendrimers. 228: 227–236
- de Raadt A, Fechter MH (2001) Miscellaneous. 215: 327–345
- Desreux JF, see Jacques V (2002) 221: 123–164
- Diederich F, Gobbi L (1999) Cyclic and Linear Acetylenic Molecular Scaffolding. 201: 43–79
- Diederich F, see Smith DK (2000) 210: 183–227
- Djakovitch L, see Astruc D (2000) 210: 229–259
- Dolle F, see Lasne M-C (2002) 222: 201–258
- Donges D, see Yersin H (2001) 214: 81–186
- Dormán G (2000) Photoaffinity Labeling in Biological Signal Transduction. 211: 169–225
- Dorn H, see McWilliams AR (2002) 220: 141–167
- Dorshow RB, see Achilefu S (2002) 222: 31–72
- Drabowicz J, Mikołajczyk M (2000) Selenium at Higher Oxidation States. 208: 143–176
- Eckert B, see Steudel R (2003) 230: 1–79
- Ehses M, Romerosa A, Peruzzini M (2002) Metal-Mediated Degradation and Reaggregation of White Phosphorus. 220: 107–140

- Eder B, see Wrodnigg TM (2001) The Amadori and Heyns Rearrangements: Landmarks in the History of Carbohydrate Chemistry or Unrecognized Synthetic Opportunities? *215*: 115–175
- Edwards DS, see Liu S (2002) *222*: 259–278
- Elaissari A, Ganachaud F, Pichot C (2003) Biorelevant Latexes and Microgels for the Interaction with Nucleic Acids. *227*: 169–193
- Esumi K (2003) Dendrimers for Nanoparticle Synthesis and Dispersion Stabilization. *227*: 31–52
- Famulok M, Jenne A (1999) Catalysis Based on Nucleic Acid Structures. *202*: 101–131
- Fechter MH, see de Raadt A (2001) *215*: 327–345
- Ferrier RJ (2001) Substitution-with-Allylic-Rearrangement Reactions of Glycal Derivatives. *215*: 153–175
- Ferrier RJ (2001) Direct Conversion of 5,6-Unsaturated Hexopyranosyl Compounds to Functionalized Glycohexanones. *215*: 277–291
- Frey H, Schlenk C (2000) Silicon-Based Dendrimers. *210*: 69–129
- Förster S (2003) Amphiphilic Block Copolymers for Templating Applications. *226*: 1–28
- Frullano L, Rohovec J, Peters JA, Geraldes CFGC (2002) Structures of MRI Contrast Agents in Solution. *221*: 25–60
- Fugami K, Kosugi M (2002) Organotin Compounds. *219*: 87–130
- Fuhrhop J-H, see Li G (2002) *218*: 133–158
- Furukawa N, Sato S (1999) New Aspects of Hypervalent Organosulfur Compounds. *205*: 89–129
- Gabriel J-C P, Davidson P (2003) Mineral Liquid Crystals from Self-Assembly of Anisotropic Nanosystems. *226*: 119–172
- Gamelin DR, Güdel HU (2001) Upconversion Processes in Transition Metal and Rare Earth Metal Systems. *214*: 1–56
- Ganachaud F, see Elaissari A (2003) *227*: 169–193
- García R, see Tromas C (2002) *218*: 115–132
- Geraldes CFGC, see Frullano L (2002) *221*: 25–60
- Gilmore MA, Steward LE, Chamberlin AR (1999) Incorporation of Noncoded Amino Acids by In Vitro Protein Biosynthesis. *202*: 77–99
- Glasbeek M (2001) Excited State Spectroscopy and Excited State Dynamics of Rh(III) and Pd(II) Chelates as Studied by Optically Detected Magnetic Resonance Techniques. *213*: 95–142
- Glass RS (1999) Sulfur Radical Cations. *205*: 1–87
- Gobbi L, see Diederich F (1999) *201*: 43–129
- Göltner-Spickermann C (2003) Nanocasting of Lyotropic Liquid Crystal Phases for Metals and Ceramics. *226*: 29–54
- Gouzy M-F, see Li G (2002) *218*: 133–158
- Gries H (2002) Extracellular MRI Contrast Agents Based on Gadolinium. *221*: 1–24
- Gruber C, see Tovar GEM (2003) *227*: 125–144
- Güdel HU, see Gamelin DR (2001) *214*: 1–56
- Guga P, Okruszek A, Stec WJ (2002) Recent Advances in Stereocontrolled Synthesis of P-Chiral Analogues of Biophosphates. *220*: 169–200
- Gulea M, Masson S (2003) Recent Advances in the Chemistry of Difunctionalized Organophosphorus and -Sulfur Compounds. *229*: 161–198
- Hackmann-Schlichter N, see Krause W (2000) *210*: 261–308
- Hadjiraoglou LP, see de Meijere A (2000) *207*: 149–227
- Häger M, Currie F, Holmberg K (2003) Organic Reactions in Microemulsions. *227*: 53–74
- Häusler H, Stütz AE (2001) d-Xylose (d-Glucose) Isomerase and Related Enzymes in Carbohydrate Synthesis. *215*: 77–114
- Haley MM, Pak JJ, Brand SC (1999) Macrocyclic Oligo(phenylacetylenes) and Oligo(phenyldiacetylenes). *201*: 81–129
- Harada A, see Yamaguchi H (2003) *228*: 237–258
- Hartmann T, Ober D (2000) Biosynthesis and Metabolism of Pyrrolizidine Alkaloids in Plants and Specialized Insect Herbivores. *209*: 207–243
- Haseley SR, Kamerling JP, Vliegthart JFG (2002) Unravelling Carbohydrate Interactions with Biosensors Using Surface Plasmon Resonance (SPR) Detection. *218*: 93–114
- Hassner A, see Namboothiri INN (2001) *216*: 1–49
- Helm L, see Tóth E (2002) *221*: 61–101

- Hemscheidt T (2000) Tropane and Related Alkaloids. *209*: 175–206
- Hentze H-P, Co CC, McKelvey CA, Kaler EW (2003) Templating Vesicles, Microemulsions and Lyotropic Mesophases by Organic Polymerization Processes. *226*: 197–223
- Hergenrother PJ, Martin SF (2000) Phosphatidylcholine-Preferring Phospholipase C from *B. cereus*. Function, Structure, and Mechanism. *211*: 131–167
- Hermann C, see Kuhlmann J (2000) *211*: 61–116
- Heydt H (2003) The Fascinating Chemistry of Triphosphabenzenes and Valence Isomers. *223*: 215–249
- Hirsch A, Vostrowsky O (2001) Dendrimers with Carbon Rich-Cores. *217*: 51–93
- Hiyama T, Shirakawa E (2002) Organosilicon Compounds. *219*: 61–85
- Holmberg K, see Häger M (2003) *227*: 53–74
- Houseman BT, Mrksich M (2002) Model Systems for Studying Polyvalent Carbohydrate Binding Interactions. *218*: 1–44
- Hricovíniová Z, see Petruš L (2001) *215*: 15–41
- Idee J-M, Tichowsky I, Port M, Petta M, Le Lem G, Le Greneur S, Meyer D, Corot C (2002) Iodinated Contrast Media: from Non-Specific to Blood-Pool Agents. *222*: 151–171
- Igau A, see Majoral J-P (2002) *220*: 53–77
- Imamoto T, see Crépy KVL (2003) *229*: 1–40
- Iwaoka M, Tomoda S (2000) Nucleophilic Selenium. *208*: 55–80
- Iwasawa N, Narasaka K (2000) Transition Metal Promoted Ring Expansion of Alkynyl- and Propadienylcyclopropanes. *207*: 69–88
- Imperiali B, McDonnell KA, Shogren-Knaak M (1999) Design and Construction of Novel Peptides and Proteins by Tailored Incorporation of Coenzyme Functionality. *202*: 1–38
- Ito S, see Yoshifuji M (2003) *223*: 67–89
- Jacques V, Desreux JF (2002) New Classes of MRI Contrast Agents. *221*: 123–164
- James TD, Shinkai S (2002) Artificial Receptors as Chemosensors for Carbohydrates. *218*: 159–200
- Janssen AJH, see Kleinjan WE (2003) *230*: 167–188
- Jenne A, see Famulok M (1999) *202*: 101–131
- Junker T, see Trauger SA (2003) *225*: 257–274
- Kaler EW, see Hentze H-P (2003) *226*: 197–223
- Kamerling JP, see Haseley SR (2002) *218*: 93–114
- Kashemirov BA, see Mc Kenna CE (2002) *220*: 201–238
- Kato S, see Murai T (2000) *208*: 177–199
- Katti KV, Pillarsetty N, Raghuraman K (2003) New Vistas in Chemistry and Applications of Primary Phosphines. *229*: 121–141
- Kawa M (2003) Antenna Effects of Aromatic Dendrons and Their Luminescence Applications. *228*: 193–204
- Kee TP, Nixon TD (2003) The Asymmetric Phospho-Aldol Reaction. Past, Present, and Future. *223*: 45–65
- Khlebnikov AF, see de Meijere A (2000) *207*: 89–147
- Kim K, see Lee JW (2003) *228*: 111–140
- Kirtman B (1999) Local Space Approximation Methods for Correlated Electronic Structure Calculations in Large Delocalized Systems that are Locally Perturbed. *203*: 147–166
- Kita Y, see Tohma H (2003) *224*: 209–248
- Kleij AW, see Kreiter R (2001) *217*: 163–199
- Klein Gebbink RJM, see Kreiter R (2001) *217*: 163–199
- Kleinjan WE, de Keizer A, Janssen AJH (2003) Biologically Produced Sulfur. *230*: 167–188
- Klibanov AL (2002) Ultrasound Contrast Agents: Development of the Field and Current Status. *222*: 73–106
- Klopper W, Kutzelnigg W, Müller H, Noga J, Vogtner S (1999) Extremal Electron Pairs – Application to Electron Correlation, Especially the R12 Method. *203*: 21–42
- Knochel P, see Betzemeier B (1999) *206*: 61–78
- Koser GF (2003) C-Heteroatom-Bond Forming Reactions. *224*: 137–172
- Koser GF (2003) Heteroatom-Heteroatom-Bond Forming Reactions. *224*: 173–183
- Kosugi M, see Fugami K (2002) *219*: 87–130

- Kozhushkov SI, see de Meijere A (1999) 201: 1–42
Kozhushkov SI, see de Meijere A (2000) 207: 89–147
Kozhushkov SI, see de Meijere A (2000) 207: 149–227
Krause W (2002) Liver-Specific X-Ray Contrast Agents. 222: 173–200
Krause W, Hackmann-Schlichter N, Maier FK, Müller R (2000) Dendrimers in Diagnostics. 210: 261–308
Krause W, Schneider PW (2002) Chemistry of X-Ray Contrast Agents. 222: 107–150
Kräuter I, see Tovar GEM (2003) 227: 125–144
Kreiter R, Kleij AW, Klein Gebbink RJM, van Koten G (2001) Dendritic Catalysts. 217: 163–199
Krossing I (2003) Homoatomic Sulfur Cations. 230: 135–152
Kuhlmann J, Herrmann C (2000) Biophysical Characterization of the Ras Protein. 211: 61–116
Kunkely H, see Vogler A (2001) 213: 143–182
Kutzelnigg W, see Klopper W (1999) 203: 21–42
Lammertsma K (2003) Phosphinidenes. 229: 95–119
Landfester K (2003) Miniemulsions for Nanoparticle Synthesis. 227: 75–123
Lasne M-C, Perrio C, Rouden J, Barré L, Roeda D, Dolle F, Crouzel C (2002) Chemistry of b^+ -Emitting Compounds Based on Fluorine-18. 222: 201–258
Lawless LJ, see Zimmermann SC (2001) 217: 95–120
Leal-Calderon F, see Schmitt V (2003) 227: 195–215
Lee JW, Kim K (2003) Rotaxane Dendrimers. 228: 111–140
Le Greneur S, see Idee J-M (2002) 222: 151–171
Le Lem G, see Idee J-M (2002) 222: 151–171
Leitner W (1999) Reactions in Supercritical Carbon Dioxide ($scCO_2$). 206: 107–132
Lemon III BI, see Crooks RM (2001) 212: 81–135
Leung C-F, see Chow H-F (2001) 217: 1–50
Levitzi A (2000) Protein Tyrosine Kinase Inhibitors as Therapeutic Agents. 211: 1–15
Li G, Gouzy M-F, Fuhrhop J-H (2002) Recognition Processes with Amphiphilic Carbohydrates in Water. 218: 133–158
Li X, see Paldus J (1999) 203: 1–20
Licha K (2002) Contrast Agents for Optical Imaging. 222: 1–29
Linclau B, see Maul JJ (1999) 206: 79–105
Lindhorst TK (2002) Artificial Multivalent Sugar Ligands to Understand and Manipulate Carbohydrate-Protein Interactions. 218: 201–235
Lindhorst TK, see Röckendorf N (2001) 217: 201–238
Liu S, Edwards DS (2002) Fundamentals of Receptor-Based Diagnostic Metalloradiopharmaceuticals. 222: 259–278
Liz-Marzán L, see Mulvaney P (2003) 226: 225–246
Loudet JC, Poulin P (2003) Monodisperse Aligned Emulsions from Demixing in Bulk Liquid Crystals. 226: 173–196
Lubineau A, Augé J (1999) Water as Solvent in Organic Synthesis. 206: 1–39
Lundt I, Madsen R (2001) Synthetically Useful Base Induced Rearrangements of Aldonolactones. 215: 177–191
Loupy A (1999) Solvent-Free Reactions. 206: 153–207
Madsen R, see Lundt I (2001) 215: 177–191
Maestri M, see Balzani V (2003) 228: 159–191
Maier FK, see Krause W (2000) 210: 261–308
Majoral J-P, Caminade A-M (2003) What to do with Phosphorus in Dendrimer Chemistry. 223: 111–159
Majoral J-P, Igau A, Cadierno V, Zablocka M (2002) Benzyne-Zirconocene Reagents as Tools in Phosphorus Chemistry. 220: 53–77
Manners I (2002), see McWilliams AR (2002) 220: 141–167
March NH (1999) Localization via Density Functionals. 203: 201–230
Martin SF, see Hergenrother PJ (2000) 211: 131–167
Mashiko S, see Yokoyama S (2003) 228: 205–226
Masson S, see Gulea M (2003) 229: 161–198
Mathey F, see Carmichael D (2002) 220: 27–51

- Maul JJ, Ostrowski PJ, Ublacker GA, Linclau B, Curran DP (1999) Benzotrifluoride and Derivatives: Useful Solvents for Organic Synthesis and Fluorous Synthesis. *206*: 79–105
- McDonnell KA, see Imperiali B (1999) *202*: 1–38
- McKelvey CA, see Hentze H-P (2003) *226*: 197–223
- Mc Kenna CE, Kashemirov BA (2002) Recent Progress in Carbonylphosphonate Chemistry. *220*: 201–238
- McWilliams AR, Dorn H, Manners I (2002) New Inorganic Polymers Containing Phosphorus. *220*: 141–167
- Meijer EW, see Baars MWPL (2000) *210*: 131–182
- Merbach AE, see Tóth E (2002) *221*: 61–101
- Metzner P (1999) Thiocarbonyl Compounds as Specific Tools for Organic Synthesis. *204*: 127–181
- Meyer D, see Idee J-M (2002) *222*: 151–171
- Mezey PG (1999) Local Electron Densities and Functional Groups in Quantum Chemistry. *203*: 167–186
- Mikołajczyk M, Balczewski P (2003) Phosphonate Chemistry and Reagents in the Synthesis of Biologically Active and Natural Products. *223*: 161–214
- Mikołajczyk M, see Drabowicz J (2000) *208*: 143–176
- Miura M, Nomura M (2002) Direct Arylation via Cleavage of Activated and Unactivated C-H Bonds. *219*: 211–241
- Miyaura N (2002) Organoboron Compounds. *219*: 11–59
- Miyaura N, see Tamao K (2002) *219*: 1–9
- Möller M, see Sheiko SS (2001) *212*: 137–175
- Morales JC, see Rojo J (2002) *218*: 45–92
- Mori H, Müller A (2003) Hyperbranched (Meth)acrylates in Solution, in the Melt, and Grafted From Surfaces. *228*: 1–37
- Mrksich M, see Houseman BT (2002) *218*: 1–44
- Muci AR, Buchwald SL (2002) Practical Palladium Catalysts for C-N and C-O Bond Formation. *219*: 131–209
- Müllen K, see Wiesler U-M (2001) *212*: 1–40
- Müller A, see Mori H (2003) *228*: 1–37
- Müller G (2000) Peptidomimetic SH2 Domain Antagonists for Targeting Signal Transduction. *211*: 17–59
- Müller H, see Klopper W (1999) *203*: 21–42
- Müller R, see Krause W (2000) *210*: 261–308
- Mulvaney P, Liz-Marzán L (2003) Rational Material Design Using Au Core-Shell Nanocrystals. *226*: 225–246
- Murai T, Kato S (2000) Selenocarbonyls. *208*: 177–199
- Muscat D, van Benthem RATM (2001) Hyperbranched Polyesteramides – New Dendritic Polymers. *212*: 41–80
- Naka K (2003) Effect of Dendrimers on the Crystallization of Calcium Carbonate in Aqueous Solution. *228*: 141–158
- Nakahama T, see Yokoyama S (2003) *228*: 205–226
- Nakayama J, Sugihara Y (1999) Chemistry of Thiophene 1,1-Dioxides. *205*: 131–195
- Namboothiri INN, Hassner A (2001) Stereoselective Intramolecular 1,3-Dipolar Cycloadditions. *216*: 1–49
- Narasaka K, see Iwasawa N (2000) *207*: 69–88
- Nierengarten J-F (2003) Fullerodendrimers: Fullerene-Containing Macromolecules with Intriguing Properties. *228*: 87–110
- Nishibayashi Y, Uemura S (2000) Selenoxide Elimination and [2,3] Sigmatropic Rearrangements. *208*: 201–233
- Nishibayashi Y, Uemura S (2000) Selenium Compounds as Ligands and Catalysts. *208*: 235–255
- Nixon TD, see Kee TP (2003) *223*: 45–65
- Noga J, see Klopper W (1999) *203*: 21–42
- Nomura M, see Miura M (2002) *219*: 211–241

- Nubbemeyer U (2001) Synthesis of Medium-Sized Ring Lactams. *216*: 125–196
- Nummelin S, Skrifvars M, Rissanen K (2000) Polyester and Ester Functionalized Dendrimers. *210*: 1–67
- Ober D, see Hemscheidt T (2000) *209*: 175–206
- Ochiai M (2003) Reactivities, Properties and Structures. *224*: 5–68
- Okruszek A, see Guga P (2002) *220*: 169–200
- Okuno Y, see Yokoyama S (2003) *228*: 205–226
- Onitsuka K, Takahashi S (2003) Metallo-dendrimers Composed of Organometallic Building Blocks. *228*: 39–63
- Osanai S (2001) Nickel (II) Catalyzed Rearrangements of Free Sugars. *215*: 43–76
- Ostrowski PJ, see Maul JJ (1999) *206*: 79–105
- Otomo A, see Yokoyama S (2003) *228*: 205–226
- Pak JJ, see Haley MM (1999) *201*: 81–129
- Paldus J, Li X (1999) Electron Correlation in Small Molecules: Grafting CI onto CC. *203*: 1–20
- Paleos CM, Tsiourvas D (2003) Molecular Recognition and Hydrogen-Bonded Amphiphilicities. *227*: 1–29
- Paulmier C, see Ponthieux S (2000) *208*: 113–142
- Penadés S, see Rojo J (2002) *218*: 45–92
- Perrio C, see Lasne M-C (2002) *222*: 201–258
- Peruzzini M, see Ehses M (2002) *220*: 107–140
- Peters JA, see Frullano L (2002) *221*: 25–60
- Petrie S, Bohme DK (2003) Mass Spectrometric Approaches to Interstellar Chemistry. *225*: 35–73
- Petruš L, Petrušová M, Hricovíniová (2001) The Bílik Reaction. *215*: 15–41
- Petrušová M, see Petruš L (2001) *215*: 15–41
- Petta M, see Idee J-M (2002) *222*: 151–171
- Pichot C, see Elaissari A (2003) *227*: 169–193
- Pillarsetty N, see Katti KV (2003) *229*: 121–141
- Pipek J, Bogár F (1999) Many-Body Perturbation Theory with Localized Orbitals – Kapuy's Approach. *203*: 43–61
- Plattner DA (2003) Metalorganic Chemistry in the Gas Phase: Insight into Catalysis. *225*: 149–199
- Ponthieux S, Paulmier C (2000) Selenium-Stabilized Carbanions. *208*: 113–142
- Port M, see Idee J-M (2002) *222*: 151–171
- Poulin P, see Loudet JC (2003) *226*: 173–196
- Raghuraman K, see Katti KV (2003) *229*: 121–141
- Raimondi M, Cooper DL (1999) Ab Initio Modern Valence Bond Theory. *203*: 105–120
- Reinhoudt DN, see van Manen H-J (2001) *217*: 121–162
- Renaud P (2000) Radical Reactions Using Selenium Precursors. *208*: 81–112
- Richardson N, see Schwert DD (2002) *221*: 165–200
- Rigaut S, see Astruc D (2000) *210*: 229–259
- Riley MJ (2001) Geometric and Electronic Information From the Spectroscopy of Six-Coordinate Copper(II) Compounds. *214*: 57–80
- Rissanen K, see Nummelin S (2000) *210*: 1–67
- Røeggen I (1999) Extended Geminal Models. *203*: 89–103
- Röckendorf N, Lindhorst TK (2001) Glycodendrimers. *217*: 201–238
- Roeda D, see Lasne M-C (2002) *222*: 201–258
- Rohovec J, see Frullano L (2002) *221*: 25–60
- Rojo J, Morales JC, Penadés S (2002) Carbohydrate-Carbohydrate Interactions in Biological and Model Systems. *218*: 45–92
- Romerosa A, see Ehses M (2002) *220*: 107–140
- Rouden J, see Lasne M-C (2002) *222*: 201258
- Ruano JLG, de la Plata BC (1999) Asymmetric [4+2] Cycloadditions Mediated by Sulfoxides. *204*: 1–126
- Ruiz J, see Astruc D (2000) *210*: 229–259
- Rychnovsky SD, see Sinz CJ (2001) *216*: 51–92

- Saláün J (2000) Cyclopropane Derivates and their Diverse Biological Activities. *207*: 1–67
- Sanz-Cervera JF, see Williams RM (2000) *209*: 97–173
- Sartor V, see Astruc D (2000) *210*: 229–259
- Sato S, see Furukawa N (1999) *205*: 89–129
- Saudan C, see Balzani V (2003) *228*: 159–191
- Scherf U (1999) Oligo- and Polyarylenes, Oligo- and Polyarylenevinylenes. *201*: 163–222
- Schlenk C, see Frey H (2000) *210*: 69–129
- Schmitt V, Leal-Calderon F, Bibette J (2003) Preparation of Monodisperse Particles and Emulsions by Controlled Shear. *227*: 195–215
- Schoeller WW (2003) Donor-Acceptor Complexes of Low-Coordinated Cationic p-Bonded Phosphorus Systems. *229*: 75–94
- Schröder D, Schwarz H (2003) Diastereoselective Effects in Gas-Phase Ion Chemistry. *225*: 129–148
- Schwarz H, see Schröder D (2003) *225*: 129–148
- Schwert DD, Davies JA, Richardson N (2002) Non-Gadolinium-Based MRI Contrast Agents. *221*: 165–200
- Sheiko SS, Möller M (2001) Hyperbranched Macromolecules: Soft Particles with Adjustable Shape and Capability to Persistent Motion. *212*: 137–175
- Shen B (2000) The Biosynthesis of Aromatic Polyketides. *209*: 1–51
- Shinkai S, see James TD (2002) *218*: 159–200
- Shirakawa E, see Hiyama T (2002) *219*: 61–85
- Shogren-Knaak M, see Imperiali B (1999) *202*: 1–38
- Sinou D (1999) Metal Catalysis in Water. *206*: 41–59
- Sinz CJ, Rychnovsky SD (2001) 4-Acetoxy- and 4-Cyano-1,3-dioxanes in Synthesis. *216*: 51–92
- Siuzdak G, see Trauger SA (2003) *225*: 257–274
- Skrifvars M, see Nummelin S (2000) *210*: 1–67
- Smith DK, Diederich F (2000) Supramolecular Dendrimer Chemistry – A Journey Through the Branched Architecture. *210*: 183–227
- Stec WJ, see Guga P (2002) *220*: 169–200
- Stedel R (2003) Aqueous Sulfur Sols. *230*: 153–166
- Stedel R (2003) Liquid Sulfur. *230*: 80–116
- Stedel R, Eckert B (2003) Solid Sulfur Allotropes. *230*: 1–79
- Stedel R, Stedel Y, Wong MW (2003) Speciation and Thermodynamics of Sulfur Vapor. *230*: 117–134
- Stedel Y, see Stedel R (2003) *230*: 117–134
- Steward LE, see Gilmore MA (1999) *202*: 77–99
- Stocking EM, see Williams RM (2000) *209*: 97–173
- Streubel R (2003) Transient Nitrilium Phosphanylid Complexes: New Versatile Building Blocks in Phosphorus Chemistry. *223*: 91–109
- Stütz AE, see Häusler H (2001) *215*: 77–114
- Sugihara Y, see Nakayama J (1999) *205*: 131–195
- Sugiura K (2003) An Adventure in Macromolecular Chemistry Based on the Achievements of Dendrimer Science: Molecular Design, Synthesis, and Some Basic Properties of Cyclic Porphyrin Oligomers to Create a Functional Nano-Sized Space. *228*: 65–85
- Sun J-Q, Bartlett RJ (1999) Modern Correlation Theories for Extended, Periodic Systems. *203*: 121–145
- Sun L, see Crooks RM (2001) *212*: 81–135
- Surján PR (1999) An Introduction to the Theory of Geminals. *203*: 63–88
- Taillefer M, Cristau H-J (2003) New Trends in Ylide Chemistry. *229*: 41–73
- Takahashi S, see Onitsuka K (2003) *228*: 39–63
- Tamao K, Miyaura N (2002) Introduction to Cross-Coupling Reactions. *219*: 1–9
- ten Holte P, see Zwanenburg B (2001) *216*: 93–124
- Thiem J, see Werschkun B (2001) *215*: 293–325
- Thutewohl M, see Waldmann H (2000) *211*: 117–130
- Tichkowsky I, see Idee J-M (2002) *222*: 151–171
- Tiecco M (2000) Electrophilic Selenium, Selenocyclizations. *208*: 7–54

- Tohma H, Kita Y (2003) Synthetic Applications (Total Synthesis and Natural Product Synthesis). *224*: 209–248
- Tomoda S, see Iwaoka M (2000) *208*: 55–80
- Tóth E, Helm L, Merbach AE (2002) Relaxivity of MRI Contrast Agents. *221*: 61–101
- Tovar GEM, Kräuter I, Gruber C (2003) Molecularly Imprinted Polymer Nanospheres as Fully Affinity Receptors. *227*: 125–144
- Trauger SA, Junker T, Siuzdak G (2003) Investigating Viral Proteins and Intact Viruses with Mass Spectrometry. *225*: 257–274
- Tromas C, García R (2002) Interaction Forces with Carbohydrates Measured by Atomic Force Microscopy. *218*: 115–132
- Tsiourvas D, see Paleos CM (2003) *227*: 1–29
- Turecek F (2003) Transient Intermediates of Chemical Reactions by Neutralization-Reionization Mass Spectrometry. *225*: 75–127
- Ublacker GA, see Maul JJ (1999) *206*: 79–105
- Uemura S, see Nishibayashi Y (2000) *208*: 201–233
- Uemura S, see Nishibayashi Y (2000) *208*: 235–255
- Uggerud E (2003) Physical Organic Chemistry of the Gas Phase. Reactivity Trends for Organic Cations. *225*: 1–34
- Valdemoro C (1999) Electron Correlation and Reduced Density Matrices. *203*: 187–200
- Valério C, see Astruc D (2000) *210*: 229–259
- van Benthem RATM, see Muscat D (2001) *212*: 41–80
- van Koten G, see Kreiter R (2001) *217*: 163–199
- van Manen H-J, van Veggel FCJM, Reinhoudt DN (2001) Non-Covalent Synthesis of Metallo-dendrimers. *217*: 121–162
- van Veggel FCJM, see van Manen H-J (2001) *217*: 121–162
- Varvoglis A (2003) Preparation of Hypervalent Iodine Compounds. *224*: 69–98
- Verkade JG (2003) P(RNCH₂CH₂)₃N: Very Strong Non-ionic Bases Useful in Organic Synthesis. *223*: 1–44
- Vicinelli V, see Balzani V (2003) *228*: 159–191
- Vliegenthart JFG, see Haseley SR (2002) *218*: 93–114
- Vogler A, Kunkely H (2001) Luminescent Metal Complexes: Diversity of Excited States. *213*: 143–182
- Vogtner S, see Klopfer W (1999) *203*: 21–42
- Vostrowsky O, see Hirsch A (2001) *217*: 51–93
- Waldmann H, Thutewohl M (2000) Ras-Farnesyltransferase-Inhibitors as Promising Anti-Tumor Drugs. *211*: 117–130
- Wang G-X, see Chow H-F (2001) *217*: 1–50
- Weil T, see Wiesler U-M (2001) *212*: 1–40
- Werschkun B, Thiem J (2001) Claisen Rearrangements in Carbohydrate Chemistry. *215*: 293–325
- Wiesler U-M, Weil T, Müllen K (2001) Nanosized Polyphenylene Dendrimers. *212*: 1–40
- Williams RM, Stocking EM, Sanz-Cervera JF (2000) Biosynthesis of Prenylated Alkaloids Derived from Tryptophan. *209*: 97–173
- Wirth T (2000) Introduction and General Aspects. *208*: 1–5
- Wirth T (2003) Introduction and General Aspects. *224*: 1–4
- Wirth T (2003) Oxidations and Rearrangements. *224*: 185–208
- Wong MW, see Steudel R (2003) *230*: 117–134
- Wrodnigg TM, Eder B (2001) The Amadori and Heyns Rearrangements: Landmarks in the History of Carbohydrate Chemistry or Unrecognized Synthetic Opportunities? *215*: 115–175
- Wytenbach T, Bowers MT (2003) Gas-Phase Confirmations: The Ion Mobility/Ion Chromatography Method. *225*: 201–226
- Yamaguchi H, Harada A (2003) Antibody Dendrimers. *228*: 237–258
- Yersin H, Donges D (2001) Low-Lying Electronic States and Photophysical Properties of Organometallic Pd(II) and Pt(II) Compounds. Modern Research Trends Presented in Detailed Case Studies. *214*: 81–186
- Yeung LK, see Crooks RM (2001) *212*: 81–135

- Yokoyama S, Otomo A, Nakahama T, Okuno Y, Mashiko S (2003) Dendrimers for Optoelectronic Applications. *228*: 205–226
- Yoshifuji M, Ito S (2003) Chemistry of Phosphanylidene Carbenoids. *223*: 67–89
- Zablocka M, see Majoral J-P (2002) *220*: 53–77
- Zhang J, see Chow H-F (2001) *217*: 1–50
- Zhdankin VV (2003) C-C Bond Forming Reactions. *224*: 99–136
- Zhao M, see Crooks RM (2001) *212*: 81–135
- Zimmermann SC, Lawless LJ (2001) Supramolecular Chemistry of Dendrimers. *217*: 95–120
- Zwanenburg B, ten Holte P (2001) The Synthetic Potential of Three-Membered Ring Azaheterocycles. *216*: 93–124

Subject Index

- Acidithiobacillus ferrooxidans 167, 177
Acidoid sol 161, 163
Agriculture 184–185
Allochromatium vinosum 172, 174–176
Allotropes 1, 3–4, 12, 17, 19, 47, 54–57
–, high-pressure 59
Aqueous sulfur sol 154
Assimilatory reduction 169
Aten's sulfur 17
- β -Po structure 70
Bacteria 171, 172
–, sulfate reducing 169
bco sulfur 70
Beggiatoa alba 172, 174, 176
Biogas 181
Bioleaching 167, 184, 186
Bioreactor 178, 183–184
Bioscrubber 183
Biosulfur 168, 183, 185
Bond length 51
Branched rings 81, 103–104, 109, 117, 127, 129, 132
- Catenane-like molecules 112
Cell membrane 172, 174–175, 177, 181
Claus process 82, 181
Coordination number 62
Crystex 15, 45–47, 55, 89
Cyanobacteria 171
Cytoplasmic membrane 181
- Density
–, crystalline sulfur 56, 176
–, liquid sulfur 83, 176
–, sulfur globules 176
Depolymerization 53
Desulfurization, wastewater 153–154, 164
DFT calculation of sulfur cation 139–142
Diamond anvil cell 60
Dichlorodisulfane 5, 11
Dichlorotetrasulfane 8
- Dicyanohexasulfane 8
Diradical, chain-length 91
Displacement reaction 91
Dissimilatory reduction 169
DLVO-theory 172
Dynamic light scattering 178
- Engel's sulfur 17
- $F_2S=S$ 129
Flavocytochrome c 180
Floor temperature 111
Flowers of sulfur 15
Frasch process 82
Free radical 57, 86, 90–91, 103, 105, 112
- Gas absorber 183–184
Geller's phase I 49
- Halorhodospira abdelmalekii 181
Helix 41
Hexasulfane 105
High-pressure/high-temperature phase 67
Hydrodesulfurization process 82
Hydrogen sulfide 157, 164
–, oxidation 154, 162–163
–, removal 181
- Isoelectric point 173, 179
- LaMer sulfur sol 157
Landfill 184
Liquid sulfur 10, 81–97, 101–113, 118, 122, 125–128
–, band gap 103
–, color 102–103, 105
–, conductivity 107
–, dielectric constant 107
–, diradical 127–128
–, electrical conductivity 106
–, magnetic susceptibility 91
–, photochemical polymerization 109

- , photochemistry 105
- , physical properties 83, 92, 109
- , polymer content 88
- , polymerization 90, 108–109
- , properties 81
- , quantitative composition 98
- , Raman spectra 95
- , reflectance spectra 105
- , UV-Vis spectroscopy 102
- , vibrational spectroscopy 94, 97, 104
- , viscosity 92
- , -, impact of halogens 93
- , -, minimum 112

- Macromolecular sulfur 41
- Melting point 52
- Metallic state 63
- Metallization 62
- Motif 17, 34, 50

- Natural gas 181

- Odén's colloidal sulfur 157
- Optical absorption edge 63

- Periplasmic space 181
- Phase diagram 60–61
- Photoinduced structural change 63
- Photoreaction 63
- Photosynthesis 171
- Plastic sulfur 43
- Polyelectrolytes 174
- Polymer adsorption 174
- , preparation 87
- , rate of formation 90
- , structure 42
- Polymerization theory 81
- Polysulfanes 92–93
- Polysulfide 176, 179, 183
- , oxidation 184
- Polythionate 156–159, 161, 164, 167, 176, 178–179, 186
- Protein membrane 177

- Quantum chemical calculation, sulfur cation 140–141

- Raffo sol 154, 157–160, 162
- , aging 159–162
- , density 158–160
- , sulfur content 156, 158–159
- Raman spectroscopy 64, 176
- Ring, large 81, 88, 90, 110, 112
- Ring opening polymerization 108

- S 41
- S_{μ} 15, 43, 89
- S_{ω} 43
- $S_{\omega 1}$ 45, 47
- $S_{\omega 2}$ 45
- S_x 11
- S_y 43, 44
- S_1 41
- S_3 117, 120–122, 124–125, 132
- , vibrational wavenumber 131
- S_4 117–132
- , fundamental vibration 124
- , vibrational wavenumber 130
- S_4^{2+} , gas phase dissociation enthalpy 143
- S_6 17, 18, 30, 31
- , high-pressure/high-temperature phase 65
- , preparation 4, 9
- S_7 19–21, 106, 109, 127
- , allotrope 19
- , concentration in liquid sulfur 96
- , preparation 1, 6
- , pseudorotation 19
- , strain energy 21
- S_8 117–119
- , allotropes 21
- , entropy, vibrational assignment 120
- , molecular structure 22
- , order-disorder transition 26
- , preparation 6
- , strain energy 22
- , thermal expansion 21
- S_9 29
- , preparation 8
- S_{10} 29
- , preparation 8
- S_{11} 32
- , preparation 9
- S_{12} 34
- , preparation 10
- , $\cdot CS_2$ 11, 96
- S_{13} 35
- , preparation 11
- S_{14} 36
- , preparation 12
- S_{15} 37
- , preparation 12
- S_{18} 37
- , preparation 1, 13
- S_{20} 38
- , preparation 13
- S-S bond 128
- , dissociation enthalpy 128
- , distance 51

- Selmi sol 154, 157, 159, 161–164
Semiconductor 62
Settler 183
 S_n molecule, enthalpy/entropy 119–122, 125, 128–129, 132
 SO_2 emission 181, 185
Sol 153–162
–, monodispersed 155
Sour gas 82
Stabilizer 15
Steric stabilization 167, 173–174
Structure, high-pressure phase 69
Sulfane monosulfonic acid 158, 161–162
Sulfate reducing bacteria 169
Sulfide, chemical oxidation 179
–, oxidation 171
– radicals 180
Sulfur, colloidal 153, 154, 164
–, commercial 6, 92, 102
–, fibrous 15, 43, 45
–, flowers 15
–, high-purity 7
–, insoluble 15
–, laminar 45
–, macromolecular 41
–, polymeric 14, 56, 81–99, 102, 105–108, 112–113
–, superconducting 60
 ϵ -Sulfur 17
 μ -Sulfur 87
–, properties 81, 84, 89
 π -Sulfur 84, 90, 98–107, 118–128, 153–164
–, critical parameter 101
–, helical structure 67
–, high purity 92
–, melting curve 61
–, melting point depression 85
–, metallic liquid 61
–, molecular nature 84, 87
–, preparation 84, 87
–, properties 81, 84
–, Raman spectra 94, 96
–, quantum-chemical calculation 117, 125
 ρ -Sulfur 17
Sulfur allotropes 1, 3–4, 12, 17, 19, 47, 54–57
– –, analysis 59
– –, density 56
– –, nomenclature 41
– –, photochemical behavior 57
– –, physical properties 52
– –, Raman spectra 94–95
– –, solubility 55
– –, thermal behavior 53
Sulfur bacteria 153–154, 163–164, 167–169, 171
Sulfur cation, enthalpy of formation 143
– –, hyperconjugation 149–150
– –, π bonding 146–148
– –, radical 138–139, 144, 146
– –, solid state structure 137
– –, solvation energy 144
– –, synthetic procedure 137
Sulfur chain, long 14
– –, –, branched 105
Sulfur cycle, biological 168
Sulfur compound oxidizing bacteria 167–181, 185
–, alkaliphilic 172, 183
Sulfur globules 167–181, 185
– –, *Allochromatium vinosum* 176
– –, *Beggiatoa alba* 176
Sulfur helix 48
Sulfur homocycle
–, enthalpies of formation 101
–, isomer 39
–, mean bond energy 101
–, retention time 98
Sulfur inclusion envelope 177
Sulfur melts
–, birefringence 89
–, doping 92
–, ESR spectra 91
–, fractional crystallization 94
–, glass-transition temperature 89
–, HPLC 97
–, Raman spectra 89, 94–95
Sulfur molecule, HOMO/LUMO gap 104
Sulfur radical cation 138–139, 144, 146
Sulfur ring 55
– –, branched 128
– –, Raman spectra 94
Sulfur sol, hydrophilic/hydrophobic 153–157, 160, 162
– –, LaMer 157
Sulfur vapor 117–119, 124–132
–, composition 117–129, 132
–, density 121, 124, 126
–, mass spectrometry 118–127, 132
–, partial pressure 120–121, 126
–, speciation, thermodynamic 117, 120–122, 125, 128
–, UV-Vis spectra 124
–, vibrational spectra 120–122, 129
Sulfurdichloride 5
Sulfuretum 169
Sulfuric acid production 184–185
Superconducting state 60, 70
Surface charge density 179

- Surfactant 56
Syngas 181
- Ta₄P₄S₂₉ 49
Tetrathiasulfuranes 113
Tetrathionate 157, 163
Thiobacillus spp. 167, 172
Thiocapsa roseopersicina 177
Thiosulfate 4, 154, 157–160, 163
Torsional barrier 50
Triple Point 61
- van der Waals attraction 172
Van Niel reaction 171
Vesicles 167, 178, 185
- Wackenroder's solution 154
Wastewater desulfurization 153–154, 164
Weimarn sol 153–156
– –, stabilization by surfactants 155
- X-ray diffraction 175, 178
XANES 176, 178
- Zero charge, point of 173

Subject Index

- Acidithiobacillus ferrooxidans 167, 177
Acidoid sol 161, 163
Agriculture 184–185
Allochromatium vinosum 172, 174–176
Allotropes 1, 3–4, 12, 17, 19, 47, 54–57
–, high-pressure 59
Aqueous sulfur sol 154
Assimilatory reduction 169
Aten's sulfur 17
- β -Po structure 70
Bacteria 171, 172
–, sulfate reducing 169
bco sulfur 70
Beggiatoa alba 172, 174, 176
Biogas 181
Bioleaching 167, 184, 186
Bioreactor 178, 183–184
Bioscrubber 183
Biosulfur 168, 183, 185
Bond length 51
Branched rings 81, 103–104, 109, 117, 127, 129, 132
- Catenane-like molecules 112
Cell membrane 172, 174–175, 177, 181
Claus process 82, 181
Coordination number 62
Crystex 15, 45–47, 55, 89
Cyanobacteria 171
Cyttoplasmic membrane 181
- Density
–, crystalline sulfur 56, 176
–, liquid sulfur 83, 176
–, sulfur globules 176
Depolymerization 53
Desulfurization, wastewater 153–154, 164
DFT calculation of sulfur cation 139–142
Diamond anvil cell 60
Dichlorodisulfane 5, 11
Dichlorotetrasulfane 8
- Dicyanohexasulfane 8
Diradical, chain-length 91
Displacement reaction 91
Dissimilatory reduction 169
DLVO-theory 172
Dynamic light scattering 178
- Engel's sulfur 17
- $F_2S=S$ 129
Flavocytochrome c 180
Floor temperature 111
Flowers of sulfur 15
Frasch process 82
Free radical 57, 86, 90–91, 103, 105, 112
- Gas absorber 183–184
Geller's phase I 49
- Halorhodospira abdelmalekii 181
Helix 41
Hexasulfane 105
High-pressure/high-temperature phase 67
Hydrodesulfurization process 82
Hydrogen sulfide 157, 164
–, oxidation 154, 162–163
–, removal 181
- Isoelectric point 173, 179
- LaMer sulfur sol 157
Landfill 184
Liquid sulfur 10, 81–97, 101–113, 118, 122, 125–128
–, band gap 103
–, color 102–103, 105
–, conductivity 107
–, dielectric constant 107
–, diradical 127–128
–, electrical conductivity 106
–, magnetic susceptibility 91
–, photochemical polymerization 109

- , photochemistry 105
- , physical properties 83, 92, 109
- , polymer content 88
- , polymerization 90, 108–109
- , properties 81
- , quantitative composition 98
- , Raman spectra 95
- , reflectance spectra 105
- , UV-Vis spectroscopy 102
- , vibrational spectroscopy 94, 97, 104
- , viscosity 92
- , -, impact of halogens 93
- , -, minimum 112

- Macromolecular sulfur 41
- Melting point 52
- Metallic state 63
- Metallization 62
- Motif 17, 34, 50

- Natural gas 181

- Odén's colloidal sulfur 157
- Optical absorption edge 63

- Periplasmic space 181
- Phase diagram 60–61
- Photoinduced structural change 63
- Photoreaction 63
- Photosynthesis 171
- Plastic sulfur 43
- Polyelectrolytes 174
- Polymer adsorption 174
- , preparation 87
- , rate of formation 90
- , structure 42
- Polymerization theory 81
- Polysulfanes 92–93
- Polysulfide 176, 179, 183
- , oxidation 184
- Polythionate 156–159, 161, 164, 167, 176, 178–179, 186
- Protein membrane 177

- Quantum chemical calculation, sulfur cation 140–141

- Raffo sol 154, 157–160, 162
- , aging 159–162
- , density 158–160
- , sulfur content 156, 158–159
- Raman spectroscopy 64, 176
- Ring, large 81, 88, 90, 110, 112
- Ring opening polymerization 108

- S 41
- S_{μ} 15, 43, 89
- S_{ω} 43
- $S_{\omega 1}$ 45, 47
- $S_{\omega 2}$ 45
- S_x 11
- S_y 43, 44
- S_1 41
- S_3 117, 120–122, 124–125, 132
- , vibrational wavenumber 131
- S_4 117–132
- , fundamental vibration 124
- , vibrational wavenumber 130
- S_4^{2+} , gas phase dissociation enthalpy 143
- S_6 17, 18, 30, 31
- , high-pressure/high-temperature phase 65
- , preparation 4, 9
- S_7 19–21, 106, 109, 127
- , allotrope 19
- , concentration in liquid sulfur 96
- , preparation 1, 6
- , pseudorotation 19
- , strain energy 21
- S_8 117–119
- , allotropes 21
- , entropy, vibrational assignment 120
- , molecular structure 22
- , order-disorder transition 26
- , preparation 6
- , strain energy 22
- , thermal expansion 21
- S_9 29
- , preparation 8
- S_{10} 29
- , preparation 8
- S_{11} 32
- , preparation 9
- S_{12} 34
- , preparation 10
- , $\cdot CS_2$ 11, 96
- S_{13} 35
- , preparation 11
- S_{14} 36
- , preparation 12
- S_{15} 37
- , preparation 12
- S_{18} 37
- , preparation 1, 13
- S_{20} 38
- , preparation 13
- S-S bond 128
- , dissociation enthalpy 128
- , distance 51

- Selmi sol 154, 157, 159, 161–164
Semiconductor 62
Settler 183
 S_n molecule, enthalpy/entropy 119–122, 125, 128–129, 132
 SO_2 emission 181, 185
Sol 153–162
–, monodispersed 155
Sour gas 82
Stabilizer 15
Steric stabilization 167, 173–174
Structure, high-pressure phase 69
Sulfane monosulfonic acid 158, 161–162
Sulfate reducing bacteria 169
Sulfide, chemical oxidation 179
–, oxidation 171
– radicals 180
Sulfur, colloidal 153, 154, 164
–, commercial 6, 92, 102
–, fibrous 15, 43, 45
–, flowers 15
–, high-purity 7
–, insoluble 15
–, laminar 45
–, macromolecular 41
–, polymeric 14, 56, 81–99, 102, 105–108, 112–113
–, superconducting 60
 ϵ -Sulfur 17
 μ -Sulfur 87
–, properties 81, 84, 89
 π -Sulfur 84, 90, 98–107, 118–128, 153–164
–, critical parameter 101
–, helical structure 67
–, high purity 92
–, melting curve 61
–, melting point depression 85
–, metallic liquid 61
–, molecular nature 84, 87
–, preparation 84, 87
–, properties 81, 84
–, Raman spectra 94, 96
–, quantum-chemical calculation 117, 125
 ρ -Sulfur 17
Sulfur allotropes 1, 3–4, 12, 17, 19, 47, 54–57
– –, analysis 59
– –, density 56
– –, nomenclature 41
– –, photochemical behavior 57
– –, physical properties 52
– –, Raman spectra 94–95
– –, solubility 55
– –, thermal behavior 53
Sulfur bacteria 153–154, 163–164, 167–169, 171
Sulfur cation, enthalpy of formation 143
– –, hyperconjugation 149–150
– –, π bonding 146–148
– –, radical 138–139, 144, 146
– –, solid state structure 137
– –, solvation energy 144
– –, synthetic procedure 137
Sulfur chain, long 14
– –, –, branched 105
Sulfur cycle, biological 168
Sulfur compound oxidizing bacteria 167–181, 185
–, alkaliphilic 172, 183
Sulfur globules 167–181, 185
– –, *Allochromatium vinosum* 176
– –, *Beggiatoa alba* 176
Sulfur helix 48
Sulfur homocycle
–, enthalpies of formation 101
–, isomer 39
–, mean bond energy 101
–, retention time 98
Sulfur inclusion envelope 177
Sulfur melts
–, birefringence 89
–, doping 92
–, ESR spectra 91
–, fractional crystallization 94
–, glass-transition temperature 89
–, HPLC 97
–, Raman spectra 89, 94–95
Sulfur molecule, HOMO/LUMO gap 104
Sulfur radical cation 138–139, 144, 146
Sulfur ring 55
– –, branched 128
– –, Raman spectra 94
Sulfur sol, hydrophilic/hydrophobic 153–157, 160, 162
– –, LaMer 157
Sulfur vapor 117–119, 124–132
–, composition 117–129, 132
–, density 121, 124, 126
–, mass spectrometry 118–127, 132
–, partial pressure 120–121, 126
–, speciation, thermodynamic 117, 120–122, 125, 128
–, UV-Vis spectra 124
–, vibrational spectra 120–122, 129
Sulfurdichloride 5
Sulfuretum 169
Sulfuric acid production 184–185
Superconducting state 60, 70
Surface charge density 179

- Surfactant 56
Syngas 181
- Ta₄P₄S₂₉ 49
Tetrathiasulfuranes 113
Tetrathionate 157, 163
Thiobacillus spp. 167, 172
Thiocapsa roseopersicina 177
Thiosulfate 4, 154, 157–160, 163
Torsional barrier 50
Triple Point 61
- van der Waals attraction 172
Van Niel reaction 171
Vesicles 167, 178, 185
- Wackenroder's solution 154
Wastewater desulfurization 153–154, 164
Weimarn sol 153–156
– –, stabilization by surfactants 155
- X-ray diffraction 175, 178
XANES 176, 178
- Zero charge, point of 173

Reviews and Monographs on the Chemistry of Sulfur-Rich Compounds

(ordered chronologically)

Gmelin Handbook of Inorganic Chemistry, 8th ed., *Sulfur*, Springer, Berlin:

- 1953**: Hydrides and Oxides of Sulfur (in German)
- 1953**: Elemental Sulfur (in German)
- 1953**: Occurrence and Technology of Sulfur and Its Compounds
(in German)
- 1960**: Sulfur Oxoacids (in German)
- 1963**: Sulfur Compounds with Nitrogen, Oxygen and Halides (in German)
- 1977**: Sulfur-Nitrogen Compounds, Part 1 (in German)
- 1978**: Sulfur Halides (in German)
- 1978**: Thionyl Halides (in German)
- 1980**: Sulfur Oxides (in German)
- 1983**: Sulfanes (in English)
- 1985-1994**: Sulfur-Nitrogen Compounds, Parts 2-10 (in English)

B. Meyer, *Elemental Sulfur: Chemistry and Physics*, Interscience, New York,
1965; with Chapters on the following topics:

1. Nomenclature of Sulfur Allotropes
2. Structures of Solid Sulfur Allotropes
3. Phase Transition Rate Measurements
4. Preparation and Properties of Sulfur Allotropes
5. Properties of Polymeric Sulfur
6. Physical Properties of Liquid Sulfur
7. Molecular Composition of Sulfur Vapor
8. Mechanical Properties of Sulfur
9. High Pressure Behavior of Sulfur
10. Electrical and Photoconductive Properties of Orthorhombic Sulfur Crystals
11. ESR Studies of Unstable Sulfur Forms
12. Vibrational Spectra of Elemental Sulfur
13. Electronic Spectrum and Electronic States of S₂
14. Reactions of Atomic Sulfur
15. Reactions of the Sulfur-Sulfur Bond

16. Preparation of Unusual Sulfur Rings
17. Liquid Solutions of Sulfur
18. Potential Applications of Sulfur

F. Tuinstra, *Structural Aspects of the Allotropy of Sulfur and the Other Divalent Elements*, Waltman, Delft, **1967**.

G. Nickless (Ed.), *Inorganic Sulfur Chemistry*, Elsevier, Amsterdam, **1968**; with Chapters on the following topics:

1. The Sulfur Atom and its Nucleus
2. Orbitals in Sulfur and its Compounds
3. Stereochemistry of Group 16 Compounds
4. Mechanisms of Sulfur Reactions
5. Structural Studies on Sulfur Compounds
6. Analytical Chemistry of Sulfur Compounds
7. Elemental Sulfur
8. The Biogeochemical Sulfur Cycle
9. Chemistry of the Sulfur-Phosphorus Bond
10. Sulfanes
11. Oxides of Sulfur
12. Compounds with Sulfur-Halogen Bonds
13. Sulfur-Nitrogen Compounds
14. Lower Oxoacids of Sulfur
15. Sulfuric Acid
16. Fluorosulfuric Acid as a Solvent System
17. Amido- and Imidosulfuric Acid
18. Metal Sulfides

M. V. Ivanov, *Microbiological Processes in the Formation of Sulfur Deposits*, Jerusalem, **1968**.

A. V. Tobolsky (Ed.), *The Chemistry of Sulfides*, Interscience, New York, **1968**.

J. A. Karchmer (Ed.), *The Analytical Chemistry of Sulfur and its Compounds*, Part I, Wiley, New York, **1970**; with Chapters on following topics:

1. Elemental Sulfur

2. Total Sulfur
3. Sulfur-Containing Gases
4. Oxygen-Containing Inorganic sulfur Compounds
5. Other Inorganic Sulfur Compounds
6. Thiols

A. Senning (Ed.), *Sulfur in Organic and Inorganic Chemistry*, Vol. 1, Dekker, New York, **1971**, with Chapters on the following topics:

1. The Sulfur-Silicon Bond
2. The Sulfur-Nitrogen Bond
3. The Sulfur-Phosphorus Bond
4. The Sulfur-Oxygen Bond
5. The Sulfur-Sulfur Bond
6. The Sulfur-Fluorine Bond
7. The Sulfur-Chlorine Bond
8. The Sulfur-Bromine Bond
9. The Sulfur-Iodine Bond

A. Senning (Ed.), *Sulfur in Organic and Inorganic Chemistry*, Vol. 2, Dekker, New York, **1972**, with Chapters on the following topics:

1. Chemistry of Atomic Sulfur
2. Diatomic Species Containing Sulfur
3. Bond Energy Terms in the Chemistry of sulfur, Selenium and Tellurium
4. Oxyacids of Sulfur
5. Pharmacology and Toxicology of Inorganic Sulfur Compounds
6. Mass Spectra of Sulfur Compounds
7. Mixed Sulfur Halides
8. Commercially Important Sulfur Compounds
9. Chromatographic Techniques in Sulfur Chemistry

A. Senning (Ed.), *Sulfur in Organic and Inorganic Chemistry*, Vol. 3, Dekker, New York, **1972**, with Chapters on the following topics:

1. Reactions of Elemental Sulfur with Inorganic, Organic and Organometallic Compounds
2. Inorganic and Organic Polysulfides
3. Quantum Chemistry of sulfur Compounds
4. Steric Aspects of Sulfur Chemistry

5. NMR spectra of Sulfur Compounds
6. Labeled Sulfur Compounds
7. Thione-Enethiol Tautomerism
8. Nomenclature of Sulfur Compounds
9. Nucleophilicity of Organic Sulfur Compounds

J. A. Karchmer (Ed.), *The Analytical Chemistry of Sulfur and its Compounds*, Part II, Wiley, New York, **1972**; with Chapters on the following topics:

1. Sulfides
2. Di- and Polysulfides
3. Thiophenes
4. Tetra- and Hexavalent Organosulfur Compounds

D. J. Miller, T. K. Wiewiorowski (Eds.), *Sulfur Research Trends*, Adv. Chem. Ser. 110, ACS, Washington, **1972**; with Chapters on the following topics:

1. Semiempirical MO Calculations on Sulfur-Containing Molecules
2. Electron Behavior in Some Sulfur Compounds
3. Spectra of Sulfur Allotropes
4. Transition Metal Complexes with Sulfur-Donor Ligands
5. Structures of Sulfur-Nitrogen Compounds
6. Influence of High Pressure on Elemental Sulfur
7. Reactions of Mercaptanes with Liquid Sulfur
8. Photolysis of Thiols
9. Addition of Sulfur Atoms to Olefins
10. Sulfur Chlorides and Organochlorides
11. Raman Spectra of Amorphous Chalcogenide Alloys
12. Fluorinated Sulfide Polymers
13. Electrical Conductivity of Liquid Sulfur and Sulfur-Phosphorus Mixtures
14. Chemical-Mechanical Alteration of Elemental Sulfur
15. Potential Applications of Sulfur

M. Schmidt, W. Siebert, in *Comprehensive Inorganic Chemistry*, Vol. 2, Chapter 23 (Sulfur), Pergamon, Oxford, **1973**, pp. 795-933 (579 references).

K. C. Mills, *Thermodynamic Data for Inorganic Sulfides, Selenides and Tellurides*, Butterworths, London, **1974**.

D. M. Greenberg (Ed.), *Metabolic Pathways*, 3rd ed., Vol. VII: *Metabolism of Sulfur Compounds*, Academic Press, New York, **1975**.

G. Brauer (ed.), *Handbuch der Präparativen Anorganischen Chemie*, Vol. 1, Enke, Stuttgart, **1975** (Preparation of basic inorganic sulfur compounds).

B. Meyer, *Sulfur, Energy, and Environment*, Elsevier, Amsterdam, **1977** (containing 1600 references with full titles). Chapters on the following topics:.

1. History of Sulfur
2. Properties of sulfur and Inorganic Sulfur Compounds
3. Analytical Chemistry of Sulfur Compounds
4. Occurrence and Sources of Sulfur
5. The Sulfur Cycles
6. Sulfur Production
7. Recovery of Sulfur from Combustion Gases
8. Environmental Control and Legislation
9. Medical Use and Health Effects
10. Sulfur in Agriculture and Food
11. Industrial Uses of Sulfur and Its Compounds
12. Sulfur Polymers
13. Sulfur Containing Materials
14. Future Trends

D. J. Bourne (Ed.), *New Uses of Sulfur-II*, Adv. Chem. Ser. 165, ACS, Washington, **1978**.

H. G. Heal, *The Inorganic Heterocyclic Chemistry of Sulfur, Nitrogen and Phosphorus*, Academic Press, London, **1980**.

H. Bothe, A. Trebst (Eds.), *Biology of Inorganic Nitrogen and Sulfur*, Springer, Berlin, **1981**.

A. Senning (Ed.), *Sulfur in Organic and Inorganic Chemistry*, Vol.4, Dekker, New York, **1982**, with Chapters on the following topics:

1. The Sulfur-Silicon Bond
2. The Sulfur-Nitrogen Bond
3. The Sulfur-Phosphorus Bond
4. The Sulfur-Fluorine Bond
5. The Sulfur-Chlorine Bond
6. The Sulfur-Bromine Bond
7. The Sulfur-Iodine Bond

M. V. Ivanov, J. R. Freney (Eds.), *The Global Biochemical Sulfur Cycle*, SCOPE 19, Wiley, New York, **1983**.

A. Müller, B. Krebs (Eds.), *Sulfur - Its Significance for Chemistry, for the Geo-, Bio- and Cosmosphere and Technology*, Elsevier, Amsterdam, **1984**; with Chapters on the following topics:

1. Elemental Sulfur and Homocyclic Compounds and Ions (R. Steudel)
2. Sulfur in the Earth's Crust, Its Origin and Natural Cycle (K. H. Wedepohl)
3. Role of Sulfur in Black Powder (F. Seel)
4. Lapislazuli and Ultramarine Pigments (F. Seel)
5. New Developments in Organic Sulfur Chemistry (G. Kresze)
6. Organometallic Sulfur Compounds (H. Vahrenkamp)
7. Thiolates as Ligands in Transition Metal Complexes (J. R. Dilworth)
8. Metal Complexes of Sulfur and Sulfur-Nitrogen Compounds (H. W. Roesky)
9. Sulfido-Complexes of Molybdenum and Tungsten (A. G. Wedd)
10. Interaction of Metal Centers Through Sulfur-Containing Ligands (O. Kahn, J.-J. Girerd)
11. Electronic and Resonance Raman Spectra of Sulfur-Containing Complexes (R. J. H. Clark)
12. Technology of Sulfuric Acid (K. Brändle)
13. Flue Gas Desulfurization (M. Schmidt)
14. Metal Sulfides in Photovoltaic and Photoelectrochemical Energy Conversion (H. Tributsch)
15. Inorganic Chemistry of Rubber Vulcanization (J. A. McCleverty)
16. Biodegradation of Sulfur Minerals (K. Bosecker)
17. Microorganisms and the Sulfur Cycle (H. G. Trüper)

18. Phototrophic Bacteria and Their Sulfur Metabolism (H. G. Trüper)
19. Cytochromes and Iron Sulfur Proteins in Bacterial Sulfur Metabolism (U. Fischer)
20. Sulfur-Containing Ligands in Metalloproteins and Enzymes (W. E. Newton)
21. Genetic Diseases of Sulfur Metabolism in Humans (F. Skovby, S. H. Mudd)

F. Bernardi, I. G. Csizmadia, A. Mangini (Eds.), *Organic Sulfur Chemistry: Theoretical and Experimental Advances*, Elsevier, Amsterdam, **1985**.

I. Hargittai, *The Structure of Volatile Sulfur Compounds*, Reidel Publ., Dordrecht, **1985** (structures determined by electron diffraction and microwave spectroscopy).

R. J. Huxtable, *Biochemistry of Sulfur*, Plenum, New York, **1986**.

W. B. Jakoby, O. W. Griffith (Eds.), *Methods in Enzymology*, Vol. 143: *Sulfur and Sulfur Amino Acids*, Academic Press, Orlando, **1987**.

M. G. Voronkov, N. S. Vyazankin, E. N. Deryagina, A. S. Nakhmanovich, V. A. Usov, *Reactions of Sulfur with Organic Compounds*, Plenum Press, New York, **1987**; with Chapters on the following topics:

1. Structure and Physical Properties of Elemental Sulfur
2. Preparation and Chemical Properties of Sulfur Allotropes
3. Action of Sulfur on Hydrocarbons
4. Reactions with Organic Halides
5. Reactions with Organic Sulfur Compounds
6. Reactions with Oxygen-Containing Compounds
7. Reactions with Nitrogen-Containing Compounds
8. Reactions with Organometallic Compounds

B. Zwanenburg, A. J. H. Klunder (Eds.), *Perspectives in the Organic Chemistry of Sulfur*, Elsevier, Amsterdam, **1987**.

J. A. Cole, S. J. Ferguson (Eds.), *The Nitrogen and Sulfur Cycles*, Cambridge Univ. Press, Cambridge, **1988**.

R. T. Oakley, *Sulfur-Nitrogen Heterocycles*, *Progr. Inorg. Chem.* **1988**, 36, 299-391.

P. Brimblecombe, A. Yu. Lein (Eds.), *Evolution of the Biochemical Sulfur Cycle*, SCOPE 39, Wiley, New York, **1989**.

E. S. Saltzman, W. J. Cooper (Eds.), *Biogenic Sulfur in the Environment*, ACS Symp. Ser. 393, ACS, Washington DC, **1989**.

W. L. Orr, C. M. White, *Geochemistry of Sulfur in Fossil Fuels*, A.C.S. Symp. Ser., Vol. 429, American Chemical Society, Washington, **1990**.

C. Chatgililoglu, K.-D. Asmus (Eds.), *Sulfur-Centered Reactive Intermediates in Chemistry and Biology*, Plenum Press, New York, **1990**; *inter alia* with Chapters on the following topics:

1. Force Field and Molecular Orbital Calculations in Organosulfur Chemistry
2. Electronic Transitions in Sulfur-Centered Radicals
3. Electronic Properties of Sulfur-Containing Substituents and Molecules
4. Reactivity of Sulfur-Centered Nucleophiles
5. Alkenethiylperoxyl Radicals
6. Thermochemistry of Sulfur-Centered Intermediates
7. Single Electron Transfer in Nucleophilic Substitution
8. Electrochemical Reduction of Sulfur Compounds
9. Pulse Radiolysis
10. ESR Spectroscopy of Sulfur-Centered Radicals
11. Three-Electron Bonded Radicals
12. Radical Cations
13. Reaction Kinetics of Sulfur-Centered Biological Radicals
14. Redox Systems with Sulfur-Centered Species
15. Repair in Radiation Biology
16. Actions of the Glutathion/Disulfide System

S. Oae, *Organic Sulfur Chemistry: Structure and Mechanism*, CRC Press, Boca Raton, **1991**.

H. R. Krouse, V. A. Grinenko (Eds.), *Stable Isotopes: Natural and Anthropogenic Sulfur in the Environment*, SCOPE 43, Wiley, New York, **1991**.

R. W. Howarth, J. W. B. Stewart, M. V. Ivanov (Eds.), *Sulfur Cycling on the Continents*, SCOPE 48, Wiley, New York, **1991**.

S. Oae, T. Okuyama (Eds.), *Organic Sulfur Chemistry: Biochemical Aspects*, CRC Press, Boca Raton, **1992**.

R. B. King (Ed.), *Encyclopedia of Inorganic Chemistry*, Vol. 7, Wiley, Chichester, **1994**; *inter alia* with Chapters on the following topics:

1. Inorganic Sulfur Chemistry (D. Woollins)
2. Sulfur-Nitrogen Compounds (T. Chivers)
3. Organic Polysulfanes (R. Steudel, M. Kustos)
4. S-Donor Ligands (M. Schröder)

Ullmann's Encyclopedia of Industrial Chemistry, Vol. A25, VCH, Weinheim, **1994**.

C. N. Alpers, D. W. Blowes (Eds.), *Environmental Geochemistry of Sulfide Oxidation*, A.C.S. Symp. Ser., Vol 550, American Chemical Society, Washington D.C., **1994**.

Holleman-Wiberg: *Lehrbuch der Anorganischen Chemie*, 101. Auflage, de Gruyter, Berlin, **1995** (textbook with 75 pages on sulfur chemistry).

M. A. Vairaramurthy, M. A. A. Schoonen (Eds.), *Geochemical Transformations of Sedimentary Sulfur*, ACS Symp. Ser. 612, Washington, **1995**.

L. L. Barton (Ed.), *Sulfate-Reducing Bacteria*, Plenum Press, New York, **1995**.

E. I. Stiefel, K. Matsumoto (Eds.), *Transition Metal Sulfur Chemistry*, A.C.S. Symp. Ser., Vol. 653, American Chemical Society, Washington D.C., **1996**.

N. N. Greenwood, A. Earnshaw, *Chemistry of the Elements*, 2nd ed., Butterworth, Oxford, **1997** (textbook with 101 pages on sulfur chemistry).

R. Steudel, *Chemie der Nichtmetalle*, de Gruyter, Berlin, **1998** (modern textbook with 60 pages on sulfur chemistry).

Z. B. Alfassi (Ed.), *The Chemistry of Sulfur Radicals*, Wiley, Chichester, **1999**.

T. Kabe, A. Ishiara, W. Qian (Eds.), *Hydrodesulfurization and Hydrodenitrogenation*, Wiley-VCH, Weinheim, **1999**.

P. N. L. Lens, L. Hulshoff Pol (Eds.), *Environmental Technologies to Treat Sulfur Pollution: Principles and Engineering*, IWA Publishing, London, **2000**; with Chapters on the following topics:

1. The Chemical Sulfur Cycle (R. Steudel)
2. The Geochemical Sulfur Cycle (J. J. Middleburg)
3. The Biological Sulfur Cycle (T. Brüser, P. N. L. Lens, H. G. Trüper)
4. Removal of Sulfur from Diesel Oil (H. R. Reinhoudt)
5. Bioleaching of Sulfide Minerals (M. Boon)
6. Sulfur Transformation during Sewage Transport (T. Hvitvedt-Jacobsen, P. H. Nielsen)
7. Biological Treatment of Organic Sulfate-Rich Wastewaters (P. N. L. Lens, F. Omil, J. M. Lema, L. W. Hulshoff Pol)
8. Biological Removal of Sulfurous Compounds from Wastewaters (B. Johnson)
9. Anaerobic Treatment of Sulfate-Rich Wastewaters (J.-P. Steyer, N. Bernet, P. N. L. Lens, R. Moletta)
10. Survey of H₂S and SO₂ Removal Processes (J. A. Lagas)
11. Novel Biological Processes for the Removal of H₂S and SO₂ (A. J. H. Janssen, H. Dijkman, G. Janssen)
12. Biological Treatment of Gases Polluted by Volatile Sulfur Compounds (V. Herrygers, H. Van Langenhove, E. Smet)
13. Methods of Odor Measurement and Assessment (R. H. Fenner, R. M. Stuetz)
14. Treatment of Solid Materials Containing Inorganic Sulfur Compounds (R. Tichý)
15. Agricultural Aspects of Sulfur (W. H. O. Ernst)
16. Biodegradation of Sulfonated Aromatic Compounds (N. C. G. Tan, J. A. Field)

17. Metal Effects on Sulfur Cycle Bacteria and Metal Removal by Sulfate Reducing Bacteria (O. J. Hao)
18. Interactions of the Sulfur and Nitrogen Cycles: Microbiology and Process Technology (P. M. Chazal, P. N. L. Lens)
19. Sulfur-Storing Bacteria and Bulking of Activated Sludge ((D. H. Eikelboom)
20. Sulfur Problems in Anaerobic Digestion (V. O'Flaherty, E. Colleran)
21. Corrosion and Sulfur Bacteria (B. J. Little, R. I. Ray, R. K. Pope)
22. Recent Developments in Research on Biogenic sulfuric Acid Attack of Concrete (E. Vincke, J. Montaney, A. Beeldens, N. De Belie, L. Taerve, D. Van Gemert, W. H. Verstraete)

Holleman-Wiberg: *Inorganic Chemistry*, Academic Press, New York, **2001** (most comprehensive inorganic chemistry textbook available).

R. Steudel, *Organic Polysulfanes* R_2S_n ($n > 2$), *Chem. Rev.* **2002**, *102*, 3905-3945.

More reviews and monographs on (mainly inorganic) sulfur chemistry are cited in the various Chapters of Volumes 230 and 231.